

**Modes and Progression of Tool Deterioration and Their Effects
on Cutting Force during End Milling of 718Plus Ni-Based
Superalloy using Cemented WC-Co Tools**

Nurul Hidayah Razak

A thesis submitted to Auckland University of Technology in fulfilment of the
requirements for the degree of Doctor of Philosophy

2017

School of Engineering, Computer and Mathematical Sciences

ABSTRACT

Understanding the detailed progression of cutting tool deterioration and how deterioration affects cutting force (F) during milling of difficult-to-cut Ni-based superalloys is important for the improvement of machinability of the alloys. It also serves to clarify whether and how an F -based method for monitoring tool deterioration is possible. This understanding is however far from sufficient, as is explained in this thesis after a comprehensive review of the literature. The aim of the present research is thus to determine and explain the modes and progression of tool deterioration and how cutting forces may vary due to the various deterioration features of the cutting tool edge.

Experimentally, the study started by using a typical milling condition with both uncoated and coated cemented carbide (WC-Co) tools. Milling was conducted in either dry or wet conditions. After each pass of a selected distance, the tool was examined in detail in the same manner. Thus, tool deterioration could be monitored more closely and failure mechanisms could be identified and explained. Following on the study on determining the modes of tool deterioration, the progress of deterioration and cutting forces during milling were carefully monitored. Through analysing the monitored tool deterioration features and measured force data, how edge wear, chipping and breakage in cutting edge and beyond the edge contribute to the variation of cutting forces could be studied and better understood. Furthermore, experiments have also been conducted using workpiece in a hardened state.

It has been observed that the commonly recognised build-up layer in the initial stage does not significantly affect the tool deterioration process. Instead, from the beginning of milling, cutting forces/stresses could cause small chipping locally in the initially sharp cutting edge. Fracturing locally with cracks propagating outside the cutting edge along the flank face in the subsurface region could also take place and was consistent with the direction of the cutting force. There was an initial period of time during which a number of microcracks had initiated in and near the cutting edge on the rake face side. These cracks soon propagated resulting in extensively fracturing and blunting of the tool. Coating of the tools had provided little protection as in the cutting edge area the coating had broken away soon after milling started. The major tool failure mode was Co binder material having heavily deformed to fracture, separating the WC grains. Loss of strength in binder material at cutting temperatures

is also discussed. As would be expected, the general trend of how F increased as the number of pass (N_{pass}) increased agreed with the general trend of increasing flank wear (VB) as N_{pass} increased. However, the F - VB_{max} plot has shown a rather poor F - VB_{max} relationship. This was the result of the different modes of tool deterioration affecting VB_{max} differently, but VB_{max} did not represent fully the true cutting edge of the deteriorating tool insert. Chipping and breakage of the inserts confined in the cutting area, resulting in the significant blunting of the edge area, causing a high rate of F increase as VB_{max} increased and completely deteriorated 6 minutes within of milling time. Fracturing along the face of thin pieces effectively increased VB_{max} without increasing the cutting edge area and without further blunting the edge, thus no increase in F was required. The high rate, meaning high $\Delta F/\Delta VB_{max}$, results from the effect of the edge deterioration/blunting on the reducing the effective rake angle and thus increasing F is suggested and discussed. The use of coolant has not been found to affect tool deterioration/life and cutting force. Explanation for this will be given considering the deformation zone for which coolant does not have an effect. An increase in feed rate has reduced the tool life and the mode of deterioration has become more edge chipping/fracturing dominant, leading to a better F - VB_{max} relationship.

Finally, it has been observed that the rate of tool deterioration is not higher when the hardened workpiece material is used. The modes and progression of deterioration of tools using hardened workpiece were determined to be comparable to those when annealed workpiece was used. Furthermore, the trends of increase in cutting force as milling pass increases have been observed to be similar for both workpiece material conditions. Interrupt milling experiments followed by hardness mapping has indicted that the workpiece hardened state has not affected the deformation area significantly, although increase in hardness in a similar amount in the severe deformed region has been found for both cases. It is suggested that temperature increases in the narrow deformation zone to be similar for both workpiece conditions and at high temperatures hardening mechanisms do not operate, and thus cutting force values do not differ significantly. Furthermore, the modes and rate of tool deterioration on the hardened workpiece was comparable to the annealed workpiece.

ACKNOWLEDGEMENTS

I would like to acknowledge and extend my heartfelt gratitude to my primary supervisor, Prof Zhan Chen for the continuous support of my Ph.D study and related research, for his patience, motivation, and immense knowledge. His guidance helped me in all the time of research and writing of this thesis. I could not have imagined having a better advisor and mentor for my Ph.D study. I also would also like to thank my secondary supervisor, AP Timotius Pasang for his continuous support guiding me through the thesis writing process by giving me his best effort.

My sincere thanks also goes to Jim Crossen, Ross Jamieson, Mark Masterston, Tim Luton, Thomas Jones and Patrick Connor for their hard work, expertise and patience. Without their precious support, it would not be possible to conduct this research.

My appreciation also extends to Karl Davidson for stimulating discussion and for the sleepless nights we were working together before the deadline. I also would like to thank Doddy, Evtaleny, and Yuan and other research group members for all the fun we have had in the last three years. I also thank my dearest friends Hemyza Budin, Har Einur Azrin, Nurul Syuhada Mohamed, Ili Ayuni Johan and Ridhuan Abd. Rahim for providing support and friendship.

Most importantly, I would like to thank The Davidsons and Wendy Millen for their great support and unconditional love during difficult times. I would not have made it this far without them. Last but not least, I would like to thank my family especially my mother, Wan Rasnah Wan Idris, who have guided me throughout my life. She has always sacrificed her time and has continuously supported me in achieving my dreams and goals. I would like to thank her for all her love, support and encouragement for me. I specially dedicate this work to my beloved late father, Razak Latif and I wish he could smile for me.

LIST OF PUBLICATIONS

The following papers have been published over the course of this research.

Journal papers:

Razak, NH, Chen, ZW and Pasang, T, Modes of Tool Deterioration during Milling of 718Plus Superalloy Using Cemented Tungsten Carbide Tools, *Wear* 316 (2014): 92-100.

Razak, NH, Chen, ZW and Pasang, T, Progression of Tool Deterioration and Related Cutting Force during Milling of 718Plus Superalloy using Cemented Tungsten Carbide Tools, *International Journal Advance Manufacturing Technology* (2016) 86: 3203-3216.

Conference paper:

Razak, NH, Chen, ZW and Pasang, T, Relationship Between Tool Deterioration and Cutting force during Milling of a Nickel-Based Superalloy Using Cemented Carbide Tool, *Proceeding of the ASME 2015 International Mechanical Engineering Congress and Exposition (IMECE2015)*, November 13-19, 2015, Houston, Texas.

TABLE OF CONTENTS

ABSTRACT.....	ii
ACKNOWLEDGEMENTS	iv
LIST OF PUBLICATIONS	v
TABLE OF CONTENTS.....	vi
LIST OF FIGURES	viii
LIST OF TABLES	xviii
NOMENCLATURE.....	xix
ATTESTATION OF AUTHORSHIP	xxi
Chapter 1: Introduction and Literature Review	1
1.1 Background of the Study.....	1
1.2 An Introduction on Tool Deterioration.....	3
1.3 Current Assessment Methods on Tool Deterioration	7
1.4 Tool Wear Mechanisms.....	10
1.5 Current Understanding on Gradual Wear.....	10
1.6 The Other Modes of Tool Deterioration.....	20
1.7 Model Relating Tool Deterioration to Milling Time or Distance	24
1.8 Effect of Cooling on Tool Deterioration	26
1.9 Effect of Tool Coating on Tool Deterioration.....	29
1.10 Effect of Workpiece Hardened State on Tool Deterioration.....	32
1.11 Effect of Tool Deterioration on Cutting Force	33
1.12 The Scope of This Study	36
Chapter 2: Experimental Design and Procedures.....	38
2.1 Milling Machine and Clamping system	38
2.2 Workpiece and Cutting Tools Materials.....	40
2.3 Workpiece Hardness and Strength Measurements	43
2.4 Milling Parameters and Conditions	45
2.5 Dynamometer and Force monitoring.....	48

2.6	Sample Preparation and Examination	50
2.7	Tool Deterioration Monitoring	52
Chapter 3: Modes of Tool Deterioration		56
3.1	Flank Deterioration – Early Stage	56
3.2	Flank Deterioration – Growth Stage.....	60
3.3	Deterioration Observed on All Three Faces	61
3.4	Deterioration of Coated Tools	65
3.5	Further Discussion on Modes and Measures of Tool Deterioration.....	67
3.6	Mode of Fracture	69
3.7	Summary	70
Chapter 4: Cutting Force and Progression of Tool Deterioration		71
4.1	Features of Forces During Milling	71
4.2	Examination on the Effect of Coating on Cutting Force	77
4.3	Effect of Tool Deterioration on Cutting Force	80
4.4	Further Discussion on Cutting Force Relating to Deterioration of Cutting Edge .	88
4.5	Examination on Cutting Edge Condition Affecting Deformation Zone	90
4.6	Effect of High Feed Rate on Cutting Force.....	94
4.7	Summary	103
Chapter 5: Tool Deterioration Influenced by Workpiece Heat Treatment State		104
5.1	Cutting Edge Deterioration	104
5.2	Trend of Cutting Force Increase Verse Milling Pass	115
5.3	Cutting Edge Condition Affecting Deformation Zone	121
5.4	Summary Plots on The Effect of Heat Treatment State	123
5.5	Overall Plots of Flank Wear and Cutting Force	125
Chapter 6: Conclusion.....		127
References		129

LIST OF FIGURES

Figure 1-1 Illustration of resultant force (F_R) and friction force (F_f) as the interaction between workpiece and cutting tool.....	1
Figure 1-2 Scanning Electron Microscope images (SEM) on tool failure of an uncoated cemented carbide tool; (a) side flank face and (b) rake face.....	3
Figure 1-3 Illustration of down-milling operation with image of tool holder and insert.....	4
Figure 1-4 Cutting edge view with (a) cutting edge (wear), (b) edge chipping and (c) heavy chipping, the primary deterioration modes further proposed in this study	5
Figure 1-5 Enlarged view near the cutting edge locations with cutting force and edge shear stress indicated	5
Figure 1-6 Standard wear nomenclature, (a) tool cutter, (b) illustration of VB assessment ..	7
Figure 1-7 Graph of flank wear, VB (mm) versus cutting time (min) [11].....	8
Figure 1-8 Illustration to indicate the true dimensional deterioration distances in a cross section	8
Figure 1-9 Measurement of tool wear. The original profile of the tool edge is shown as the discontinuous line [9].....	11
Figure 1-10 (a) Flank wear of an insert after six passes of down milling ($v_c = 30$ m/min, $f = 0.03$ mm/rev, $DOC = 1.2$ mm, $a_e = 2$ mm) from Li et al. [22] and (b) Illustration of VB assessment from various publications and true assessment of tool deterioration	12
Figure 1-11 Flank wear of TiAlN/AlCrN insert [11].....	13
Figure 1-12 Flank wear of a carbide tool at cutting speed, (V)=113.1m/min and feed rate, (f) = 0.05m/tooth [3].....	13
Figure 1-13 Maximum flank wear width and maximum chipped edge with on a cutter flute [4]	14
Figure 1-14 Illustration of cutting edge, flank face and rake face	14
Figure 1-15 Mapping of speculative wear causes, types and consequences, given by Zhu et al. [12] (there is a serious uncertainty in Zhu et al.'s quoting in regard to the sources of the map).....	16
Figure 1-16 (a) Images of the adhesion mechanism during the adhesion of workpiece material to tool, Illustration indicated the adhesive mechanism based on suggested opinion by Zhu et	

al. [12], (b) after taking off the tool material and (c) illustration the bonding strength BUL (σ_{BUL}) σ_{WC-Co}) and interface between the WC-Co (σ_{int}) σ_{WC-Co})..... 17

Figure 1-17 Example of tool failure due to (a) abrasive mechanism, and (b) adhesion mechanism [12]..... 18

Figure 1-18 SEM images of the cutting corner location (top: rake face, left: side flank face and right: bottom flank face) of tools after end milling cutting ($v_c = 100$ m/min, $f = 0.15$ mm/rev and $DoC = 1.0$ mm) by Kadirgama et al.[5], (a) PVD TiAlN coated WC-Co tool after 180 mm milling (b) CVD TiN/TiCN/Al₂O₃ coated WC-Co tool after 742 mm milling and (c) Illustration to aid the attachment and notch (s) location..... 21

Figure 1-19 SEM images of tool inserts: (a) an insert in an initial stage with rake face and flank face as indicated and clearly without a notch, (b) a down view on the rake face after notching (we have observed, outlined/labelled in white although authors have not) during ball-nose end milling by Kasim et al. [11]. Tool inserts were TiAlN/AlCrN coated (cutting conditions were not specified by authors) and (c) Illustration from Figure 1-19a, chipping at flank face (we identified) 22

Figure 1-20 Photos of a coated tool insert after: (a) 22.1 min, (b) 24.1 min, (c) 27.5 min, (d) 29.5, (e) 35.5 min and (f) 42.9 min under cutting condition of ($v_c = 50$ m/min, $f = 0.1$ mm/rev and axial depth of cut = 0.5, $a_e = 1.0$ mm) via dry condition. Top: rake face, left: bottom flank face and right: side flank face, scale on the photo is our approximation based on value of axial depth of cut [8]..... 22

Figure 1-21 Photos of a coated tool insert after: (a) 20.8 min, (b) 28.8 min, (c) 44.9 min, (d) 57.0 min, 64.3 min and (f) 72.4 min under cutting condition of ($v_c = 50$ m/min, $f = 0.1$ mm/rev and axial depth of cut = 0.5, $a_e = 1.0$ mm) via MQL . Top: rake face, left: bottom flank face and right: side flank face, scale on the photo is our approximation based on value of axial depth of cut [8]..... 23

Figure 1-22 Scanning electron microscope (SEM) micrograph showing tool fracturing ... 24

Figure 1-23 Change in corner wear with cutting length for MQL machining with the ordinary nozzle. Cutting conditions: cutting speed, 1.3 m/s (78 m/min); depth of cut, 0.11 mm; feed rate, 0.1 mm/rev [29]..... 26

Figure 1-24 Tool lives of three coated tools in MQL, wet and dry cutting, Cutting conditions: cutting speed, 1.0 m/s; feed rate, 0.1 mm/rev; depth of cut, 0.1mm; air pressure of MQL, 0.40MPa; Oil consumption of MQL, 16.8 ml/h [30] 27

Figure 1-25 Tool wear VB with cutting time under different cutting conditions [8] 27

Figure 1-26 Evolution of tool life in dry, oil based emulsion, cold air and cryogenic turning of Inconel 718 [48]..... 28

Figure 1-27 Notch wear progression under different cooling conditions [34].....	28
Figure 1-28 Development of average flank wear when face milling Inconel 718 and feed rate of 0.08 mm per tooth [17]	29
Figure 1-29 Tool wear plot in terms of length cut [36]	30
Figure 1-30 Performance of TiAlN-multilayer variants in turning Inconel 718 [37].....	30
Figure 1-31 Tool lives of three coated tools in MQL, wet and dry cutting, Cutting conditions: cutting speed, 1.0 m/s; feed rate, 0.1 mm/rev; depth of cut, 0.1mm; air pressure of MQL, 0.40MPa; Oil consumption of MQL, 16.8 ml/h [30]	31
Figure 1-32 Box plots, whisker and outliers of tool life with different cutting tool coatings [40].....	32
Figure 1-33 Illustration of resulted force (F_R) and friction force (F_f) as the interaction between workpiece and cutting tool for (a) annealed state and (b) hardened state workpiece of Ni-based alloy.....	33
Figure 1-34 Cutting force (N) versus cutting time (min), (a) F_x and (b) F_y [8]	33
Figure 1-35 Effect of tool wear on cutting force [11].....	34
Figure 1-36 Measured flank wear progression with other observed wear modes during the end milling of Inconel 718. $V_c=140$ m/min, $FR=0.15$ mm/tooth, $DoC=0.75$ mm, $a_e=0.2$ mm [11].....	34
Figure 1-37 Cutting force of different machining conditions, Aramcharoen and Chuan [33]	35
Figure 1-38 Evolution of the three components and the magnitude of the cutting force (N) as a function of T_{mr} ($^{\circ}C$). $V_c=30$ m/min, $FR=0.10$ mm/tooth, and $DoC=0.2$ mm, Kong et al. [41].....	35
Figure 2-1 A Pacific FU.125 milling machine and the arrangement of dynamometer and workpiece	38
Figure 2-2 Illustrations of down-milling experiment: (a) image showing assembly of dynamometer for forces (F_x , F_y and F_z) measurement, 718Plus workpiece, tool holder and insert, coolant nozzle, and (b) schematic of viewing down on the workpiece and tool-insert with various stages of the tool during the pass indicated.....	39

Figure 2-3 (a) A drawing of workpiece blocks, (b) actual workpiece with different block viewing	40
Figure 2-3 Continued	41
Figure 2-4 (a) Photo of an insert mounted on a tool holder and actual images of three faces of a tool insert, (a) rake face, (b) side flank face and (c) bottom flank face. (Regions marked by the pink rectangular are cutting areas and thus the major interest/focus areas to be analysed)	42
Figure 2-5 An illustration of the radius cutting edge between cutting insert and the workpiece	42
Figure 2-6 Example of distance between Vickers indentations	43
Figure 2-7 The dimension of tensile specimens.....	44
Figure 2-8 Plot of engineering stress against engineering strain: (a) annealed sample 1, (b) annealed sample 2, (c) hardened sample 1 and (d) hardened sample 2	44
Figure 2-9 Engineering stress (MPa) versus engineering strain; (a) annealed sample 1 and (b) heat treatment sample 1	45
Figure 2-10 Dynamometer setting (a) dynamometer forces F_x , F_y and F_z direction on the machine setting (b) configuration of dynamometer, charge amplifier and milling machine	49
Figure 2-11 An illustration of cutting tool insert mounted on epoxy resin.....	50
Figure 2-12 An illustration of an interrupt milling pass with line drawn indicating sectioned sample was made on the machined surface.....	51
Figure 2-13 Machined surface of 718Plus Ni-based superalloy (a) an illustration a cross section machined surface on a bakelite resin and (b) micrograph of the cross section machined surface.....	51
Figure 2-14 Cutting tool insert position at the SEM sample holder for three different view; (a) side flank face, (b) bottom flank face and (c) rake face	52
Figure 2-14 Continued	53
Figure 2-15 Example of flank wear assessment on SEM images on the side flank face; (a) a new tool insert before milling, (b) higher magnification image in location A, (c) higher location magnification image in location B showing fine WC grains in edge location (cutting	

edge) before milling (d) Tool deteriorated after the fourth milling pass. Tooling condition: uncoated carbide and wet (TC12-1).....	53
Figure 2-15 Continued	54
Figure 2-16 SEM images sequences for every passes; (a) side flank face, (b) bottom flank face and (c) rake face. Tooling condition: uncoated carbide and wet (TC12-1).....	54
Figure 2-16 Continued	55
Figure 3-1 SEM images of insert TC1 side flank face before and after various passes: (a) before milling with edge outlined, designated as zero pass edge outline (ZPEO), (b) after the first pass together with ZPEO, (c) after the second pass with ZPEO and (d) after the third pass (magnification different). Tooling condition: uncoated carbide and dry	57
Figure 3-2 Cutting edge features: (a) higher magnification image in location A of Figure 3-1b, showing 718 BUL material next to WC grains edge, (b) higher magnification image in location marked B in (a) showing fine WC grains in edge location, (c) EDS spectrum with analytical spot * marked in (a) and (d) EDS spectrum with analytical spot + marked in (a)	58
Figure 3-3 Illustration of a cross section of new tool insert (SEM images) and workpiece (drawings) indicating features during milling: (a) low magnification SEM image in and around cutting edge location together with drawings indicating the various features in the surrounding and (b) high magnification SEM image in a cutting edge location displaying fine WC grains bound by Co-binder	59
Figure 3-4 SEM images of insert TC2 side flank face before and after various passes: (a) before milling with edge outlined, designated as zero pass edge outline (ZPEO), (b) after the first pass together with ZPEO, (c) after the second pass together with ZPEO, (d) after the third pass together with ZPEO and (e) A higher magnification of image 3-4d indicating plastic lowering on the tool insert	62
Figure 3-5 SEM images of insert TC2 bottom flank face before and after various passes: (a) before milling with zero pass edge outline (ZPEO), (b) after the first pass together with ZPEO, (c) after the second pass together with ZPEO and (d) after the third pass together with ZPEO. Tooling condition: uncoated carbide and dry.....	63
Figure 3-6 SEM images of insert TC2 rake face before and after various passes: (a) before milling with zero pass edge outline (ZPEO), (b) after the first pass together with ZPEO, (c) after the second pass together with ZPEO and (d) after the third pass together with ZPEO, (d) after the third pass together with ZPEO, Chip flow direction is indicated by arrow in each pass. Tooling condition: uncoated carbide and dry.....	64
Figure 3-7 Higher magnification images showing cracks as pointed to by arrows in cutting edge: (a) at location A of Figure 3-5c and (b) at location B of Figure 3-6c	65

Figure 3-8 SEM images of insert TC3 (TiAlN coated) side flank face after (a) before milling, (b) first pass (c) second passes and (d) third passes. Tooling condition: coated carbide and dry	66
Figure 3-9 SEM images of insert TC4 (TiAlN coated) side flank face after two passes, (a) low magnification and (b) very high magnification in location A in (a). Tooling condition: coated carbide and dry	66
Figure 3-10 Schematic summary of severity of tool deterioration observed in this study ..	69
Figure 4-1 Schematic view looking down on the workpiece and tool-insert with various stages of the tool during the pass indicated.....	72
Figure 4-2 The whole F_x , F_y , F_z and F curves (recorded data) of (a) the first milling pass and (b) the fourth milling pass. Tooling condition: uncoated and coolant (TC7-2).....	73
Figure 4-3 F_x , F_y , F_z and F data/curves of the first pass during (a) the initial and within 3 s of milling engagement and (b) a half milling cycle time in early milling stage. Tooling condition: uncoated and coolant (TC7-2)	74
Figure 4-4 Geometrical representation of milling, viewing down: (a) at the start of milling engagement meaning the first cycle of a pass, and (b) during a normal milling cycle that the tool insert cuts the workpiece with a full lateral distance (radial depth of cut), a_e . Distance of FR and thus d_{c-w} are not drawn in proportion	75
Figure 4-5 F_x , F_y , F_z and F data/curves of the fourth pass during (a) a 3 s period just before the insert reached the end of the workpiece and (b) a half milling cycle time within a period. Tooling condition: uncoated and coolant (TC7-2).....	76
Figure 4-6 Cutting force (F) data/curves of the first pass during the initial 3s of milling engagement of tool conditions; (a)-(b) uncoated and dry, (c)-(d) coated and dry, (e)-(f) uncoated and coolant and (g)-(h) coated and coolant	78
Figure 4-7 SEM images of side flank faces after the first pass of milling of tool conditions: (a)-(b) uncoated and dry, (c)-(d) coated and dry, (e)-(f) uncoated and coolant and (g)-(h) coated and coolant.....	79
Figure 4-8 Average maximum force values F_{x-e-m} , F_{y-e-m} , F_{z-e-m} and F_{e-m} verses the number of passes for the four tooling conditions, (a) uncoated and dry, (b) coated and dry, (c) uncoated and coolant and (d) coated and coolant.....	82
Figure 4-9 SEM images of coated insert and wet (coolant) conditions (TC8-1): (a) side flank face of the insert after the first pass (coating eroded on edge and workpiece build-up are indicated), (b) left - side flank face, mid - bottom flank face and right - rake face, respectively,	

of the insert after five passes, and (c) left - higher magnification image in location marked C in (b) and right – EDS spectrum with analytical spot + marked in the left image. In the right image of (b), how the side flank face view corresponds in the right image and bottom flank view in the mid image are indicated 83

Figure 4-10 VB_{max} verses the number of passes for the four milling conditions, (a) uncoated and dry, (b) coated and dry, (c) uncoated and coolant and (d) coated and coolant..... 84

Figure 4-11 F_{e-m} values plotted as a function of VB_{max} 85

Figure 4-12 SEM images of (a) from left to right side flank face, bottom flank face and rake face of insert TC7-2 after four passes (the edge outline of the insert before milling has been superimposed), corresponding to point B in 4-11 and (b) higher magnification image in location marked B in (a) and EDS spectrum (on spot +) on the right..... 86

Figure 4-13 SEM images of side flank faces: (a) insert TC7-1 after 4 passes and (b) insert TC5-2 after 5 passes. In each image, the edge outline of the insert before milling has been superimposed 87

Figure 4-14 Schematic illustration of milling with (a) the cutting insert in the initial state before deterioration, (b) the insert having worn and thus the radius of cutting edge having enlarged, $r1 < r2$, and (c) the insert having worn and flank face material having fractured off, $r3 \ll r2$ (Note: $r4$ does not need to be equal to $r2$ and $r1$ of the initial cutting edge is not indicated). The projection of the resultant of total force in working plane, F_a , is indicate in (a) and SEM viewing directions and thus VB are indicated (c) 88

Figure 4-15 Illustration of the deforming zone on the machined cross-section surface 90

Figure 4-16 Micro hardness map on the machined cross-section surface; left images are of new tool image and right image is a deteriorated tool after the fourth pass (a)-(b) annealed workpiece, uncoated and dry (TC9), (c)-(d) annealed workpiece, uncoated and wet (coolant) (TC10)..... 91

Figure 4-16 Continued 92

Figure 4-17 SEM images of uncoated and dry (TC9) after the fourth pass (a) side flank face (b) bottom flank face 94

Figure 4-18 F curves (recorded data) of (a) the first milling pass of TC9, (b) the final pass milling pass of TC9, (c) the first milling of TC10 and (d) the final milling pass of TC10.. 94

Figure 4-19 The whole F_x , F_y , F_z and F curves (recorded data) of (a) the first milling pass and (b) the third pass. Tooling condition: uncoated carbide and dry (TC11-1)..... 95

Figure 4-20 F_x, F_y, F_z and F curves of the first pass during (a) the initial within 3s of milling engagement and (b) a half milling cycle time in the early milling stage. Tooling condition: uncoated carbide and dry (TC11-1)	96
Figure 4-21 F_x, F_y, F_z and F curves of the first pass during (a) 3-s period just before the insert reached the end of the workpiece and (b) a half milling cycle time within a period. Tooling condition: uncoated carbide and dry (TC11-1)	97
Figure 4-22 Average maximum force values $F_{x-e-m}, F_{y-e-m}, F_{z-e-m}$ and F_{e-m} versus the number of passes for the two tooling (a) TC11 and (b) TC12	98
Figure 4-23 VB_{max} versus the number of passes for the two milling conditions, TC11 and TC12.....	100
Figure 4-24 SEM images of side flank face; (a) before milling, (b) first milling pass, (c) second milling pass and (d) third milling pass. Tooling condition: TC11-2	100
Figure 4-25 SEM images of third pass; (a) bottom flank face and (b) rake flank face, tooling condition: TC11-2	101
Figure 4-26 SEM images of side flank face; (a) before milling, (b) first milling pass, (c) second milling pass and (d) third milling pass. Tooling condition: TC12-1	101
Figure 4-27 F_{e-m} versus VB_{max} for a feed rate of 0.1 mm/rev conditions.....	102
Figure 5-1 VB_{max} versus the number of passes of milling a hardened workpiece : (a) dry (TC13) and (b) wet (coolant) (TC14).....	104
Figure 5-2 SEM images Tool TC13-1 side flank face before and after various milling passes of a hardened workpiece: (a) before milling with edge outlined, designated as zero pass edge outline (ZPEO), (b) after the first pass together with ZPEO, and (c) after the second pass together with ZPEO.....	105
Figure 5-3 SEM images Tool TC13-1 bottom flank face before and after various milling passes of a hardened workpiece: (a) before milling with edge outlined, designated as zero pass edge outline (ZPEO), (b) after the first pass together with ZPEO, and (c) after the second pass together with ZPEO.....	105
Figure 5-3 Continued	106
Figure 5-4 SEM images Tool TC13-1 rake face before and after various milling passes of a hardened workpiece: (a) before milling with edge outlined, designated as zero pass edge outline (ZPEO), (b) after the first pass together with ZPEO, and (c) after the second pass together with ZPEO.....	106

Figure 5-5 SEM images Tool TC13-2 side flank face before and after various milling passes of a hardened workpiece: (a) before milling with edge outlined, designated as zero pass edge outline (ZPEO), (b) after the first pass together with ZPEO, (c) after the second pass together with ZPEO, (d) after the third pass together with ZPEO, and (e) after the fourth pass together with ZPEO..... 107

Figure 5-6 SEM images Tool TC13-2 of rake face before and after various milling passes of a hardened workpiece: (a) before milling with edge outlined, designated as zero pass edge outline (ZPEO), (b) after the first pass together with ZPEO, (c) after the second pass together with ZPEO, (d) after the third pass together with ZPEO, and (e) after the fourth pass together with ZPEO..... 108

Figure 5-7 SEM images Tool TC14-1 side flank face before and after various milling passes of a hardened workpiece: (a) before milling with edge outlined, designated as zero pass edge outline (ZPEO), (b) after the first pass together with ZPEO, (c) after the second pass together with ZPEO, (d) after the third pass together with ZPEO, and (e) after the fourth pass together with ZPEO..... 110

Figure 5-8 SEM images Tool TC14-1 bottom flank face before and after various milling passes of a hardened workpiece: (a) before milling with edge outlined, designated as zero pass edge outline (ZPEO), (b) after the first pass together with ZPEO, (c) after the second pass together with ZPEO, (d) after the third pass together with ZPEO, and (e) after the fourth pass together with ZPEO..... 111

Figure 5-9 SEM images Tool TC14-2 side flank face before and after various milling passes of a hardened workpiece: (a) before milling with edge outlined, designated as zero pass edge outline (ZPEO), (b) after the first pass together with ZPEO, (c) after the second pass together with ZPEO, (d) after the third pass together with ZPEO, and (e) after the fourth pass together with ZPEO..... 112

Figure 5-10 SEM images of tool TC14-2 in milling a hardened workpiece: (a) higher magnification image in location of Figure 5-9d at location A, showing crack initiation at side flank face view, and (b) higher magnification of 5000X magnification at side flank face 113

Figure 5-11 SEM images Tool TC14-2 rake face before and after various milling passes of a hardened workpiece: (a) before milling with edge outlined, designated as zero pass edge outline (ZPEO), (b) after the first pass together with ZPEO, (c) after the second pass together with ZPEO, (d) after the third pass together with ZPEO, and (e) after the fourth pass together with ZPEO..... 113

Figure 5-11 Continue 114

Figure 5-12 SEM images of tool TC14-2 in milling a hardened workpiece: (a) higher magnification image in location of Figure 5-11d at location point B, showing crack initiation at rake face view, and (b) higher magnification of 5000X magnification at the rake face 114

Figure 5-13 The whole F_x , F_y , F_z and F curves (recorded data) of a hardened workpiece (a) the first milling pass and (b) the fourth milling pass. Tooling condition: uncoated and coolant (TC14-1).....	115
Figure 5-13 Continued	116
Figure 5-14 F_x , F_y , F_z and F data/curves of a hardened workpiece for the first pass during (a) the initial and within 3 s of milling engagement and (b) a half milling cycle time in early milling stage. Tooling condition: uncoated and coolant (TC14-1).....	116
Figure 5-14 Continued	117
Figure 5-15 F_x , F_y , F_z and F data/curves of the first pass during (a) a 3-s period just before the insert reached the end of the workpiece and (b) a half cycle time within a period. Tooling condition: uncoated and coolant (TC14-1)	118
Figure 5-16 Average maximum force values F_{x-e-m} , F_{y-e-m} , F_{z-e-m} and F_{e-m} versus the number of passes four two cooling conditions, (a) TC13-1, (b) TC13-2, (c) TC14-1 and (d) TC14-2	119
Figure 5-17 F_{e-m} values as a function of VB_{max}	121
Figure 5-18 Micro hardness map on the cross section machined surface; (a) a new tool insert after the first pass (left image) and a deteriorated tool insert after the fourth milling pass (right image). Tool condition: uncoated tool and dry (TC15)	122
Figure 5-19 SEM images rake face of a deteriorated tool after the fourth pass of milling hardened workpiece in dry condition (TC15)	122
Figure 5-20 F curves (recorded data) of tool insert (a) a new tool after the first pass (b). 123	
Figure 5-21 (a) Cutting force (F_{e-m}) and (b) flank wear (VB_{max}) values plotted against the number of passes (N_{pass}) for milling experiments conducted using annealed workpiece (TC5 and TC7) and hardened workpiece (TC13 and TC14).....	124
Figure 5-22 F_{e-m} values plotted as a function of VB_{max} for experiments using both annealed and hardened workpieces	125
Figure 5-23 (a) Cutting force (F_{e-m}) and (b) flank wear (VB_{max}) values plotted against the number of passes (N_{pass}) for various tool conditions using annealed and heat treatment workpieces.....	126

LIST OF TABLES

Table 2-1	Composition specification of 718Plus (wt%).....	40
Table 2-2	Heat treatment of 718 Plus.....	41
Table 2-3	Summary of milling condition of 718Plus experimental conditions.....	47

NOMENCLATURE

ω - Spindle Speed

$\tau_{Cutting}$ - Shear Stress

θ_e - Effective Rake Angle

a_e - Radial Depth of Cut

BUE – Build-Up Edge

BUL - Build-Up Layer

Co - Cobalt

CrN - Chromium Nitride

d_{c-w} / h - Thickness of Cut

DoC - Depth of Cut

EDS - Energy Dispersive Spectrometry

f or FR - Feed Rate

F or $F_{Cutting}$ - Cutting Force

F_a - working plane

$F_{Cutting-R}$ - Cutting Edge Action Force

F_f - Friction Force

F_R - Resultant Force

F_x - Force in x -direction

F_y - Force in y -direction

F_z - Force in z -direction

F_{x-m} - The maximum F_x started to decrease when the end of the pass was reached

F_{y-m} - The maximum F_y started to decrease when the end of the pass was reached

F_{z-m} - The maximum F_z started to decrease when the end of the pass was reached

F_m - The maximum F started to decrease when the end of the pass was reached

F_{x-e-m} - The maximum F_x of 3 s period just before the insert reached the end of workpiece

F_{y-e-m} - The maximum F_y of 3 s period just before the insert reached the end of workpiece

F_{z-e-m} - The maximum F_z of 3 s period just before the insert reached the end of workpiece

F_{e-m} - The maximum F of 3 s period just before the insert reached the end of workpiece

HRC - Hardness Rockwell C

HV - Hardness Vickers

ISO - International Organisation for Standardisation
MAZ - Milling Affected Zone
MQL - Minimum Quantity Lubrication
Ni - Nickel
 N_{pass} - Number of Tool Passes
PCD - Polycrystalline Diamond
PVD - Physical Vapour Deposition
 r_e - Cutting Edge Radius
 r_{e-eff} - Effective Radius of the Cutting Edge
SEM – Scanning Electron Microscope
 t_0 - Original Cutting Edge Geometry
TC -Tool Condition
TDA - Tool Deterioration Area
 t_i - Original Cutting Edge Geometry after the wearing process
TiAlN - Titanium Aluminium Nitride
TiC - Titanium Carbide
TiN - Titanium Nitride
 v - Forward Speed
 V - Tool Forward Speed
 VB - Flank Wear
 $VB1$ - Uniform Flank Wear
 $VB2$ - Non-Uniform Wear
 $VB3$ - Localised Flank Wear
 VB_{max} - Maximum Flank Wear (localised)
 V_c – Cutting Speed
VTW - Volume Tool Wear
 V_{wear} - Volume of Wear
WC - Tungsten Carbide
WC-Co - Cemented Tungsten Carbide
ZPEO - Zero Pass Edge Outline

ATTESTATION OF AUTHORSHIP

I hereby declare that this submission is my own work and that, to the best of my knowledge and belief, it contains no material previously published or written by another person (except where explicitly defined in the acknowledgements), nor material which to a substantial extent has been submitted for the award of any other degree or diploma of a university or other institution of higher learning.

Auckland


Signature _____

Chapter 1: Introduction and Literature Review

1.1 Background of the Study

In general, machinability is characterised by the ease of a material to be machined and is directly related to their material properties, explained by Astakhov [1] who is recognised as the leading expert on machining. Astakhov [1] explained that machinability can be assessed by considering certain machining characteristics such as tool wear, magnitude of cutting forces, and surface roughness of the machined workpiece. In machining, the cutting tool is subjected to shearing and ploughing between the cutting tool and the workpiece. This means that during machining, the cutting tool (insert) is subjected to compressive and frictional force, as (traditionally) illustrated in Figure 1-1. An important requirement in machining is the high strength, high wear resistance, and high toughness of tool materials. For machining low to mid strength materials such as mild steel or aluminium alloys the commonly used tool materials such as high speed steels and cemented tungsten carbide (WC-Co) are satisfactory in terms of tool life and surface quality. However, machining difficult-to-cut material such as nickel-based superalloys, tool life is an important consideration from the cost and sustainable manufacturing point of view. This means tool life can be the major factor in considering machinability of difficult-to-cut materials.

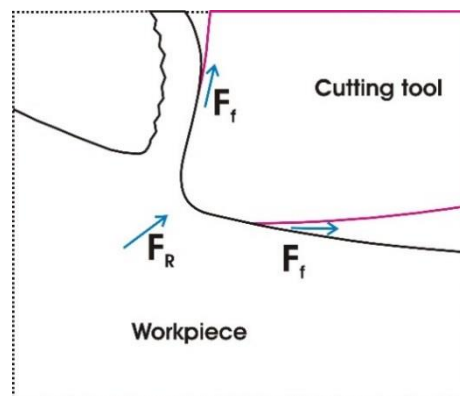


Figure 1-1 Illustration of resultant force (F_R) and friction force (F_f) as the interaction between workpiece and cutting tool

As nickel (Ni) superalloys are of high importance for aerospace applications, their machinability focusing on tool life has been the subject of a strong research effort for a very long period of time and has repeatedly been reviewed in the last 21 years [2-15]. As summarised by Pervaiz et al. [2], tool life and cutting forces are among the main criteria in

rating machinability during machining of Ni-based superalloys. Liao et al. [3] demonstrated that chipping and breakage of tool cutting edge dominated, although an observation on failure progression was not made. Studies by Chen and Li et al.[4], Kadirgama et al.[5], Devillez et al.[6], Olovsjo and Nyborg [7], Zhang et al.[8] , Uzun et al. [9], Imran et al. [10], and Kasim et al.[11], have shown that local tool fracturing is common; however, failure analysis to understand the initiation and propagation of cracks in the tool is difficult and have not been conducted in depth. Zhu et al. [12] categorised wear mechanisms in machining nickel-based superalloys as material loss through the process of adhesion, oxidation, and abrasion. Research work on the use of various coatings to improve tool life has also been included in the review with debonding furthermore classified as a wear mechanism. It is clear, however, that tool failure analysis presented in literature as reviewed by Zhu et al. [2] is insufficient so that the operation of the various suggested mechanisms and how they relate to tool failure/life could be illustrated. Because of this, how tools deteriorate during machining nickel-based superalloys is not fully understood and there could be misinterpretations regarding the mechanisms. It is important that the progression of tool deterioration during milling of nickel-based superalloys is understood so that a meaningful measurement of tool life and improvement in tool can be made.

There has been an effort to develop monitoring methods of tool wear of WC-Co tools, based on the measurement of cutting forces during milling of Ni-based superalloys. Chen and Li [4] experimentally determined a regression model relating to cutting forces in x direction (F_x), y direction (F_y), and z direction (F_z) to flank wear (VB) during milling of 718Plus Ni-based superalloy. For the purpose of tool monitoring, there is a need to develop a reliable model to predict how cutting forces relate to tool deterioration as explained by Chinchankar and Choudhury et al. [13]. Considering nickel-based superalloys, as stated above it is also clear that the understanding on how cutting forces respond to the various modes of tool deterioration during various stage of the tool life is insufficient. This understanding is required in order to clarify whether and how cutting force can be used for predicting and monitoring the state of tool during milling.

With respect to insufficient in the understanding of tool deterioration modes pointed out above, primarily, this study is conducted with a motivation to observe and explain the phenomena and progression of tool deterioration of cemented carbide tools during end milling of nickel-based superalloys. Milling was chosen as the machining process in this study as most published work on Ni alloy machinability study has focused on turning.

Secondly, cutting forces during milling are monitored in order to investigate the influence of edge wear, chipping and breakage in cutting tool edge and beyond the edge on the variation of cutting forces. A final series of experiments were conducted using a hardened workpiece in order to understand the effect of increased hardness/strength on the rate of tool deterioration and the corresponding modes. Following the detailed literature review, the scope of the present research and the sequence of this Ph.D research will be given.

1.2 An Introduction on Tool Deterioration

Short tool life is of major concern when machining nickel-based superalloys [8, 23]. To understand this problem, a scanning electron microscope (SEM) image of cutting tool failure taken from this preliminary experiment in milling a 718Plus nickel-based alloy is examined as depicted in Figure 1-2. In this image, it can be seen that the cutting tool has experienced severe damage, resulting in a short tool life. Reduction in tool life increases tool cost, down time consumption, and thus reduces efficiency in the manufacturing industry. Due to these machining difficulties, cutting tool materials with high wear resistance, high strength, and high toughness are required. Advanced cutting tool materials include cemented tungsten carbide (WC), ceramic, polycrystalline diamond (PCD) and polycrystalline cubic boron nitride (PCBN) [18] are commonly used in industry. In addition, coatings such as titanium carbide (TiC), titanium nitride (TiN) and titanium aluminium nitride (TiAlN) are also applied in order to extend the tool life [9, 14, 23, 25, 26].

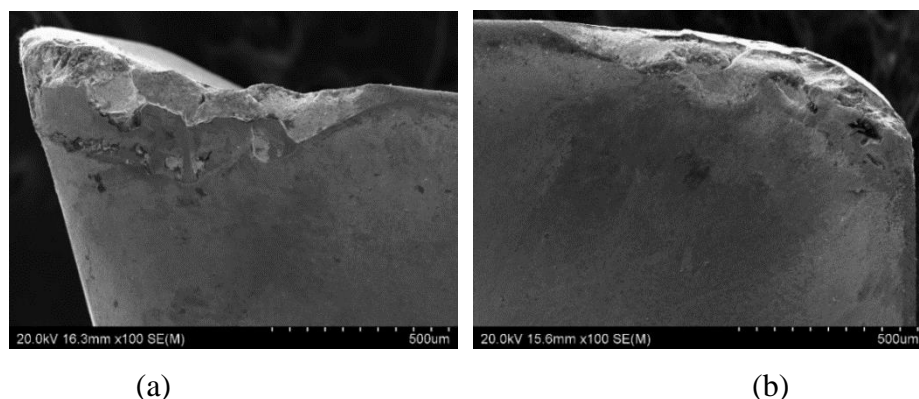


Figure 1-2 Scanning Electron Microscope images (SEM) on tool failure of an uncoated cemented carbide tool; (a) side flank face and (b) rake face

In material removal practice, milling is defined as interrupted cutting, where every individual cutting insert enters and exits the cut continuously [8, 27]. To understand the milling

operation, an illustration indicating the fundamental components of down-milling including the tool holder, cutting tool insert, workpiece and machine (not shown) is presented in Figure 1-3. A cemented carbide (WC) cutting tool with a cobalt (Co) binder was used in this present study to machine 718 superalloy as depicted in Figure 1-3. The settable parameters of the milling machine were forward speed (v), spindle speed (ω), depth of cut (DoC) and radial depth of cut (a_e). The milling pass starts by rotating the tool into the pass at a tool forward speed (V), entering at the location labelled “Start of the milling pass” and completing when the tool exits the other end of the block labelled “Finish of milling pass”.

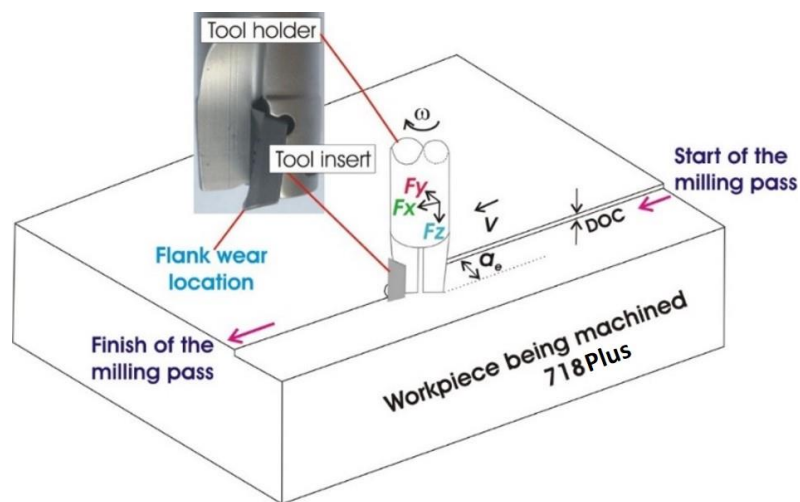


Figure 1-3 Illustration of down-milling operation with image of tool holder and insert

During milling of 718Plus Ni-based superalloy, the cutting tool is subjected to high cutting forces in order to shear the workpiece material. As the intermittent cutting continues, a sharp cutting tool edge experiences a gradual tool wearing process or fails suddenly depending on the cutting condition. According to the ISO standard [15] of testing of tool wear and tool life during milling, tool deterioration is classified by two major forms; tool wear which is a progressive loss of tool material and brittle fracture (chipping) which results from crack initiation during milling. Having considered these two major forms of tool deterioration, a used schematic diagram is shown in Figure 1-4 to illustrate the condition at the cutting edge location and possible forces acting on the tool. This research attempts to more explicitly categorise and suggest that there should primarily be three possible individual forms in which the cutting tool can deteriorate. The first mode is wear (cutting edge wear specifically) which is a gradual process of material in the cutting edge being eroded away, as shown in Figure 1-4a where f refers to the feed rate, t_0 refers to the original cutting edge geometry and t_i refers to one after the wearing process. Second, edge chipping forms by small tool piece(s)

fracturing off locally within the cutting edge primarily under the influence of shear stress ($\tau_{Cutting}$), shown in Figure 1-4b. The third mode is heavy chipping where large tool piece (s) fracture off, with cracking extended to various distances beyond the cutting edge largely resulting from cutting force ($F_{Cutting}$), shown in Figure 1-4c.

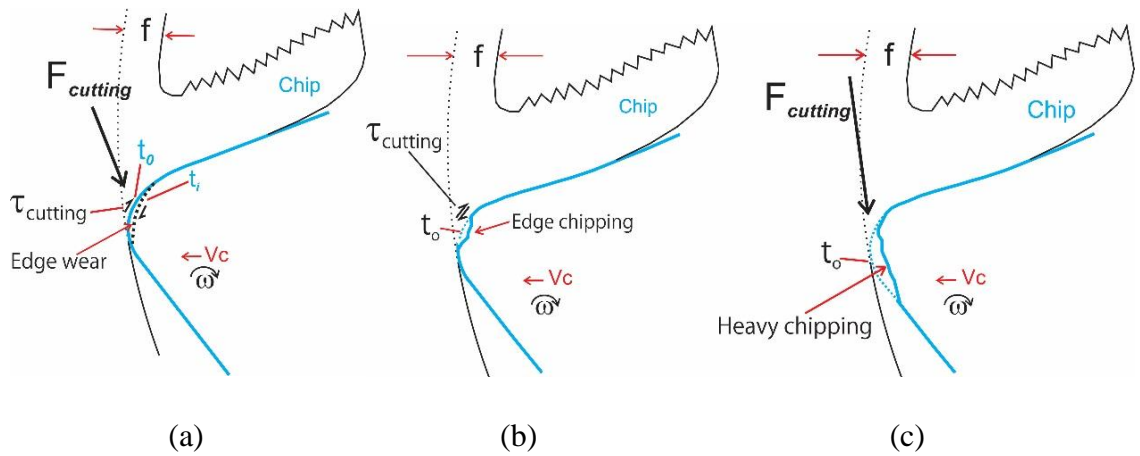


Figure 1-4 Cutting edge view with (a) cutting edge (wear), (b) edge chipping and (c) heavy chipping, the primary deterioration modes further proposed in this study

In order to have a better picture on how the cutting edge of the tool may behave, an illustration of cutting force and shear distribution on the cutting edge is presented in Figure 1-5. For this illustration, cemented tungsten carbide (WC-Co) is used as a cutting tool insert which it is extensively used in machining nickel-based alloys [16]. The WC-Co tools consists of particles of a hard phase of tungsten carbide (WC) cemented in soft phase binder usually cobalt (Co). The combination of strength and toughness of WC-Co tools are considered superior to other tool materials [8, 22].

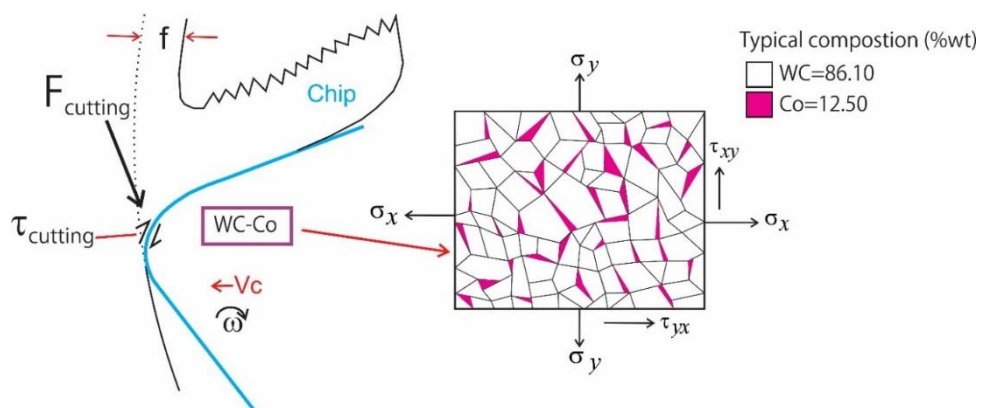


Figure 1-5 Enlarged view near the cutting edge locations with cutting force and edge shear stress indicated

During milling, cutting tool forces the workpiece to shear in order to remove the layer of material machined and concurrently, the cutting tool is subjected to a cutting force and shear stress (τ). Conversely, if the shear force acting on the cutting edge is low, WC particles may experience gradual loss with small grains being worn off. Next, if the shear stress is high, the tool could experience local chipping or fracturing in the form of small tool pieces dislodging. Furthermore, if the cutting force is more severe, the tool may deteriorate in the form of heavy chipping. Thus, considering these three modes of deterioration, this study has been conducted to reveal, under the complicated mechanical condition, how the cutting tool deteriorates. This has not been previously discussed in the literature review. The study further aims to improve to the understanding on how cutting force responses to each of the modes of deterioration. The understanding of deterioration modes employed in the milling process is essential for future improvement of the machinability of nickel-based superalloys.

Aside from focusing on modes of deterioration, it is crucial to understand how proper is the assessment of tool wear using the traditional wear criterion of flank wear (VB) as in many publications of nickel-based superalloy machining over many years [7,10, 11, 13, 15, 21, 31-35]. In traditional assessment, only a single dimension (1D) measurement on the flank face area is considered and is not a true presentation to present total cutting tool loss which is a three dimensional phenomenon (3D). In most referred publications, the process of tool deterioration is not well described and hence the assessment of tool life could be misleading. Therefore, the aim of this study is to systematically monitor the progression of tool deterioration and examine how the cutting tool deteriorates so that the mechanism of the tool edge changes geometrically can be understood. Thus, the assessment of tool life is meaningful.

Following the background of the study given above, a detailed literature review is presented in the following section. How tool deterioration during milling of nickel-based superalloys is assessed (section 1.3) will first be reviewed. A comprehensive review on the current understanding of gradual wear is presented in section 1.4. A review of other modes of tool deterioration covering chipping/fracturing is discussed in section 1.5. Current suggested models for predicting tool wear and the effect of cooling, tool coating, hardened workpiece on tool deterioration are reviewed in section 1.6, 1.7, 1.8 and 1.9 respectively. Furthermore, the effect of tool deterioration on cutting force is discussed in section 1.10. Following the comprehensive literature review, the scope and sequence of this Ph.D research will be explained.

1.3 Current Assessment Methods on Tool Deterioration

Testing of tool wear and tool life via ISO 8688-2 tool life testing in milling – part 2 [15] in the milling of Ni alloys is widely reported; [7,10, 11, 13, 15, 21, 31-35]. According to the ISO standard, tool deterioration is defined as all physical changes of the cutting part of the tool caused by the process of cutting. In this standard, tool deterioration is classified in two major forms; tool wear, a progressive loss of tool material and brittle fracture (chipping) resulting from crack initiation during milling. Generally, flank wear (VB) as illustrated in Figure 1-6, is the most common representation of the gradual material loss process on the flank face land [17]. In Figure 1-6 $VB1$, $VB2$ and $VB3$ refer to uniform flank wear, non-uniform wear and localised flank wear respectively. The measurement of tool deterioration refers to a numerical value expressing the magnitude of tool deterioration for a defined aspect.

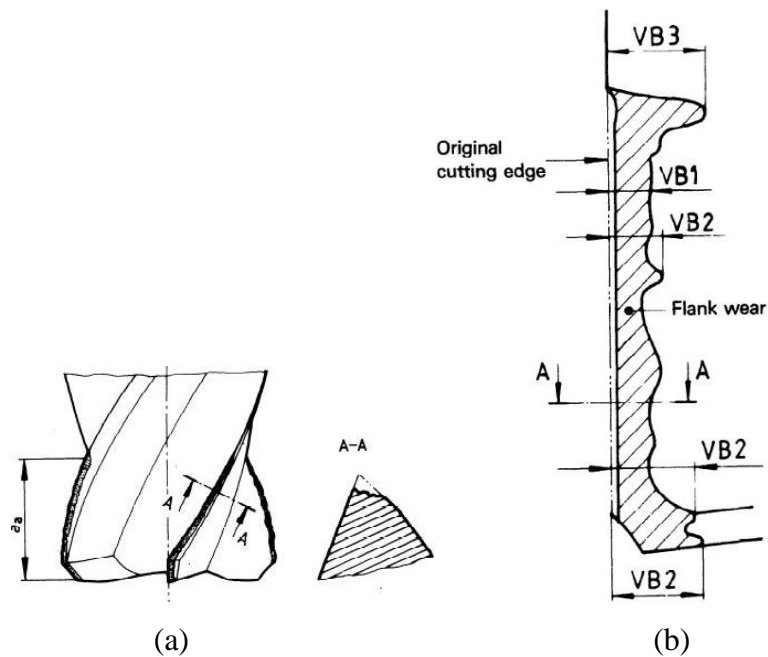


Figure 1-6 Standard wear nomenclature, (a) tool cutter, (b) illustration of VB assessment

With respect to VB , there are two recommended criteria to indicate the life of tool. The first is uniform wear, where the average flank width affected reaches 0.3 mm and the second is localised wear (VB_{max}) which represents the maximum flank width affected reaches 0.5mm. The measurement of VB is taken parallel to the surface of the wear land and perpendicular to the original cutting edge as shown in Figure 1-6. From this specific wear criterion, a tool life graph such as in Figure 1-7 (taken from Kasim et al. [11]) is plotted to represent the state of

tool wear [14-16, 22-23, 27]. Although this tool life graph is widely used by the researchers, if VB is not assessed correctly the plotted graph could be misleading.

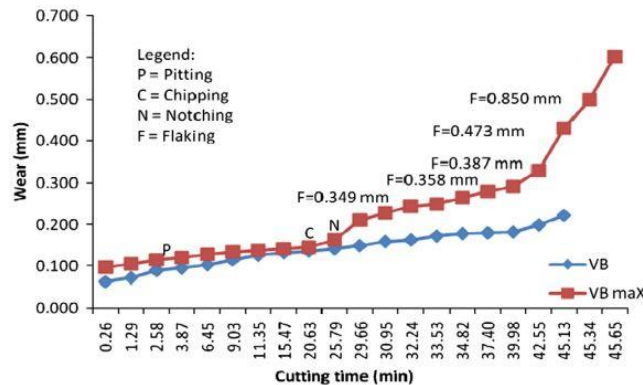


Figure 1-7 Graph of flank wear, VB (mm) versus cutting time (min) [11]

Thus, the methods of understating the fundamentals of tool wear assessment to establish a proper measurement are discussed forthwith. As tool wear refers to material tool loss it is a three dimensional (3D) phenomenon. Kuttolamadom [18] stated tool wear has been assessed in a single dimension (1D) for many years. If bulk deformation of the tool is not considered, tool deterioration can be as an individual form or combination and is schematically illustrated in a cross-sectional view shown in Figure 1-8 where, a piece or pieces had fractured off in or near the cutting edge. The deterioration width as a function of depth from the flank face (at X within $X1$ and $X0$) is given by:

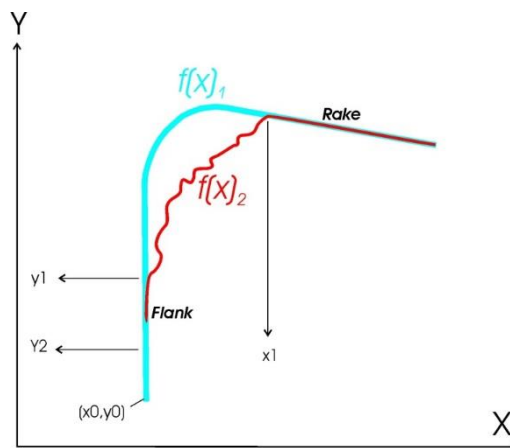


Figure 1-8 Illustration to indicate the true dimensional deterioration distances in a cross section

$$F(x)_z = [f(x)_{1max} - f(x)_{2max}]_z \quad \text{Equation 1-1}$$

For a particular Z, the total deteriorated area (TDA) is:

$$TDA = \int_{x_0}^{x_1} F(x) dx = \int_{x_0}^{x_1} [f(x)_{1max} - f(x)_{2max}] dx \quad \text{Equation 1-2}$$

However, according to the ISO standard a measurement (VB which is defined as “the width of a flank wear land”) should be made and this measurement can be illustrated in Figure 1-8 as;

$$VB_a = f(x)_{1max} - y_1 \quad \text{Equation 1-3}$$

Subscript “ a ” signifies the correct measurement following the ISO standard. The value VB may indicate deterioration but clearly it is not a measure of total deterioration, which should be as in Equation 1-2. Often, researchers [14-16, 22, 23, 27] measured VB without a reference to the $f(x)_{1max}$, thus applying the following equation:

$$VB_{E1} = f(x)_{2max} - y_1 \quad \text{Equation 1-4}$$

Whereby, subscript “ E ” signifies an incorrect measurement and VB_{E1} is measured without a reference as indicated later in Figure 1-16. A considerably more common error in measuring VB occurs from the presence of a build-up layer (BUE) denoted by VB_{E2} as in Equation 1-5, included in the measurement [14-16, 22, 23, 27]. This can occur irrespective of the ISO standard specifically stating the removal of the layer prior to measuring VB . Mechanical procedures and chemical etching can be used to remove the presence of BUE or other workpiece material debris off on the cutting tool. It should be noted that mechanical technique may damage the tool and chemical etching may dissolve the cobalt (Co) binder if a cemented carbide tool is used. Chen and Li [4] provided the only publication reporting the removal of the build-up edge, although an explanation on how the BUE was removed was not provided. From analysing their images illustrating the flank wear width, it would be very difficult to remove the BUE. No build-up was evident in the images and the measurements conducted did not consider the formation of BUE.

$$VB_{E2} = f(x)_{2max} - y_2 \quad \text{Equation 1-5}$$

It is important to note that regardless of whether VB can be measured correctly, the measured value is not a true measurement of deterioration as a 2D view cannot be accurately used to represent a 3D volume. The graph commonly used to indicate tool life, shown above in Figure 1-7 is debatable because VB does not represent volume material loss.

1.4 Tool Wear Mechanisms

Tool wear describes the progressive/gradual loss of tool material when tool-workpiece surfaces rub together, resulting in a loss of material and in a change in the tool geometry [19]. In metal cutting, adhesion wear, abrasive wear, erosive wear and tribocorrosion wear have been identified as the wearing processes. In the case of adhesion wear, according to the established mechanism [19], the mating surface comes close enough together to form strong bonds. If the bonds established are stronger than the local strength of the material, a particle may transfer from one to another. After this has occurred numerous times, a loose fragment may form and separate as wear debris. Besides that, this mechanism is also classified as attrition mechanism [20]. Abrasion wear is defined as the removal of small fragments when a hard body slides over a softer surface and in order for abrasive wear to occur, one of the contacting surfaces needs to be harder than the surface being abraded at least 1.3 times [19]. Furthermore, impact of hard particles on surfaces is the main reason of erosive wear to be occurred [21]. Material loss in this process is measured as the ratio of the mass removed material with respect to the mass of the erosive particles. In addition, tribocorrosion wear has also been viewed as the wearing mechanism in cutting tool, which involves material loss by corrosion due to chemical attack on a surface. These mechanisms of tool wear may apply to a large range/type of workpiece materials. For difficult-to-cut materials particularly for Ni-based superalloys, tool wear modes have been specifically studied for a long time. Thus, in the next section (section 1.5), a detailed discussion is presented on the current understanding of the wear mechanisms during machining Ni-based superalloys.

1.5 Current Understanding on Gradual Wear

In order to understand the wear mechanism specifically in machining Ni-based superalloys, first analysed in this review are the existing publications related to flank wear, a term extensively used to represent the state of tool deterioration. Following this, a critical discussion on the current understanding of gradual wear mechanisms commonly addressed by researchers attributing to the “wearing” process is discussed. Examining all the relevant

research (journal) publications in the last ten years; [6-8, 10-11, 16, 20-21, 29, 32, 35-37] the term “flank wear” has continued to be widely used. However, “flank wear” does not describe the process of wear (cutting edge wear) as has already been explained in Figure 1-4a. There is no justification of the mechanics that wear should appear on the flank face because it is outside the cutting edge region where the workpiece-tool interfaces. This point is already explained with more detail in section 1.2. Of the all relevant publications on tool wear, only Uzun et al. [9] has attempted to illustrate cutting edge wear as the form of tool deterioration. They illustrate in a true geometrical sense the loss of cutting tool material in the cutting edge location in Figure 1-9. However, the loss must be compounded by wear and local fracturing. This compounding is justifiable, as wear is a very slow process, dominated by local fracturing. As evident in Figure 1-9, the original geometry of the cutting tool was quite sharp. Local fracturing appears to have dominated at the workpiece-tool interface rapidly deteriorating the tool. Thus, a gradual wear process was not demonstrated in this publication.

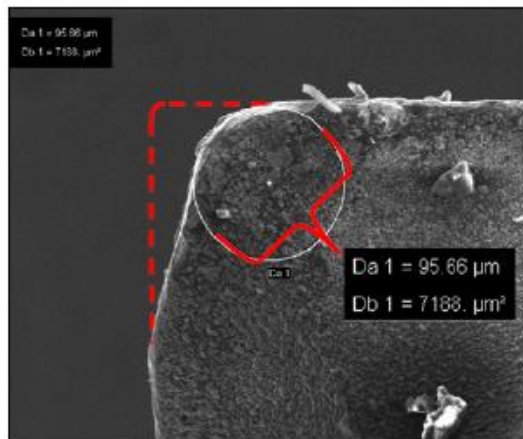


Figure 1-9 Measurement of tool wear. The original profile of the tool edge is shown as the discontinuous line [9]

Subsequently, we shall refer to some examples of “flank wear” represented in the publications; [6-8, 10-11, 16, 20-21, 29, 32, 35-37], so as to illustrate why flank wear may not be a reasonable measure of wear. The first example we have taken is from a study conducted by Li et al. [22]. They conducted milling experiments including down milling of a nickel-based superalloy using tools of cemented WC with Co binder (WC-Co) similar to that suggested in Figure 1-5. Figure 1-10 is a typical “Flank wear” photo presented by them. The “flank wear” distance detailed in the figure was measured to be 0.3 mm. A more plausible explanation is that the distance detailed is the measurement of Ni build-up on the flank face. Flank wear distance (VB) as described by the following publications; [6-8, 10-

11, 16, 20-21, 29, 32, 35-37] is consolidated in Figure 1-10b. The *VB* region clearly does not represent the material loss but, tool deterioration area (TDA) does represent the amount of material loss as discussed in section 1.3.

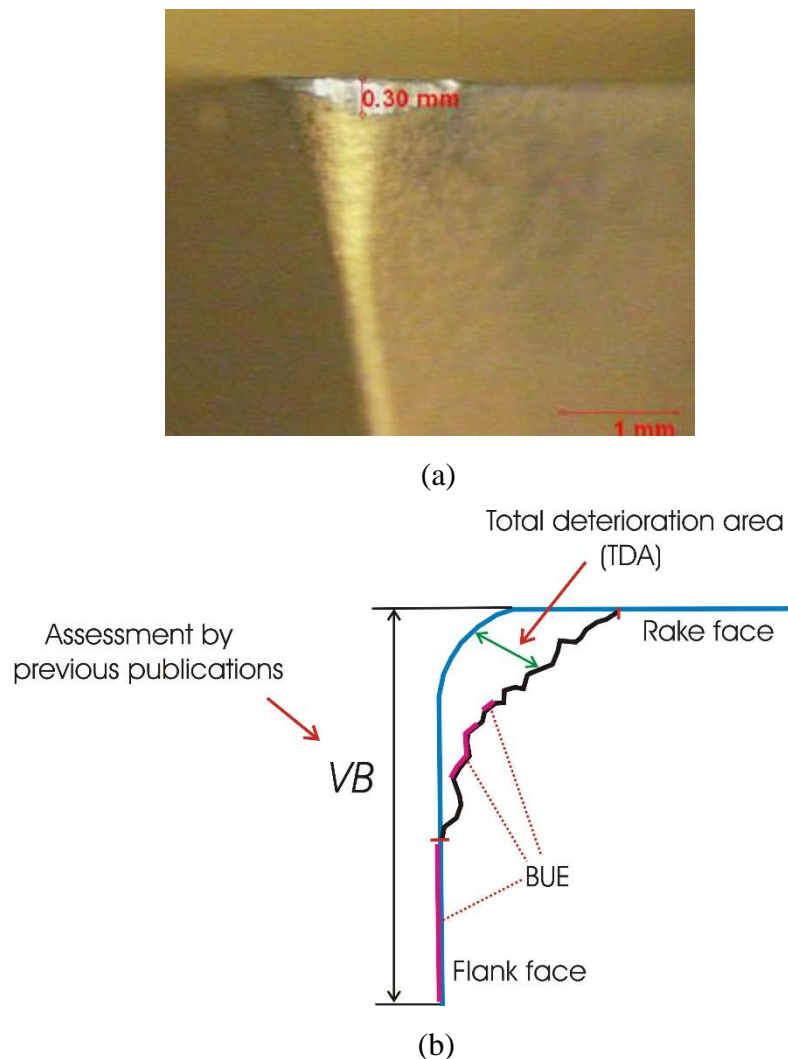


Figure 1-10 (a) Flank wear of an insert after six passes of down milling ($v_c = 30$ m/min, $f = 0.03$ mm/rev, $DOC = 1.2$ mm, $a_e = 2$ mm) from Li et al. [22] and (b) Illustration of *VB* assessment from various publications and true assessment of tool deterioration

There are three deficiencies presented by Li et al. [22] as shown in Figure 1-10a. Firstly, it did not show the actual material loss as it may be an attachment of Ni superalloy. If there is an attachment, it is unknown if there is any material loss underneath the attachment. Secondly, the view plane of the flank face does not provide the geometrical view of the flank face edge, thus not representing true flank face loss. Thirdly, assuming there is tool material loss, reviewing the mechanism of the material loss is not possible, thus presenting little knowledge on flank wear. The second example is from Kasim et al. [11] as in Figure 1-11. They carried out ball end milling experiments of Inconel 718 using WC with multi-layer

PVD TiAlN/AlCrN coating. In this publication, firstly there is no clear demonstration to prove that the tool has worn. Secondly, the assessment of wear at that position cannot be used to detect the evidence of tool loss. Thirdly, the tool possibly had some coating delamination but this was not related to the loss of the underlying material.

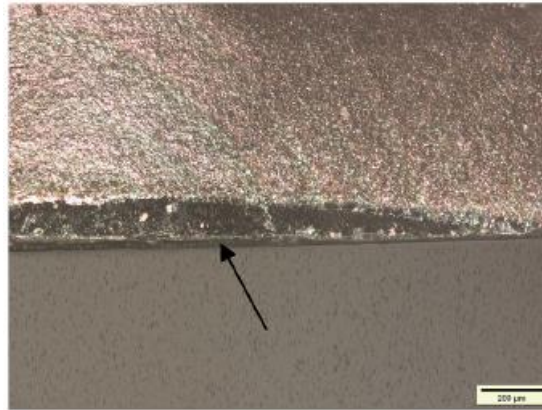


Figure 1-11 Flank wear of TiAlN/AlCrN insert [11]

The third example is from the study by Liao et al. [3] on end milling of Inconel 718 superalloy using cemented carbide tool. They stated that flank wear on the cutting tool was identified when the cutting speed increased to 56.5 m/min. From the image in Figure 1-12, there is no clear evidence to indicate the wear on the flank face, however the smearing traces between the cutting tool and workpiece were visible on the flank area.

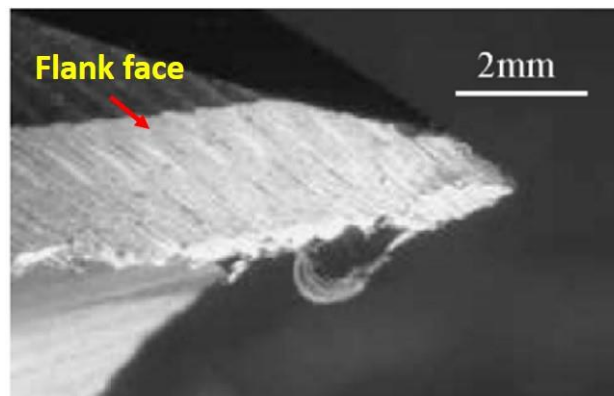


Figure 1-12 Flank wear of a carbide tool at cutting speed, (V)=113.1m/min and feed rate, (f) = 0.05m/tooth [3]

Moreover, in the fourth example, Chen and Li et al. [4] developed a tool wear observer model for online tool condition monitoring and control in machining. The result showed the maximum flank wear width to have a value of 0.75 mm as shown in Figure 1-13. It was mentioned in the publication that a projection of the cutter flute's rake face perpendicular to

microscope's focus plane was used as a reference to measure the flank wear width since the original edges vanished. Nevertheless, the accuracy of this artificial reference is uncertain and the value measured may not be valid for plotting the graph of the tool life, presented in the later part of the discussion. Furthermore, the term maximum flank wear was incorrect in describing the wear process of this cutting flute because it was certainly not a progressive wear process. This figure clearly suggested that the cutting flute has gone through the heavy chipping process where fracturing off extended beyond the cutting edge.

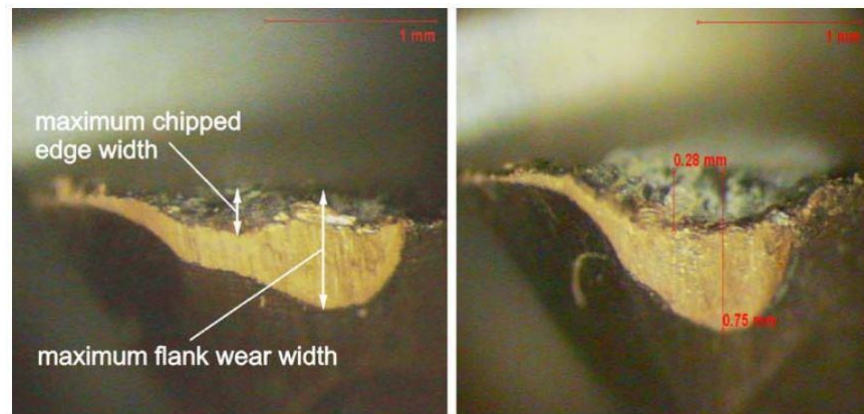


Figure 1-13 Maximum flank wear width and maximum chipped edge with on a cutter flute [4]

Based on the present literature review, the classification of the tool wear is inadequate, attributable to the lack of understanding of the definition of wear. From the view point of mechanics, tool wear is a progressive loss affecting the cutting edge first (cutting edge is the main contact area, rather than flank that is outside the cutting edge) rather than the flank face as illustrated in Figure 1-14. Thus, “flank wear” may not be an appropriate term as there is only gradual cutting edge wear. Furthermore, as discussed in section 1.2 the previous assessments of tool wear has failed to measure the material loss adequately.

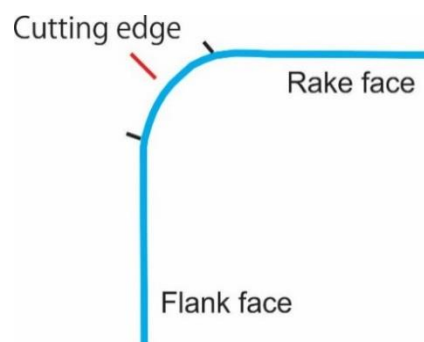


Figure 1-14 Illustration of cutting edge, flank face and rake face

Particular to this “wear” process, collated literature suggested a number of mechanisms of the “wearing” process. In a comprehensive review encompassing 34 journal papers by Zhu et al. [12] on the topic of tool wear during machining of nickel alloys, “wear” mechanisms during machining of the alloys have also been categorised as material loss through the processes of adhesion, diffusion, oxidation and abrasion, further shown in Figure 1-15. Various coatings were used to improve tool life, the debonding of these coatings classified as a mechanism of wear. This review specifically focuses on milling. Discussed firstly is the mechanism of adhesion. Zhu et al. [12] defined adhesive mechanisms as workpiece material adhered to the cutting tool, and adhesive form including the formation of build-up edge (BUE) which may occur on the flank and rake face.

This attachment may fragment the tool and erode the cutting tool [6, 10, 21, 25, 38]. This latter fragmentation process has however not been supported by evidence in any of the publications reviewed. Akhtar et al. [23] a year later adapted Zhu et al.’s [12] similar concept of on adhesion mechanism in a review of tool wear mechanisms of the machining of Nickel based super-alloys. However, it’s stated that this adhesion occurred at high cutting temperatures and stresses. Under this condition, the workpiece material adhered at the tool flank and rake face forming BUE. It has been suggested, but not directly demonstrated that the adherent BUE material may be unstable and may dislodge dragging the particles of tool, resulting in several grooves and cracks on the subsurface of the tool. Also reported is a predominance in chemical and diffusion wear at high cutting speeds and temperatures. This, however, should be viewed as speculation as there was no further scientific elaboration on how the mechanism could occur. Moreover, Kadirgama et al. [5] in their study of tool life and wear mechanism when machining Hastelloy C-22HS Ni-based alloy observed that the repeated formation of BUE on the cutting tool assisting the phenomena of attrition, finally leading to chipping.

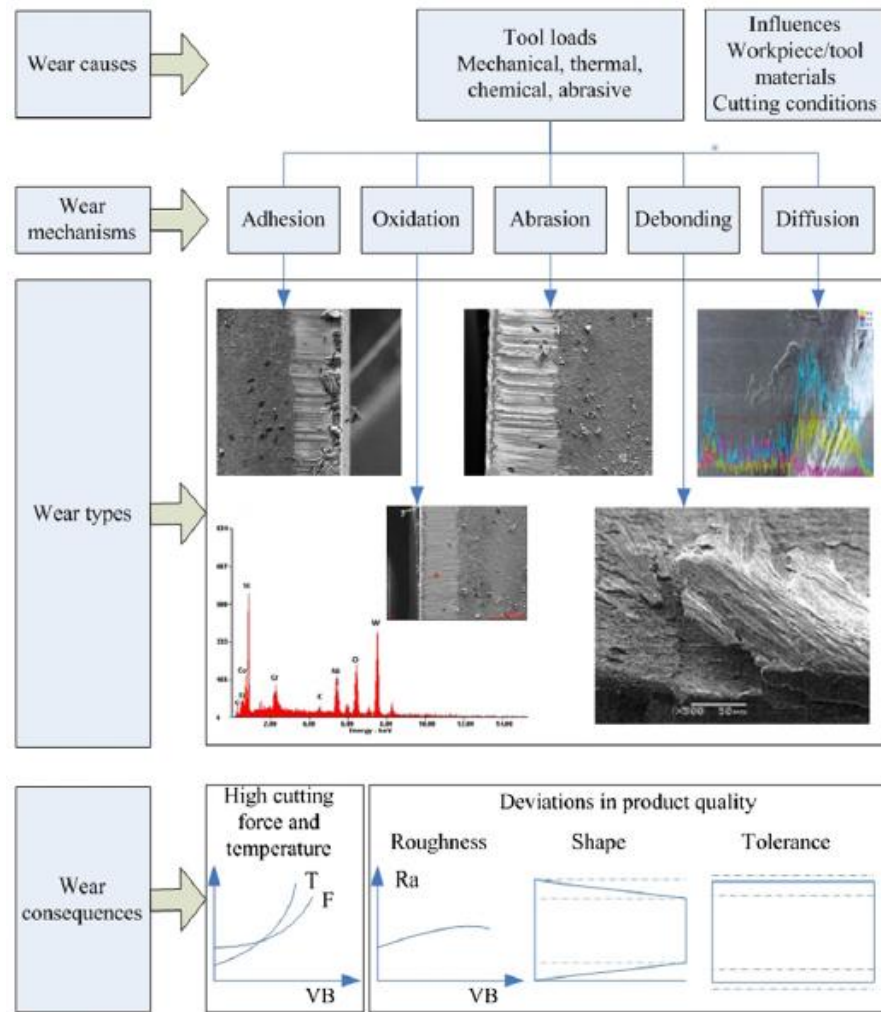


Figure 1-15 Mapping of speculative wear causes, types and consequences, given by Zhu et al. [12] (there is a serious uncertainty in Zhu et al.'s quoting in regard to the sources of the map)

Returning to the review of Zhu et al. [12], from the photo in Figure 1-15 under the BUE adhesion there appears a deposited (smeared) layer, with unknown influence on tool wear. To aid further discussion on adhesion “wear”, an illustration is given in Figure 1-16. Suggestion of adhesion wear can be interpreted as a process leading from what is illustrated in Figure 1-16b and Figure 1-16c. The primary problem of the adhesion wear theory is the requirement of a BUE bond strength to be higher than the strength of the tool material (Figure 1-16d), so that when the build-up layer (BUL) is removed, part of the tool will fracture off. However, there is no data available pertaining to this and there is no reasonable scientific base to suggest that workpiece-BUL and interface bonding strength is higher than the strength of the tool material. Thus, Zhu et al’s adhesion theory may not be unreasonable. However, the mechanism of heavy chipping illustrated in Figure 1-4c could lead to what is illustrated in Figure 1-16c.

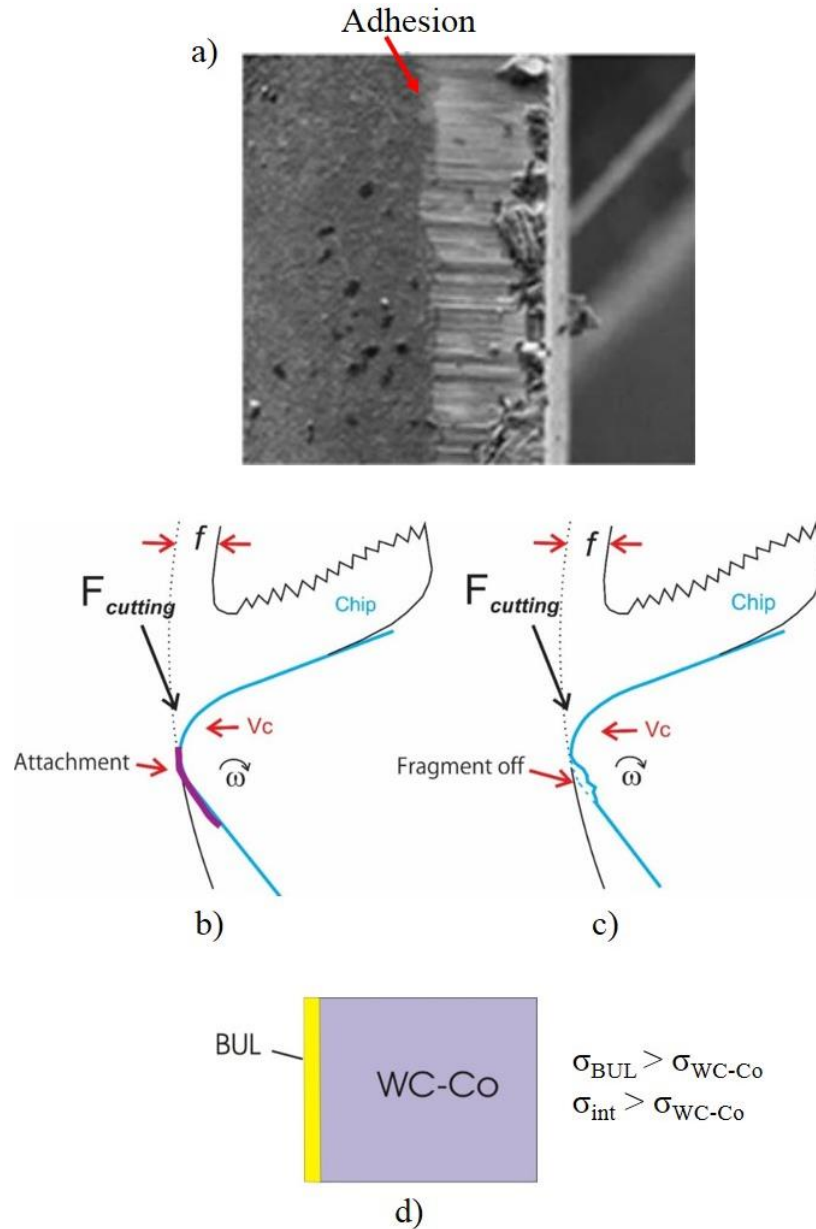


Figure 1-16 (a) Images of the adhesion mechanism during the adhesion of workpiece material to tool, Illustration indicated the adhesive mechanism based on suggested opinion by Zhu et al. [12], (b) after taking off the tool material and (c) illustration the bonding strength BUL ($\sigma_{BUL} > \sigma_{WC-Co}$) and interface between the WC-Co ($\sigma_{int} > \sigma_{WC-Co}$)

Equivalent to the concept of Zhu et al's. [12] BUE, Kasim et al. [11] claimed that this formation leads to further severe tool failure mechanisms such as pitting. However, they did not explain how this could occur as pitting is a corrosion process of a material taking time to grow and to damage the tool. The unsuitably used term of pitting wear is furthered discussed in section 1.4 on the other modes of tool deterioration. Conversely, Uzun et al. [9] concluded

that flank “wear” was through an abrasive “wear” mechanism, further suggesting a link of this abrasion to the corrosiveness of particles in the workpiece. This latter suggestion is incomprehensive, as abrasion is a mechanical action while corrosion is through chemical reaction/dissolution. A tool wear observer model for online tool condition monitoring and control in machining nickel based alloys was developed by Chen and Li [4]. TiAlN coated carbide cutting tools were used in the study, with flank wear and chipping observed as dominant failure of the tools. The reported abrasion mechanism has been suggested to be the cause of these tool failures even though they also found adhering layer on the cutting tool resulting from the adhesion mechanism. However, the adhering layer should not significantly weaken the tools.

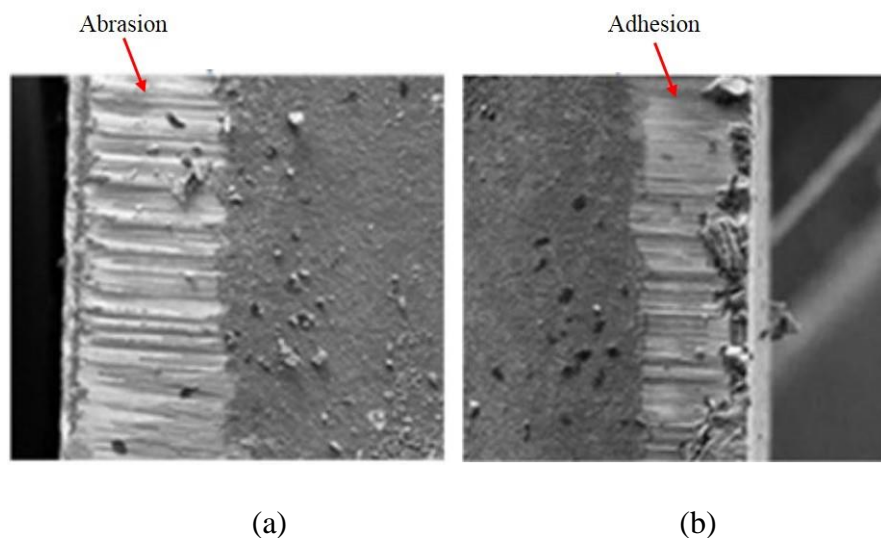


Figure 1-17 Example of tool failure due to (a) abrasive mechanism, and (b) adhesion mechanism [12]

Additionally, Li et al. [22] also indentified flank wear and chipping on multilayer (TiN//Al₂O₃/TiCN) coated carbide tools in end milling a nickel-based superalloy. They suggested that high temperatures generated when milling at high cutting speeds in dry conditions increased the tendency of the coatings to peel off by the abrasive mechanism. Zhu et al. [12] provided an image of a tool failure resulting from the abrasion mechanism as shown in Figure 1-17a. It is clear that the cutting tool experienced indentical features as given previously on adhesion wear (Figure 1-17b). Thus, there is no significant evidence for the suggested mechanism. It also should be noted that this similar appearance of cutting tools must have led to confusion in deterimining the exact mechanism of each cutting tool. Another example of insufficient understanding on “wear” mechanisms commonly related to flank wear is diffusion wear. Based on literature, high cutting temperatures generated during

machining Ni based superalloys are the most influential factor leading to diffusion wear, [4, 39]. Akhtar et al. [23] summarised that diffusion wear resulted from the application high cutting speeds which causes high temperature in the machining zone, thus promoting diffusion of the workpiece elements into the cutting tool. Similarly, Chen and Li [4] observed during milling at cutting speeds in excess of 30 m/min diffusion wear occurred detrimental to the TiAlN coated tungsten carbide tool.

In the early review paper by Ezugwu et al. [40,41] flank wear on carbide, ceramic and CBN cutting tools were associated to diffusion wear. A hypothesis proposed by Zhu et al. [12] is that cobalt (Co) in tools could be depleted due to diffusion causing diffusion wear. This hypothesis is based on a similar opinion expressed by Ezugwu et al. [24]. Ezugwu et al. [25] further elaborated suggesting that the carbide grains in the tools may dissolve and diffuse into the chips machined from the workpiece resulting in tool material loss. Furthermore, tungsten carbide may diffuse into the Co binder weakening the bonding between the binder and carbide grains causing tool material detachment. Dissolution limited by solid state diffusion is normally a slow process, and the duration of heating sequences during the machining operation is extremely short. The kinetics of diffusion were not considered and tool material transportation by diffusion lead tool material loss has not been proved. Thus, diffusion wear may not be simply viewed as an established mechanism that can explain how wear of the tool takes place during milling of nickel alloys.

The last two mechanisms which are reported rarely in literature are oxidation and debonding. Mechanism of oxidation are described where the coating has peels off exposing the tool substrate to air. Little, however, has been scientifically explained why exposing tool substrate to air should aid the mechanical action of tool deterioration. The final mechanisms that suggest tool wear is debonding failure and applies solely to coated cutting tools. Zhu et al. [12] noted debonding failure is very intricate as it consists of all the mechanisms discussed above of; adhesive, abrasive, diffusion and oxidation. Yet, the coating layer on the cutting tool is very thin and does not necessarily provide good protection to the cutting tool. Additionally, if the coating does peel off, it does not mean to cutting material loss as suggested in many publications.

Based on this critical review on the definition of flank wear and extensive discussion on adhesive, abrasive, diffusion, oxidation and debonding mechanisms, it can be concluded that the “theory” behind of each of the mechanisms is largely speculative. The discussion above has demonstrated that the speculative “wear” mechanisms attributing to flank wear promoting severe tool deterioration are not fully understood. In the following section a further literature review on the other modes of tool deterioration in milling nickel based superalloys are presented.

1.6 The Other Modes of Tool Deterioration

In this section, an extended review on the other modes of deterioration when milling nickel-based superalloys is discussed. Many researches [6, 7, 15, 18-20, 38] over the last ten years have demonstrated that the tool chipping is the dominant of tool failure mechanism machining nickel superalloys. Here, a review of several examples from publications representing these studies in regards to failure modes during end milling is given. The first example of which is from a study conducted by Kadirgama et al. [5], where a tool was used to mill a workpiece in a pass of 180mm. Notch wear occurred in the cutting corner of the tool as labelled in Figure 1-18. Although not defined by Kadirgama et al. [5] in their research, notch wear is commonly referred to as wear resulting from a local piece of tool fragmenting off the cutting edge [6, 15, 18, 38]. Looking further in these publications, it seems researchers mean the size of fragmentation in notch wear is normally significantly larger than the width of cutting edge. Thus, a notch results from either many small edge chips in the same location or a small number of heavy chips detached from the tool edge. Note chips here refer to tool material loss due to chipping of tool, not chips of workpiece from milling.

A further point needs to be made for Figure 1-18a, despite of notch wear being stated by the authors, upon review there is no evidence of a notch in the cutting edge/corner. Rather, an attachment locally can be observed which can be explained in Figure 1-18c. In their milling tool that was used for further milling, however, one notch was evident in the side flank face and another in the bottom flank face, as in Figure 1-18b. These are referred by the authors as chipping and catastrophic failure respectively. It is clear in the publication that because the form of wear was not clarified in the initial stages of machining, the individual deterioration processes and their combinations leading to the formation of notching was not identified.

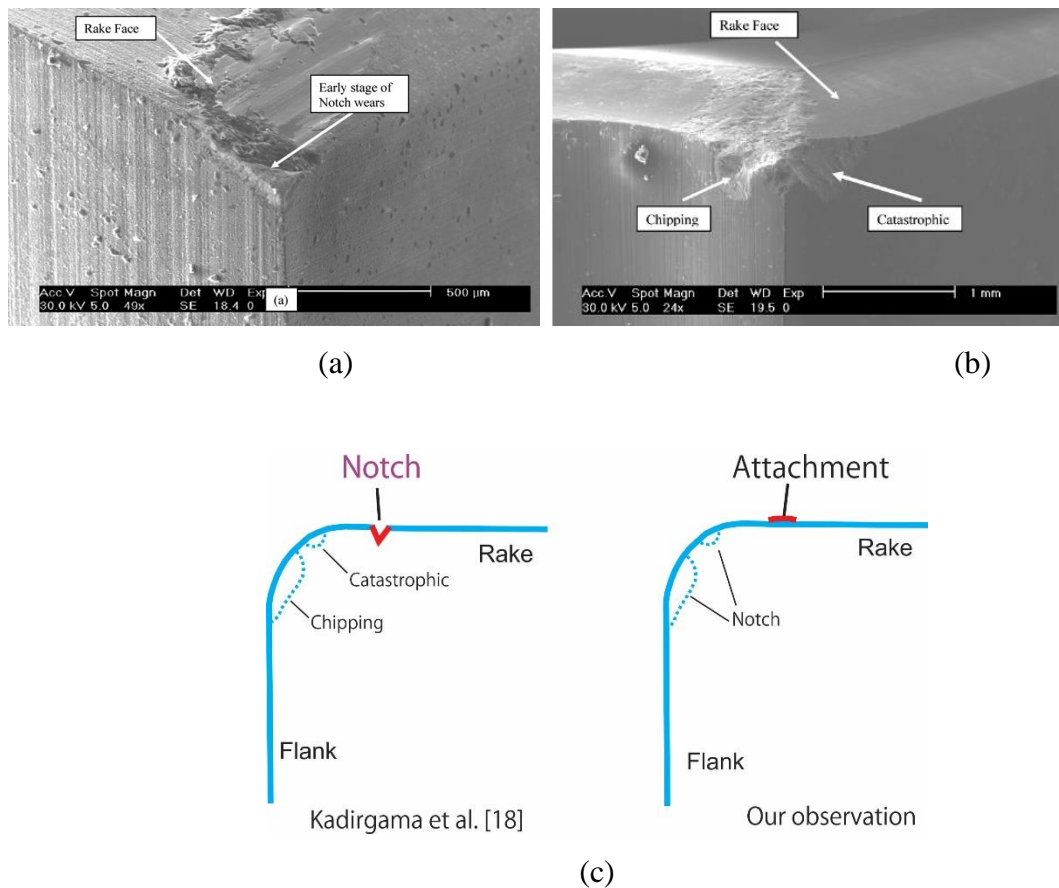


Figure 1-18 SEM images of the cutting corner location (top: rake face, left: side flank face and right: bottom flank face) of tools after end milling cutting ($v_c = 100$ m/min, $f = 0.15$ mm/rev and $DoC = 1.0$ mm) by Kadirgama et al.[5], (a) PVD TiAlN coated WC-Co tool after 180 mm milling (b) CVD TiN/TiCN/Al₂O₃ coated WC-Co tool after 742 mm milling and (c) Illustration to aid the attachment and notch (s) location

The second example is taken from a study carried out by Kasim et al. [11], whose experiments were based on using ball-end mill tool inserts. As illustrated in Figure 1-19a, edge chipping or pitting as it is referred to by the authors clearly occurs in the initial stage of cutting. From this paper, it is clear that authors did not relate “pitting” to a particular form of tool deterioration rather than to mean it as a form of edge chipping as we have defined. In the image, points of “abrasion” and “attrition” have been labelled by the authors although the evidence of such wear was not demonstrated. The unreasonable labeling of “abrasion” in Figure 1-19a, will be clarified in the discussion of our preliminary in Chapter 4. For a longer milled distance tool insert, as shown in Figure 1-19b, severe notching occurred, for which we labelled and outlined the notch in the Figure 1-19c. The authors did not note the notch nor examine the notching process because of this, any link between the build-up edge (BUE) and flaking relation to notching was unclear.

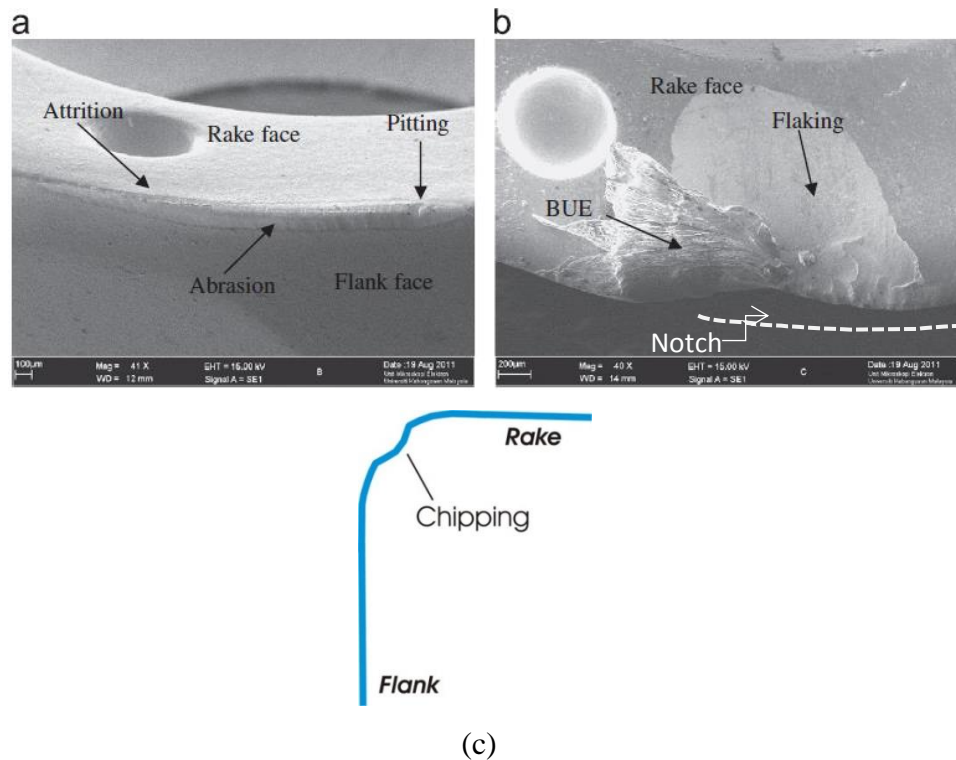


Figure 1-19 SEM images of tool inserts: (a) an insert in an initial stage with rake face and flank face as indicated and clearly without a notch, (b) a down view on the rake face after notching (we have observed, outlined/labelled in white although authors have not) during ball-nose end milling by Kasim et al. [11]. Tool inserts were TiAlN/AlCrN coated (cutting conditions were not specified by authors) and (c) Illustration from Figure 1-19a, chipping at flank face (we identified)

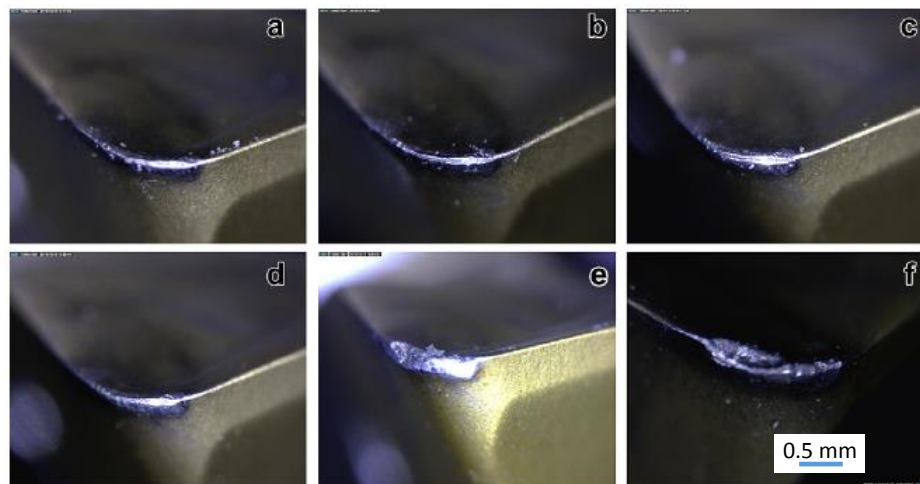


Figure 1-20 Photos of a coated tool insert after: (a) 22.1 min, (b) 24.1 min, (c) 27.5 min, (d) 29.5, (e) 35.5 min and (f) 42.9 min under cutting condition of ($v_c = 50$ m/min, $f = 0.1$ mm/rev and axial depth of cut = 0.5, $a_e = 1.0$ mm) via dry condition. Top: rake face, left: bottom flank face and right: side flank face, scale on the photo is our approximation based on value of axial depth of cut [8]

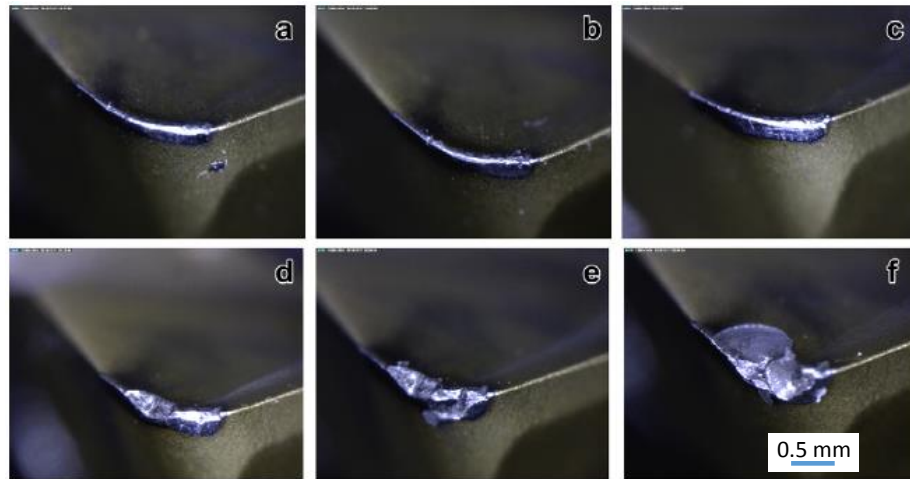


Figure 1-21 Photos of a coated tool insert after: (a) 20.8 min, (b) 28.8 min, (c) 44.9 min, (d) 57.0 min, 64.3 min and (f) 72.4 min under cutting condition of ($v_c = 50$ m/min, $f = 0.1$ mm/rev and axial depth of cut = 0.5, $a_e = 1.0$ mm) via MQL. Top: rake face, left: bottom flank face and right: side flank face, scale on the photo is our approximation based on value of axial depth of cut [8]

The third example is from Zhang et al. [8]. Images of their tools are shown in Figure 1-20 and Figure 1-21 after of milling Inconel 718 under dry and minimum quantity lubrication (MQL) cutting conditions, respectively. The tool insert examination was done visually by camera imagery. It is clear from these images that deterioration had only progressed in the cutting corner location where the tool contacted and cut the workpiece. Visually, the tool shown in Figure 1-20 deteriorated at a more gradual rate up to 30 minutes of cutting, followed by a faster deterioration as notching formed beyond the original cutting edge. From our approximation based on the value of axial depth of cut, the notch size is around 0.2mm.

In Figure 1-21, rapid deterioration started after 45 minutes of cutting, suggesting the possibility of an extended tool life when lubricated conditions. However, examination only visually (aided by photos) cannot reveal tool features below 0.5 mm (our approximation based on the value of axial depth of cut). These features need to be revealed in detail for the understanding of wear and fracturing behaviors as a 0.5 mm notch exceeds $VB \sim 0.3$ mm. Figure 1-22 is our own example of a scanning electron microscope (SEM) micrograph of side flank face based on the preliminary experiments demonstrating the tool fracturing is assessed using a sufficient scale of magnification. This low SEM magnification image is three times the magnification and at a much resolution than the optical photographs presented by Zhang et al. [8] in Figure 1-20 and Figure 1-21.

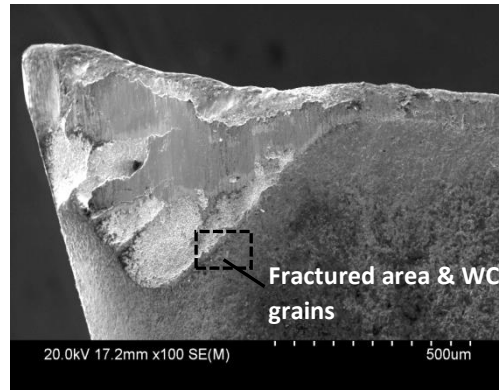


Figure 1-22 Scanning electron microscope (SEM) micrograph showing tool fracturing

From the review of the previous publications discussed above, notching as a form of tool material in the cutting edge fragmenting off has been well recognized although other terms have been used. However, fracturing processes and chipping leading to the final notches in the tools have not been explained in detail. Notch formation relating to cutting forces, as suggested in Figure 1-5, during milling has not been extensively discussed in the literature. In a more direct way, the modes of local failure forming a notch has never been discussed and understood. As can be observed in the referred literature, most notches formed without a noticeable amount of deformation, suggesting a brittle mechanism of fracture.

1.7 Model Relating Tool Deterioration to Milling Time or Distance

There have been attempts to empirically relate VB or V_{wear} (volume of wear) to milling distance. A function determining material loss on a cutting tool due to adhesive wear within a time interval is developed by Huang and Liang [26] and derived as:

$$V_{wear-adhesion} = K_{adhesion} e^{aT} V_c w \bar{\sigma} \Delta t \quad \text{Equation 1-6}$$

Where $K_{adhesion} = \frac{p_0 k_0 (1 - p_{abrasion} \%)}{b}$ is the coefficient of adhesive wear in m^3/N and is assumed constant for tool and workpiece. a refers to hardness constant, T is temperature, V_c is the velocity at the flank face with wear length VB slides laterally the workpiece, w refers to width of cut, $\bar{\sigma}$ is the normal average stress and Δt is the time interval. In the $K_{adhesion}$ equation P_0 refers to the probability of forming substantial wear on the tool, K_0 is a constant, σ is clearance angle and b is a hardness constant. They further developed another

mathematical function of tool wear for abrasive and diffusion wear as presented in Equation 1-8.

$$V_{wear-abrasion} = k_{abrasion} K \left(\frac{P_a^{n-1}}{P_t^n} \right) V_c w V B \bar{\sigma} \Delta t \quad \text{Equation 1-7}$$

Where tool volume loss from abrasion within a time interval is calculated from the following inputs; P_a represents the hardness of the abrasive particle, P_t represents tool hardness, n and K are a known function of P_t/P_a or T and defined as:

$$\begin{cases} n = 1.0, K = 0.333, & \text{for } T < 0.8 \\ n = 3.5, K = 0.189, & \text{for } 1.25 > T > 0.8 \\ n = 7.0, K = 0.416, & \text{otherwise} \end{cases}$$

$K_{abrasion} = P_{abrasion} \% \tan \frac{\theta}{2}$ is a constant referring to the dimensionless abrasive wear. In diffusion wear, the total material loss can be determined by;

$$V_{wear-diffusion} = K_{diffusion} \sqrt{V_c V B e}^{-(K_Q/T+273)} w \Delta t \quad \text{Equation 1-8}$$

In this case, $K_{diffusion}$ is assumed constant for the same tool-workpiece combination and K_Q is constant for activation energy.

In addition, Archard determined the tool volume loss attributed from oxidation wear by;

$$V_{wear-oxidation} = K_{oxidation} \frac{W}{3\sigma T} V_c \Delta t \quad \text{Equation 1-9}$$

Where $K_{oxidation}$ is chemical wear coefficient, W is the applied load, \bar{T} is average temperature.

Derived mathematical equations in the review above, provide an idealistic approximation in determining the volume tool loss and give insight into tool wear control during machining. Irrespective of the equations presented, the physical evidence explaining the formation and progression of tool wear is not well demonstrated as the mathematical algorithm is only a numerical representation without revealing how the tool deterioration process occurs.

1.8 Effect of Cooling on Tool Deterioration

The difficulty of machining nickel based superalloys leads to high cutting temperatures and rapid tool wear [27], resulting in the tendency of chips to weld on the cutting tool forming a build-up edge noted by Liao et al. [3]. In general, the function of cutting fluid/coolant is to reduce the cutting temperature (cooling effect) and reduce the cutting forces by lubrication enhancing tool life, [28]. Obikawa et al. [29] claimed that the application of minimum quantity lubrication (MQL) in machining Inconel 718 could prolong tool life, enhance the surface quality of the machined workpiece, and improve in dimensional accuracy. An example of which is presented in Figure 1-23, where it can be observed that a wet condition has resulted in the longest tool life ~ 47.8 min, while a MQL condition with pressure of 15 ml/h resulted in a life 3.8 min shorter than wet cutting.

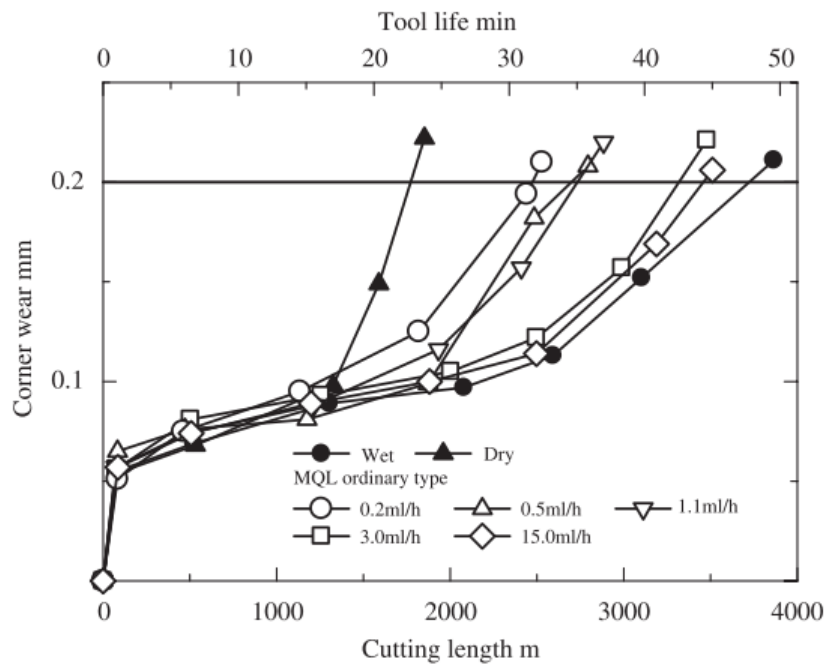


Figure 1-23 Change in corner wear with cutting length for MQL machining with the ordinary nozzle. Cutting conditions: cutting speed, 1.3 m/s (78 m/min); depth of cut, 0.11 mm; feed rate, 0.1 mm/rev [29]

A study investigating high speed MQL finish-turning of Inconel 718 using cemented carbide tools with various coating layer types was presented by Kamata and Obikawa et al. [30]. In their study, an MQL environment at various pressures was found to improve the life of the tool in comparison to dry turning as shown in Figure 1-24. This shows that the use of MQL could be a good alternative to wet and dry cutting in order to decrease cutting fluid consumption and improve environmental conservation.

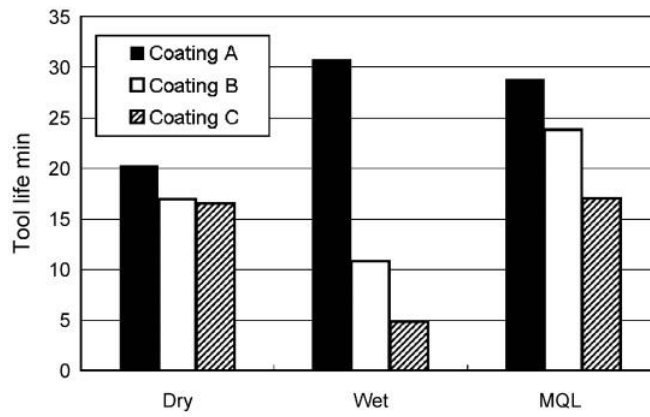


Figure 1-24 Tool lives of three coated tools in MQL, wet and dry cutting, Cutting conditions: cutting speed, 1.0 m/s; feed rate, 0.1 mm/rev; depth of cut, 0.1mm; air pressure of MQL, 0.40MPa; Oil consumption of MQL, 16.8 ml/h [30]

Cryogenic cooling experiments investigating the influence of on the surface integrity in the turning Inconel 718 and were compared to dry and MQL environments by Pusavec et al. [31]. They note that the application of cooling (cryogenic and MQL) in machining can retain the temperature below thermal softening, improving the cutting tool life drastically in comparison to dry machining conditions. The MQL cutting condition was observed to increase tool life by a factor of 1.57 compared to dry milling in the work by Zhang et al. [8] in end milling Inconel 718, as seen in Figure 1-25.

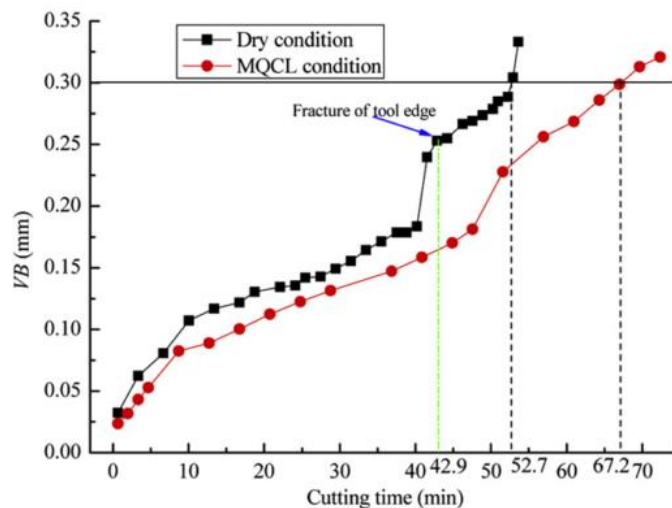


Figure 1-25 Tool wear VB with cutting time under different cutting conditions [8]

Moreover, Fernandez et al. [32] concluded that cryogenic cutting prolonged the life of PVD coated carbide tools in comparison to dry cutting conditions when machining Inconel 718. This is clarified in Figure 1-26 where it is shown that the rate of wear in cryogenic cutting was the lowest with progressive wear deterioration compared to the other cutting conditions.

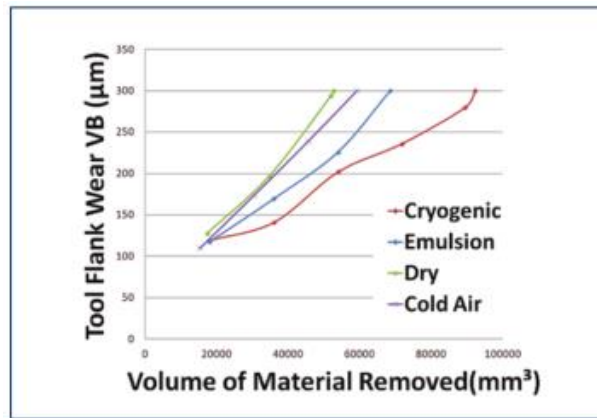


Figure 1-26 Evolution of tool life in dry, oil based emulsion, cold air and cryogenic turning of Inconel 718 [48]

Aramchareon and Chuan [33] investigated the effect of cryogenic cooling on milling of Inconel 718 using WC-Co tools, reporting that cryogenic cooling in milling resulted in a reduction in cutting temperatures and cutting forces, enhancing the cooling effect close to the cutting edge of the tool, thus improving the life of cutting tool. Similar findings were presented by Kaynak et al. [34] in the cryogenic cooling and tool wear progression of turning NiTi alloys. Tool wear reduced, prolonging tool life evident from Figure 1-27. From the graph presented, tool deterioration progression under cryogenic conditions was gradual from the beginning and remained slow after 50 m/min while other conditions experienced an extremely high rate of tool wear. Thus, cryogenic cooling is a proven method to enhance the machinability of Ni based alloys as it increases the tool life significantly. Unexpectedly from this experiment the role of MQL in increasing tool life was not evident.

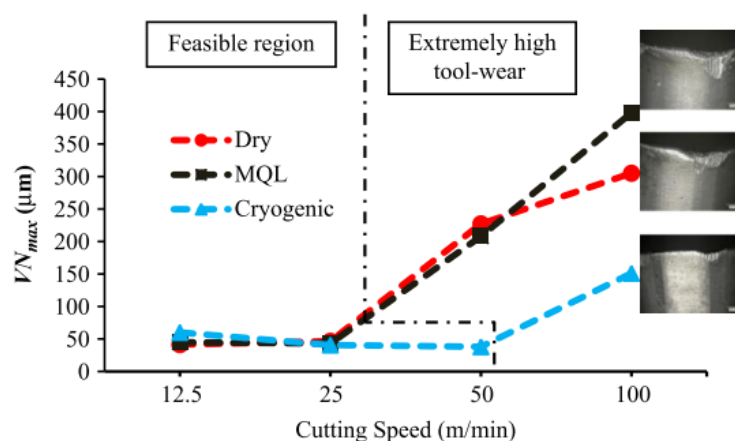


Figure 1-27 Notch wear progression under different cooling conditions [34]

Although data from a number of studies as cited above may have suggested that using coolant may prolong tool life, they all base on using VB . As has been discussed, VB does not represent

the amount of tool material loss. Furthermore, the use of coolant may affect BUE. As explained, BUE does not need to be part of tool wear/deterioration. In all these studies cited, again detailed examination of deterioration has not been conducted.

1.9 Effect of Tool Coating on Tool Deterioration

Alternatively, it is viewed that increased tool life in machining nickel based superalloys can be obtained by the application of a coating on the tool. As recounted by Ghani et al. [35] coating layers enhance the lubricity of the tool, increasing the mechanical and chemical resistance as well as reducing cutting temperature. In micro milling of Inconel 718, Ucut et al. [9] believed that tool coatings generate a barrier reducing the tendency of build-up on the tool and decreased the friction at the tool-workpiece interface. It is reported by Jawaid et al. [17] in Figure 1-28 that the performance of uncoated carbide tools exceeds that of a PVD-TiN-coated tool at low cutting speeds (25 m/min). However, with the increase of cutting speed to 50 m/min, the coated PVD-TiN was superior to the uncoated due to the high wear resistance and low conductivity of the TiN coating layer.

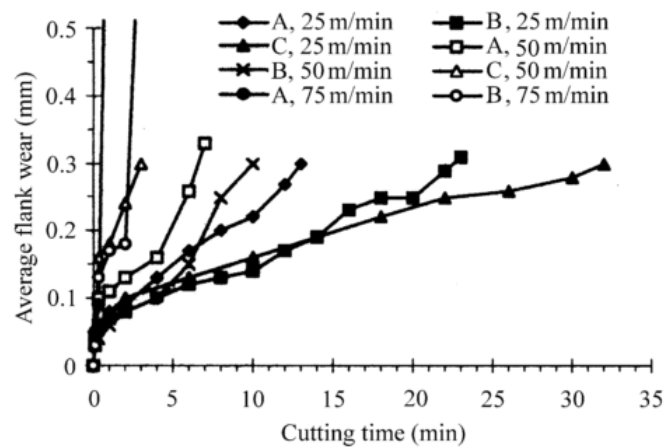


Figure 1-28 Development of average flank wear when face milling Inconel 718 and feed rate of 0.08 mm per tooth [17]

Analysis of variance (ANOVA) results on the tool life of a high speed ball nose end milling Inconel 718 presented by Sharman et al. [36], showed the tool coating to be the dominant factor affecting tool life with 45.3% percentage contribution ratio (PCR). Additionally, in Figure 1-29, it is evident that the use of TiAlN coating demonstrated a longer tool life compared to the CrN coating resulting from its high hardness and oxidation resistance and the longest tool life obtained from TiAlN coated tools occurred at 90 m/min. At 90 m/min,

debonding of the coating and BUE was observed on CrN coated tools as a result of CrN's high chemical affinity for Inconel 718 in comparison to TiAlN.

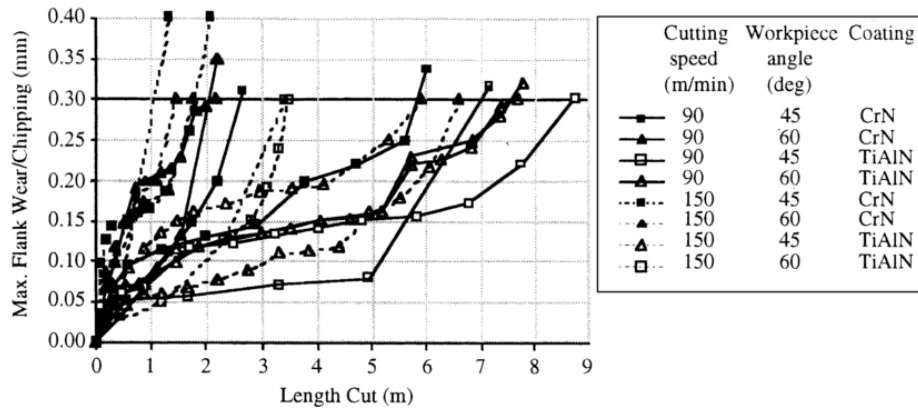


Figure 1-29 Tool wear plot in terms of length cut [36]

Multilayer PVD coatings were tested by Prengel et al. [37] in the machining of Inconel 718. As seen from the result shown in Figure 1-30, TiAlN-multilayer coatings have performed better than TiAlN-monolayer especially at elevated cutting speeds of 61 and 76 m/min. This was attributed from their hardness of coatings according to authors however, the hardest coatings of TiN/TiCB/TiAlN-multilayer experienced the shortest tool life because of the premature coating peeling off from high compressive residual stress. The PVD TiAlN coated carbide tools were also recommended by Dudzinski et al. [28] for turning Inconel 718 at an elevated maximum cutting speed of 100 m/min.

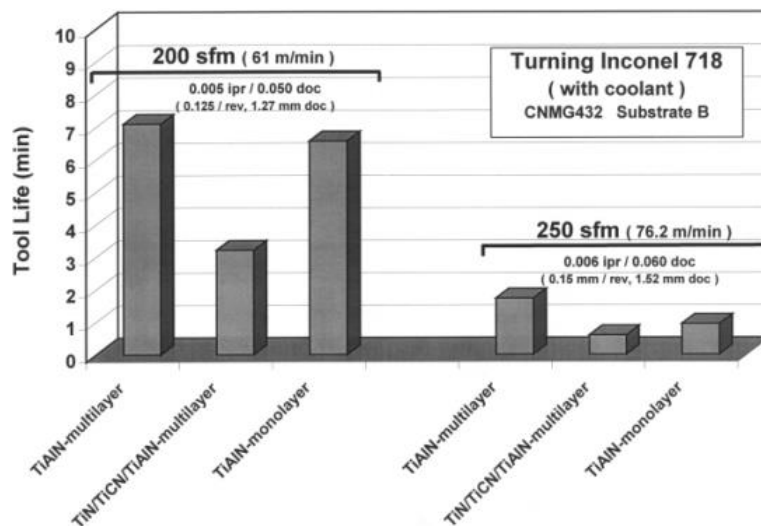


Figure 1-30 Performance of TiAlN-multilayer variants in turning Inconel 718 [37]

Li et al. [38] evaluated the tool life of coated carbide tools and ceramic inserts in high speed turning of annealed Inconel 718. Micro-breakout, chipping, abrasive and adhesion wear were

identified as the wear mechanisms in machining the nickel-based alloy. However, as has already been explain, wear modes in literatures are quite speculative. Ceramic tools were recommended for a longer tool life in the machining of Ni based alloys, however coated carbide tools are more financially economical.

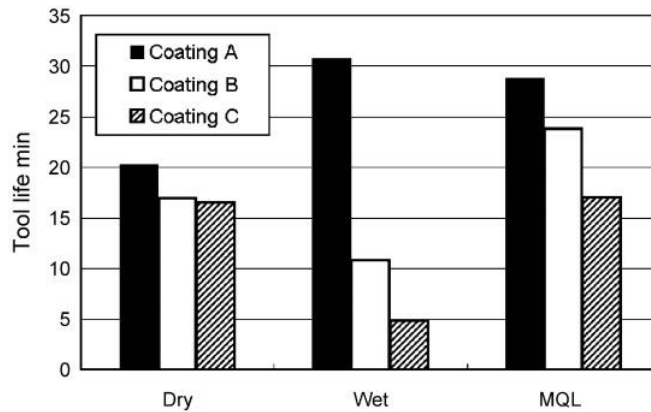


Figure 1-31 Tool lives of three coated tools in MQL, wet and dry cutting, Cutting conditions: cutting speed, 1.0 m/s; feed rate, 0.1 mm/rev; depth of cut, 0.1mm; air pressure of MQL, 0.40MPa; Oil consumption of MQL, 16.8 ml/h [30]

In addition, coatings of fine thickness are implemented to increase the tool life as noted by Ducros et al. [39]. They claimed that the high corrosion durability and resistance to prevent the adhering chip on the cutting tool was evident for TiN/AlTiN and CrN/TiN nano-layer tools compared to the uncoated tool. The meaning by corrosion is however not clear. Moreover, Kamata and Obikawa et al. [46] conducted experiments in high speed finish-turning of Inconel 718 with different coated tools in MQL, dry and wet environments. Three different coatings were used; TiCN/Al₂O₃/TiN (CVD) referred as tool A, TiN/AlN superlattice (PVD) referred as tool B and TiAlN (PVD) referred as tool C. The tool life of multi-coated TiCN/Al₂O₃/TiN layers was observed to be longer than other coating layers in MQL condition as observed in Figure 1-31. Note, the limitation of assessment for tool life and the influence of BUL need to be clarified, before the effect of coating on tool life can be understood better.

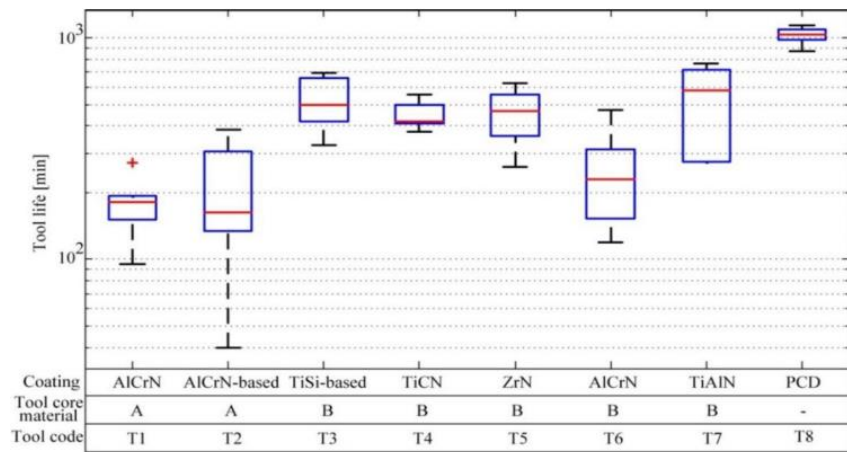


Figure 1-32 Box plots, whisker and outliers of tool life with different cutting tool coatings [40]

Recently Sortino et al. [40] performed a study on innovative tool coatings for increasing tool life in milling nickel-coated nickel silver using both cemented carbide and PCD tools. The PCD tool was found to have a superior tool life, twice that of the cemented carbide as shown in Figure 1-32. They also found that the application of tool coatings prolonged the tool life. Based on the review above, the application of tool coating may prolong in tool life when machining nickel-based superalloys, however the significance of applying this fine coating layer especially when machining very difficult-to-cut material is not well demonstrated and needs to be understood.

1.10 Effect of Workpiece Hardened State on Tool Deterioration

An effort has been made to search the literature on research to investigate the influence of increasing strength of workpiece on tool deterioration for machining Ni alloys, little has been found. The resultant force (F_R) acting at the tool during machining is represented in Figure 1-33. As visible in Figure 1-33b, the F_R for a hardened workpiece may exceed that of the annealed state (Figure 1-33a), as an increase in workpiece strength requires higher cutting forces to shear the workpiece, potentially resulting in severe tool deterioration. Due to the lack of knowledge, this study aims to investigate the effect of increase in workpiece hardness/strength on tool deterioration.

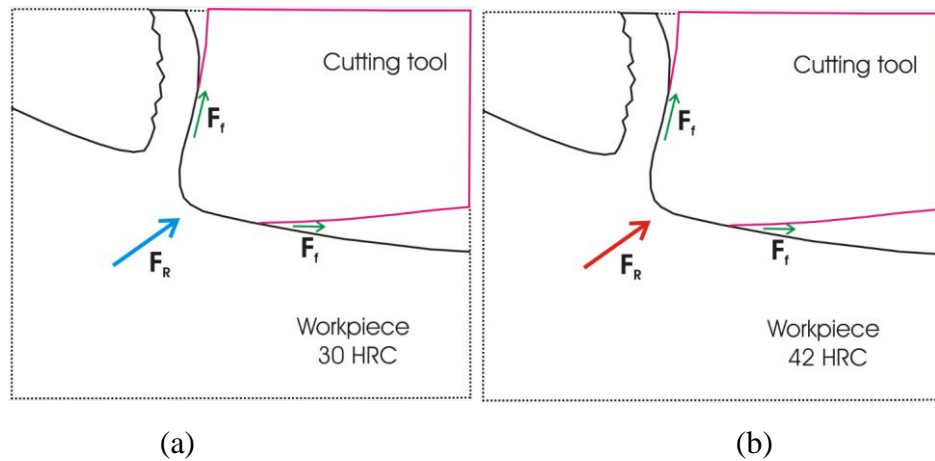


Figure 1-33 Illustration of resulted force (F_R) and friction force (F_f) as the interaction between workpiece and cutting tool for (a) annealed state and (b) hardened state workpiece of Ni-based alloy

1.11 Effect of Tool Deterioration on Cutting Force

In this section a detailed review on the relationship between tool deterioration and cutting force in the milling of nickel-based superalloys is discussed. This relationship is crucial for improving the machinability of the alloys and clarifies how a cutting force based method for monitoring tool deterioration works as there is great research interest in this area. A trend of increasing values of F_x , F_y and of VB as N_{pass} increased are presented in Figure 1-34 by Zhang et al. [8] from their experiments on tool life and cutting forces in end milling Inconel 718 under dry and minimum quantity cooling lubrication cutting conditions. They observed a linear relationship between cutting force variation components and the flank wear width as number pass increased.

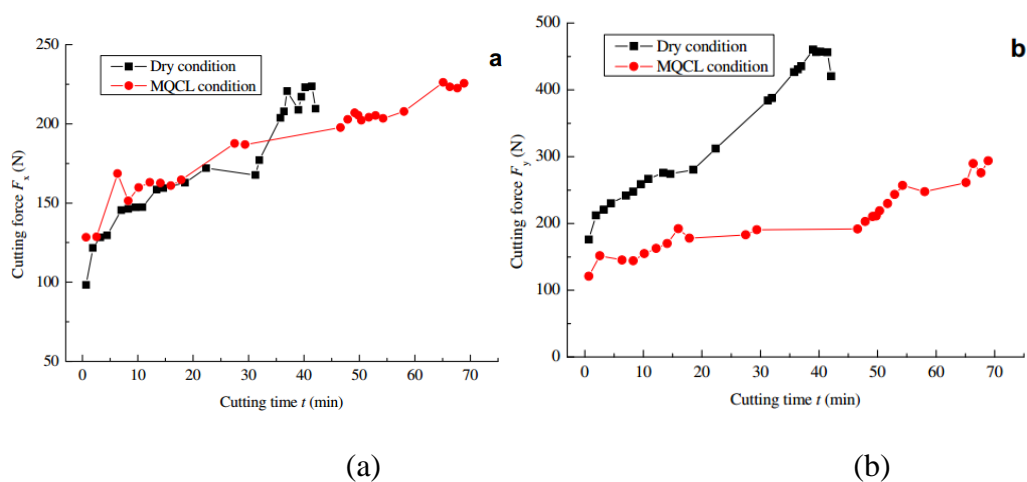


Figure 1-34 Cutting force (N) versus cutting time (min), (a) F_x and (b) F_y [8]

In the study by Kasim et al. [11] on milling Inconel 718 alloy, the measured value of notch occurred at the maximum value of VB (VB_{max}). In Figure 1-35a brief very sharp increase in VB_{max} after cutting time of just over 4 minutes, followed closely by a very sharp increase in F , although the milling condition has not been explained. However, this finding is contradicted by the curve in Figure 1-36. VB and VB_{max} are seen to increase sharply after ~ 43 minutes of milling, with the milling condition stated in the published paper.

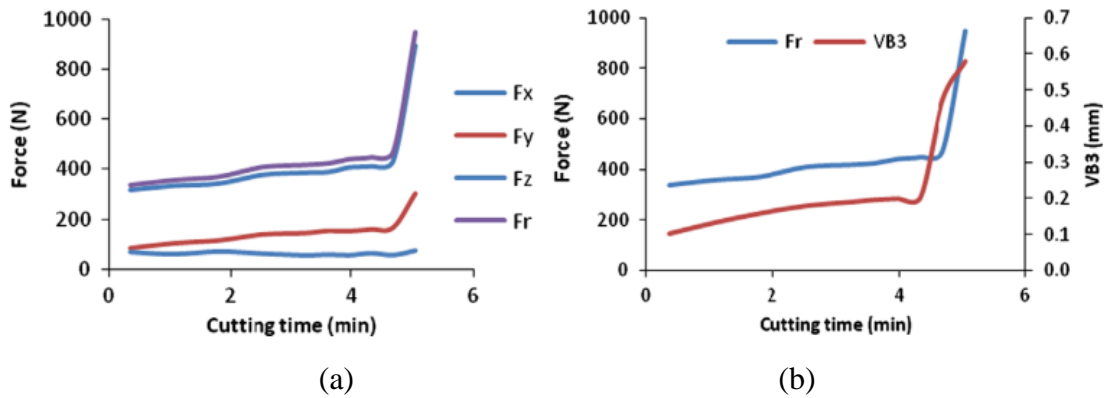


Figure 1-35 Effect of tool wear on cutting force [11]

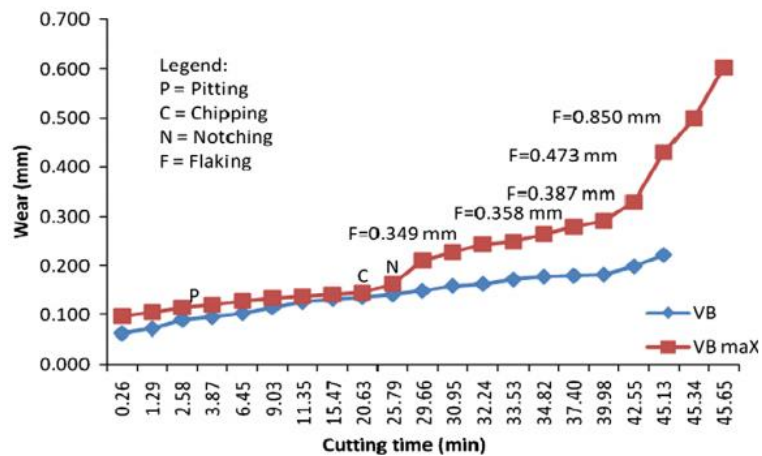


Figure 1-36 Measured flank wear progression with other observed wear modes during the end milling of Inconel 718. $V_c=140$ m/min, $FR=0.15$ mm/tooth, $DoC=0.75$ mm, $a_e=0.2$ mm [11]

Furthermore, Aramcharoen and Chuan [33] investigated the effect of cryogenic cooling on milling of Inconel 718 using WC-Co (note they named it tungsten carbide) tools. Tool wear and F were the major aspects of study and they claimed that the use of cryogenic cooling resulted in improved tool life but did not result in a reduction in F as clearly shown in Figure 1-37. From this graph, this is no information proving a decrease in cutting force, hence increasing the tool life regardless of machining condition.

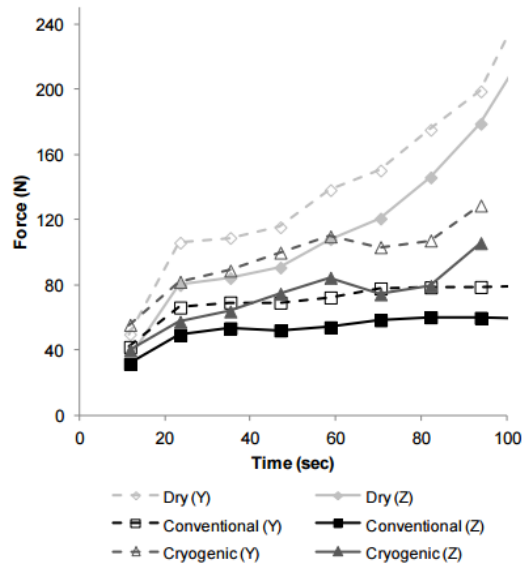


Figure 1-37 Cutting force of different machining conditions, Aramcharoen and Chuan [33]

Kong et al. [41] studied the effect of heating the workpiece on machinability and showed that laser heating during milling of a Ni-based alloy significantly reduced VB and F values. However, despite of the well-recognised importance of F and the progression of tool deterioration as part of the assessment of machinability, correlating the two was not addressed in these two studies presented in Figure 1-38 investigating the effect of the thermal condition on machinability during milling.

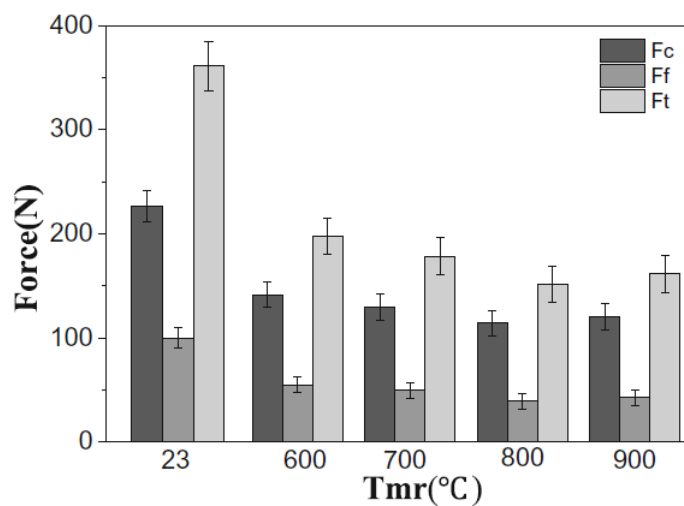


Figure 1-38 Evolution of the three components and the magnitude of the cutting force (N) as a function of Tmr (°C). $V_c=30$ m/min, $FR=0.10$ mm/tooth, and $DoC=0.2$ mm, Kong et al. [41]

There has been an effort to develop methods of monitoring tool wear of WC-Co tools, based on F measurement during milling of Ni-based superalloys. Li et al. [22] experimentally

determined a regression model relating F to VB during milling of Inconel 718. However, as has been explained, VB only indirectly indicates wear even when VB is accurately measured. Similarly, empirical relationship relating VB to F_x , F_y , F_z , and torque was made using neural networks by Kaya et al. [42]. More recently, a method to track a force model coefficient (K) used as a wear parameter to monitor VB of WC-Co tools was developed by Nouri et al. [43]. It is shown that the beginning increase in K value could be related to the transition of gradual wear to chipping and/or accelerated wear, although the authors also concluded that the wear mechanisms need to be verified. It should be pointed out, as has been detailed previously in section 1.3 VB_{max} is a measure to indicate the affected width of flank face. This width is not required to be the width of tool-workpiece contact area during milling along the flank face. For tool monitoring purposes, there is a need to develop a reliable model to predict how F relates to the state of tool (deterioration), as explained by Chinchankar and Choudhury [44]. Similarly, in Lauro et al.'s [45] comprehensive review on monitoring machining processes, a major method of monitoring is by analysing F results in order to improve tool life. With consideration of Ni-based superalloys, it is also clear from the review above the understanding on how F responds to the various modes of tool deterioration along the life of the tool is insufficient.

1.12 The Scope of This Study

Based on the literature review above, the deterioration modes of the commonly used WC-Co cutting tools during milling of Ni superalloys have not been well understood, and the notching process has not been studied in detail. Further, literature has not covered the basic deterioration forms and tool deterioration mode combinations. Similar basic processes contributing to the formation of the final notches and other forms of tool material loss have also not been adequately considered. The speculative wear mechanisms suggested by various researchers do not relate to the major forms of deterioration which are chipping/fracturing and thus notching. Therefore, the suggested mechanisms may not be physically reasonable. Moreover, the proposed assessment method for the tool deterioration which is a 3D (volume) in nature is currently conducted in the literature only providing a numerical value of the 2D (area) side view. This latter measuring method does not provide correct information to understand the tool deterioration and even the 2D measurement has not been properly conducted. Besides that, as recently reviewed, the understanding on how total force (F) provides information on the state of cutting tool is still vague and needs to be improved. The progression of tool deterioration, from the general wear and edge chipping to breakage

response to the variation of F has not been not critically discussed. Therefore, the understanding on how F is effected by the modes of tool deterioration needs to be developed, with the knowledge from this study providing an insight for improving tool deterioration monitoring methods. Furthermore, knowledge of the modes of tool material failure and tool's response using various cutting parameters and coatings are insufficient and rarely analysed in literature. As explained in section 1.9, there is no publication discussing the influence of a hardened workpiece on the modes of tool deterioration in Ni alloys. With no prior reference, the importance of investigating how an increase in hardness affects the modes of deterioration of 718Plus Ni-based superalloy is required. Thus, this Ph.D study intends to answer the following questions:

1. In a typical milling condition, what are the predominant tool deterioration modes and how individually each and in combination progress (es) as milling pass increases?
2. How does PVD coating of tools affect the tool deterioration modes and progress of tool deterioration?
3. Is deterioration rate affected by using coolant?
4. How does cutting force response to the various modes and progress of tool deterioration?
5. How does increasing feed rate affect tool deterioration and cutting force?
6. How does strength increase in workpiece by heat treatment affect cutting force and tool deterioration?

In the next chapter, experimental procedures and details of analytical facilities are described and explained. In chapters 3 to 5, detailed results of experiments and analysis are presented and discussed. Questions 1-3 above will be answered in Chapter 3 (objective 1) questions 4 and 5 will be answered in Chapter 4 (objective 2) and question 6 will be answered in Chapter 5 (objective 3).

Chapter 2: Experimental Design and Procedures

The three objectives of this research were stated and explained in the previous chapter. In the first objective, a series of end milling experiments were conducted and a detailed examination of the cutting edge deterioration process was described. This series of experiment started with the use of uncoated tools and milling in dry conditions and later included the use of coated cutting tools and the use of coolant. It was established from the early stage that the edge was severely damaged. For the second objective, an extensive series of milling experiments including both monitoring the progress of tool deterioration and cutting force was conducted. This series of experiments also included the use of an increase in feed rate. Finally, for the third objective, milling experiments examining the effect of hardened workpiece on tool deterioration where the workpiece was heat treated to a higher strength state than as-received material. Details of the experimental, measuring and analytical procedures are described below in this chapter.

2.1 Milling Machine and Clamping system

All experiments were conducted using a Pacific FU.125 down-milling machine as shown in Figure 2-1. During a down milling experiment, the workpiece was positioned firmly on a Kistler™ dynamometer as shown in Figure 2-2a.

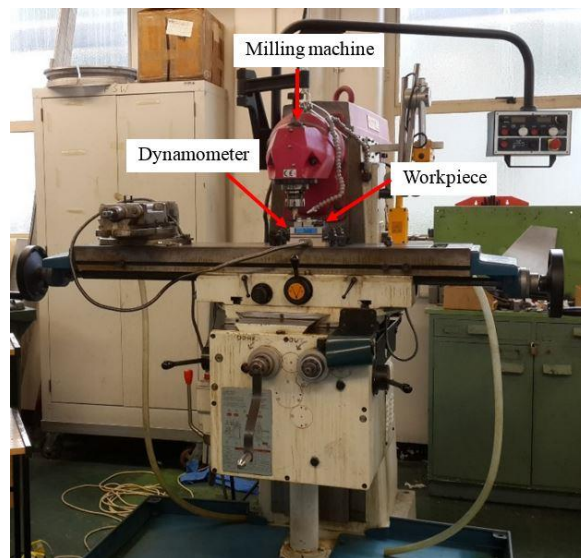
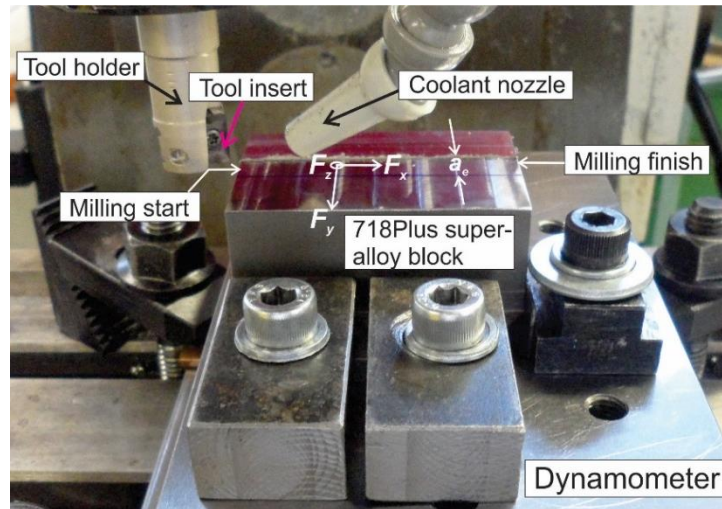
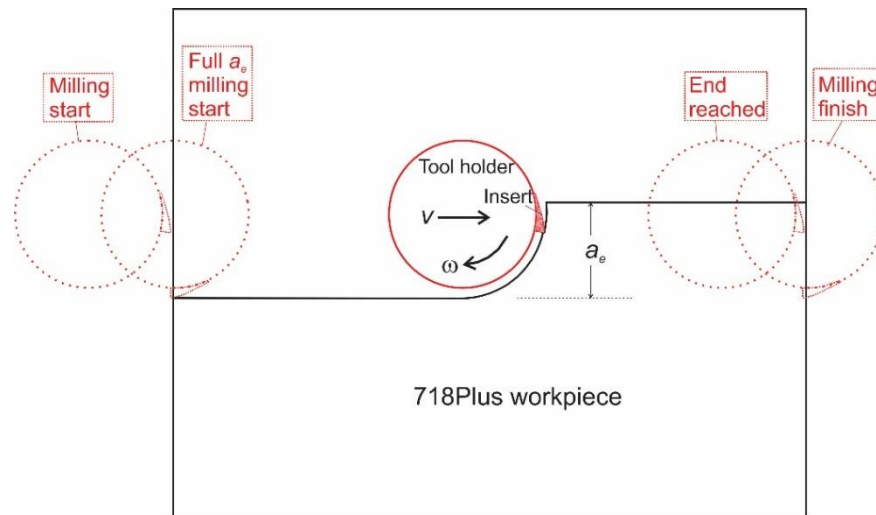


Figure 2-1 A Pacific FU.125 milling machine and the arrangement of dynamometer and workpiece

A milling pass started by the rotating tool entering the location pointed to as “Milling start” in Figure 2-2b and finished when the tool exited the other end of the block. The length of the workpiece per pass was ~ 60 mm. The workpiece was clamped on a dynamometer for cutting force measuring. For the conditions of wet milling, coolant (HOCUT 795B, from Houghton Australia, to water ratio 1:10) with a flow rate set at 0.02 l/s through the nozzle was directed to the milling location, as is also indicated in Figure 2-2a.



(a)



(b)

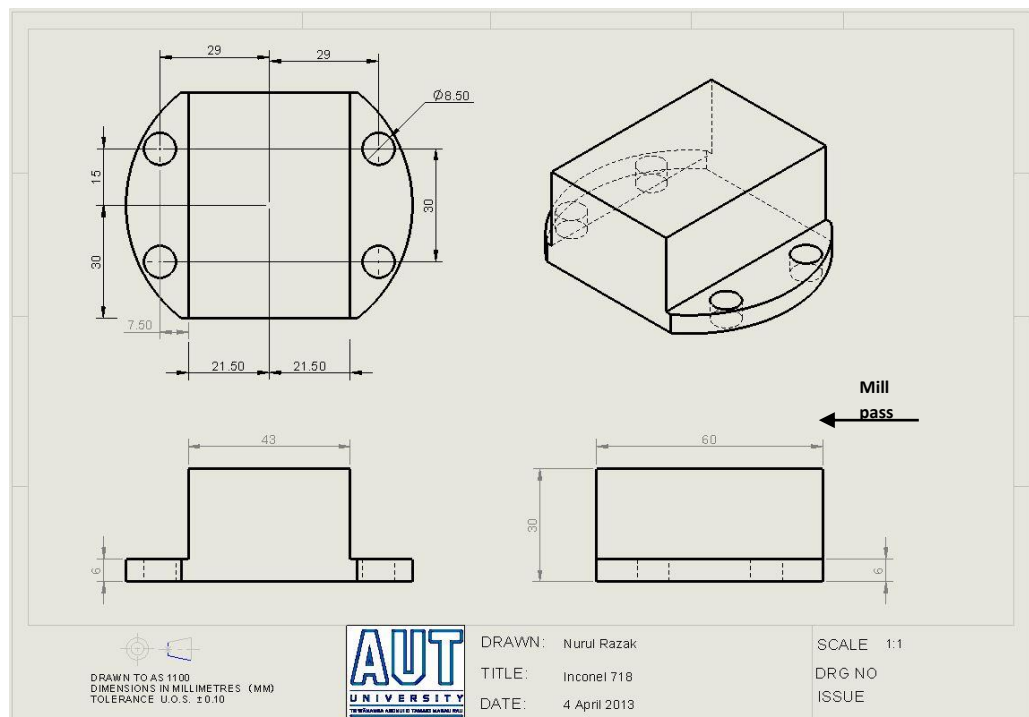
Figure 2-2 Illustrations of down-milling experiment: (a) image showing assembly of dynamometer for forces (F_x , F_y and F_z) measurement, 718Plus workpiece, tool holder and insert, coolant nozzle, and (b) schematic of viewing down on the workpiece and tool-insert with various stages of the tool during the pass indicated

2.2 Workpiece and Cutting Tools Materials

Superalloy 718Plus was the nickel-based alloy used in this study with the compositional specification provided in Table 2-1. The as-received bar (76 mm in diameter) was in a solutionised state approximately 30 HRC (302 HV) as stated in technical data sheet of ATI 718Plus [59-61]. The workpieces were machined out from the as-received bar to a block with overall dimensions of 60 x 42 x 30 mm shown in Figure 2-2a. Images in Figure 2-3b was the actual workpiece. The workpiece was made in this way to make sure they could be positioned properly on the dynamometer. The milling pass shown in Figure 2-2b occurred along the long edge of the block (60 mm) as denoted in Figure 2-3.

Table 2-1 Composition specification of 718Plus (wt%).

Ni	Cr	Fe	Co	Nb	Mo	W	Ti	Al	Si	Mn	Cu	C	Others
Bal	19	8	8	5.2	2.5	0.8	0.5	1.2	0	0	0.3	0.01	0
	-	-	-	-	-	-	-	-	-	-		-	-
	21	10	10	5.8	3.1	1.4	1.0	1.7	0.35	0.35		0.05	0.035



(a)

Figure 2-3 (a) A drawing of workpiece blocks, (b) actual workpiece with different block viewing

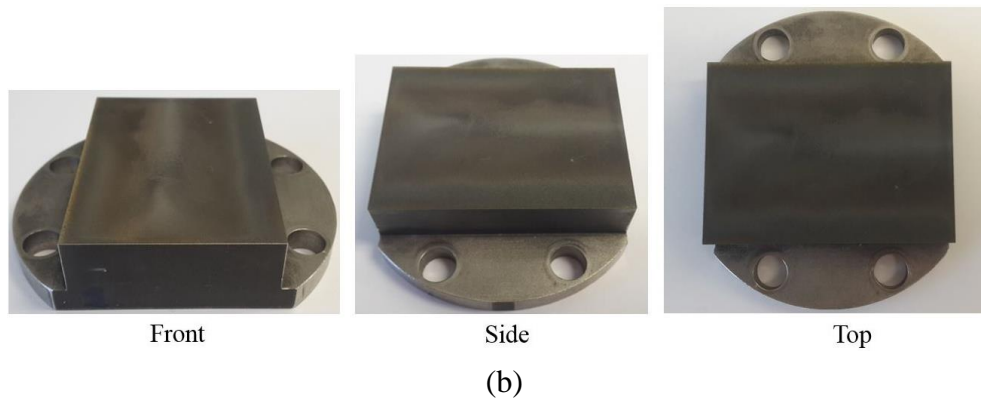


Figure 2-4 Continued

A summary of the heat treatment process is presented in Table 2-2. These conditions are adapted from the ordinary thermal process used in manufacturing, consisting of solutionising under identical conditions to our study. However, two aging stages are defined in the ordinary procedure the first stage is identical to the ageing of the workpieces in this study [60, 61]. Comparably, Whitmore et al. [46] conducted a single aging step after solutionizing for the same material as our work. They solutionised the workpiece at 980 °C for 30 min, followed by aging at 788°C for 4 hours and air cooling. This resulted in a sample with a hardness of 4.5 GPa (~ 46 HRC) and yield strength of 1060 ± 10 MPa at 0.2 % offset [46]. By adapting the conditions used in by Rao et al. [70] and Whitmore et al.'s research the following heat treatment procedure was used; Solutionizing at 982°C for 1hr, rapid quenching in water followed by age hardening at 788°C for 8 hours and air cooling. The heat treatment process was conducted in a McGregor induction furnace with each workpiece treated separately and wrapped in stainless steel foil to prevent surface oxidation. After heat treating the samples were tested for their hardness. The hardness of the samples were ~ 42 HRC (412 HV) which were comparable to the hardness value of fully aged condition in ATI material data sheet [47].

Table 2-2 Heat treatment of 718 Plus

Process	Temperature (°C)	Time (hour)	Notes
Solutionising	982	1	water quenched
Ageing	788	8	air cooled

To have a greater insight into the mechanical properties of 718Plus Ni-based superalloy in an annealed and hardened condition, tensile tests were conducted. Tensile test samples are of shape and dimension in Figure 2-7 and discussed in the testing process below in section 2.3.

The inserts were supplied by ISCAR with the uncoated inserts of part code; APKR 1003PDR-HM IC 28 and PVD TiAlN coated inserts of APKR 1003PDR-HM IC 928. A dual insert tool holder with a single insert arrangement was used as in Figure 2-4, enabling unambiguous tool deterioration monitoring of each tool. The tool holder was of 16 mm diameter and the base circle radius from the cutting edge to the tool insert was 9 mm as illustration in Figure 2-5.

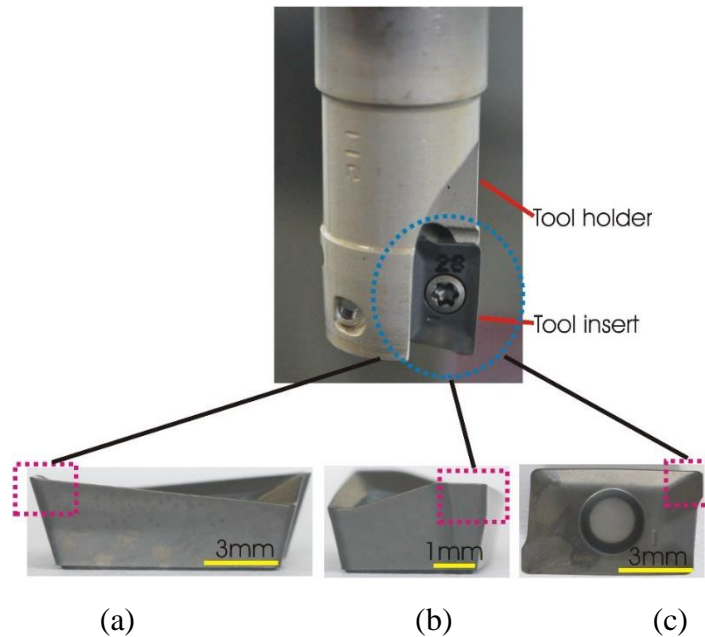


Figure 2-5 (a) Photo of an insert mounted on a tool holder and actual images of three faces of a tool insert, (a) rake face, (b) side flank face and (c) bottom flank face. (Regions marked by the pink rectangular are cutting areas and thus the major interest/focus areas to be analysed)

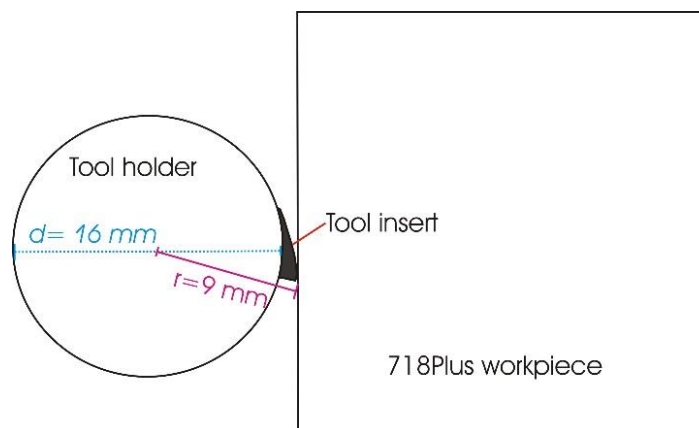


Figure 2-6 An illustration of the radius cutting edge between cutting insert and the workpiece

2.3 Workpiece Hardness and Strength Measurements

The hardness of the workpiece material was measured using a micro-hardness tester (MODEL LECO M-400-GI). The measurement procedure was conducted based on ASTM standard E384. An indentation load of 300gf at constant dwell time of 10 seconds was used to measure the hardness of annealed and hardened workpieces. However, for machined surface samples that will be discussed in section 2.6 for tool conditions TC9, TC10 and TC15 as shown later in Table 2-3; a 50gf load was applied for a dwell time of 10 seconds creating a hardness distribution of higher resolution with more indents applied. TC9 and TC10 were conducted on an annealed workpiece using uncoated tool in dry and wet (coolant) condition respectively. Meanwhile TC15 was conducted on a hardened workpiece using uncoated and dry condition. According to the instruction manual book of this hardness tester, it is recommended to have at least four times more than the diagonal length between two indentations. It is also suggested to have a distance of at least 2.5 times more than the diagonal length from the edge of the specimen as depicted in Figure 2-6. Based on this guideline, a hardness indentation could only be taken about 40 μm from the surface (edge of specimen).

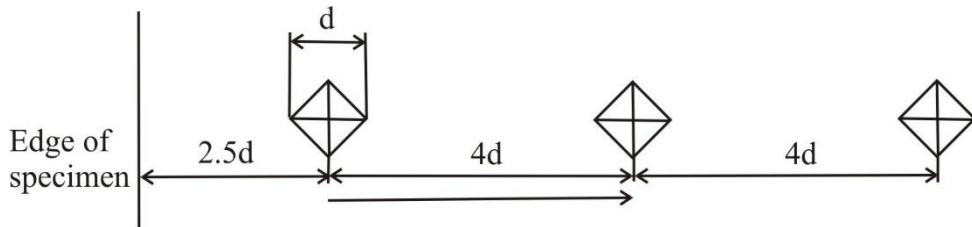


Figure 2-7 Example of distance between Vickers indentations

In addition, tensile test samples were produced from 718Plus Ni-based superalloy in the annealed and hardened state and tested on a Tinius Olsen H50KS tensile testing machine with a load of 50 KN at room temperature. Dimensions of the tensile test samples are presented in Figure 2-7. Figure 2-8 shows the tensile data for annealed and hardened samples and Figure 2-9 demonstrates the yield strength values taken from annealed and hardened samples in Figure 2-8a and Figure 2-8c. At the 0.02% offset the values of annealed (Figure 2-10a) and hardened (Figure 2-9b) samples were ~600 MPa and 1000 MPa respectively. The value of the hardened value was comparable to yield data strength produced by Whitmore et al. [46].

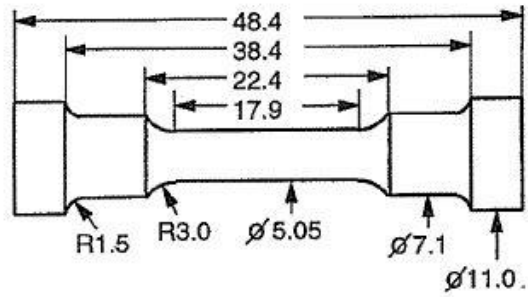


Figure 2-8 The dimension of tensile specimens

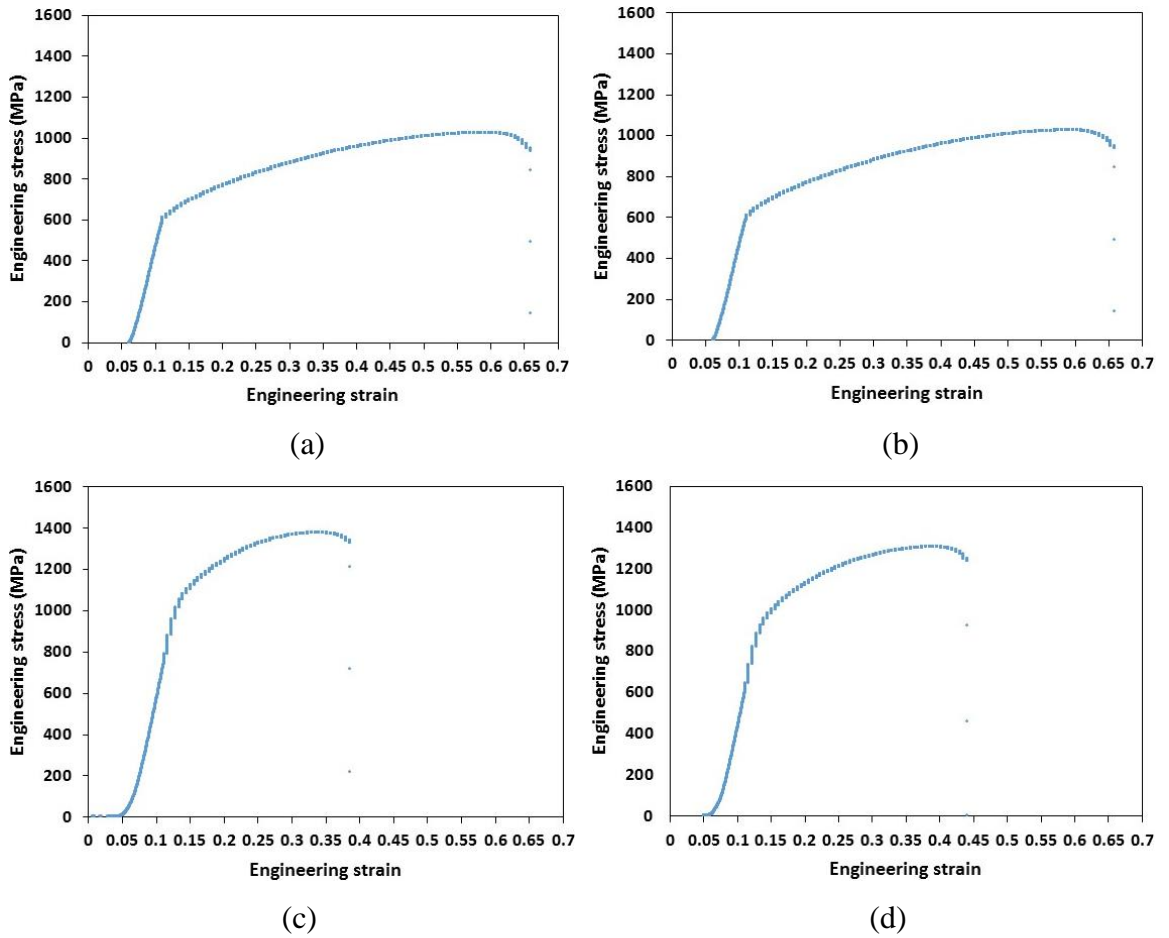
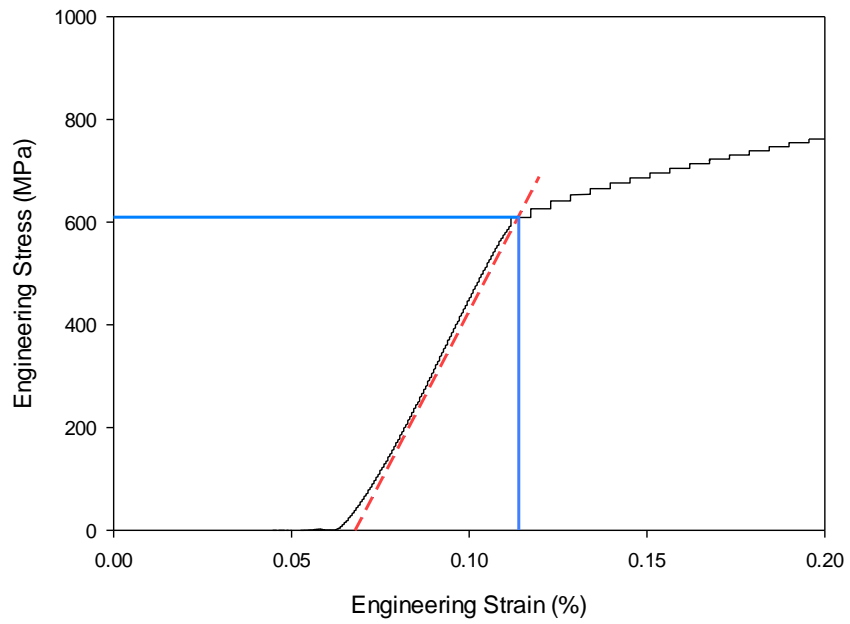
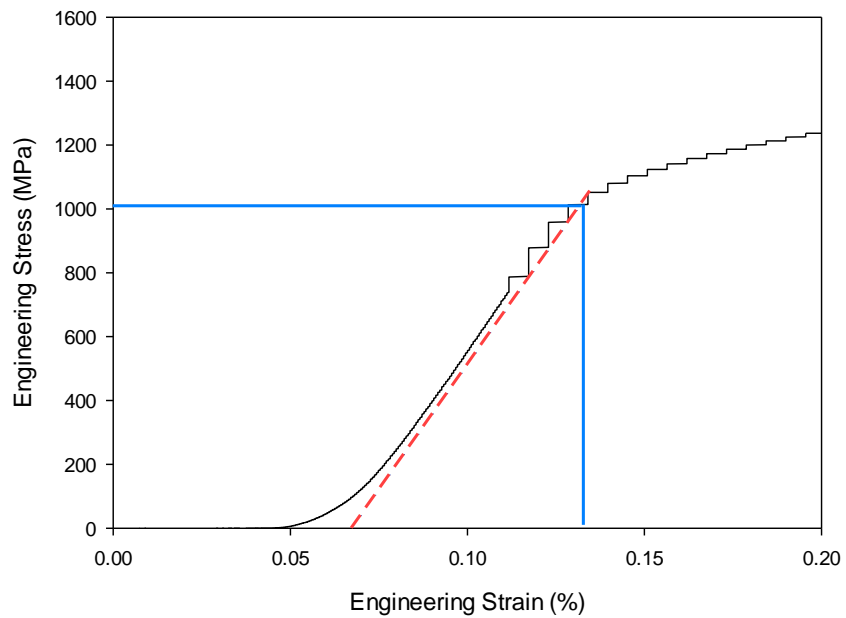


Figure 2-9 Plot of engineering stress against engineering strain: (a) annealed sample 1, (b) annealed sample 2, (c) hardened sample 1 and (d) hardened sample 2



(a)



(b)

Figure 2-10 Engineering stress (MPa) versus engineering strain; (a) annealed sample 1 and (b) heat treatment sample 1

2.4 Milling Parameters and Conditions

Milling experiments on 718Plus Ni-based superalloy were separated into four separate series as summarised in Table 2-3 with each of the milling and tool conditions (TC). For each of objective series, 718Plus Ni-based superalloy workpiece was milled using a tungsten carbide tool. The objective for experiments in series 1 was to monitor and examine the cutting edge deterioration process. In this series, four tool conditions were used (TC1-TC4) which

included uncoated carbide and coated carbide tools in dry condition. Superalloy 718Plus workpiece in their annealed state with an average hardness of 30 HRC was used. A spindle rotation speed of 1,000 rpm and traverse speed of 50 mm/min were set to obtain a cutting speed (V_c) of 50 m/min and feed rate (FR) of 0.05 mm/rev. Furthermore, the depth of cut (DoC) and radial depth of cut (a_e) were set 1.0 mm and 9.0 mm respectively. For milling Ni-based alloys, V_c of 50 m/min is regarded as a medium cutting speed [2]. Values of feed rate (FR), depth of cut (DoC) and radial depth of cut (a_e) may also be regarded as ordinary values. However, after reviewing the relevant studies on milling of Ni-based superalloys, [6, 5-17, 23, 38] suitable and optimised values are not clearly defined.

In series 2, an extensive series of milling experiments with the objective (objective 2) of monitoring the progress of tool deterioration and cutting force were conducted. A further aim was to investigate the effect of increasing feed rate on tool deterioration, which is part of objective 2. The same machining conditions used in Series 1 (objective 1) were used in Series 2 in dry and wet conditions except the value of DoC , which was set to 0.5 mm. DoC was reduced due to the high cutting forces observed after a preliminary milling pass to be ~ 800 N using 1.0 mm DoC and hence the DoC was reduced to 0.5 mm. In tooling conditions TC9-TC10, similar milling conditions were used but only using uncoated tool inserts, however it was conducted in an interrupt milling pass. An interrupt milling pass, defined as the milling pass terminated midway along the full milling pass distance, to be discussed further in section 2.6. These experiments were conducted to investigate the correlation between the shear deformation on the machined surface and tool deterioration. Meanwhile for tooling conditions TC11-TC12, experiments were conducted solely using uncoated carbide tools in both wet (coolant) and dry conditions with an increase of FR to 0.1 mm/rev. The spindle rotation speed (1,000 rpm) was identical to series 1 however, the forward traverse speed was set to 100 mm/min resulting in a cutting speed (V_c) and feed rate (FR) of 50 m/min and 0.1 mm/rev respectively. This series of experiments has aimed to investigate the influence of elevated feed rate values on tool fracturing modes.

A hardened workpiece of with the hardness of 42 HRC hardness was used in series 3 with the same cutting parameters as series 2. Experiments were conducted at two tooling conditions (TC13-TC14) solely using uncoated carbide tools under wet (coolant) and dry cutting conditions. Of importance is the understanding on how the cutting tool responds to the harder workpiece material and its influence on the modes of tool deterioration. It is also of significance to observe and monitor the changes in cutting force when the tool experiences

the high resultant force from the increased hardness/strength of the workpiece. Identical machining conditions in tooling condition (TC9-TC10) were used in tool condition (TC15), which was an interrupted experiment.

Table 2-3 Summary of milling condition of 718Plus experimental conditions.

Series	TC	Milling condition						
		Tool	Coolant	V_c (m/min)	FR (mm/rev)	DoC (mm)	a_e (mm)	Hardness (HRC)
1	TC1	uncoated	dry	50	0.05	1	9	30
	TC2	uncoated	dry	50	0.05	1	9	30
	TC3	coated	dry	50	0.05	1	9	30
	TC4	coated	dry	50	0.05	1	9	30
2	TC5-1	uncoated	dry	50	0.05	0.5	9	30
	TC5-2	uncoated	dry	50	0.05	0.5	9	30
	TC6-1	coated	dry	50	0.05	0.5	9	30
	TC6-2	coated	dry	50	0.05	0.5	9	30
	TC7-1	uncoated	wet	50	0.05	0.5	9	30
	TC7-2	uncoated	wet	50	0.05	0.5	9	30
	TC8-1	coated	wet	50	0.05	0.5	9	30
	TC8-2	coated	wet	50	0.05	0.5	9	30
	TC9	uncoated	dry	50	0.05	0.5	9	30
	TC10	uncoated	wet	50	0.05	0.5	9	30
	TC11-1	uncoated	dry	50	0.1	0.5	9	30
	TC11-2	uncoated	dry	50	0.1	0.5	9	30
	TC12-1	uncoated	wet	50	0.1	0.5	9	30
	TC12-2	uncoated	wet	50	0.1	0.5	9	30
3	TC13-1	uncoated	dry	50	0.05	0.5	9	42
	TC13-2	uncoated	dry	50	0.05	0.5	9	42
	TC14-1	uncoated	wet	50	0.05	0.5	9	42
	TC14-2	uncoated	wet	50	0.05	0.5	9	42
	TC15	uncoated	dry	50	0.05	0.5	9	42

A repetition experiment was conducted for each tooling condition. For Series 2 and Series 3 of experiments, the cutting force was measured using a Kistler™ dynamometer for all experiments. After each milling pass or experiment the tool insert was removed from the tool holder and examined using a Hitachi SU-70 field emission scanning electron microscope (SEM) prior to the next milling pass. Positioning of inserts in the SEM sample holder was as consistent as possible, with wear images taken on the side flank face, bottom flank face and rake face. Details of these images will be explained in section 2.7. Every TC was repeated

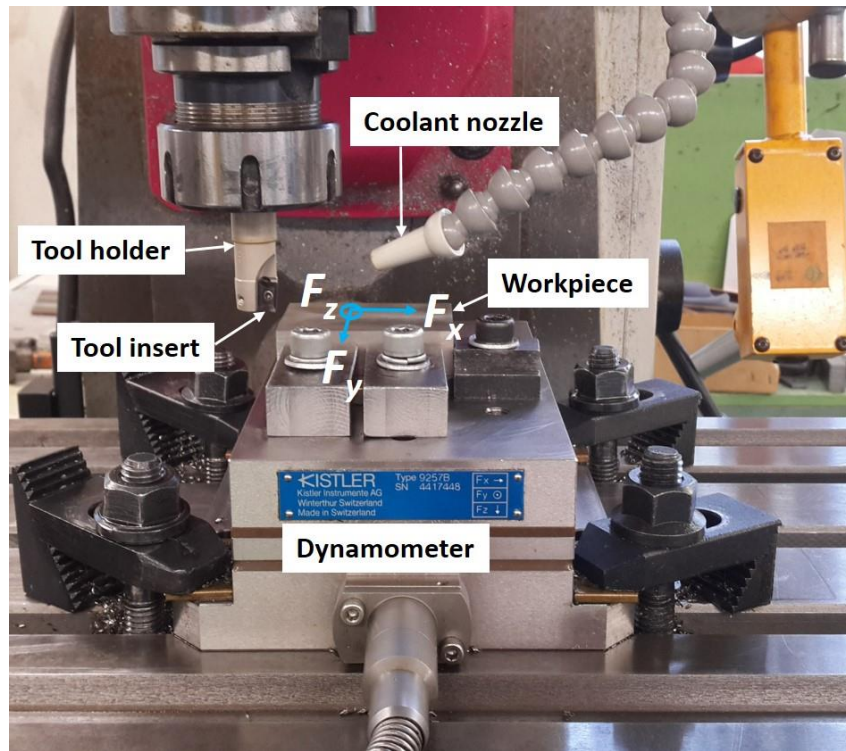
for few passes and it was intended for VB_{max} to reach 0.5 mm wear criterion as stated in the ISO Standard 8688-2, which is maximum flank wear of 0.5 mm.

2.5 Dynamometer and Force monitoring

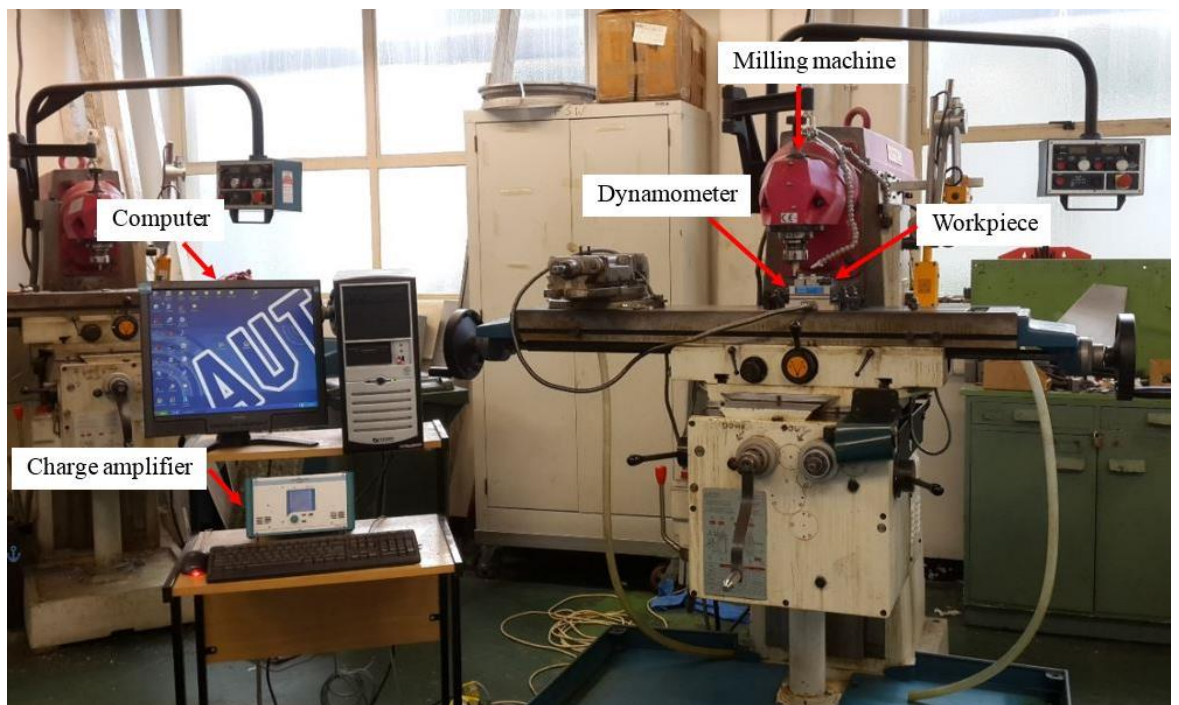
A Kistler 9257B three-component piezoelectric force dynamometer was used to measure the cutting forces. It was mounted on the bed of Pacific FU.125 down-milling three axis-milling machine, x , y and z directions denoted in Figure 2-10a. The dynamometer set up on the milling machine is shown in Figure 2-10b. Model 5004 Kistler dual mode of charge amplifier shown in Figure 2-10a was used to convert the dynamometer output signal into a voltage signal applicable for the data acquisition system. The input sensitivities of charge amplifier is set corresponding to the output sensitivity of the force dynamometer in the direction of the forces. The x , y and z forces were measured and exported to a tab-delimited text file, followed by conversion into a digital format such as a Microsoft Excel file.

During the experiment the sampling rate was set at 1,000/s. Since each milling cycle (revolution) took 0.06 s (=60/1000 s/rev), there were 60 (=1,000/s \times 0.06s) force data points in each cycle. For each milling pass, dynamometer data recording commenced just prior to the tool insert engagement with the workpiece after the tool started moving forward relative to the machine bed. The start is indicated as “Milling start” in Figure 2-2a (section 2.1). In just under 10s the tool moved a distance equal to the radius of the tool (holder plus insert), by which time the insert has started milling the whole width equal to a_e , marked as “Full a_e milling” in Figure 2-2b (section 2.1). The cutting force (F) is determined by:

$$F = \sqrt{F_x^2 + F_y^2 + F_z^2} \quad \text{Equation 2-1}$$



(a)



(b)

Figure 2-11 Dynamometer setting (a) dynamometer forces F_x , F_y and F_z direction on the machine setting (b) configuration of dynamometer, charge amplifier and milling machine

2.6 Sample Preparation and Examination

Before samples were examined under scanning electron microscope (SEM), several procedures needed to be carried out. First, cutting tool insert was removed from the tool holder and then it was cleaned using soapy water and further cleaned with ethanol liquid in ultrasonic bath cleaning machine in order to remove stain/lubricant on their surface for about 30 s. In order to measure the cutting edge radius of carbide and examine the WC grains and the Co binder, a cross section of a new carbide tool insert was conducted. The tool insert was mounted in a cold setting resin to hardener mixture of 15:2 ml respectively per sample as shown in Figure 2-11. Then, the sample was cooled to room temperature overnight before removal from the mould.

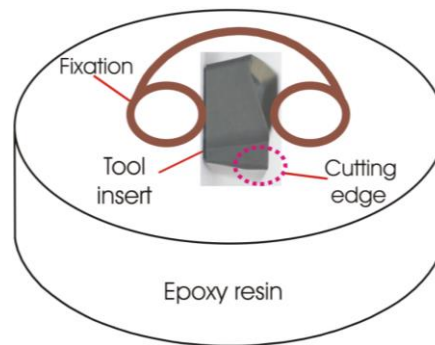


Figure 2-12 An illustration of cutting tool insert mounted on epoxy resin

Following the mounting process, the sample was ground on a Metaserv LJ7006-84 grinding machine using 180, 500, 1200 and 2400 grit silicon carbide (SiC) papers. Further grinding of the samples was completed on a TegraPol-25 automatic sample grinding machine using a MDMol grinding pad in a DiaPro-Allegro Largo suspension (9 μm abrasive) for 4 minutes. A final polishing stage was conducted using a MDLargo polishing pad with DiaPro-Mol suspension (3 μm abrasive) for 3 minutes and MDChem polishing pad with OP-S suspension (0.04 μm abrasive) for about 1 minute.

With the objective to investigate the correlation between the shear deformation of machined surface and tool deterioration, interrupt milling pass was conducted in tool conditions TC9, TC10 and TC15 (refer to Table 2-3). The milling pass was terminated in the centre of the workpiece as illustrated in Figure 2-12, following which the tool returned to its initial start position. Machined surface workpieces from the first pass and final pass (tool deteriorated) of each tool conditions were selected for the sample cross sectioning. From these selections

of milling passes, the shear deformation corresponding to the tool condition can be understood. The workpiece was sliced ~ 2.5 mm below the surface by wire electrical discharge machining (EDM). The sliced section denoted as ‘A’ in Figure 2-12 was cut using a BUEHLER ISO met low speed saw with a CBN blade recommended for nickel-based superalloys. This low speed saw was used to minimise the amount of induced sectioning damage to the material. The sample was mounted in a Bakelite resin with cross section exposed as shown in illustration Figure 2-13a and microhardness map which will be discussed in Chapter 4 (section 4-5) was mapped based on the micrograph of the cross section as presented in Figure 2-13b. The sample was ground and polished following the same methods as above. Consequently, the sample was electro-polishing in a 100 mg CuCl₂, 100 ml methanol and 100 ml HCl solution for 20 seconds and later rinsed in ethanol.

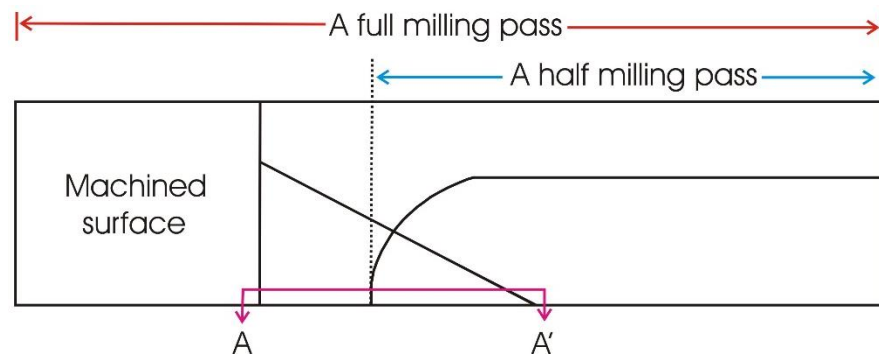


Figure 2-13 An illustration of an interrupt milling pass with line drawn indicating sectioned sample was made on the machined surface

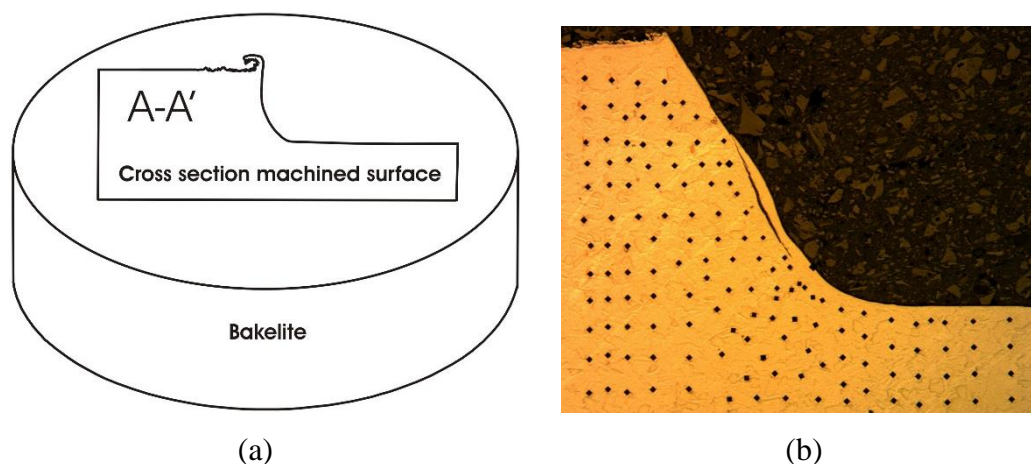


Figure 2-14 Machined surface of 718Plus Ni-based superalloy (a) an illustration a cross section machined surface on a bakelite resin and (b) micrograph of the cross section machined surface

2.7 Tool Deterioration Monitoring

A Hitachi SU-70 field emission scanning electron microscope (SEM) was used to monitor the progression of tool deterioration and chip formation in this study. The default 20 kV accelerated voltage was chosen to capture all images. The cutting tool insert was placed in the sample holder in three positions exposing the side flank face, bottom flank face and rake face. Figure 2-14 details the mounting position of the cutting tool insert in the SEM sample holder for consistent imagery. This consistency was vital for monitoring the progression of tool deterioration in every experiment of milling pass which lacking in the studies in literature. Furthermore, prior to conducting an experiment SEM images were taken for each of the new insert at 100X magnification. For the first pass, the images were taken at 100X magnification with subsequent pass imagery obtained at magnifications adapted to the level of wear evident on the tool in order to obtain overall image of tool deterioration. Energy dispersive Spectrometry (EDS) was used to analyse the chemical composition of the cutting insert primarily on the BUE formation.

After capturing the SEM images, flank wear was measured for each pass as according to ISO Standard 8688-2. In order to monitor the progression of flank wear for each pass, zero pass tool insert was created where an outline was made following the edge of the tool insert. This zero pass edge outline (ZPEO) was fit/placed onto each subsequent pass insert edge image. Figure 2-15 a-d exemplifies the assessment of flank wear. Meanwhile Figure 2-15b shows a higher magnification of tool cutting edge before milling indicating that WC grains cannot be seen in a new insert. All SEM images were then sequentially organised as per that of Figure 2-16, for every experimental milling pass ensuring accurate monitoring of the incremental tool deterioration

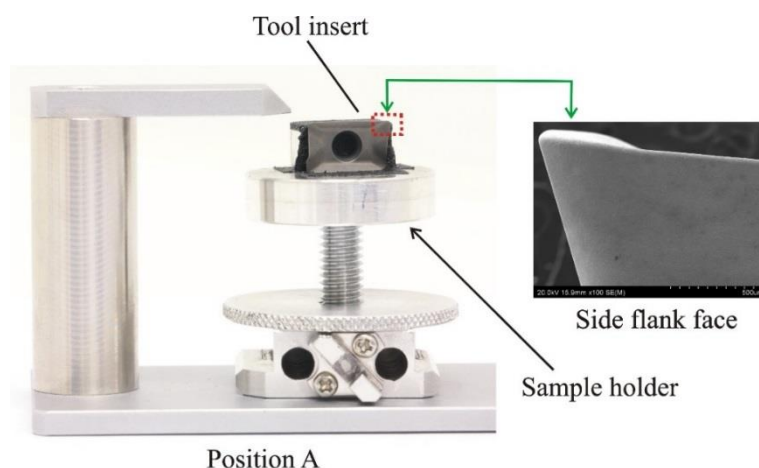


Figure 2-15 Cutting tool insert position at the SEM sample holder for three different view; (a) side flank face, (b) bottom flank face and (c) rake face

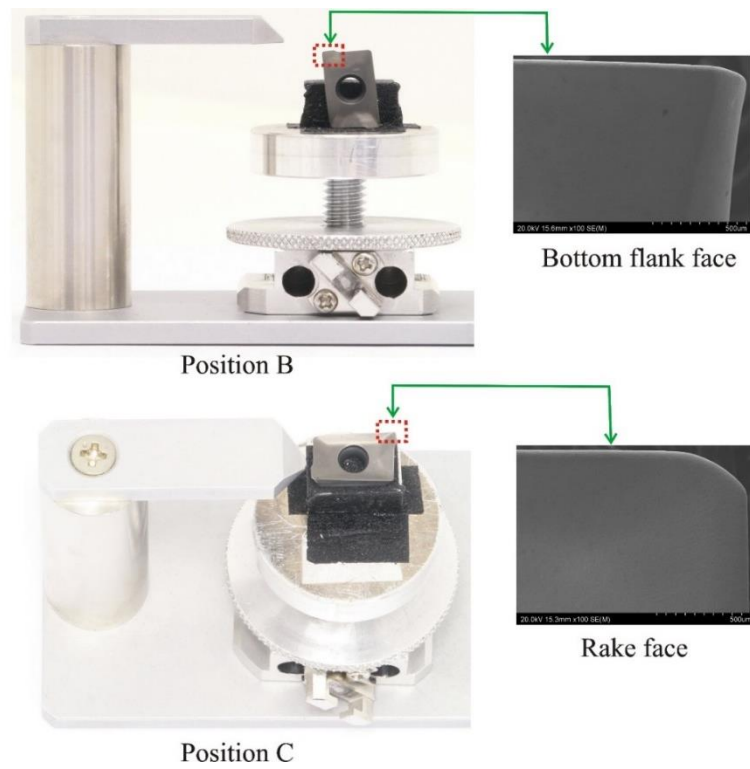


Figure 2-16 Continued

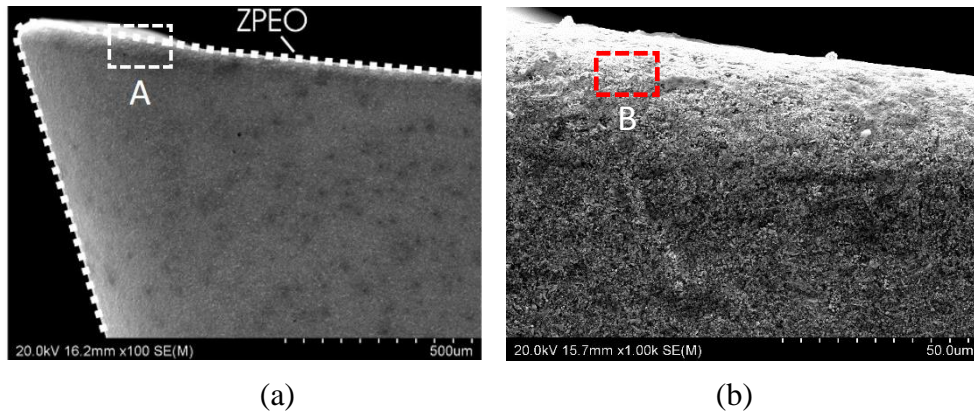


Figure 2-17 Example of flank wear assessment on SEM images on the side flank face; (a) a new tool insert before milling, (b) higher magnification image in location A, (c) higher location magnification image in location B showing fine WC grains in edge location (cutting edge) before milling (d) Tool deteriorated after the fourth milling pass. Tooling condition: uncoated carbide and wet (TC12-1)

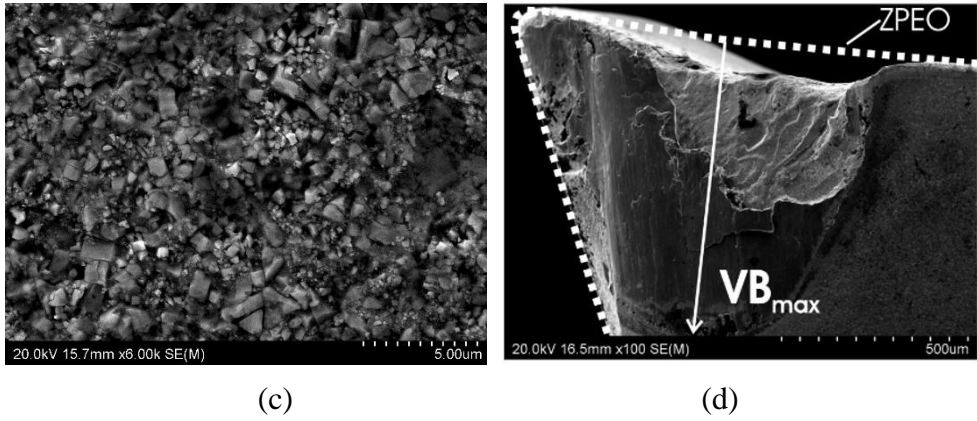


Figure 2-18 Continued

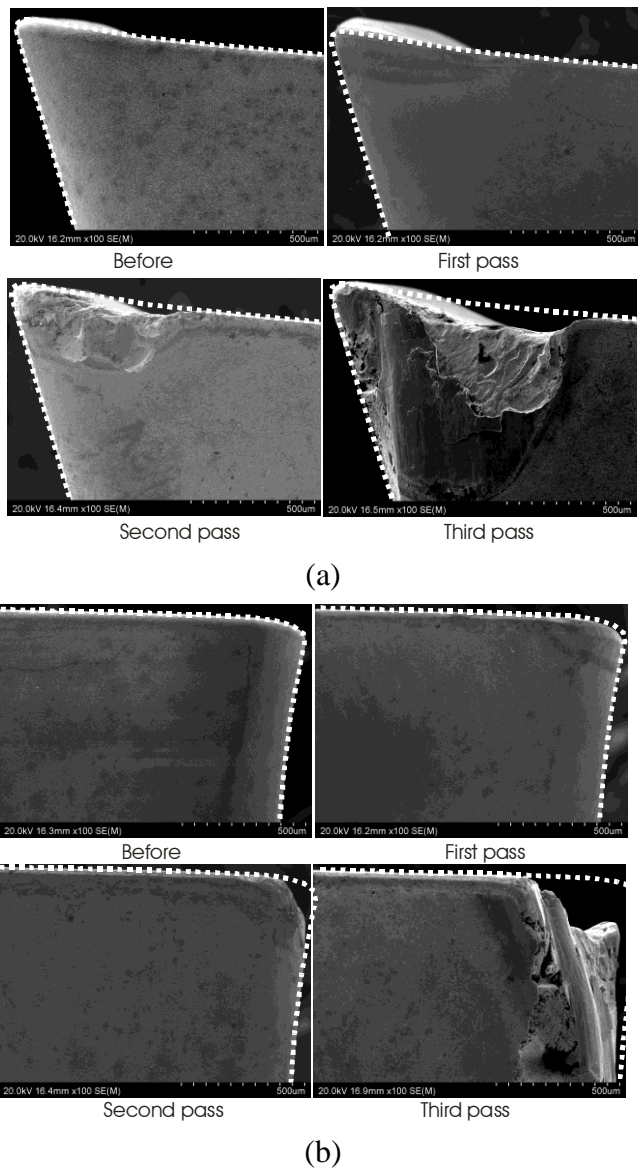
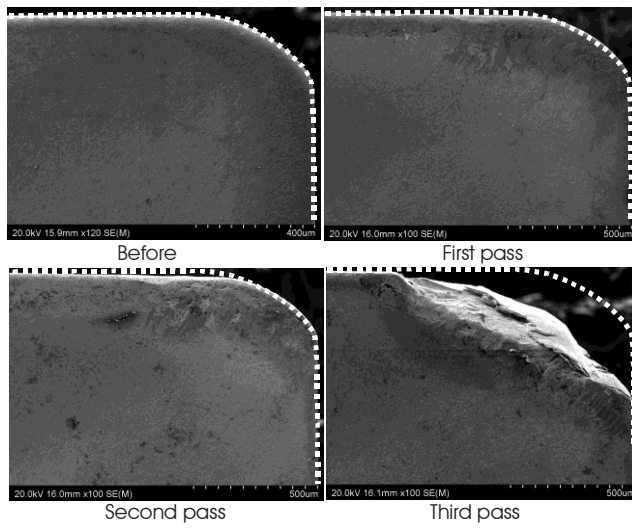


Figure 2-19 SEM images sequences for every passes; (a) side flank face, (b) bottom flank face and (c) rake face. Tooling condition: uncoated carbide and wet (TC12-1)



(c)

Figure 2-20 Continued

Chapter 3: Modes of Tool Deterioration

In this chapter, observations on the tool deterioration process from its initial stage to severe cutting edge damage are presented first. Through these observations and general consideration on cutting edge geometry, the modes of deterioration can be suggested and the deficiency of using flank face measurement alone is discussed. The results of milling experiments using coated tools are presented with a corresponding discussion on the effect of thin tool coatings on the deterioration modes reported subsequently reported. Furthermore, observations through failure analysis on the cutting edge fracture surfaces are presented and the fracture mechanism of the WC-Co composite tool material during milling of hard-to-cut 718Plus alloy is explained.

3.1 Flank Deterioration – Early Stage

SEM images of the side flank face presented in Figure 3-1 show the sequential deterioration of the tool insert. It should be noted that the SEM image of the tool flank face is rotated 90° relative to the flank face view shown in Figure 2-10. An outline corresponding to the zero pass tool insert profile is used as a reference. The zero pass edge outline (ZPEO) is placed onto each subsequent pass insert edge as seen in Figure 3-1. Comparing the images of a new (Figure 3-1a) and used tool (after one pass – Figure 3-1b) via the ZPEO, little geometrical change of the insert was observed. However, a build-up layer (BUL) formed not extending to the top of the edge. This detail is evident in Figure 3-2a and 3-2b, higher magnification images of location A in Figure 3-1b. SEM energy dispersive spectroscopy (EDS) analysis (Figure 3-2c) clearly shows that compositionally the BUL is of the 718 workpiece material, with top edge (Figure 3-2a and b) compositionally identified by EDS as WC-Co (Figure 3-2d).

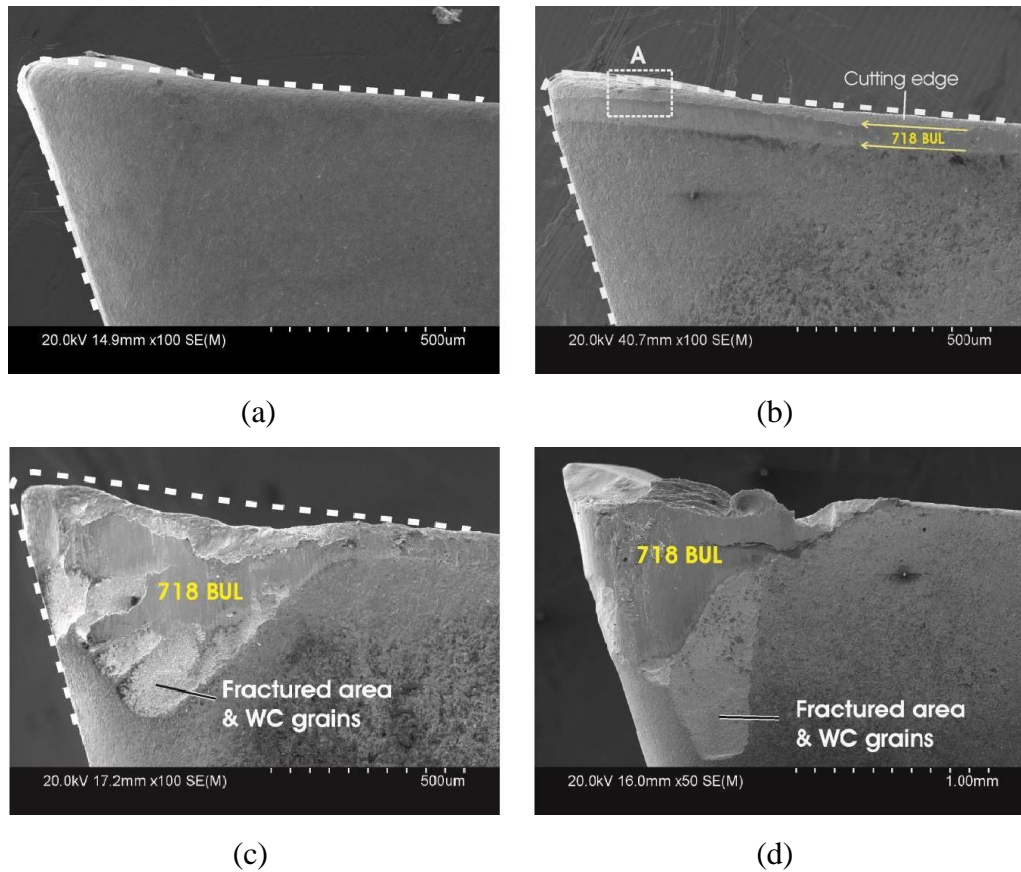


Figure 3-1 SEM images of insert TC1 side flank face before and after various passes: (a) before milling with edge outlined, designated as zero pass edge outline (ZPEO), (b) after the first pass together with ZPEO, (c) after the second pass with ZPEO and (d) after the third pass (magnification different). Tooling condition: uncoated carbide and dry

During milling, the tool cutting edge forces the workpiece material to shear, fracture, and flow out in the form of chips. A short distance behind the cutting edge, the tool flank may rub against the workpiece material, generating a BUL. To aid the discussion Figure 3-3 is presented with a schematic illustration representing the cutting edge, workpiece and chip formation, together with SEM of a cross section of the cutting edge. BUL location is indicated in Figure 3-3. The radius of cutting edge is around 0.05mm. On the flank face, the cutting edge ends where the tool insert and workpiece separate. Knowing this, the position of cutting edge as viewed under SEM can be estimated, as marked in Figure 3-3. This view and the SEM images in Figure 3-1b and 3-2a show that after the first milling pass, BUL starts from the last part of the cutting edge extending a short distance ~ 0.05 mm behind the cutting edge along the flank face. Extension of the BUL is justifiable as high pressure acting at the cutting edge location during milling leads to a small amount of workpiece material being continuously extruded slightly behind the cutting edge on the flank face, thereby extending the rubbing distance in that location.

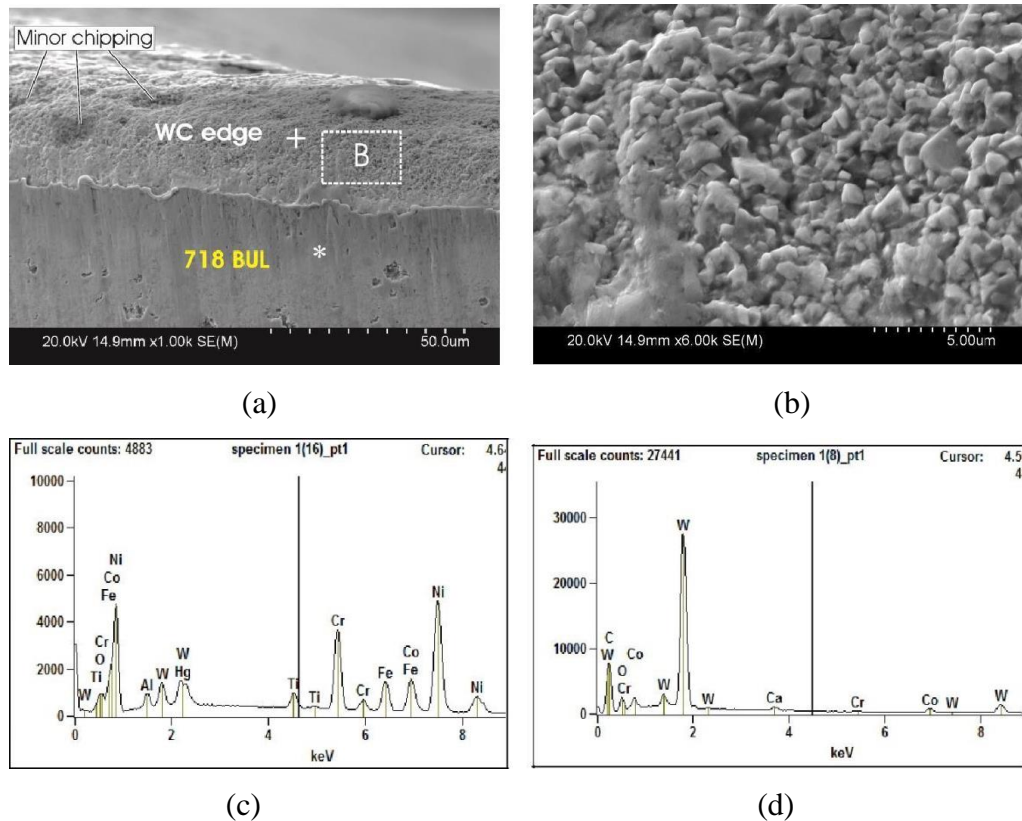
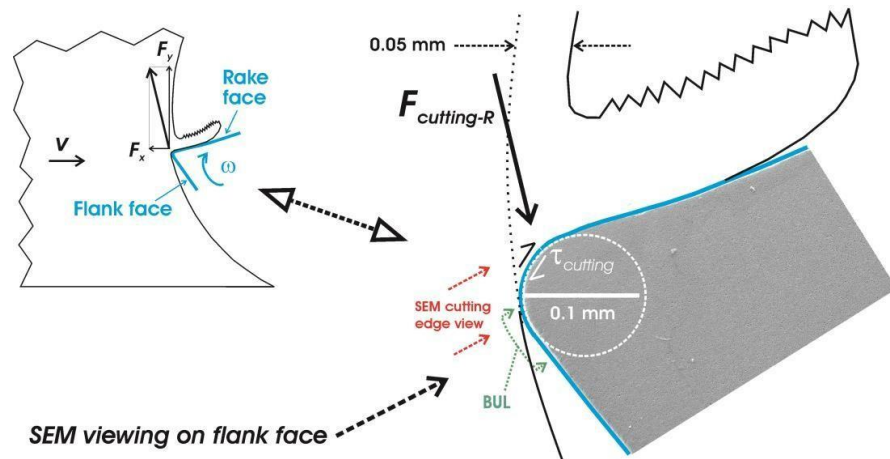


Figure 3-2 Cutting edge features: (a) higher magnification image in location A of Figure 3-1b, showing 718 BUL material next to WC grains edge, (b) higher magnification image in location marked B in (a) showing fine WC grains in edge location, (c) EDS spectrum with analytical spot * marked in (a) and (d) EDS spectrum with analytical spot + marked in (a)

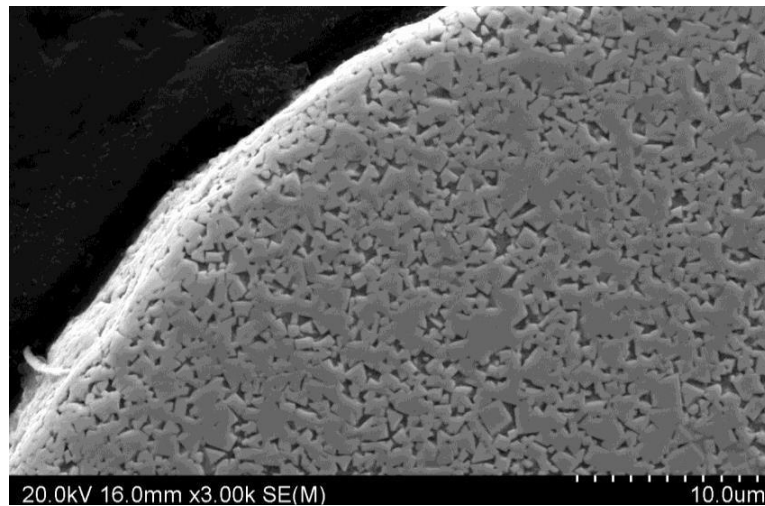
In the main portion of the cutting edge after the first pass as shown in Figure 3-2b, WC grains in the tool are clearly visible. Contrariwise, WC grains are not clearly seen in new inserts. Evident in Figure 3-3b in the dense packed microstructure of the surface of the cutting edge appearing flat when the insert is new. The irregular cutting edge surface in Figure 3-2b displaying angular WC grains suggests that although no significant deterioration of the tool has occurred, some WC grains may have detached and eroded away. The erosion is a slow, gradual wear process, hence no apparent geometrical change of the cutting after the first pass. It should be noted that some small “pieces” lost within the cutting edge also has started to be apparent, as can be viewed on the left side of the SEM image of Figure 3-2a, marked as minor chipping.

Further clarification regarding the minor geometrical change of the cutting edge and the physical change marked by BUL is required. Clearly, as indicated in Figure 3-3, BUL is not an indication of wear on the flank face. BUL is a smeared layer in the trailing part of the

cutting edge on flank face, which does not require tool loss to bond the BUL to the tool. By measuring the distance including the cutting edge and BUL in Figure 3-1b, a VB of roughly 0.1mm is attained. The ISO standard [15] true value of VB indicates wear, without an measurement quantifying the volume of tool material loss. As further explained in the ISO standard, adhesive material (such as BUL) affects the measurement of VB . Thus the measurement of VB in Figure 3-1b is erroneous and not meaningful with concern to tool deterioration.



(a)



(b)

Figure 3-3 Illustration of a cross section of new tool insert (SEM images) and workpiece (drawings) indicating features during milling: (a) low magnification SEM image in and around cutting edge location together with drawings indicating the various features in the surrounding and (b) high magnification SEM image in a cutting edge location displaying fine WC grains bound by Co-binder

As discussed, measurement of VB in the milling of Ni alloys is commonly reported. In the recent work on milling Inconel 718 by Kasim et al. [11], gradual wear excluding notch wear resulted in a VB of $\sim 0.1\text{--}0.2$ mm. By observing the SEM micrograph in Kasim et al.'s work, a strong correlation to this study (Figure 3-1b) is evident particularly the cutting edge of the tool and its vicinity in flank. This suggests a BUL of a similar width and a bare cutting edge however, Kasim et al. [11] did not consider it as a BUL, but rather the location having been worn due to abrasive wear. It should be noted that no compositional analysis was conducted by Kasim et al. [21] on the area as it was based on an earlier study by Sharman et al. [36]. In this referred study, however, there is no similar SEM observation on the cutting edge and they did not suggest abrasion wear.

3.2 Flank Deterioration – Growth Stage

The insert (TC1) non-uniformly deteriorated severely along the cutting edge during the second pass, as clearly presented in Figure 3-1c. The non-uniform material loss was the result of chipping (fracturing) locally along the cutting edge and likely repeatedly too during this second pass. Fracture further extended ~ 0.5 mm from the edge in addition to the cutting edge location. The possible cause of this relatively large fracture is discussed with aid from the illustration in Figure 3-3. As in most cutting processes, the cutting edge forces the workpiece material to shear off along the rake face. There is then an action force acting on the cutting edge, indicated as $F_{Cutting-R}$ in Figure 3-3, which can be elevated if the workpiece material is of high strength. As already stated and is commonly understood, during milling of high strength Ni alloys, capable of retaining high strength at high temperatures resultant high cutting forces are needed. The direction of $F_{Cutting-R}$ possibly aided the fracturing process starting from the edge location of the rake face and propagating a distance in the subsurface along the flank face. The cutting edge location on the rake face is a high stress region where workpiece material is expected to separate and shear off. Thus, a high shear stress ($\tau_{Cutting}$) is expected which can lead to wear and chipping in the cutting edge area.

Severity of fracturing both along and within the cutting edge area considerably worsened in the following pass (third pass) on insert TC1, evident from the micrograph in Figure 3-1d. Although only the flank face is visible, a large amount of tool material loss and a considerable blunting of the cutting edge/corner were apparent. Furthermore, a large amount of build-up in and near the cutting corner region is visible from the micrograph. This build-up should result from the rubbing and forging of the workpiece material ahead of the tool at the

fracturing and thus blunting of the tool became very severe during this third pass. Continual rubbing and forging would lead to total cutting function loss of the tool and end of life of the tool.

3.3 Deterioration Observed on All Three Faces

In the experiments with insert TC2, the tool was examined in more detail not only on the side flank face (Figure 3-4), but also the bottom flank face (Figure 3-5) and the rake face (Figure 3-6). Solely considering the side flank face, the condition of insert TC2 (Figure 3-4b) is similar to insert TC1 (Figure 3-1b), after the first pass. After the second pass however, insert TC2 (Figure 3-4c) differs from insert TC1 (Figure 3-1c) as there was no fracture extending a distance away from the cutting edge. Small fracture/chipping along the cutting edge was clear. In the next pass, visible in Figure 3-4d is severe fracturing and blunting of the tool, leading to rubbing and forging of the workpiece material instead of cutting similar to that of insert TC1 (Figure 3-1d). The build-up in the fractured locations evident in Figure 3-4d has a swollen appearance.

Higher magnification images (Figure 3-4e) support literature definition of this phenomenon as “plastic lowering” [15, 63]. Further plastic deformation of the cutting tool is observed with reference to the ZPEO (yellow outlined) on the SEM image, consisting of tool geometry enlargement and drooping downwards. A high pressure location and stress concentration on the cutting edge during milling is likely to cause edge deformation on the tool. Kadirgama et al. [5] observed similar plastic deformation on the cutting wedge after uninterrupted machining Hastelloy C-22HS for 180 mm. High temperatures during milling leading to creep deformation were proposed as the potential cause of this phenomenon. Additionally, Astakhov [48] found that high temperature creep is the major factor attribute to plastic lowering at the cutting wedge. A tool-chip interface between 1000-1200 °C was seen to result in plastic deformation of the cutting edge [64, 65]. The observation made in this work suggests that locally in the cutting edge region, high temperature and high force acting on the edge simply results in a slight deformed edge.

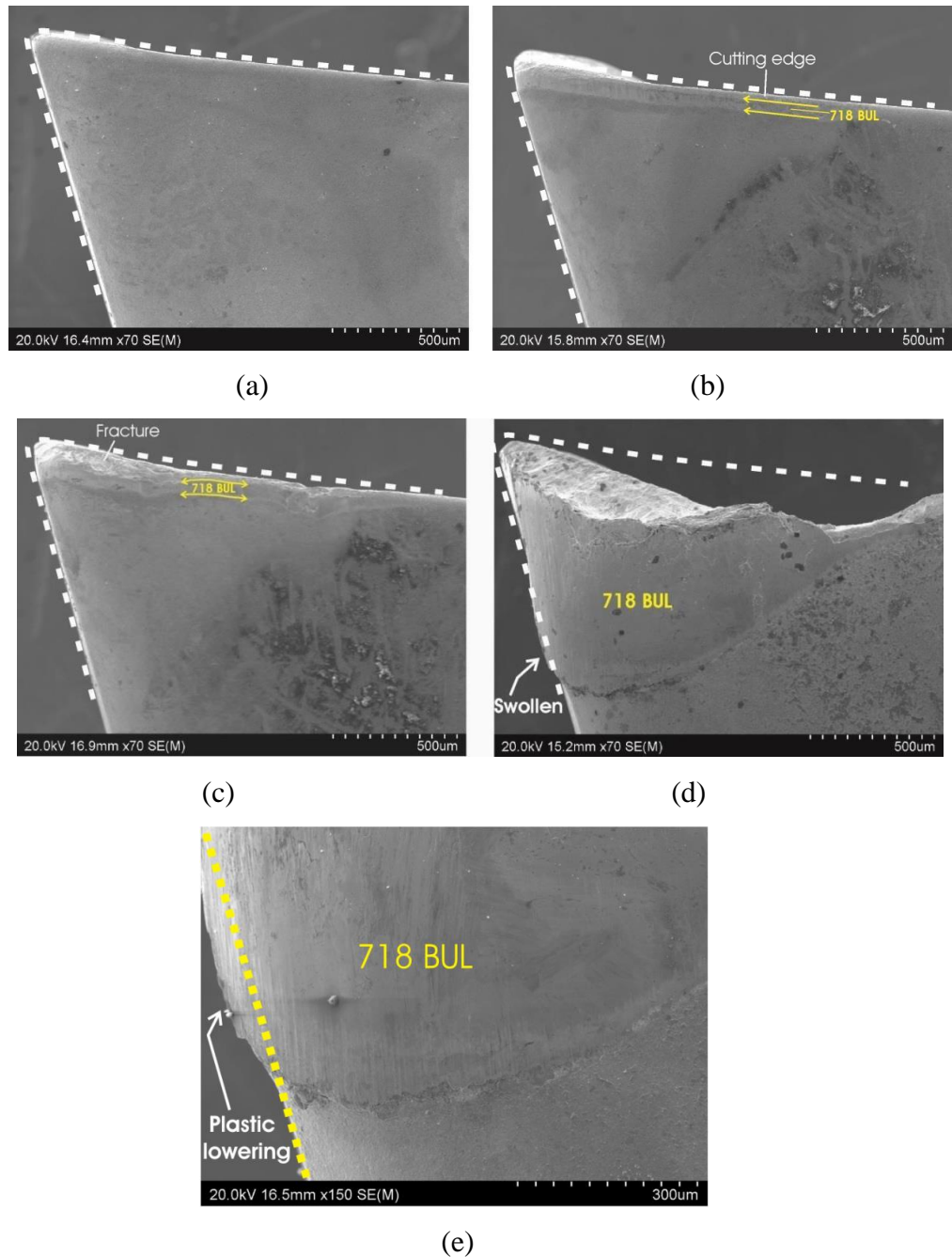


Figure 3-4 SEM images of insert TC2 side flank face before and after various passes: (a) before milling with edge outlined, designated as zero pass edge outline (ZPEO), (b) after the first pass together with ZPEO, (c) after the second pass together with ZPEO, (d) after the third pass together with ZPEO and (e) A higher magnification of image 3-4d indicating plastic lowering on the tool insert

Images of insert TC2 are displayed in Figure 3-5 with the view of the bottom flank face. Minimal tool material loss is visible in Figure 3-5b, however there is local chipping near the cutting corner. In the following pass, significant tool material loss and blunting in the cutting corner is clear in Figure 3-5c. This loss cannot be viewed properly when the tool is viewed in the side (major) flank face as in Figure 3-4c. Higher magnification imagery (Figure 3-7a)

of a small chipping site in Figure 3-5c (location A) shows the rather locally rough surface indicating uneven fracture of small pieces. A crack is apparent and this crack is assumed to propagate during the next pass, fracturing pieces away. As discussed previously for the view on the side flank face, substantial tool material loss and blunting occurred during the next pass (third pass). This is better shown in the image viewed from the bottom flank face (Figure 3-5d) showing swelling of the tool insert. In the viewing the rake face, after each run the used tool was positioned in the SEM chamber and the images in Figure 3-6 were taken normal (90° rotated) to the rake face, explained previously in Chapter 2 (section 2.6). Figure 3-6b confirms no observable tool material loss resulting from flank wear after the first pass. The images taken of the rake face (Figure 3-6c) do not indicate the magnitude of tool material loss in the cutting edge (corner) after the second pass, as evident in Figure 3-5c of the bottom flank face. Cracking is visible in the rake face of the tool, in and near the cutting edge parallel to the flank face. An example of which is given in Figure 3-7b. Crack initiation on the rake face in or near the cutting edge (corner) is expected, as there is strong cutting forces acting on the tool during milling as alluded to in Figure 3-3.

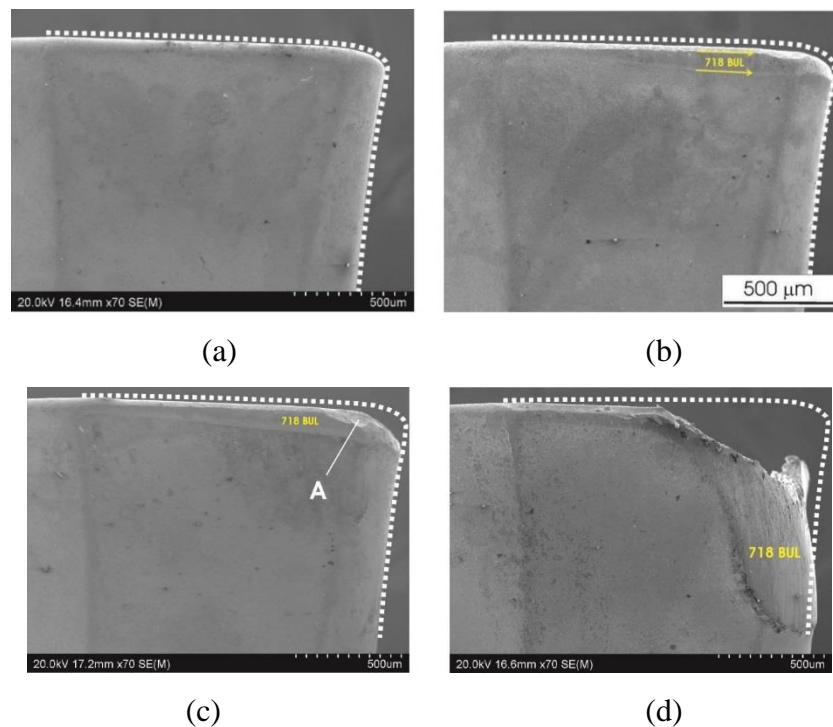


Figure 3-5 SEM images of insert TC2 bottom flank face before and after various passes: (a) before milling with zero pass edge outline (ZPEO), (b) after the first pass together with ZPEO, (c) after the second pass together with ZPEO and (d) after the third pass together with ZPEO. Tooling condition: uncoated carbide and dry

Crack propagation accelerated in the third pass and a large volume of tool material fractured off, clearly seen in Figure 3-6d. The rake face view, together with the view of the bottom flank face (Figure 3-5d), can aid a quantitative measurement on the amount of tool material loss if such measurement is needed in practice. Both views clearly show that the cutting corner is where tool fracture is at its greatest. The large amount of tool material fracturing off in the third pass is consistent with the many cracks in the tool sample observed after the second pass (examples shown in Figure 3-7). The severity of tool deterioration after three passes in insert TC2 experiment may be viewed as comparable to that of the insert TC1 experiment.

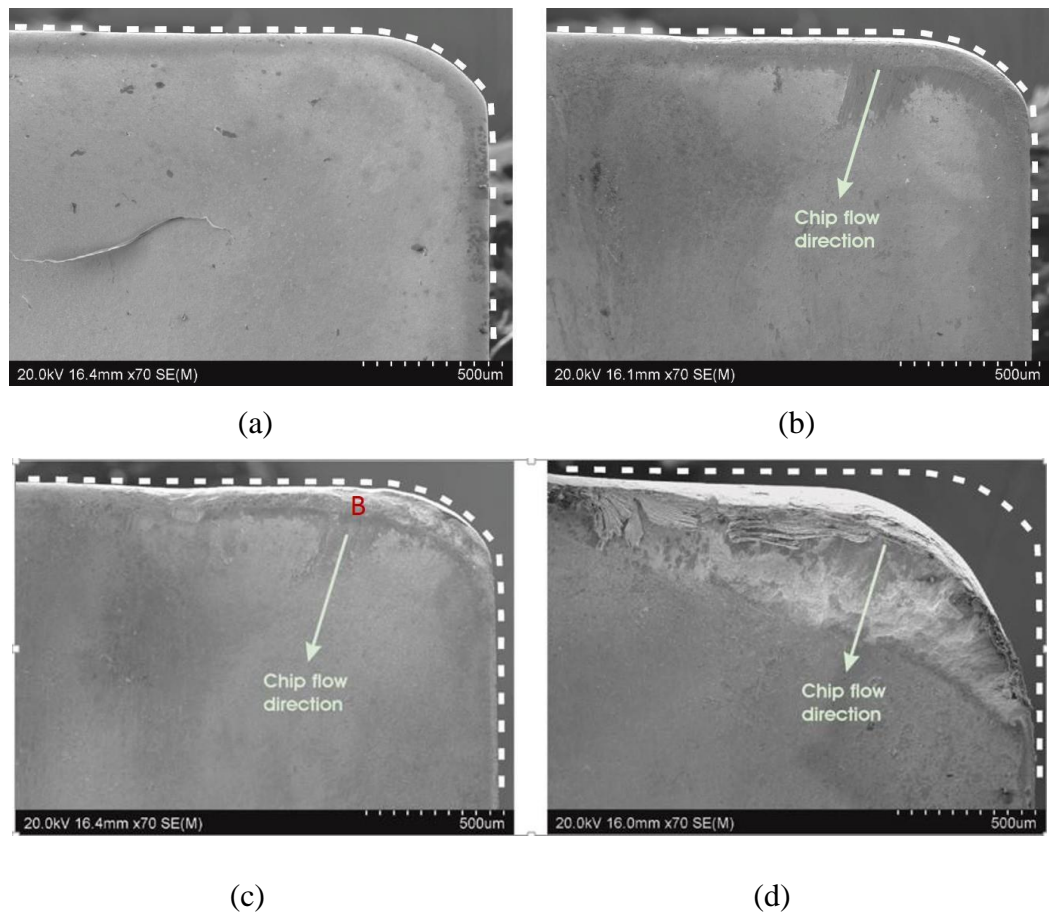


Figure 3-6 SEM images of insert TC2 rake face before and after various passes: (a) before milling with zero pass edge outline (ZPEO), (b) after the first pass together with ZPEO, (c) after the second pass together with ZPEO and (d) after the third pass together with ZPEO, Chip flow direction is indicated by arrow in each pass. Tooling condition: uncoated carbide and dry

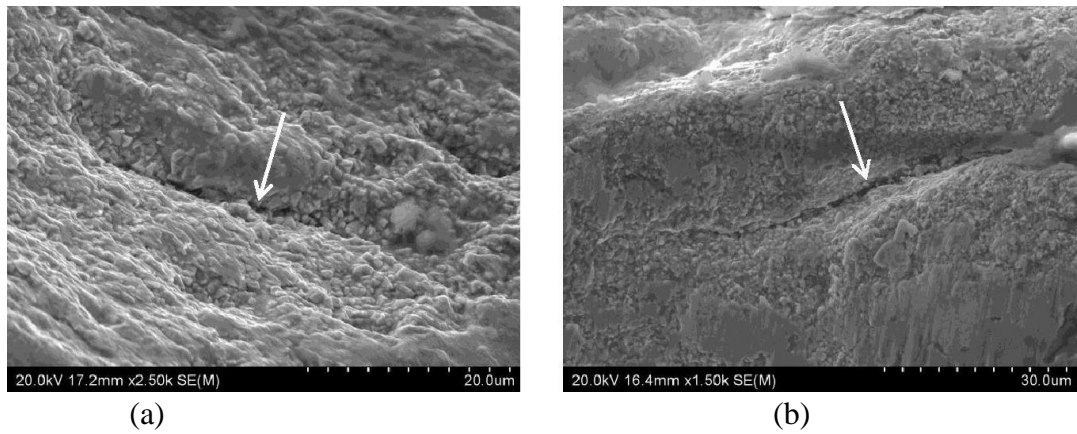


Figure 3-7 Higher magnification images showing cracks as pointed to by arrows in cutting edge: (a) at location A of Figure 3-5c and (b) at location B of Figure 3-6c

3.4 Deterioration of Coated Tools

Qualitatively, coating has altered little the course of the tool deterioration process. As shown in Figure 3-8a, the TiAlN coated Tool TC3 wore through its coating after one pass in the edge area and a long and narrow band of 718 BUL formed similar to that observed on uncoated tools. Damage to the coating was only contained to the edge area and below (away from) the BUL band, the coating was unaffected however, fracture/chipping locally along the cutting edge was quite severe. Evidently, the coating has provided minor protection to the tool and the cutting force impacting/acting on the edge as indicated in Figure 3-3, may have lead to deterioration of the coating on the cutting edge area during this first pass. Figure 3-8b is the corresponding image for insert TC3 after three milling passes. Very severe fracturing and blunting occurred on the side flank face and a large amount of build-up material from rubbing/forging is visible. This build-up may have periodically fractured off, suggested by the large crack across the material in Figure 3-8b.

A further experiment using a coated tool (TC4) presented in Figure 3-9a, confirmed the general tool deterioration process with clear shear fracture extending a distance from the cutting edge. This fracture type is identical to that observed in the uncoated insert TC1 (Figure 3-1c) after two passes, although the severity of fracture in Tool 1 is greater. But in insert TC2 (Figure 3-4) which was uncoated, no large local fracture extending along distance was observed during the tool deterioration process. Local fracture extending significantly outside the cutting edge was also absent in insert TC3 experiment during the second pass. Long distance shear fracture may or may not take place within the first two passes however,

the initiation of many cracks during the second pass caused a high amount of fracturing and tool blunting during the third pass consistent in every experiment conducted.

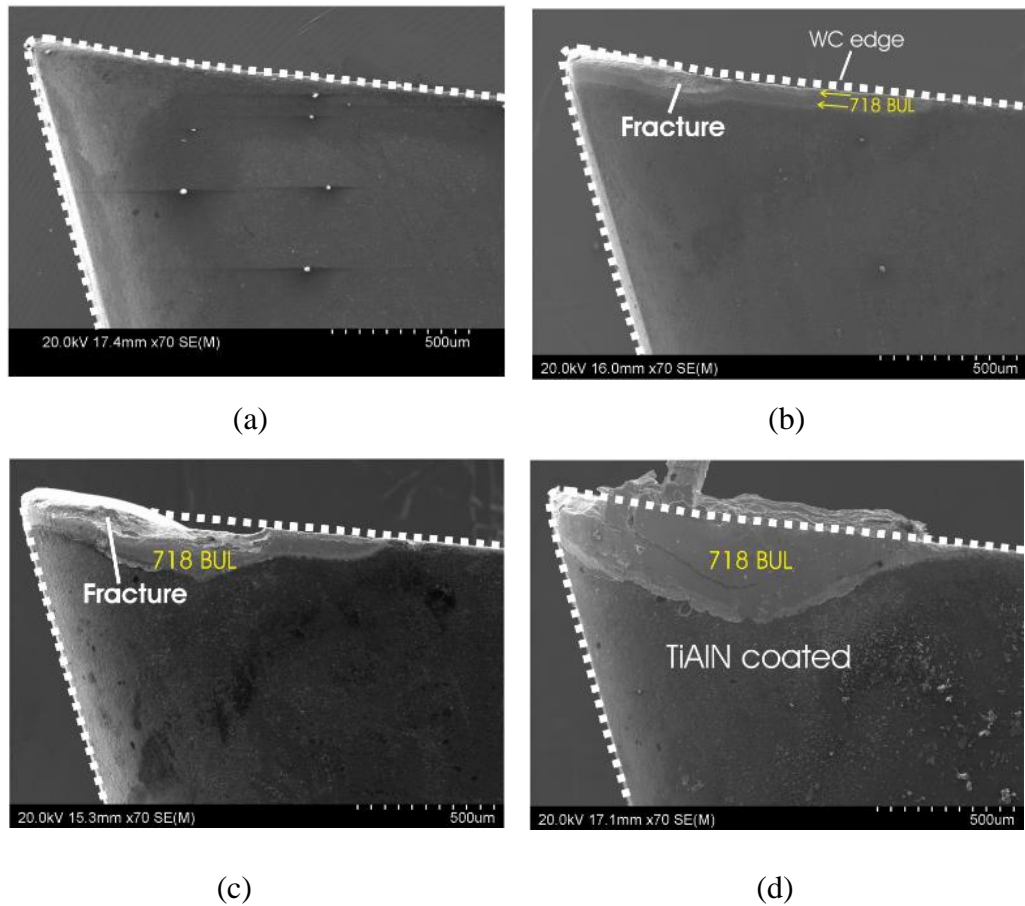


Figure 3-8 SEM images of insert TC3 (TiAlN coated) side flank face after (a) before milling, (b) first pass (c) second passes and (d) third passes. Tooling condition: coated carbide and dry

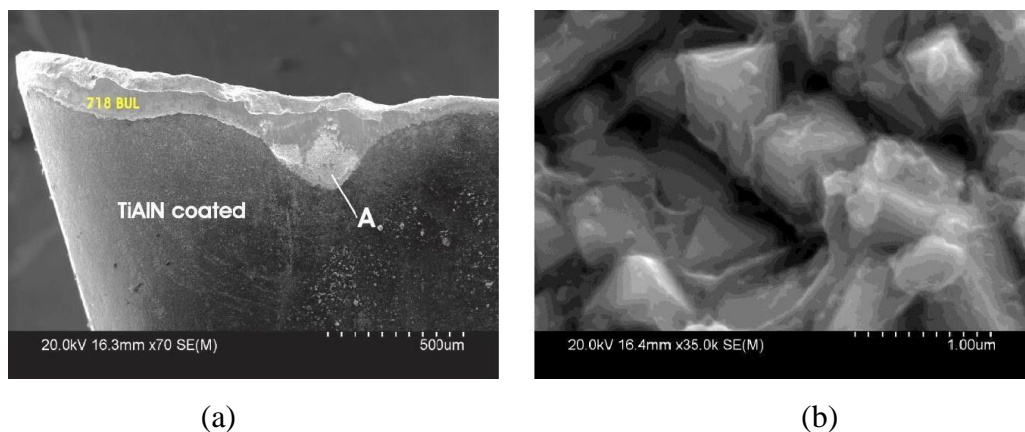


Figure 3-9 SEM images of insert TC4 (TiAlN coated) side flank face after two passes, (a) low magnification and (b) very high magnification in location A in (a). Tooling condition: coated carbide and dry

3.5 Further Discussion on Modes and Measures of Tool Deterioration

It may be generalised that after milling has started, $F_{Cutting-R}$ and $\tau_{Cutting}$ should quickly break and erode away any non WC material or coating in the direct workpiece-tool contact cutting edge. $F_{Cutting-R}$ and $\tau_{Cutting}$ will then cause chipping/fracturing along the cutting edge, further to this $F_{Cutting-R}$ can cause cracking locally with propagation in the flank face side away from the cutting edge. At the same time (in the second pass), multiple cracks initiate on the rake face in and near the cutting edge and propagate along the tool. During the third pass, as cracks propagate and more tool material is fractured off, tool blunting becomes very severe and deterioration accelerates.

As explained previously, measurements of the width of flank wear VB are commonly conducted to represent tool wear, [6-8, 15, 16, 21, 23]. However, as has also been explained, deposits such as BUL affect the accuracy of the VB measurement. The commonly reported VB values in literature are generally measured without considering the deposits. The significance of this effect is seen in the initial milling stage when BUL quickly establishes without measurable changes in shape and size of the tool cutting edge. The inclusion of BUL in VB may explain the initial small but rapid tool wear widely reported, which may mislead the understanding of the tool deterioration process. Chen and Li [4] considered BUE but they failed to explain how the build-up was removed. From their images illustrating the flank wear width, it is difficult to accept the measured wear did not include the build-up width.

As explained previously, assuming accurate measurements of VB were conducted, VB is not necessarily indicative of the amount of tool material lost. It should be noted that tool deterioration directly means tool material loss, according to the ISO standard [15]. In recent work, Uzun et al. [9] took SEM images of bottom flank face estimating the radius of the tool cutting edge of a micro milling 718 alloy establishing the change in cutting edge radius. The radius change as the milling distance increased studied under SEM, provided a more direct assessment of tool deterioration and tool fracturing behaviour. However, as has been explained and illustrated in Figures 3-4 to 3-6, single side tool views may lead to an incomplete assessment of tool deterioration. In the TC2 insert experiment, only the view on the bottom flank does not provide an accurate assessment of the sizeable deterioration in tool cutting edge/corner location.

Nevertheless, Kuttolamadam et al. [49] recently addressed the inadequacies of traditional assessment methods of measuring tool wear and developed a volume tool wear (VTW) quantification method [50]. The overall process of assessing VTW consists of capturing point cloud of data of the cutting tool using a 3D optical surface profiler, importing the 3D data into a suitable format engineering software and constructing a parametric surface/actual model that captures significant surface features. The tool volume damaged during milling is compared to a 3D model of the unused tool and its bounding areas, in order to determine the tool material loss. Despite the thorough evaluation on the tool wear, the technique employed by Kuttolamadam et al. [49] and the model developed does not consider BUL formation. Kuttolamadam et al. [49] does not discuss BUL formation, however in a similar study on turning TiAl4V by Chetan et al. the same BUL was evident on the flank face [51]. Furthermore, the VTW model assumes pure loss of the tool material without considering the VTW rate with gradual BUL formation. It should be mentioned Kuttolamadam et al. [49] valuable publication was published in 2015 is however after we have reported our present work in 2014 [52].

Although the volume of tool material loss was not measured, the term “severity of deterioration” can be used as a quantitative measure to summarise and indicate how severely a tool has deteriorated. A summary plot is drawn in Figure 3-10 illustrating after three passes, all 4 tools have completely deteriorated and thus the severity can be treated as having reached a maximum of 10 with zero corresponding to no deterioration. The small progressive edge wear was considered insignificant and did not reach a severity value of 1 even after three passes, suggesting tools without fracture could retain a long life. During the first pass, edge micro-chipping took place the size of which could be as big as the initial and small cutting edge or many times smaller. As the chipping is small the severity is treated as <1 . During the second pass, edge chipping became more severe extending shear fracture to the outside the cutting edge at various distances. This increased the severity but it either could remain low (treated as ~ 1) or could become much higher (>2 indicatively). Regardless, cracks initiated in the second and third pass accelerated fracturing during the third pass with a rapid increase in severity to a maximum of 10.

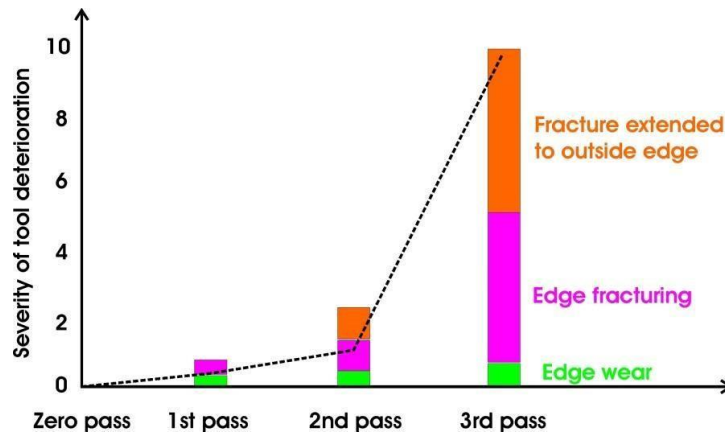


Figure 3-10 Schematic summary of severity of tool deterioration observed in this study

3.6 Mode of Fracture

In considering tool fracture behaviour, refer to Figure 3-9a where the extended area of fracture is away from the cutting area and alloy 718 material has not rubbed onto the fractured surface. Thus, features of fracture can be further examined. In the very high magnification image of Figure 3-9b, a ridge appearance of the Co-binder between WC grains is observed suggesting substantial tearing of the binder material. The original Co-binder material (see also Figure 3-3b) between WC grains tears and deforms leading to fracture under the strong loading condition during milling. Under high cutting forces and temperatures, the low strength and ductile binder material likely deformed and tore, unbinding and thus fracturing in the regions between WC grains. Thus, although it may be seen as an “intergranular” fracture, it is primarily due to the ductile fracture of Co binder material, although WC–Co interface debonding cannot be ruled out.

In the textbook “Engineering Materials 2 “ by Ashby and Jones, page 254 in [53], WC-Co cutting tool material failure mechanism during machining has been stated to be predominantly cracking through the WC grains. This mechanism is however not supported by the observation made here during milling of Ni-based superalloy which is failure through the Co binder dominant.

As expressed in the review by Zhu et al. [12], it is generally known that the very high temperature in the cutting area during machining of Ni alloys is a major factor in shortening tool life in which the author notes temperatures in excess of 1000 °C during milling. These temperature measurements may have based on measurements made by Kitagawa et al. [54]

in the turning of 718 alloy. For a set V_c of 50 m/min, temperature measured in a location near the cutting edge was close to 1000 °C, thus the maximum temperature in cutting edge is expected to be greater than 1000 °C. The strength of the Co-binder is quite low above 1000 °C, an example of which the compressive strength of Co alloys at 1000 °C is slightly below 200 MPa but $d\sigma/dT \approx 15$ MPa/10 °C [55]. Therefore, if the temperature is increased from 1000 °C to 1050 °C, the flow stress will decrease to ~ 120 MPa. Henceforth, it is reasonable to assume that the Co binder to deform to failure during machining as $F_{Cutting-R}$ and $\tau_{Cutting}$ need to be sufficiently high for workpiece material removal.

3.7 Summary

The short life of WC–Co tool inserts during the milling of 718Plus Ni alloy is the result of a tool deterioration process dominated by fracturing. After milling starts, chipping fracture follows in the cutting edge region, at the same time cracking/ fracturing can extend a longer distance in the subsurface region along the flank face. The forms of these fracture processes directly relate to the forces acting on the cutting region. The process commences by crack initiation in the binder between WC grains and propagates between the grains. The major contribution of this fracture mode is the deformation to fracture of Co binder material. As tool fracturing and thus blunting proceeds, the tool loses its function of cutting the workpiece. Instead, rubbing/forging between the workpiece and the tool dominates. Views from the bottom flank face and rake face in a consistent manner, in addition to viewing the major flank face not only allow the fracturing progression to be revealed but also allow for a correct estimation of tool material loss. Although tool life is short, there is a stage of incubation when cracks initiate in or near the cutting edge on the side of rake face before severe fracturing and thus accelerating tool blunting. Qualitatively, coating of the tool by TiAlN has little effect on the tool deterioration process. This is because the coating in the cutting edge region breaks off under the milling conditions, soon after milling starts.

Chapter 4: Cutting Force and Progression of Tool Deterioration

The results and observations from the extensive series of experiments on cutting force (F) monitoring as the tool deteriorates are presented in this chapter first. Cutting force is correlated with the conventional flank wear (VB_{max}) which has been measured for each pass. This correlation affected by the various deterioration modes will then be explained in detail. Results from the effect of edge deterioration/blunting in reducing the effective rake angle and thus increasing F is suggested and discussed. Following this, the indirect observation on deformation zone during cutting is presented and is used to explain why the use of coolant does not affect tool deterioration and cutting force. Finally, results are presented for and a discussion is made on the effect of increasing feed rate on tool deterioration and cutting force.

4.1 Features of Forces During Milling

The understanding of features of the force during milling 718Plus nickel based alloy was achieved by conducting four milling with different tooling conditions (TC) which were TC5, TC6, TC7 and TC8 (refer to Table 2-3 in Chapter 2). TC5 refers to uncoated and dry, TC6 to coated and dry, TC7 refers to uncoated and wet (coolant) and TC8 refers to coated and wet (coolant). A repetition experiment was conducted for each tooling condition.

In the International Standard ISO 3002/4 [72]: Basic quantities in cutting and grinding Part 4: F_f , F_{fN} , F_p are used to represent F_x , F_y and F_z . In this study, F_x , F_y , F_z and F are used as the terminology to represent the cutting forces because they are commonly used in most published literature [6, 7, 21, 23, 49, 54]. In each milling pass, after the tool has started moving forward (relative to the machine bed), the recording of the dynamometer data was turned on normally just before the tool insert started engaging in milling. This start is indicated as “Milling start” as shown Figure 4-1. It then took just under 10 s for the tool to have moved a distance equal to the radius of the tool (holder plus insert), by which time the insert started milling the whole width equal to a_e , marked as “Full a_e milling” in Figure 4-1.

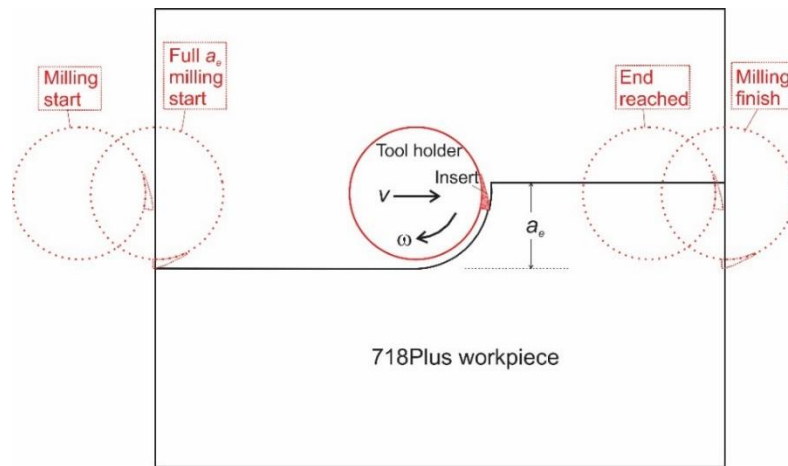


Figure 4-1 Schematic view looking down on the workpiece and tool-insert with various stages of the tool during the pass indicated

In order to observe and monitor the features, cutting force data from two milling passes, one from the first and the other from the fourth of the same insert are plotted in Figure 4-2. They are used to illustrate the various features of F_x , F_y and F_z and the cutting force (F) (also designated in ISO 3002/4):

$$F = \sqrt{F_x^2 + F_y^2 + F_z^2} \quad 4-1$$

The initial milling stage is further discussed using data plotted in Figure 4-3. During the first milling cycle, maximum F_x and F_y values (both ~ 50 N) were low and $F_z \approx 0$. Within this first cycle F (not shown in detail) increased and reduced to zero within 0.002 s. Geometrically, we may use the illustration in Figure 4-4a to explain. If we assume the insert in a rotating cycle has just reached the workpiece, cutting will start next cycle, cutting an area as hatched with a lateral distance ~ 1.8 mm ($= 2 \times \sqrt{(8 - 0.05)^2 - 8^2}$ mm $= 2 \times 0.89$ mm), thus taking ~ 0.002 s ($\approx [1.8 \text{ mm}/3.14 \times 16 \text{ mm}] \times 0.06 \text{ s}$).

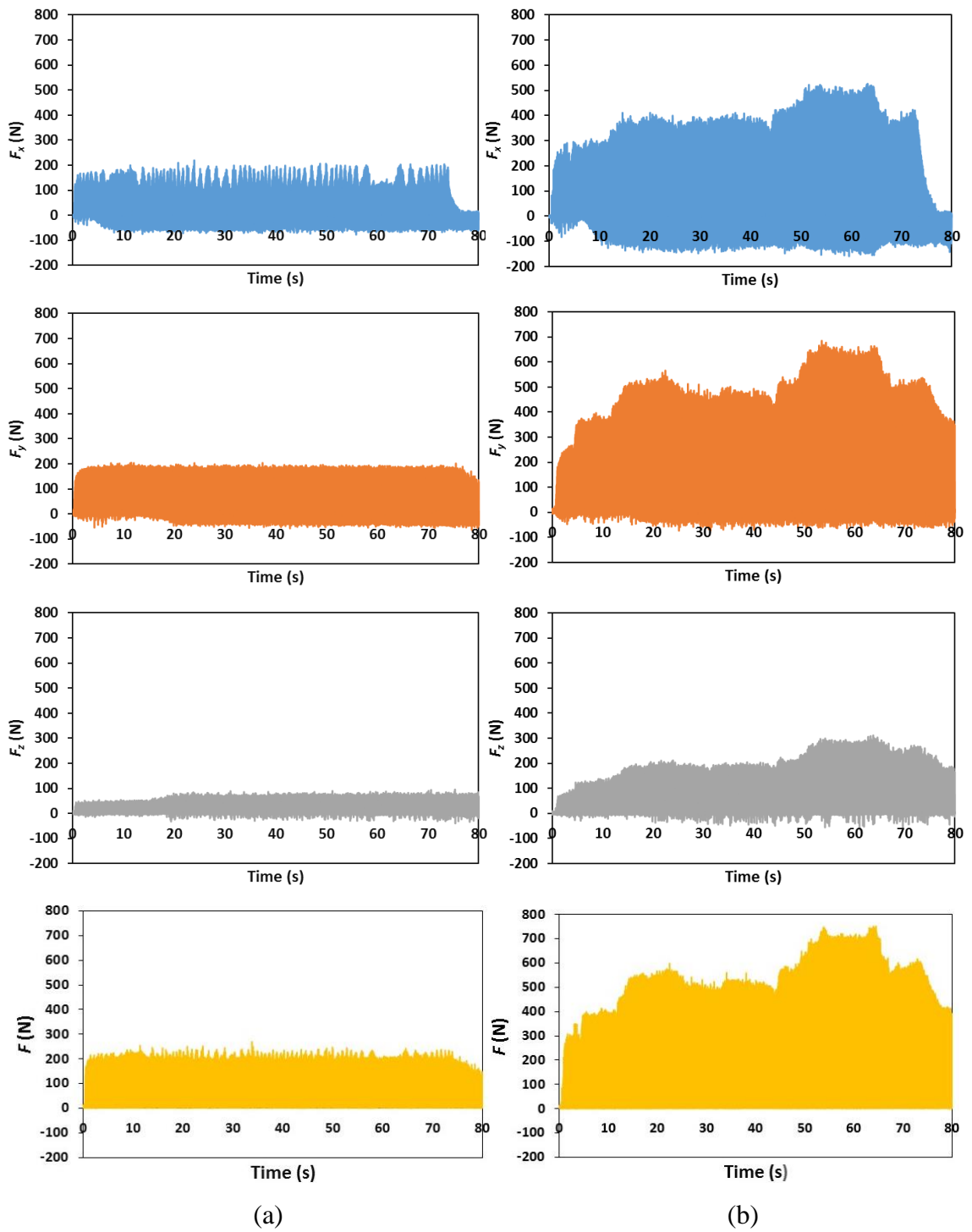


Figure 4-2 The whole F_x , F_y , F_z and F curves (recorded data) of (a) the first milling pass and (b) the fourth milling pass. Tooling condition: uncoated and coolant (TC7-2)

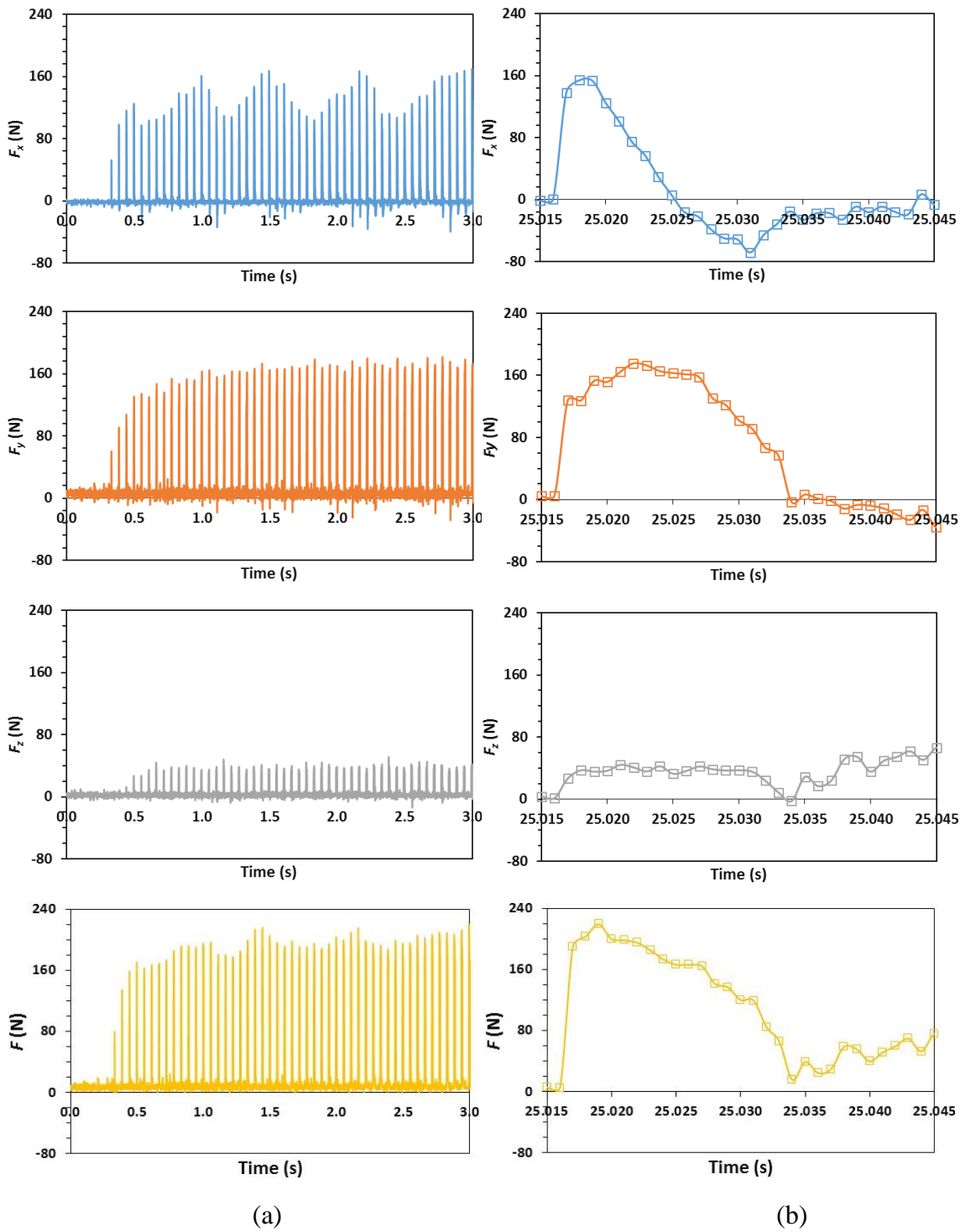


Figure 4-3 F_x , F_y , F_z and F data/curves of the first pass during (a) the initial and within 3 s of milling engagement and (b) a half milling cycle time in early milling stage. Tooling condition: uncoated and coolant (TC7-2)

In the next few cycles, along with an increasing cutting width from ~ 1.8 mm, maximum F_x , F_y , F_z and thus F values rapidly increased. Later, after the start of full a_e milling, the cutting length from the start to finish within a cycle, as indicated in Figure 4-4b, was 14 mm ($= R_{tool+insert} \times 3.14/2 + 1$ mm). Along this length, the thickness of cut (d_{c-w}) was 0.05 mm (value of FR) initially, then decreasing gradually to zero. In a cycle, as plotted in Figure 4-

3b, F soon reached the peak and then gradually decreased to close to zero within 0.018 s ($\approx 25.034\text{s}-25.016\text{s}$). This is consistent with the decreasing d_{c-w} along the cutting length with a calculated cutting time close to 0.017 s ($\approx \text{cycle time} \times \text{cutting length} / \text{circumference of the tool/insert} = 0.06 \text{ s} \times 14 \text{ mm} / (3.14 \times 16 \text{ mm})$).

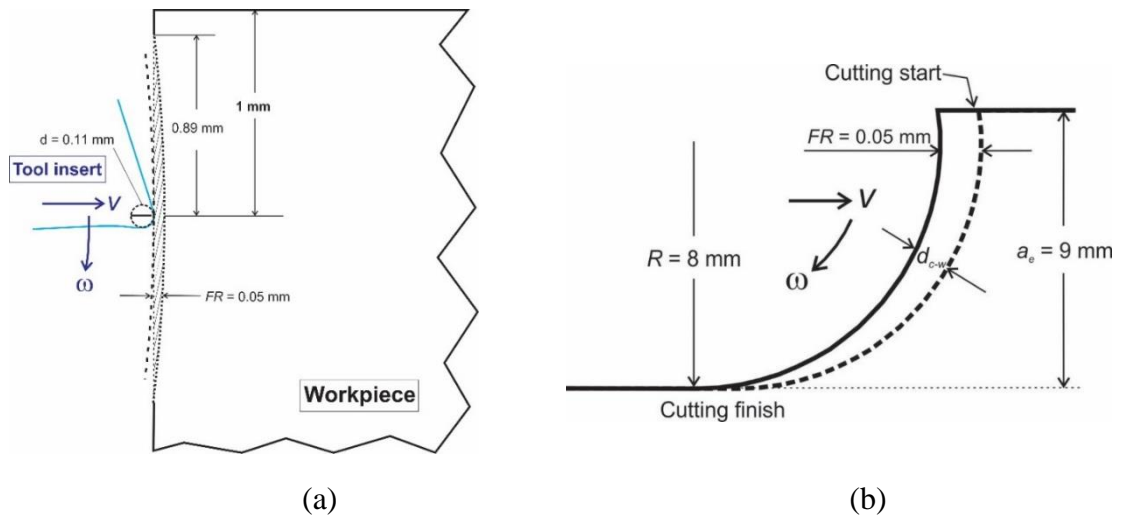


Figure 4-4 Geometrical representation of milling, viewing down: (a) at the start of milling engagement meaning the first cycle of a pass, and (b) during a normal milling cycle that the tool insert cuts the workpiece with a full lateral distance (radial depth of cut), a_e . Distance of FR and thus d_{c-w} are not drawn in proportion

After the initial milling engagement, the tool continued for $\sim 72 \text{ s}$ to reach the other end marked as “End reached” in Figure 4-1. The maximum force values (denoted as F_{x-m} , F_{y-m} , F_{z-m} and F_m) started to decrease when the end was reached, at 73-74 s (72 s plus 1-2 s of dynamometer turned on ahead of milling engagement) of the force recording time, as shown in Figure 4-2b. Thus, average F_{x-m} , F_{y-m} , F_{z-m} and F_m values during a 3 s period before the force values started to decrease, meaning between 70 to 73 s, as shown in Figure 4-5 for the example of the 4th pass, can be taken as the force values corresponding to the end of that pass. These F_{x-m} , F_{y-m} , F_{z-m} and F_m values toward the end of the pass are denoted as F_{x-e-m} , F_{y-e-m} , F_{z-e-m} and F_{e-m} , as also indicated in Figure 4-5a. These values are used to approximately relate the state of the tool insert condition (deterioration) after that milling pass. There are two major features that can be seen by comparing the force data of the first pass to the data of the fourth (and final) pass, shown in Figures 4-2, 4-3, and 4-5. First, F_m increased from $\sim 200 \text{ N}$ to 600 N or higher.

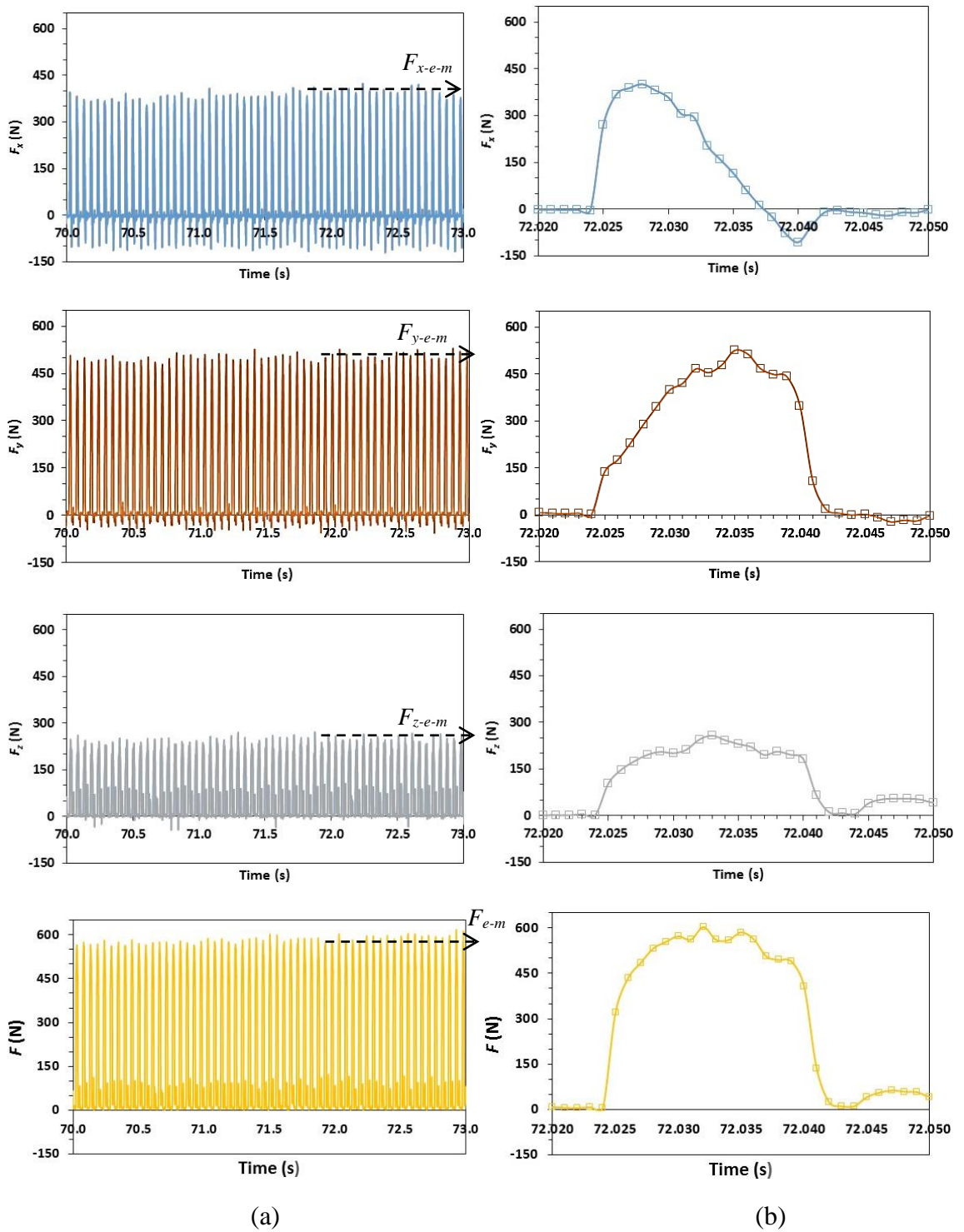


Figure 4-5 F_x , F_y , F_z and F data/curves of the fourth pass during (a) a 3 s period just before the insert reached the end of the workpiece and (b) a half milling cycle time within a period. Tooling condition: uncoated and coolant (TC7-2)

Second, comparing Figure 4-5b to Figure 4-3b (different scales), the rapid increase in F in the beginning of a cycle was the same but for the fourth pass F remained high for most of the cutting length within the same cutting time of ~ 0.016 s. Furthermore, there are three

further features that need to be noted. The first is a periodicity observed in F_{x-m} , but not in F_{y-m} and F_{z-m} in first pass as shown in Figure 4-2a and Figure 4-3a. The source of this is unclear. The values of ΔF_{x-m} were between 60-70 N and $\Delta F = 20-30$ N which is $\sim 10\%$ F in the first pass, but during the subsequent passes when F_{x-m} increased the periodicity became less clear and ΔF_{x-m} reduced. As shown in Figure 4-5a, when F_{x-m} was high, periodicity disappeared and thus ΔF_{x-m} was zero. The second further feature, which can be observed in Figure 4-2b, refers to the varying and irregular (up and down) force values particularly observed in the final pass when the tool insert has deteriorated significantly. The third further feature is the effect of the blunting of the tool insert and trend of cutting force that could be observed by taking examples of F_{y-m} from Figure 4-3b and Figure 4-5b. By comparing these Figures, a rapid increase in F_{y-m} (Figure 4-3b) occurred within the first 0.003s of the first milling pass with a gradual increase to reach the maximum F_{y-m} and slow gradual decrease until the end of the pass. This indicates that the tool insert was still sharp and has a high tendency to mill the workpiece. Meanwhile in Figure 4-5b, a more gradual increase in F_{y-m} is observed resulted by the tool blunting and fracture evident by the rapid decrease of F_{y-m} at the end of the milling pass.

4.2 Examination on the Effect of Coating on Cutting Force

As demonstrated in previous chapter, the use of coating does not significantly affect tool life. Reasons for this have already been shown and explained. In order to investigate the significance of applying the coating layer, the cutting force (F) of the initial 3 s of milling engagement for the first pass of each uncoated and coated tools (TC5-TC8) is presented in Figure 4-6. By monitoring the initial force, the effect of the coated tool on the cutting force (F) can be witnessed. From the figure, it is observed that the average values (initial) of F for coated tools were 210-270 N which shown in Figure 4-6 (c-d) and Figure 4-6 (g-h). Meanwhile for uncoated tools, F values were 170-205 N as presented in Figure 4-6 (a-b) and Figure 4-6 (e-f). This means that F values at the initial 3 s of milling for coated tools were slightly higher than the uncoated tools. Thus, based on the F values measured application of a coating does not provide lubrication to reduce frictional and thus the total force as suggested in literature, it was unlikely that the coating provided a protection layer to the tool insert. Furthermore, Figure 4-7 shows the tool condition at the end of the first milling pass. After the first pass, build-up edge (BUE) dominated on the flank face of the uncoated and coated tools resulting in a VB_{max} 0.1 mm overall.

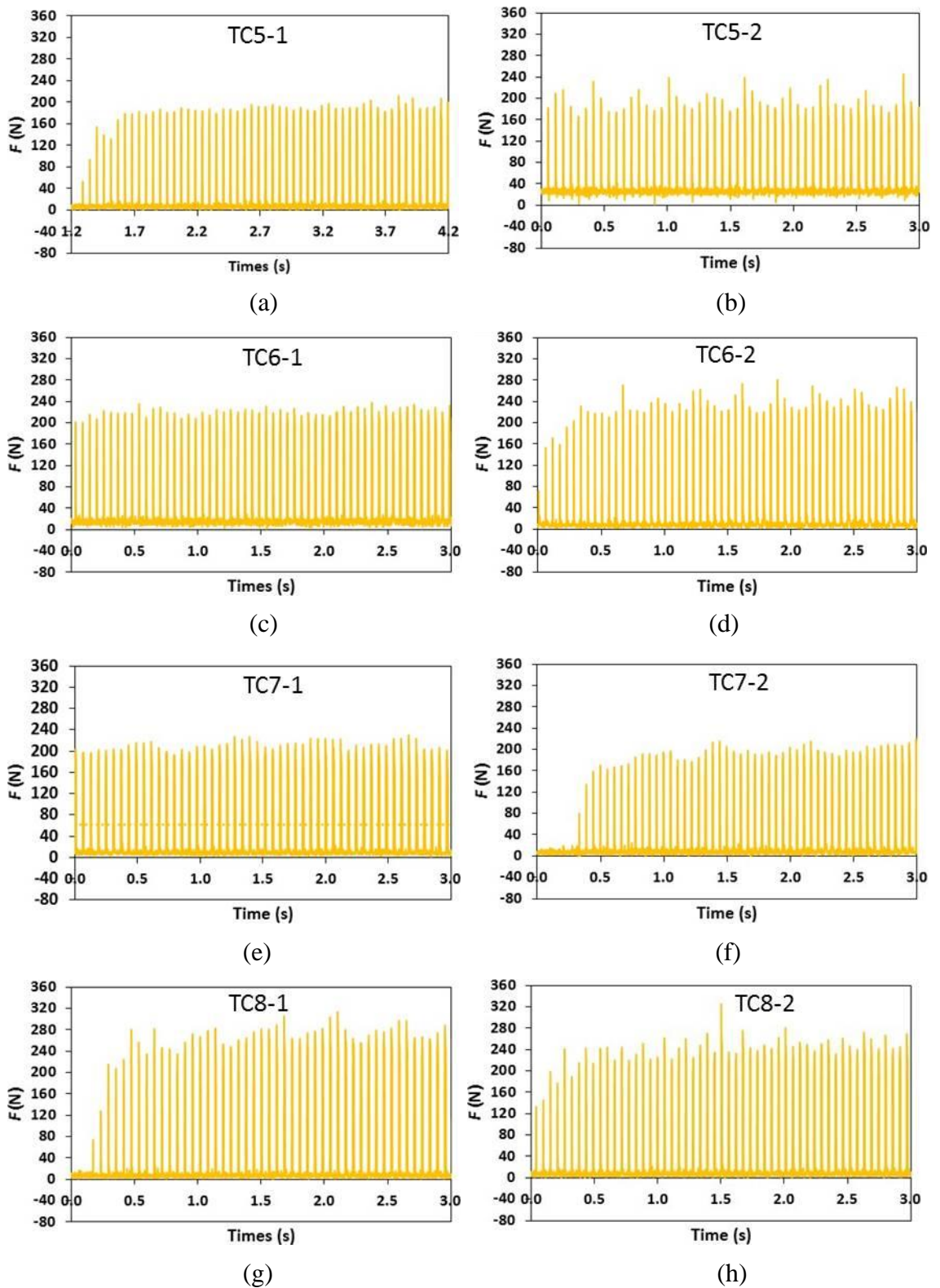


Figure 4-6 Cutting force (F) data/curves of the first pass during the initial 3s of milling engagement of tool conditions; (a)-(b) uncoated and dry, (c)-(d) coated and dry, (e)-(f) uncoated and coolant and (g)-(h) coated and coolant

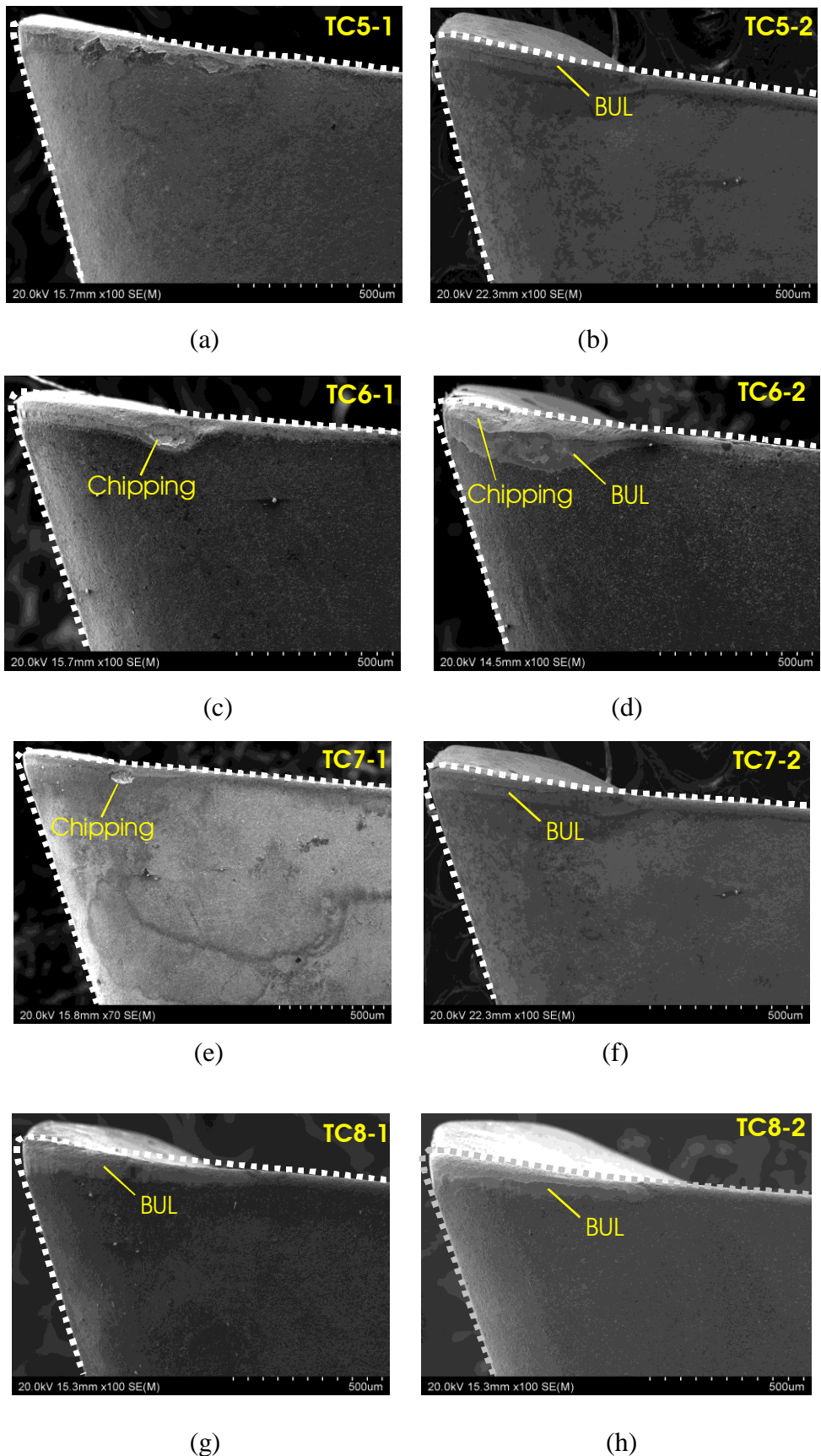


Figure 4-7 SEM images of side flank faces after the first pass of milling of tool conditions: (a)-(b) uncoated and dry, (c)-(d) coated and dry, (e)-(f) uncoated and coolant and (g)-(h) coated and coolant

However for coated tools in tool condition TC6-1 (Figure 4-7c) and TC6-2 (Figure 4-7d), chipping on the flank face of TC6-1 and on the cutting edge (TC6-2) dominated causing VB_{max} of 0.13 mm and 0.22 mm respectively. These values of VB_{max} were marginally higher than those measured after the first pass for the uncoated tools. Based on this observation, the coating layers of the coated tools were peeling off after the first pass and the performance of the coated tools were almost similar to the uncoated tools as has already been concluded in the previous chapter. TiAlN coating layer with a thickness of 4 μm [56] on the tool insert does not provide extra protection to the tool insert when machining difficult-to-cut material. Thus, the application of coating layers on the tool inserts does not necessarily assist in reducing the initial wear and cutting forces.

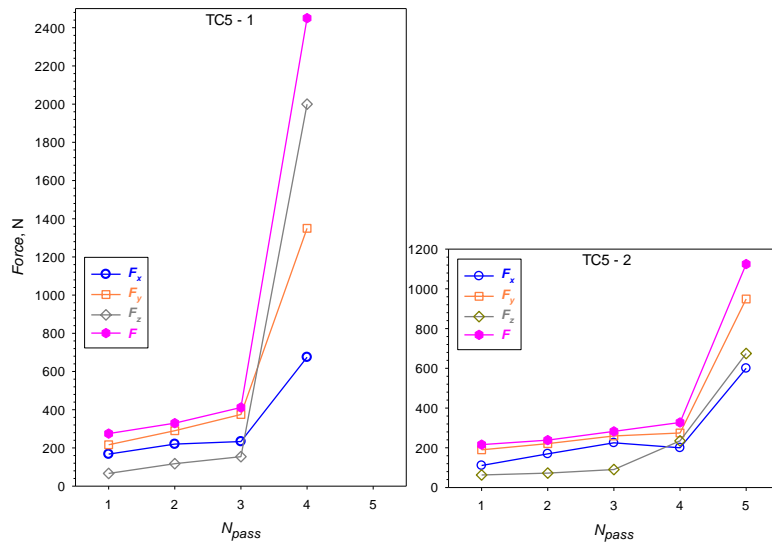
4.3 Effect of Tool Deterioration on Cutting Force

As has been explained in (Chapter 1) the understanding of the effect of tool deterioration on the cutting force (F) during milling 718Plus Ni-based superalloy is important to improve the machinability of the alloy. It also clarifies whether the cutting force (F) method is suitable to monitor tool deterioration. In order to investigate this correlation, the maximum cutting forces towards the end of the milling pass (F_{x-e-m} , F_{y-e-m} , F_{z-e-m} and F_{e-m}) against the number of passes (N_{pass}) are plotted in in Figure 4-8. In all the first passes, force values were low with an average F_{e-m} value equal to 266 N (standard deviation 33 N from 8 data/experiments), whereas a small increase from an average F_m value equal to 222 N (standard deviation 20 N) was measured in the beginning of full a_e milling in the first passes. In the second passes, ΔF_{e-m} remained small in six experiments, but in two experiments (Figure 4-8b) F_{e-m} increased considerably. It should be noted that although these two were from the same tooling condition, the second experiment was conducted after a number of milling experiments at other conditions. Excluding these two, in the other six, small to moderate (ΔF_{e-m} up to 80N) increases of F_{e-m} can be seen in the third passes. In the fourth passes, ΔF_{e-m} values ranged from zero to 150 N (TC5-2, TC7-1, TC7-2, TC8-1 and TC8-2), although in one (TC5-1) ΔF_{e-m} exceeded 2,000 N. In the milling experiments with F_{e-m} less than 400 N in the fourth passes (TC5-2, TC8-1 and TC8-2) a further pass was conducted following.

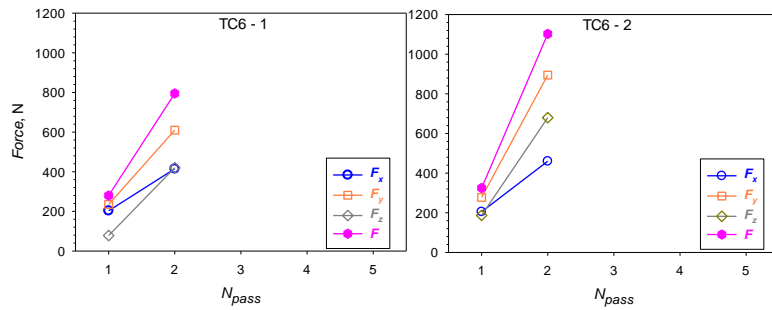
The data in Figure 4-8 may have suggested that milling using coolant could reduce F . The effect of using coating on F may be confusing. For one case, in the second passes, F_{e-m} values had already become very high (> 800 N) when dry cutting conditions were used with coated

inserts as shown in Figure 4-8b. While alternately, in the two wet (coolant) milling experiments using coated inserts, after five passes F_{e-m} is still ~ 500 N or slightly higher as can be seen in Figure 4-8d. The disappearance of the coating in the cutting edge area, exposing WC grains after the first pass in wet (coolant) milling conditions is clearly shown in Figure 4-9a. This erosion of the coating is the same as that which occurred in the dry milling condition and has been explained with more detail in Chapter 3. Considering that F_{e-m} is quite consistent and low in the first passes and that coating, if it is a coated insert, has been eroded away in cutting edges also in first passes, any trends of F_{e-m} variation as N_{pass} increased was not due to the coating.

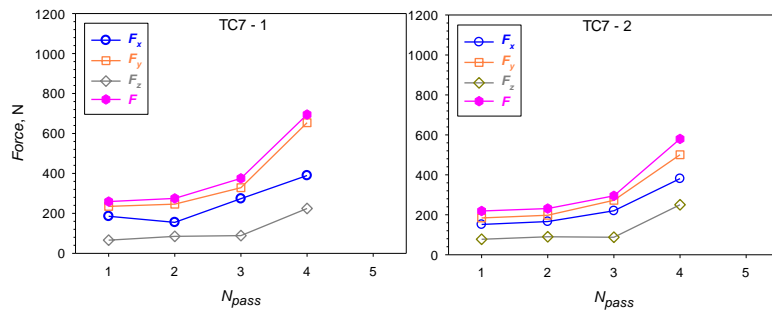
Clearly, as shown in Figure 4-9b, the cutting edge deteriorated quite significantly after five passes, although the insert could still be regarded as being usable as the F_{e-m} value of 505 N, was not very high. As already explained in the Chapter 1, the established method to indicate deterioration during milling of Ni superalloy is flank wear, in the form of VB (uniform) or VB_{max} (non-uniform) following ISO 8688-2 [22]. Accurate measurements of the affected width in flank wear was conducted using SEM images aided by the outline of the insert before milling to enable the measurement of the truly affected distance, which is VB_{max} , as indicated in Figure 4-9. In Figure 4-10, VB_{max} values are plotted against N_{pass} . In most cases, VB_{max} was ~ 0.1 mm after the first pass, which includes the projected distance of cutting edge and the build-up layer on the flank face, shown in Figure 4-9a. It should be pointed out that, as has been explained in Chapter 3, a portion of the build-up layer (BUL) is part of the cutting edge but a portion of the layer extends outside the edge, that the insert material underneath may not have been mechanically affected. Thus, a measured VB or VB_{max} , is a slightly overestimated value of the affected width. An example of SEM energy dispersive spectroscopy (EDS) analysis is given in Figure 4-9c, showing that compositionally BUL is of the 718Plus Ni-based superalloy workpiece material.



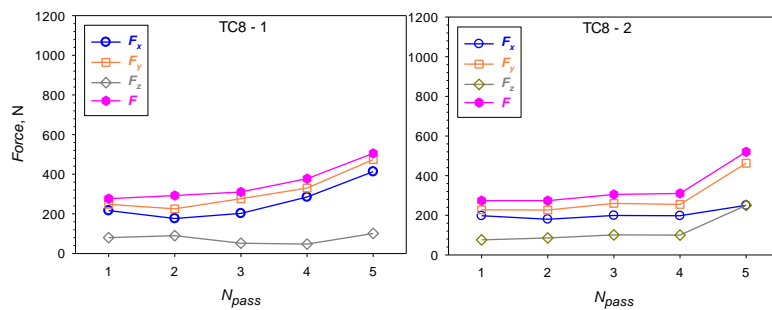
(a)



(b)



(c)



(d)

Figure 4-8 Average maximum force values F_{x-e-m} , F_{y-e-m} , F_{z-e-m} and F_{e-m} versus the number of passes for the four tooling conditions, (a) uncoated and dry, (b) coated and dry, (c) uncoated and coolant and (d) coated and coolant

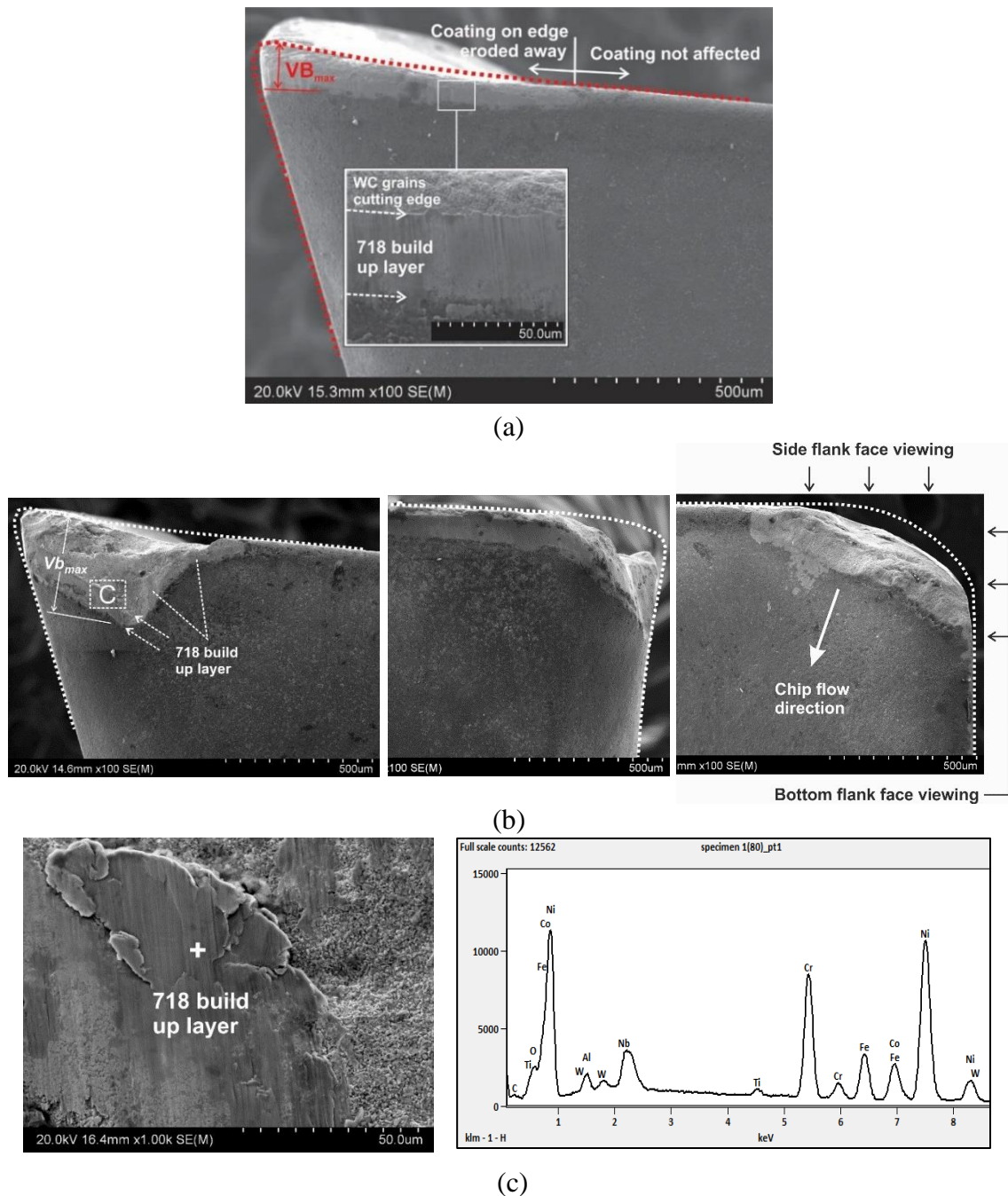


Figure 4-9 SEM images of coated insert and wet (coolant) conditions (TC8-1): (a) side flank face of the insert after the first pass (coating eroded on edge and workpiece build-up are indicated), (b) left - side flank face, mid - bottom flank face and right - rake face, respectively, of the insert after five passes, and (c) left - higher magnification image in location marked C in (b) and right – EDS spectrum with analytical spot + marked in the left image. In the right image of (b), how the side flank face view corresponds in the right image and bottom flank view in the mid image are indicated

In general, there are similarities in the trends of increasing VB_{max} (Figure 4-10) and of increasing F_{e-m} (Figure 4-8) with sequential N_{pass} . However, $F_{e-m} - VB_{max}$ correlation needs to be examined more closely and thus F_{e-m} values have been plotted against VB_{max} in Figure

4-11. It is noted in the figure that data from all TC conditions scatter widely. A high dF/dVB_{max} curve and a low dF/dVB_{max} curve closely fitting the upper and lower boundary data respectively, are drawn in the figure to aid discussion. Extrapolating VB_{max} to ~ 0.1 mm would correlate to the lowest F_{e-m} value (~ 200 N) in first passes.

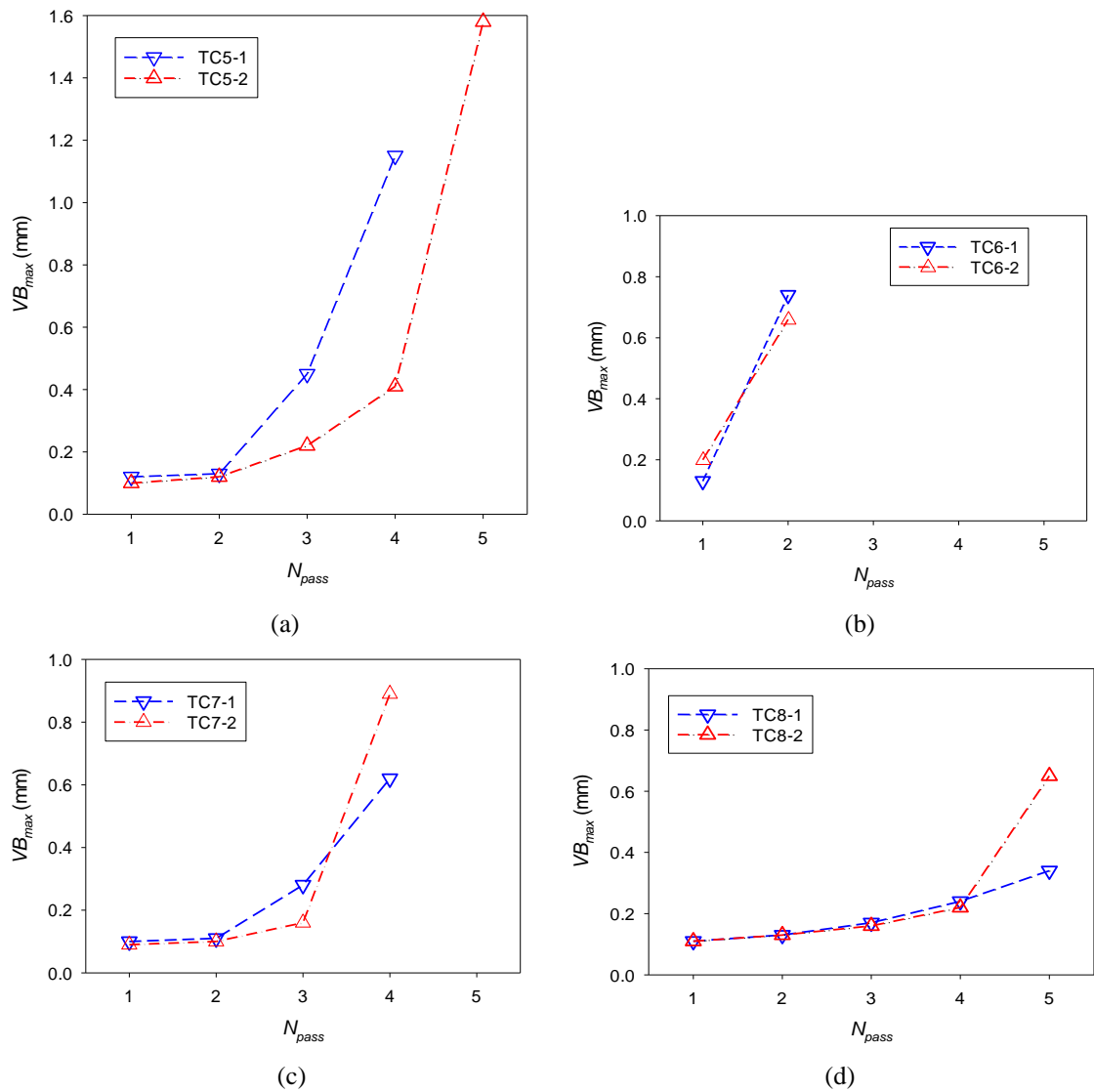


Figure 4-10 VB_{max} verses the number of passes for the four milling conditions, (a) uncoated and dry, (b) coated and dry, (c) uncoated and coolant and (d) coated and coolant

Figure 4-11 shows that F_{e-m} generally increases as VB_{max} increases but, particularly when $VB_{max} > \sim 0.3$ mm, F_{e-m} increasingly relates poorly to VB_{max} . As is widely known and used, ISO 8688-2 specifies criteria for the tool to deteriorate to an unacceptable level when VB has reached 0.3 mm or $VB_{max} = 0.5$ mm. A new method to evaluate the machinability of difficult-to-cut materials by evaluating the constants of Taylor's formula of tool life, as proposed by Wang et al. [23], also is based on ISO VB or VB_{max} criteria. Thus, if F is to be used for

indicating the state of the tool, F needs to correlate well with VB or VB_{max} . Since the correlation is poor in this work (Figure 4-11), further examination below is mandatory. The point marked as point A in Figure 4-11 is for the insert (TC8-1) after five passes, shown in Figure 4-9b. As $VB_{max} = 0.34$ mm, the insert should still be usable, according to ISO 8688-2. The corresponding F_{e-m} is 505 N. As shown in Figure 4-9b, viewing of the side flank face alone and the measured VB_{max} value may indicate but are far from providing sufficient information on how the insert has deteriorated. Further views on the bottom flank face and particularly on the rake face as in the mid and right images of Figure 4-9b respectively, have demonstrated geometrically how the cutting edge/corner of the insert has been eroded and blunted. For point B in Figure 4-11, $F_{e-m} = 580$ N. If the high dF/dVB_{max} curve in the figure was followed and for an F_{e-m} increase from 505 N to 580 N, VB_{max} should be ~ 0.4 mm and the insert should still be usable. However, insert of point B has followed the low dF/dVB_{max} curve in Figure 4-11 and thus, for $F_{e-m} = 580$ N, $VB_{max} \approx 0.9$ mm. The high VB_{max} value means the insert has deteriorated well beyond the acceptable level, according to ISO 8688-2, although F_{e-m} is correspondingly not high.

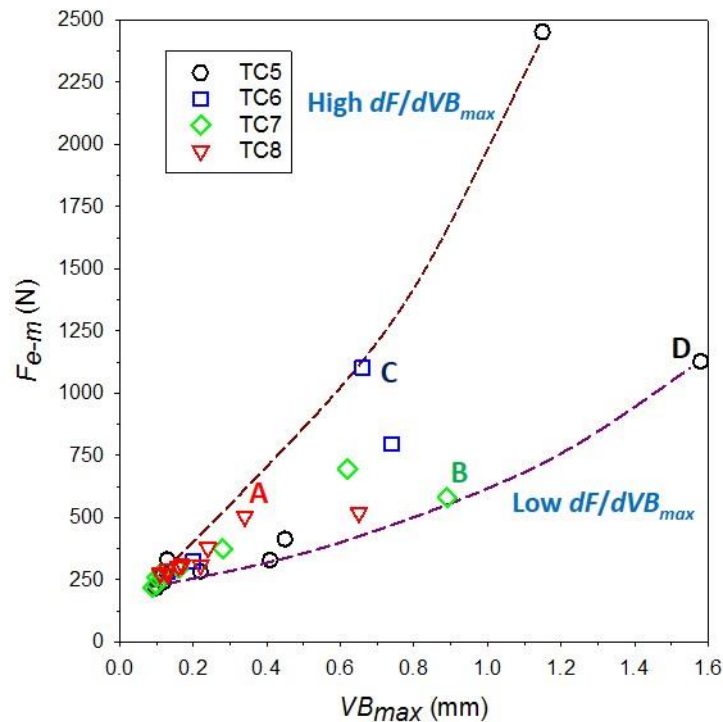
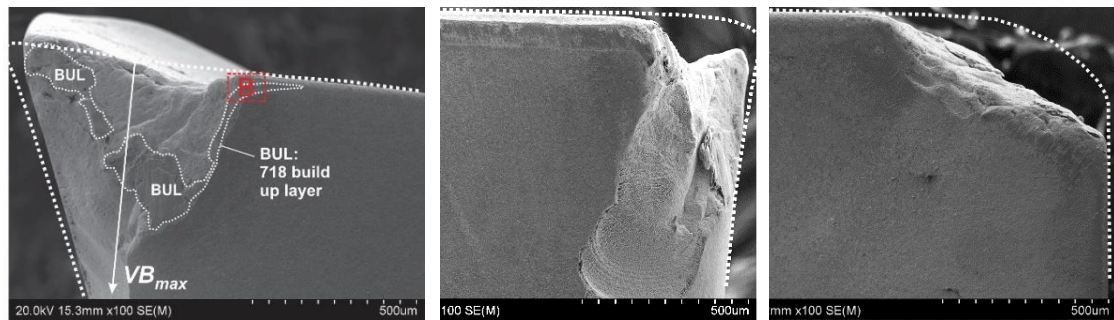


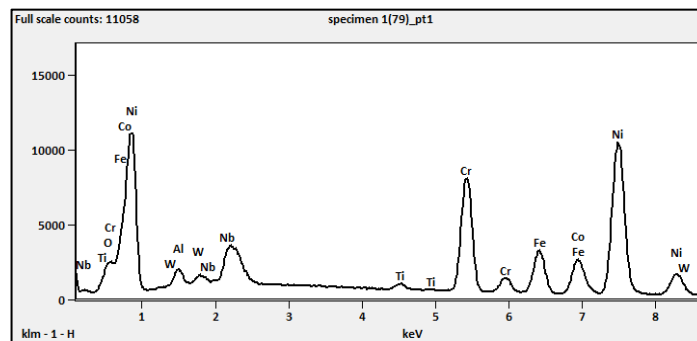
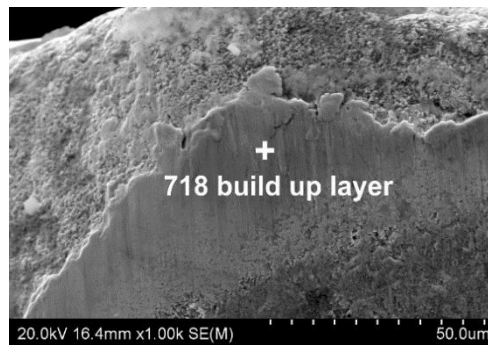
Figure 4-11 F_{e-m} values plotted as a function of VB_{max} .

The major reason for the poor $F_{e-m} - VB_{max}$ relationship may be explained by comparing images in Figure 4-12 to those in Figure 4-9, for the discussed data of point A and point B. As shown in Figure 4-9a and as explained previously, a uniform 718 Ni-Based layer build-

up at the rear portion extending a small distance just behind (below the figure) the cutting edge on the flank face side. The major cutting edge is the area where WC grains have been exposed. Deterioration of the point A insert has resulted in the irregular shape of the cutting edge seen in Figure 4-9b, and a 718 build-up layer can also be observed along the boundary of the irregular cutting edge.



(a)



(b)

Figure 4-12 SEM images of (a) from left to right side flank face, bottom flank face and rake face of insert TC7-2 after four passes (the edge outline of the insert before milling has been superimposed), corresponding to point B in 4-11 and (b) higher magnification image in location marked B in (a) and EDS spectrum (on spot +) on the right

The cutting edge of point B (Figure 4-11) insert, as shown in Figure 4-12 (left), was quite irregular with the deterioration mode of fracturing a long, thin layer along the flank face. Thus $VB_{max} = 0.89$ mm and extended beyond the image. However, the area of fracture below

the 718 Ni-Based build-up layer areas (marked BUL) in Figure 4-12 should have made no contact with the workpiece during milling, meaning that F_{e-m} should only correlate to a fraction of the measured VB_{max} (0.89 mm) and would not correlate the whole measured VB_{max} as well. Further EDS analysis is given in Figure 4-12b, showing that compositionally the BUL is of the 718 workpiece material.

A further pair of data (point C and point D in Fig 4-11) and the corresponding images in Figure 4-13 exemplifies the same justification for the poor $F_{e-m} - VB_{max}$ relationship. For point C, $VB_{max} = 0.66$ mm and $F_{e-m} = 1103$ N, corresponding to a high dF/dVB_{max} point. As can be seen in Figure 4-13a, the cutting corner has broken off and severely eroded away. The result of this should be a large area of the cutting corner contacting and likely forging/rubbing the workpiece during milling, although the real contact width cannot be accurately determined. The large area of 718 alloy build-up may be expected due to forging and rubbing, which is also the reason for the high F_{e-m} value (1103 N). In this point C insert, however, there was no large fracturing of a thin piece along the flank face, thus VB_{max} (= 0.66) is not very high although it has exceeded the unacceptable level at 0.5 mm. For point D (a low dF/dVB_{max} point), $F_{e-m} = 1125$ N, similar to the F_{e-m} value of point C. As shown in Figure 13b, a very long and thin layer fractured off along the flank face, thus $VB_{max} = 1.58$ mm. Judging by the build-up layer area, drawn for clarity in Figure 4-13b, the real cutting contact may not be more than 0.5 mm.

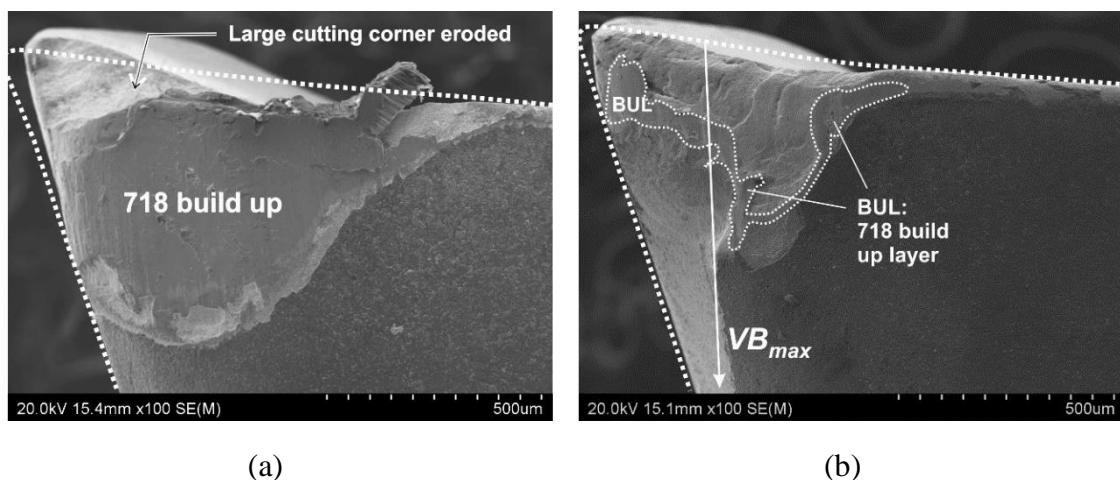


Figure 4-13 SEM images of side flank faces: (a) insert TC7-1 after 4 passes and (b) insert TC5-2 after 5 passes. In each image, the edge outline of the insert before milling has been superimposed

4.4 Further Discussion on Cutting Force Relating to Deterioration of Cutting Edge

This discussion is aided by using the schematic illustrations of insert-workpiece cross sections on the working plane, represented in Figure 4-14. As is illustrated in Figure 4-4a, the cutting edge radius (r_e) is ~ 0.055 mm and was estimated by drawing the edge outline of an insert in its original form as reported previously [8]. The illustration in Figure 4-14a closely represents a moment in the milling cycle, by carefully tracing the whole tool holder holding a (new) insert and then positioning them together with the workpiece outline.

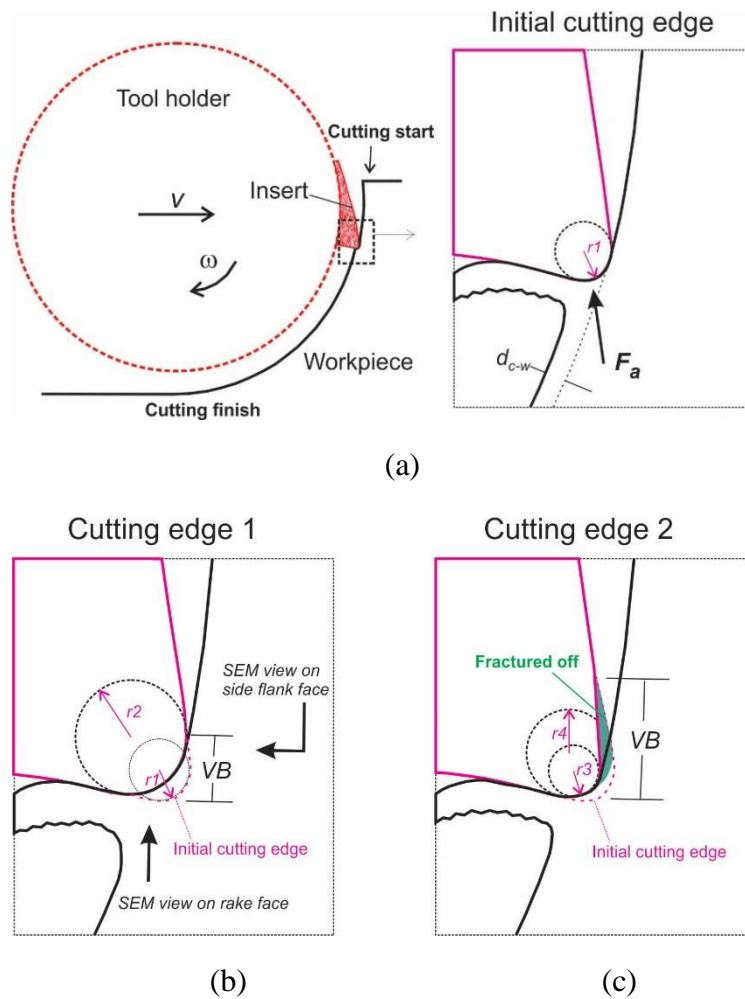


Figure 4-14 Schematic illustration of milling with (a) the cutting insert in the initial state before deterioration, (b) the insert having worn and thus the radius of cutting edge having enlarged, $r_1 < r_2$, and (c) the insert having worn and flank face material having fractured off, $r_3 \ll r_2$ (Note: r_4 does not need to be equal to r_2 and r_1 of the initial cutting edge is not indicated). The projection of the resultant of total force in working plane, F_a , is indicate in (a) and SEM viewing directions and thus VB are indicated (c)

It should be noted that, as is clear from viewing Figure 4-9, Figure 4-12 and Figure 4-13, progression of tool deterioration has meant that there has been severe erosion of the cutting corners. For the purpose of discussion, Figure 4-14b indicates in general an insert after severe edge deterioration although irregularity of the cutting edge due to edge chipping has not been further detailed. The effective radius (r_{e-eff}) of the cutting edge has increased considerably, which should result in a sizeable increase in F_m . This may be represented by the high dF/dVB_{max} points in Figure 4-11. Figure 4-14c represents a different form of insert deterioration. Although edge wear and edge chipping are still part of the overall deterioration, fracturing of a thin piece along the flank face is the distinctive feature and “plastic lowering” phenomena on the cutting tool as has been discussed in Chapter 3 (section 3.3). This is the case of the inserts shown Figure 4-12 and Figure 4-13b and as has been stated, the large part of the fractured area was not within the cutting edge therefore taking no part in cutting. Then r_{e-eff} is not necessarily high, despite the high measured value of VB_{max} , as schematically illustrated in Figure 4-14c. Thus, as for the case for point B (and also point D) in Figure 4-12, F_{e-m} was not very high. Not only for point B and point D, it can be verified (an observation was made during each VB_{max} measurement on the SEM image) that many data points in Figure 4-11 are similar to point B and point D although the degrees of fracturing are lower. Thus, it can be stated that in Figure 4-11, the high dF/dVB_{max} curve may closely represent the $F - VB_{max}$ relationship when there is insignificant fracture extending outside the cutting edge along the flank face. Following the high dF/dVB_{max} curve, for $VB_{max} = 0.5$ mm as suggested in ISO 8688-2, F measured 875 N. This value with respect to the milling condition applied, could be used to judge whether the tool insert has deteriorated to an unfavourable level.

In milling difficult-to-cut alloys such as Ni based superalloys, FR (0.05 mm/rev) value is small and a representative value has also been used here. As is illustrated in Figure 4-4, maximum d_{c-w} (= 0.05 mm) is comparable to r_e (≈ 0.055 mm), meaning $r_e/d_{c-w} = 0.055/0.05$ mm/mm = 1 when the insert is new. This ratio means the effective rake angle (θ_e), following Denkena et al. [24], decreases and become more negative along and around the cutting edge from $\sim 0^\circ$ in the location adjoining flank face, although the θ of the insert is a positive value. As explained by Grzesik [25], it is well understood, that θ is the most influential parameter affecting F and as it decreases the resultant F increases rapidly. Thus, for a small uncut chip thickness (h , which has the same meaning as d_{c-w} in this study), as r_e/h increases the specific F should increase at a rapid rate as illustrated by Fleisher et al. [26]. Then, tool deterioration

that results in significant blunting of the cutting edge and thus a significant increase in r_{e-eff} should increase F_m with similar intensity, as is the case of the high dF/dVB_{max} curve in Figure 4-11. How readily locally thin piece(s) may fracture extending beyond the cutting edge may relate to the consistence of quality and properties of the insert (WC-Co) material, which cannot be predicted at present. This has prevented a clear $F - VB_{max}$ relationship to be established.

4.5 Examination on Cutting Edge Condition Affecting Deformation Zone

Understanding the effect of tool deterioration induced cutting edge blunting on the cutting force, as discussed in last section, may be further evaluated by examining the deformation zone in the workpiece. A simplified representation of the deformation zone is added and illustrated in Figure 4-15, following Figure 4-14. It is assumed that the deformed zone has experienced a microstructural change, including both work hardening and softening due to frictional and deformation heat. Thus, the hardness map of the cross section may suggest how coolants application may affect deformation.

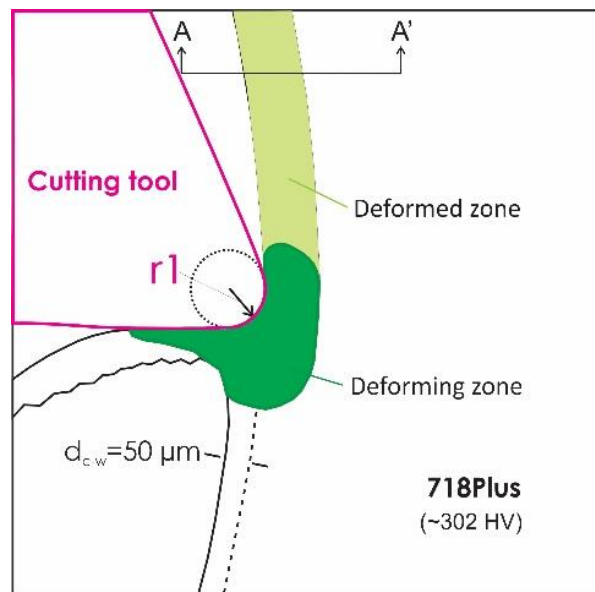


Figure 4-15 Illustration of the deforming zone on the machined cross-section surface

A deformation zone sample was obtained by reversing the machine bed movement suddenly during a milling experiment. The deformed zone in the workpiece is thus preserved and a cross-section, A-A in Figure 4-15, could then be made. The experimental and measurement procedures have been described in Chapter 2 (2.6). Hardness distribution maps are presented

in Figure 4-16 for dry (a and b) and wet (coolant) cutting (c and d) conditions respectively. The depth of cut as observed in Figure 4-16 is ~ 0.5 mm, which is the set value of the milling experiments. In each cutting condition, the map on the left of the figure is for first pass using the new tool and the map on the right is for the tool that has been used for a number of passes.

It is clear from observing the shapes of the milled surfaces of the cross-sections on the two right maps (b & d) with comparison to the two on the left (a & c) of Figure 4-16, that there is severe tool edge loss in the tools after four passes. It must be noted, as explained in Chapter 2 (section 2.3), a hardness indentation could only be taken about $40 \mu\text{m}$ from the surface. In these maps (Figure 4-16), the hardness band at each 25 HV interval is marked by a specific colour. Data points within the same band (colour) of hardness are linked and the profile of hardness change near the milled surface can therefore be visualised. The two deformed zones are marked in the figure, zone 1 consisting of shearing by the cutting edge during milling and zone 2 behind the cutting edge with zero shear. For purpose of clarity it is necessary to first discuss the hardness change using Figure 4-16a. In zone 1 the highest hardness band is 450-475 HV nearest to the milled surface.

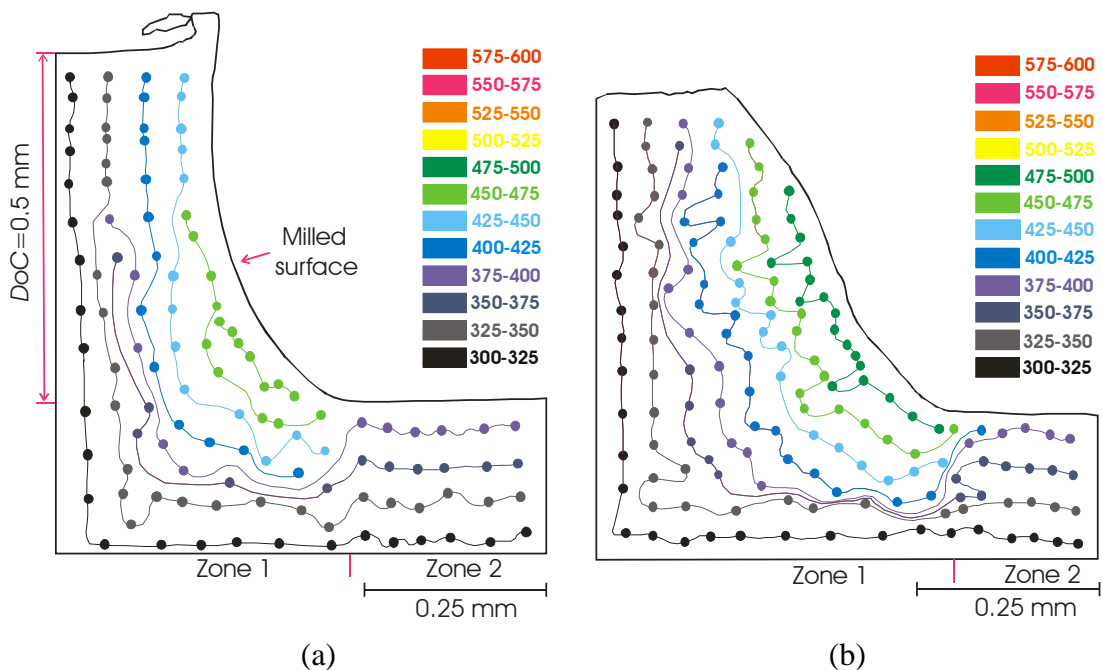


Figure 4-16 Micro hardness map on the machined cross-section surface; left images are of new tool image and right image is a deteriorated tool after the fourth pass (a)-(b) annealed workpiece, uncoated and dry (TC9), (c)-(d) annealed workpiece, uncoated and wet (coolant) (TC10)

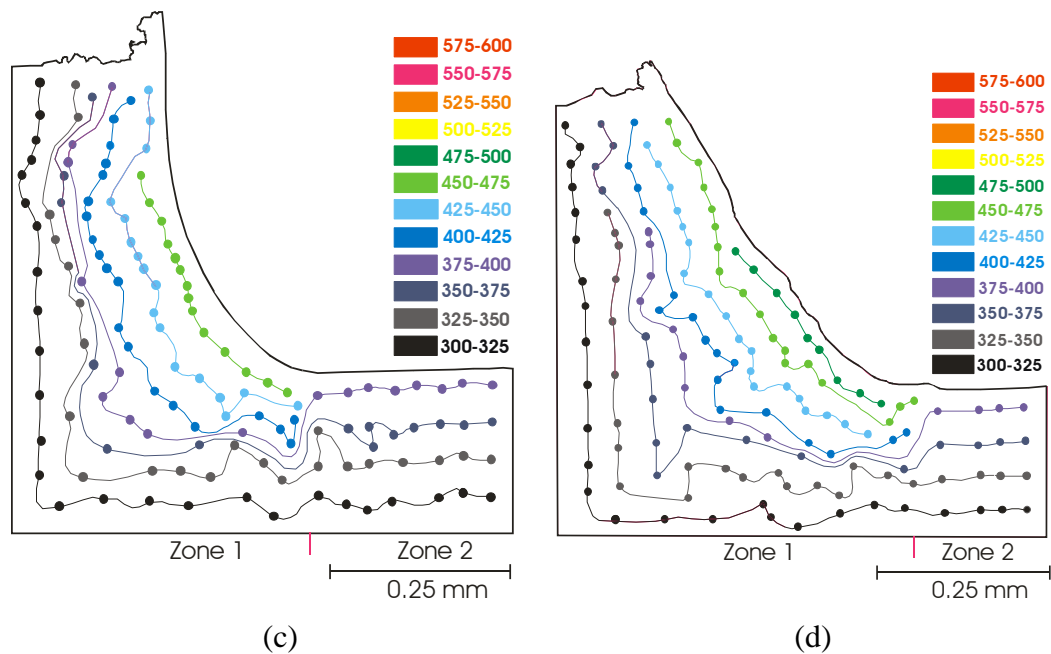


Figure 4-17 Continued

The surface hardness, which was unable to be measured should exceed this band. The hardness (band) of the unaffected workpiece material is 300-325 HV. Thus, it can be observed that the depth of milling affected zone in zone 1 ranges from ~ 0.2 mm in the workpiece surface region to ~ 0.3 mm in the bottom part of the zone. In zone 2, hardness values horizontally are rather uniform, from 375-400 HV near the milled surface to 300-325 HV ~ 0.2 mm below the milled surface. Note that in the transition from zone 1 to zone 2, the transition of hardness values is rapid. This means that hardness has increased considerably in the workpiece adjacent to and near the cutting edge during cutting (in zone 1 and before transition).

Furthermore, the bottom of the deformed zone 1 transits into zone 2 with hardness reducing significantly. The considerable increase in hardness towards the cutting surface in zone 1 is consistent with the view of severe work hardening of Ni-superalloy during machining [57], although a microstructural change relating to this increase has not been conducted in the present work. Due to the absence of further analysis, the hardness transition phenomenon in the bottom deformed zone cannot be further explained. With regard to the sample milled with a deteriorated tool shown in Figure 4-16b, the highest hardness band was 475-500 HV, demonstrating a slight but clear increase in hardness in the milled surface region compared to the hardness band of the same region of the new cutting edge sample. Also clearly, with comparison to using the new cutting tool (Figure 4-16a), the deformed zone (Figure 4-16b) has widened from slightly over 0.2 mm in the workpiece surface to ~ 0.45 mm to in the

bottom of zone 1. This suggests that the blunted tool cutting edge has forged/compressed a larger region. This is consistent with the severe (deterioration) blunting of the cutting edge shown in Figure 4-17(a) and Figure 4-17(b) and the corresponding large increase in cutting force shown in Figure 4-18b. The rapid hardness transition from zone 1 to zone 2 (in Figure 4-16b) is however similar to that in the sample of using the new cutting tool (Figure 4-16a).

The understanding on why the use of coolant has not affected tool deterioration and cutting force, as discussed earlier in this chapter may now be further examined. Comparing Figure 4-16c to Figure 4-16a, the size of milling affected zone and the hardness values do not appear to differ significantly for the two conditions. It would thus suggest that cutting force required for the cutting deformation does not differ significantly, regardless of whether coolant is used or not. This is confirmed by examining the force data in Figure 4-18 (a and c), both being ~ 200 N which is the value when a new cutting tool is used, as is well explained earlier in this chapter. The comparison using the hardness maps for the two tool deteriorated samples, as shown in Figure 4-16b and Figure 4-16d, also does not suggest a large difference in deformation behaviour and the corresponding cutting force values (Figure 4-18). The highest hardness value band and the overall hardness gradient are comparable for the two conditions, although a slightly narrower zone 1 for condition using coolant could be the case.

The insignificant differences in the size of deformation zone, cutting force and tool deterioration for the two conditions (dry machining and wet machining) may seem unusual. This is because the use of coolant should significantly aid the milling (friction and deformation) heat being taken away and thus it should be expected that a considerably lower temperature in workpiece would result. The strength (flow stress) of workpiece at a lower temperature should be higher and thus a higher cutting force should result. However, the seemingly unusual phenomenon may relate to the size of the deformation zone that has been identified in this work, as shown in Figure 4-16 and discussed above. For dry milling conditions, the width of the deformation zone is ~ 0.2 mm on the workpiece surface, as indicated in Figure 4-16a and Figure 4-16b. It is possible that coolant directed at the cutting tool rotating at a high speed (1000 rpm) may not reach the workpiece-cutting edge junction at a close enough range (< 0.2 mm). Thus, temperature in the very thin (0.2 mm on surface) deformation zone does not reduce. As a result, dry milling and wet (coolant) milling are similar in terms of cutting force and tool deterioration.

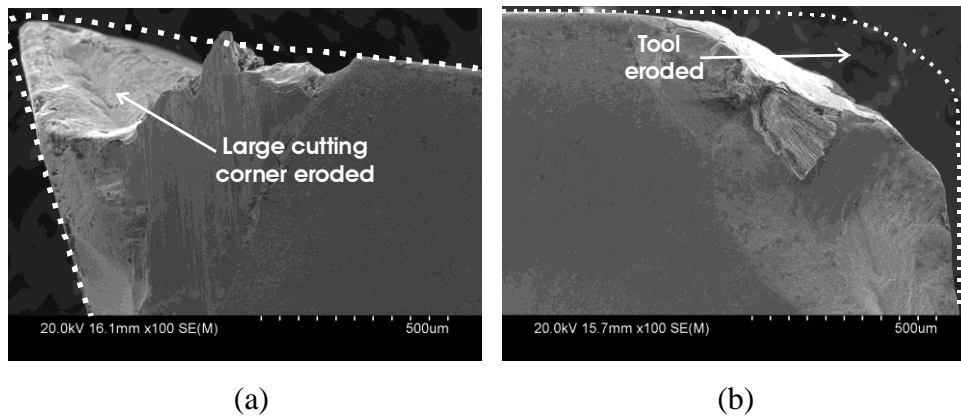


Figure 4-18 SEM images of uncoated and dry (TC9) after the fourth pass (a) side flank face (b) bottom flank face

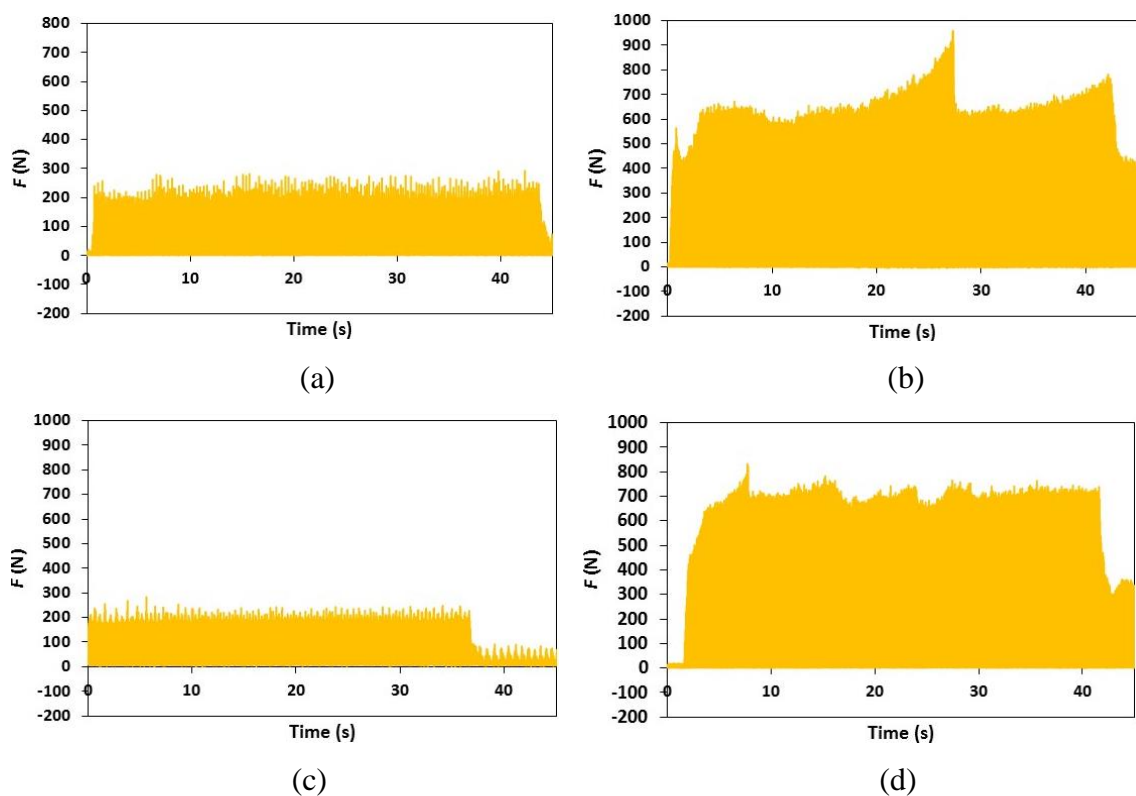


Figure 4-19 F curves (recorded data) of (a) the first milling pass of TC9, (b) the final pass milling pass of TC9, (c) the first milling of TC10 and (d) the final milling pass of TC10

4.6 Effect of High Feed Rate on Cutting Force

In order to investigate the effect of feed rate on cutting force during milling of Ni-based 718Plus, two tooling conditions (TC) were used (refer Table 2-3 in Chapter 2); TC11 referring to uncoated carbide tools machining in dry conditions and TC12 referring to uncoated carbide tools machining in wet (coolant) conditions. In these TCs, an increased feed rate of 0.1 mm/rev was used while cutting speed, depth of cut and radial depth were

kept constant with previous experiments. Cutting force values from two milling passes, the first and third pass from the same insert (TC11-1) are plotted in Figure 4-19.

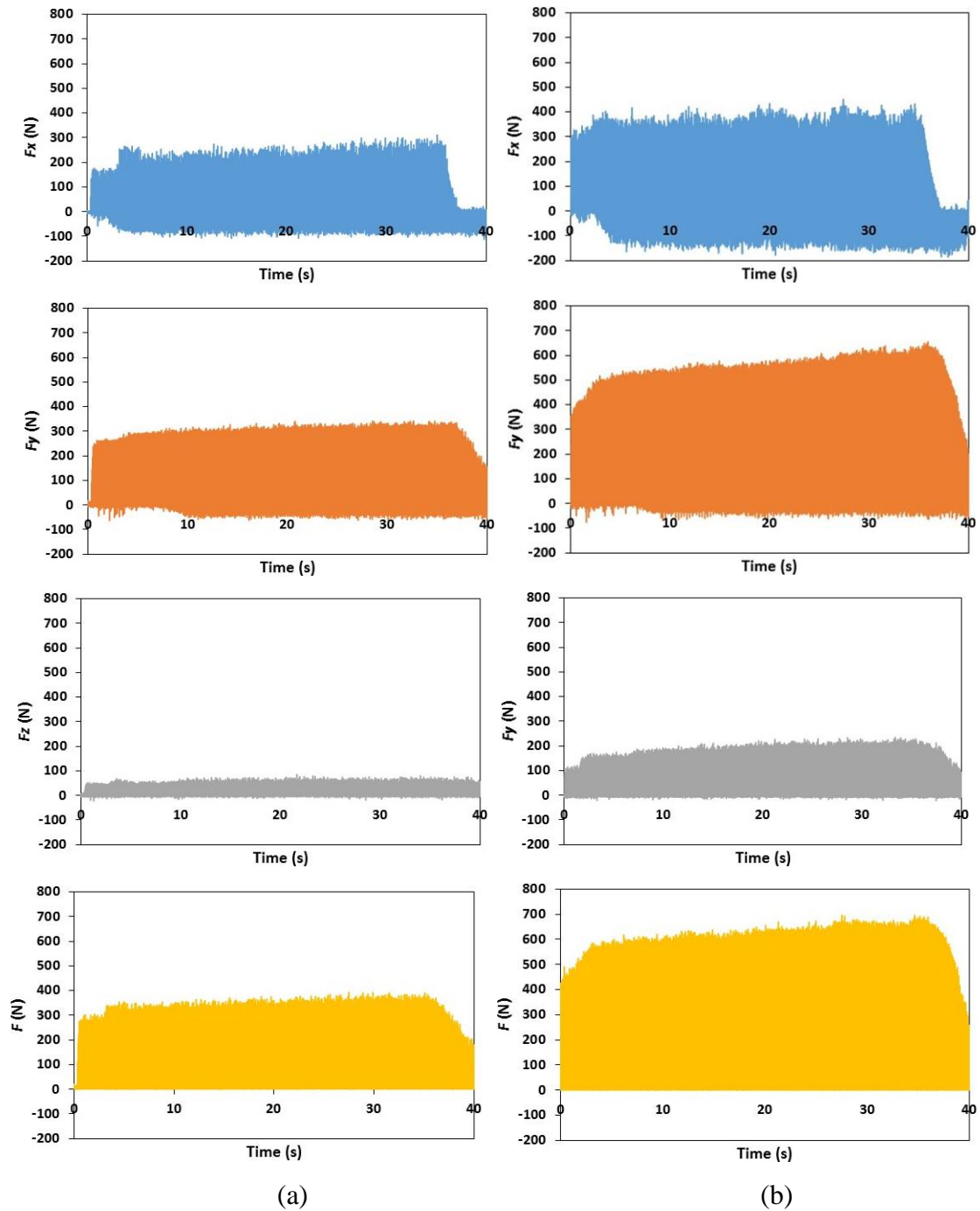


Figure 4-20 The whole F_x , F_y , F_z and F curves (recorded data) of (a) the first milling pass and (b) the third pass. Tooling condition: uncoated carbide and dry (TC11-1)

Greater detail of the initial milling stage is further presented in Figure 4-20. At the first milling cycle, maximum F_x and F_y values were 60 and 80 N respectively, with a F_z of ~ 0 N all slightly higher than the forces when $FR= 0.5$ mm/rev (section 4.1). Within this first

cycle, F (not shown in detail) increased and reduced to zero within 0.03 s, 0.01 s faster than milling at a FR of 0.05 mm/rev.

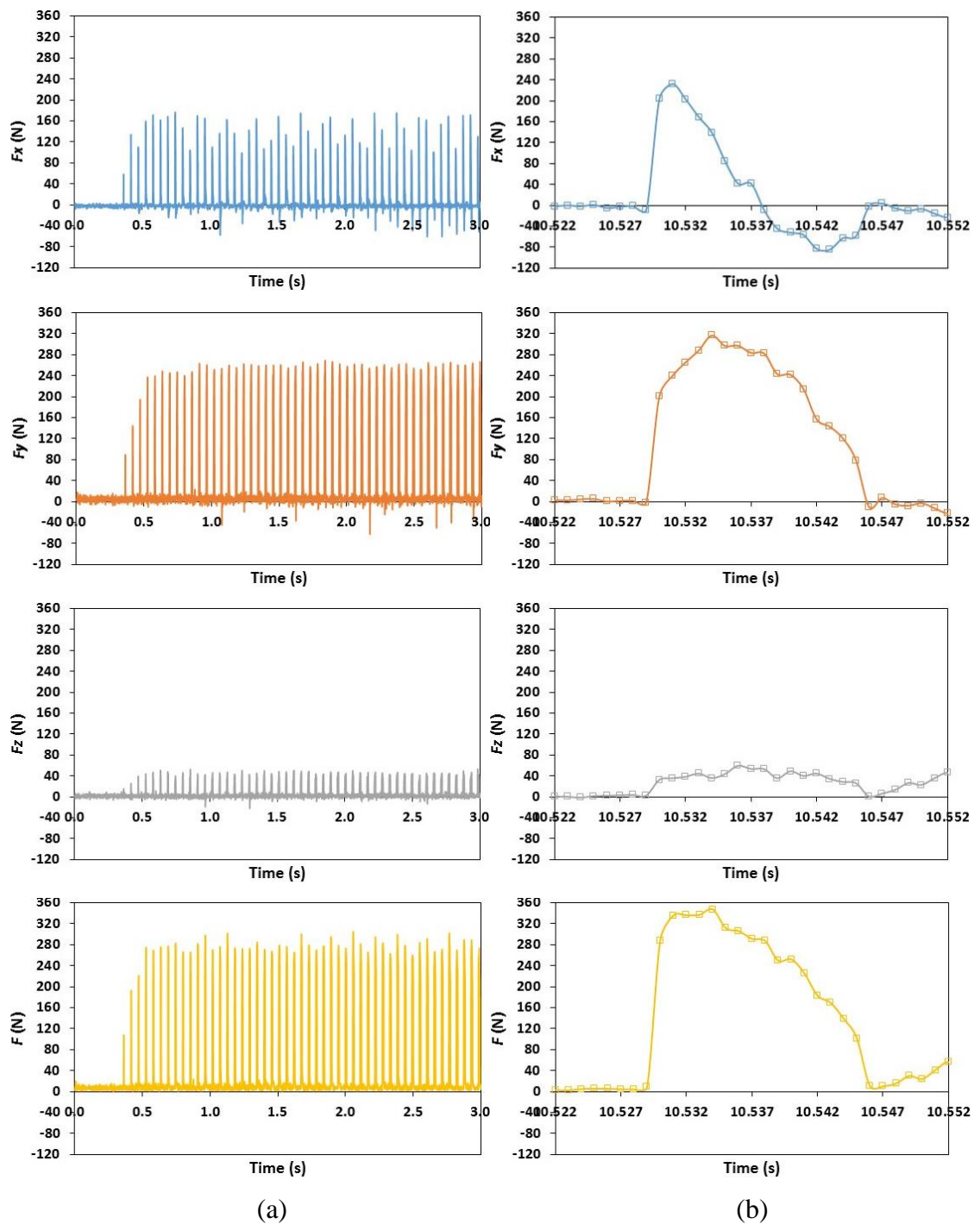


Figure 4-21 F_x , F_y , F_z and F curves of the first pass during (a) the initial within 3s of milling engagement and (b) a half milling cycle time in the early milling stage. Tooling condition: uncoated carbide and dry (TC11-1)

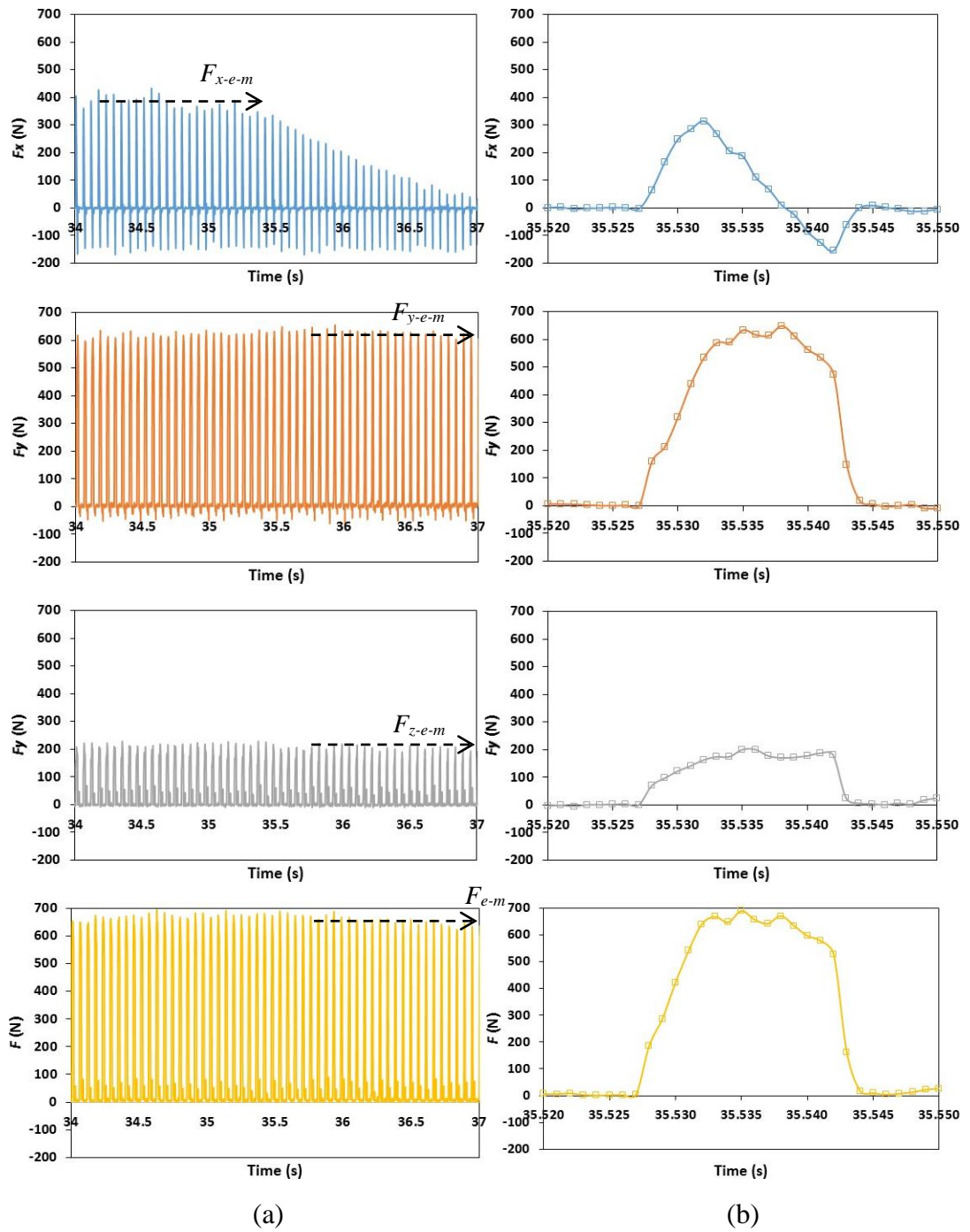


Figure 4-22 F_x , F_y , F_z and F curves of the first pass during (a) 3-s period just before the insert reached the end of the workpiece and (b) a half milling cycle time within a period. Tooling condition: uncoated carbide and dry (TC11-1)

After the initial engagement, the tool insert continued milling for 35 s to reach to the other end of the workpiece. The maximum force values (F_{x-m} , F_{y-m} , F_{z-m} and F_m) started to decrease when the end was reached at 37-38 s as shown in Figure 4-19. Hence, average F_{x-m} , F_{y-m} , F_{z-m} and F_m values during the 3 s period before the force values started to decrease (34-37 s) as shown Figure 4-21 for the third pass, can be used as the force values corresponding to the

end pass (F_{x-e-m} , F_{y-e-m} , F_{z-e-m} and F_{e-m}) indicated in Figure 4-23a. There are two main features to be observed through comparing the force data of the first pass to the third (and final) pass in Figure 4-19, 4-20 and 4-21. First, F_m has increased from ~ 360 to 680 N or higher. Second, the prompt increase in F in the beginning of the cycle was similar, however for the third pass F stayed high for most of the cutting length within the same cutting time of ~ 0.016 s (comparing Figure 4-21b and Figure 4-20b). Besides that, at the first pass a periodicity was observed in F_{x-m} but not in F_{y-m} and F_{z-m} (Figure 4-19a and Figure 4-20a). This periodicity was identical to $FR=0.05$ mm/rev as explained in the previous section. Figure 4-22 is plotted to show the values of F_{x-e-m} , F_{y-e-m} , F_{z-e-m} and F_{e-m} against N_{pass} .

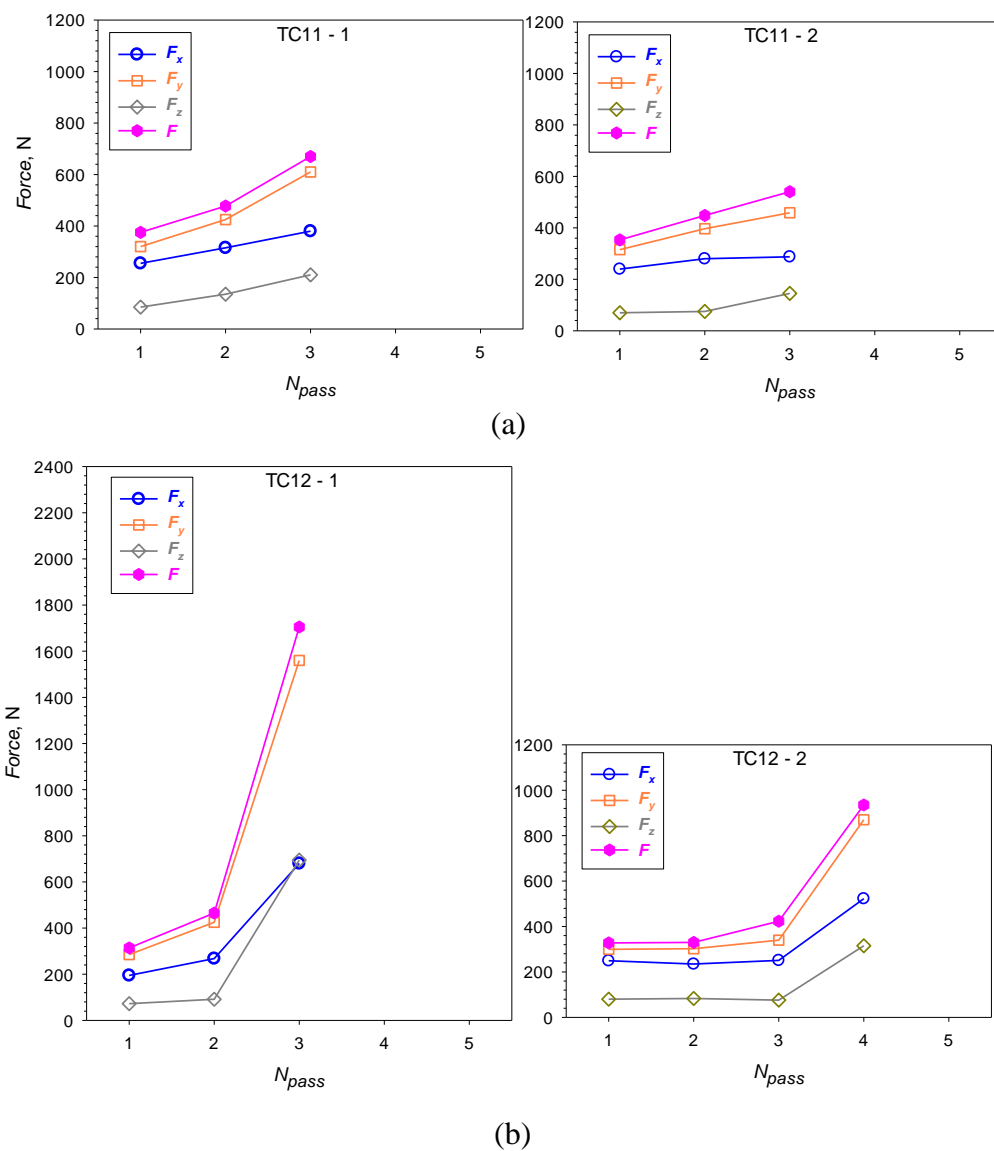


Figure 4-23 Average maximum force values F_{x-e-m} , F_{y-e-m} , F_{z-e-m} and F_{e-m} versus the number of passes for the two tooling (a) TC11 and (b) TC12

The average F_{e-m} for all first passes were higher compared to the base cutting parameter FR (0.05 mm/rev) with an average of 342 N (standard deviation 27.1 N from 4 data/experiments), a small increase from an average F_m value equal to 324.5 N (standard deviation 20 N) measured in the start of full a_e milling for the first passes. After the second passes, F_{e-m} for all tooling conditions accelerated about 450-480 N except in experiment TC12-2 where it was ~ 330 N (Figure 4-22b) which is identical to F_{e-m} after the first pass (~ 327.5 N). After the third pass, ΔF_{e-m} values were 0-220 N (TC11-1, TC11-2 and TC12-2) while in TC12-1, ΔF_{e-m} was 1240 N. For TC11-1, TC11-2 and TC12-1, milling experiments stopped after their third pass. However due to the small increment of F_{e-m} for TC12-2, a further pass continued (fourth pass) with $F_{e-m} \sim 935$ N. The functions of coolant in reducing F values were confusing. In Figure 4-24 (TC12-1), F_{e-m} values after the third pass were 1705 N (very high), however for TC12-2, F was 423 N (low) and the milling further continued for the next pass (fourth pass). The value of F after the third pass of TC12-1 was even higher compared to dry milling for TC11-1 and TC11-2.

Figure 4-23 shows plotted graphs of VB_{max} versus the number of passes. Overall, VB_{max} after the first pass was $\sim 0.12 - 0.16$ mm except for TC12-2, which was quite higher ($VB_{max} \sim 0.2$ mm). These rates were greater than that of $FR = 0.05$ mm/rev ($VB_{max} \sim 0.1$ mm) on average for every first pass, which is reasonable due to the higher value of $FR = 0.1$ mm/rev. Moreover, it was noticed that when $FR=0.1$ mm/rev was used, the N_{pass} of tool insert decreased to three passes on average, except for TC12-2 (four passes). By using $FR=0.05$ mm/rev, the tool inserts lasted for four to five passes. In Figure 4-23, the number of passes of TC11-2 stopped after the third pass, albeit the VB_{max} was only 0.26 mm (low) and not yet reached the ISO 8688-2 criterion ($VB_{max} = 0.5$ mm). After the third pass the F_{e-m} value was ~ 540 N, regarded as a high force and no further milling passes were conducted. Figure 4-24 shows the VB_{max} progression of TC11-2, where a gradual wearing process took place at the cutting edge (Figure 4-24 a) after the first pass. After the third pass, it can be observed that the side flank face was covered by BUL and quite severe chipping on the cutting edge has taken place. Rather large chipping was found on the flank area (furthest end of the cutting edge) that must have triggered the high F_{e-m} values (540 N). Figure 4-25 (a-b) shows SEM images on the bottom flank and rake face. In these views, it is clearly seen that the cutting edge of the tool insert has deteriorated significantly (material loss), resulting in a high F_{e-m} after the third pass although the VB_{max} was only 0.26 mm.

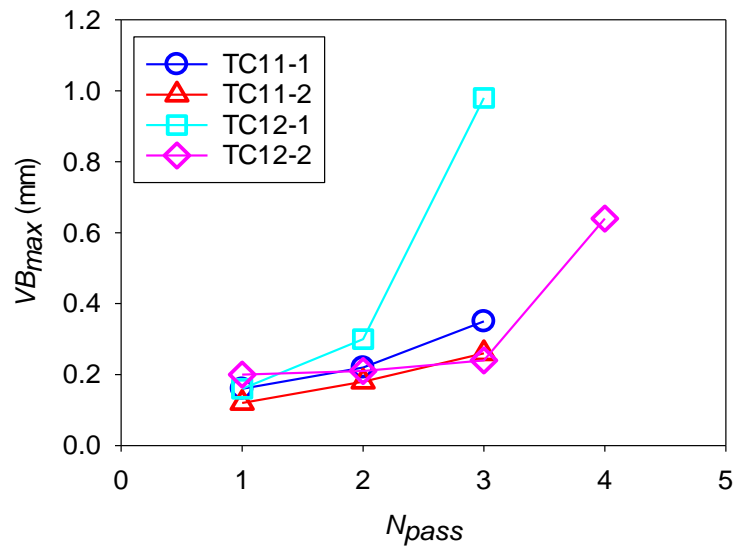


Figure 4-24 VB_{max} versus the number of passes for the two milling conditions, TC11 and TC12

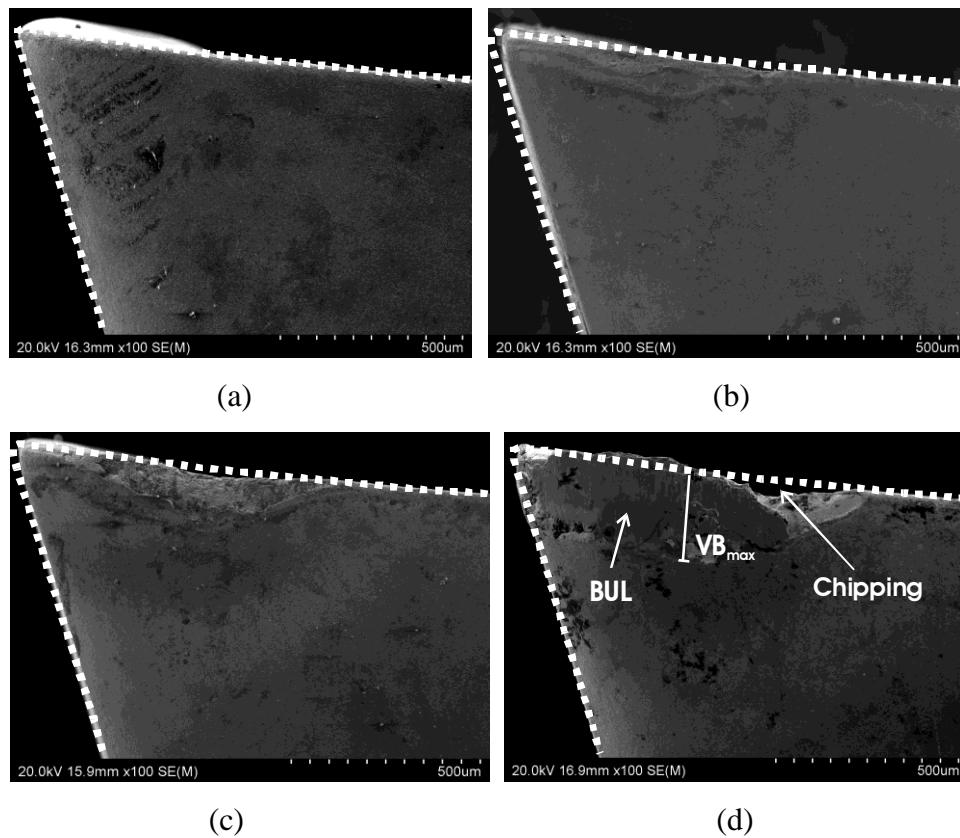


Figure 4-25 SEM images of side flank face; (a) before milling, (b) first milling pass, (c) second milling pass and (d) third milling pass. Tooling condition: TC11-2

Additionally, Figure 4-26 shows SEM images for TC12-1. As mentioned earlier, F_{e-m} value for this particular experiment was very high at ~ 1705 N after the third pass. In the first pass, gradual wear dominated with BUL occurring on the flank face and cutting edge and VB_{max} measuring 0.16 mm (Figure 4-26b).

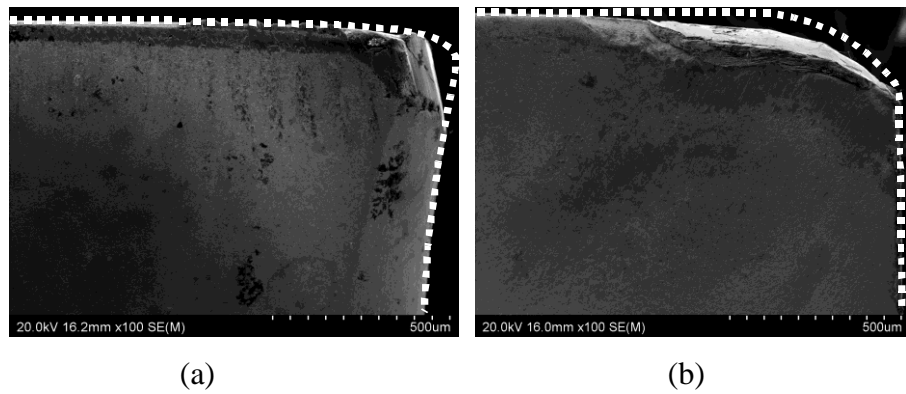


Figure 4-26 SEM images of third pass; (a) bottom flank face and (b) rake flank face, tooling condition: TC11-2

Then, in the second pass, chipping occurred on the cutting edge (Figure 4-26c) and VB_{max} accelerated to 0.3 mm. However, during that pass F_{e-m} was only ~ 465 N (not high) suggesting further milling could be completed. After the third pass (Figure 4-26d), large fracturing extended outside the cutting edge area and the cutting corner broke eroding away, thus resulting in a F_{e-m} value of 1705 N and $VB_{max} \sim 0.98$ mm.

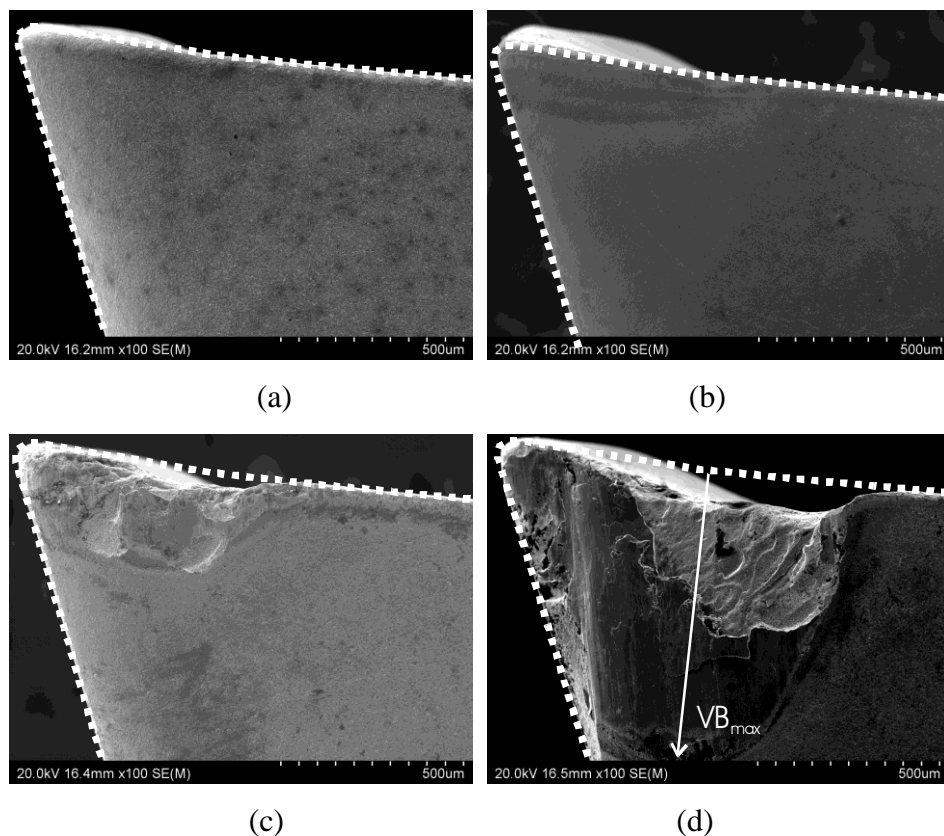


Figure 4-27 SEM images of side flank face; (a) before milling, (b) first milling pass, (c) second milling pass and (d) third milling pass. Tooling condition: TC12-1

As has been explained previously (section 4.2), VB_{max} and F (F_{e-m}) increase as N_{pass} increases and in general the rate of increases are low initially and become high subsequently for experiments using $FR = 0.05$ mm/rev. The overall tool life (N_{pass} to failure) is low using that FR value. These features apply the higher FR value (0.1 mm/rev) experiments, as the above data and observation presented in this section have shown, with in general a shortened tool life. An important illustration given in section 4.2 is the poor correlation between F_{e-m} and VB_{max} for the low FR value experiments. This is, as has been explained, due to the fact that VB_{max} does not represent correctly the true state of tool deterioration and the change of cutting edge geometry. In Figure 4-27, data of F_{e-m} and VB_{max} are plotted for $F = 0.1$ mm/rev experiments, while the high and low dF/dVB_{max} curves from the low FR experiments (from Figure 4-11) have been provided as a comparison. Two effects of the use of increased FR can be seen. The first is, on average, increasing FR has resulted in higher F_{e-m} values. The second is the apparently good correlation between F_{e-m} and VB_{max} and the overall trend can closely be represented by a curve similar to the high dF/dVB_{max} curve of low FR value.

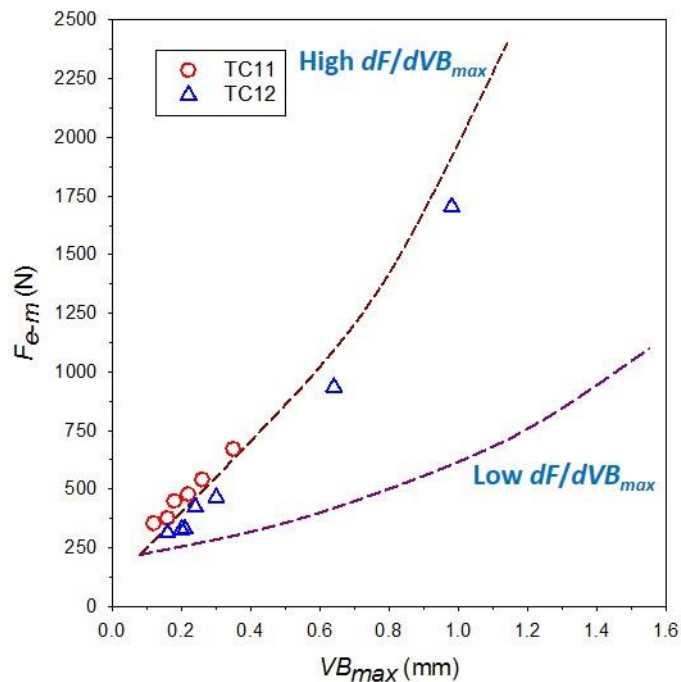


Figure 4-28 F_{e-m} versus VB_{max} for a feed rate of 0.1 mm/rev conditions

The increased cutting force (F or F_{e-m}) is expected as a higher FR value simply means a higher deformation zone, thus needing a higher cutting force. The good F_{e-m} and VB_{max} correlation should then mean VB_{max} being a good representation of tool deterioration for experiments using the higher FR value. The reason for this may be provided by using the illustration in Figure 4-11 and Figure 4-14 using the proposed mechanism for poor F_{e-m} and

VB_{max} correlation for low FR value experiments given and explained in that section (4.2). An increase in FR means a higher load bearing area on the rake face. This should result in heavier edge chipping/fracturing but not fracturing a long distance along the side flank face. As shown in Figure 4-27, the highest VB_{max} value has resulted from severe edge chipping/fracturing and no long fracturing along the flank face has been observed in this series of high FR value experiments. This edge chipping/fracturing dominant mode of tool deterioration has resulted in a good F_{e-m} and VB_{max} correlation and is the reason for a high dF/dVB_{max} trend to be followed. VB_{max} values dominated by fracturing a long distance along the flank face can vary widely, but for the deterioration mode of edge wear and edge chipping a VB_{max} value is more proportional to the true amount of tool edge eroded away. This edge erosion resulting in edge blunting should thus relate directly to the cutting force.

4.7 Summary

Modes of insert deterioration relate to F differently. The trend of increasing VB_{max} as (N_{pass}) increases broadly agrees with the trend of increasing F as N_{pass} increases. However, the present experimental data have suggested that F correlate poorly with VB_{max} because $\Delta F/\Delta VB_{max}$ can vary considerably. This is the result that, in a specific milling experiment, a deterioration mode may be more dominant than the other as the insert deteriorates. The mode of severe chipping and breakage confined to the cutting edge thus causing severe blunting of the edge corresponds to relatively high $\Delta F/\Delta VB_{max}$. This is suggested to be the result of edge blunting having a major effect on causing the effective rake angle to decrease due to the small feed rate values normally used in milling Ni-based alloys, thus a major effect of increasing F . The mode of fracturing a thin layer extending to outside the cutting edge along the flank face increases the VB_{max} value but the extra VB_{max} does not contribute to the cutting edge contact width and thus no extra F is required. This results in low $\Delta F/\Delta VB_{max}$. It was observed that the rate of tool deterioration when $FR=0.1$ mm/rev was used is higher compared to $FR= 0.05$ mm/rev. The mode of deterioration is edge wear and edge chipping/fracturing dominant which results in high $\Delta F/\Delta VB_{max}$ results. The increase of hardness of when milled with a deteriorated tool is higher compared with that of a new tool.

Chapter 5: Tool Deterioration Influenced by Workpiece Heat Treatment State

In this last chapter, the effect of increased workpiece strength/hardness on the cutting edge deterioration and cutting force is addressed. Additionally, how cutting edge deteriorations influence for the deformation zone is explained and discussed in detail for the an annealed and hardened workpieces. In this work, comparison has only been conducted for uncoated inserts in dry and wet condition.

5.1 Cutting Edge Deterioration

Plots of flank wear maximum (VB_{max}) against number of pass (N_{pass}) are presented in Figure 5-1a and b for dry and wet (coolant) milling respectively. A repetition experiment was conducted for each tooling condition represented in the figures. In Figure 5-1a, tool condition TC13-1 was conducted only for two passes although the VB_{max} value was ~ 0.22 mm after the second pass. In accordance to the previous discussion, a milling pass is terminated when total cutting force (F) exceeds ~ 550 N. In the case for TC13-1, the F was about 585 N after two passes.

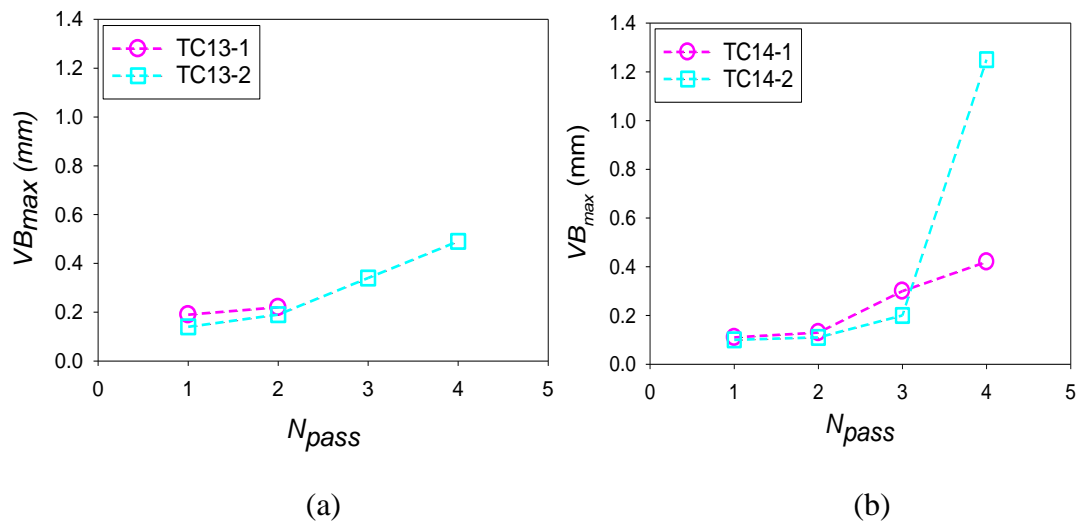


Figure 5-1 VB_{max} versus the number of passes of milling a hardened workpiece : (a) dry (TC13) and (b) wet (coolant) (TC14)

As shown in Figure 5-2b, small fractures and minor chipping were observed along the cutting edge after the first pass of TC13-1 experiment. As the milling continued in the second pass, a significant portion of the cutting corner was found to be broken off as shown in Figure 5-2c.

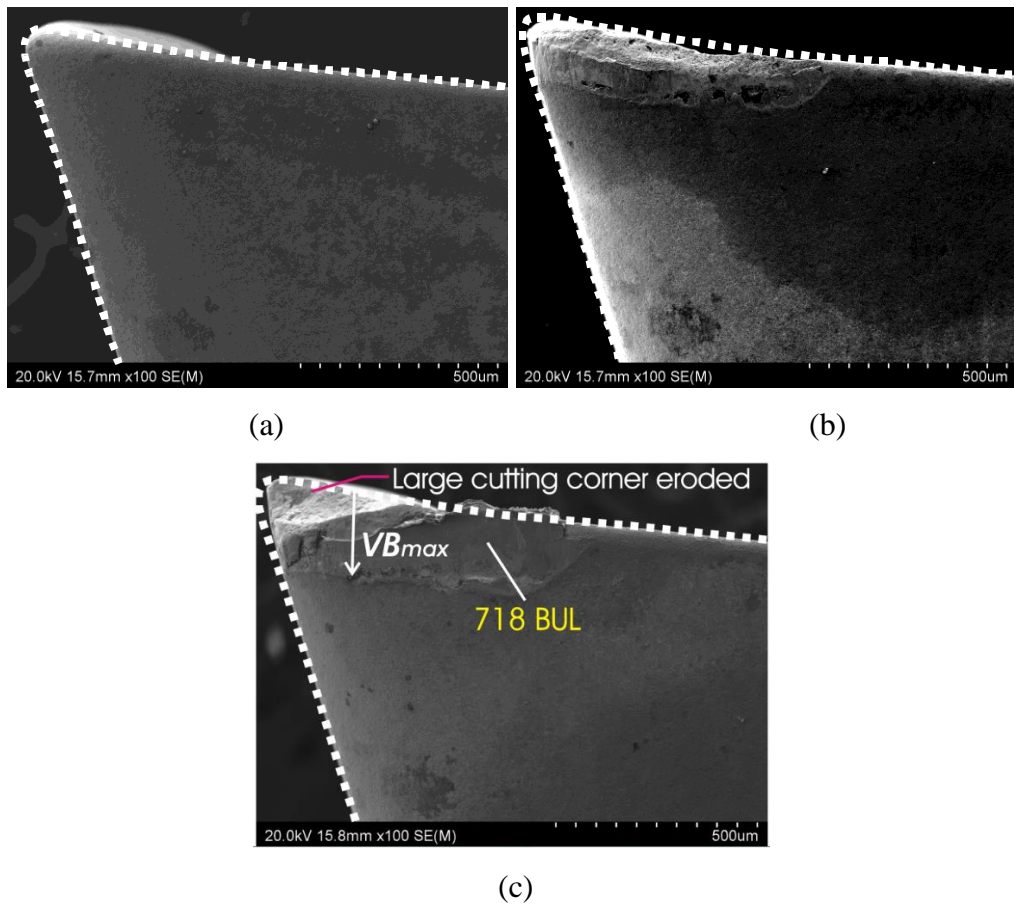


Figure 5-2 SEM images Tool TC13-1 side flank face before and after various milling passes of a hardened workpiece: (a) before milling with edge outlined, designated as zero pass edge outline (ZPEO), (b) after the first pass together with ZPEO, and (c) after the second pass together with ZPEO

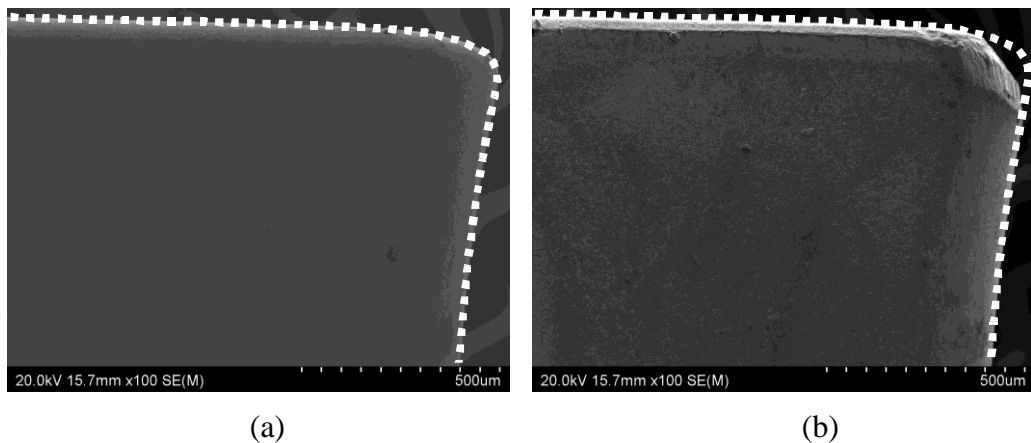
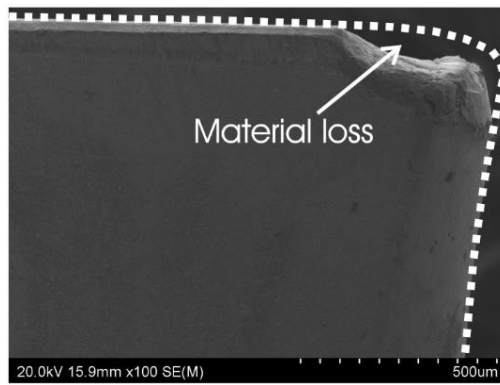


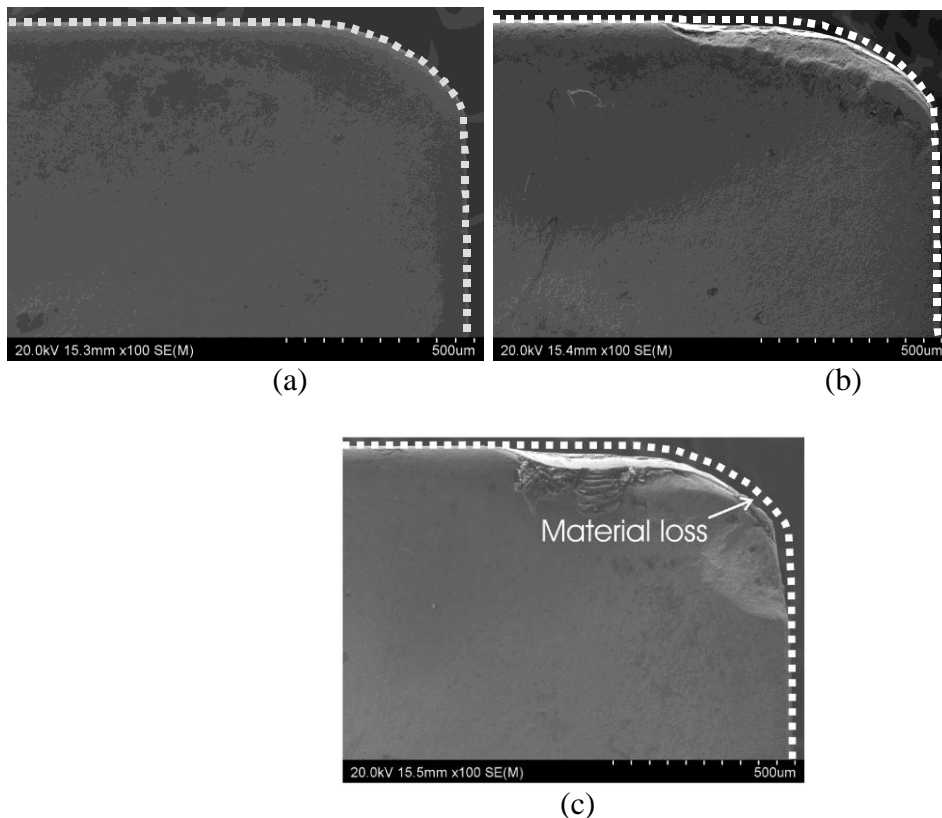
Figure 5-3 SEM images Tool TC13-1 bottom flank face before and after various milling passes of a hardened workpiece: (a) before milling with edge outlined, designated as zero pass edge outline (ZPEO), (b) after the first pass together with ZPEO, and (c) after the second pass together with ZPEO



(c)

Figure 5-4 Continued

A further SEM image presented in Figure 5-3c as viewed from the bottom flank face, shows the significant tool material loss at the cutting corner although observing on the rake face in Figure 5-4c does not show the cutting edge loss. This early but heavy fracturing/chipping in the cutting edge/corner while VB is low corresponds to a relatively high cutting force.



(a)

(b)

(c)

Figure 5-5 SEM images Tool TC13-1 rake face before and after various milling passes of a hardened workpiece: (a) before milling with edge outlined, designated as zero pass edge outline (ZPEO), (b) after the first pass together with ZPEO, and (c) after the second pass together with ZPEO

Four passes were conducted with tool condition TC13-2 (dry milling) with a gradual increase in VB_{max} from ~0.18 mm after the first pass reaching a maximum of 0.55 mm after the fourth pass. From Figure 5-5 (b-c), no significant deterioration is visible on the cutting tool after the first and second pass however, build-up edge (BUE) was apparent behind the cutting edge after the first pass.

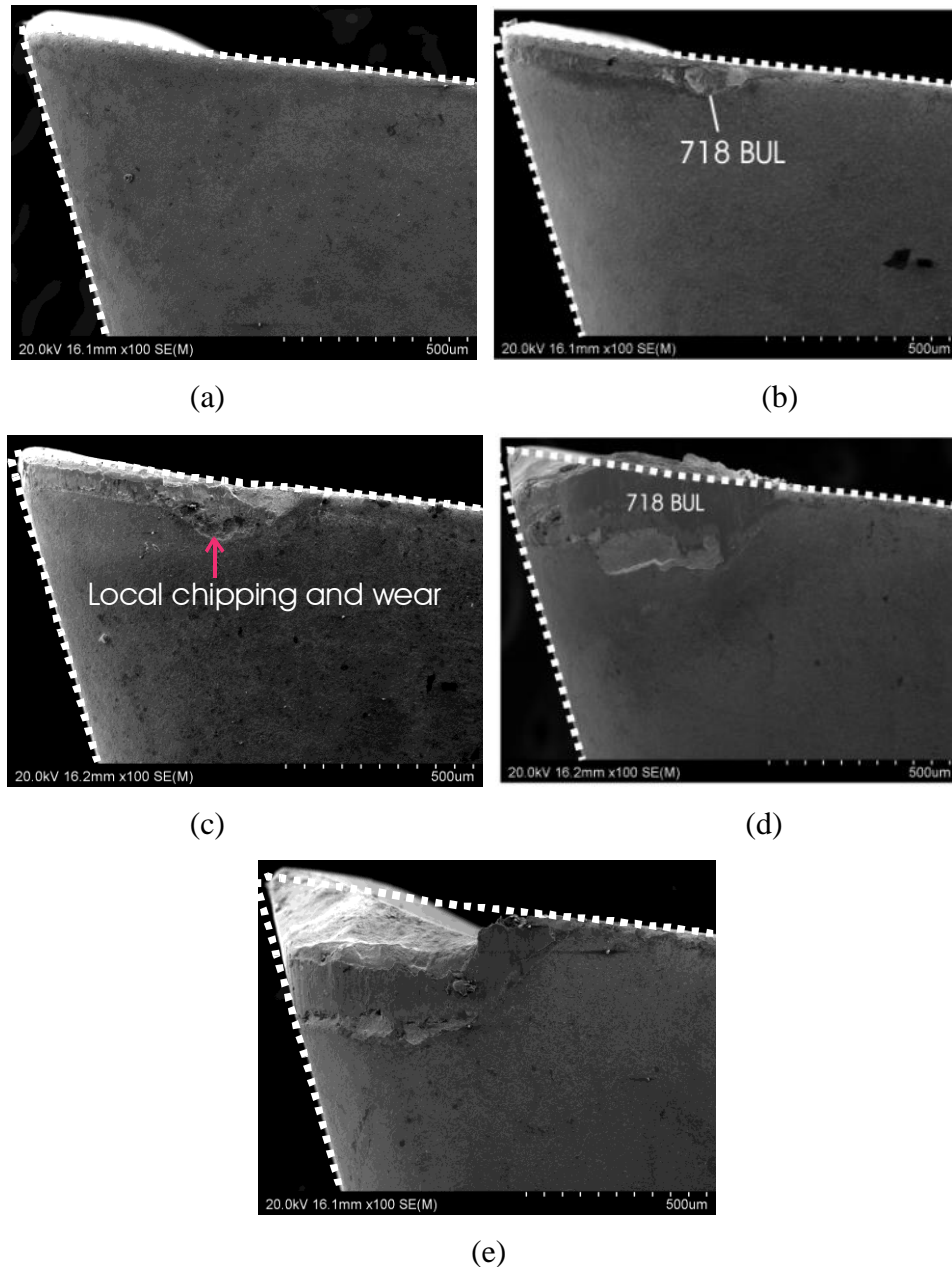


Figure 5-6 SEM images Tool TC13-2 side flank face before and after various milling passes of a hardened workpiece: (a) before milling with edge outlined, designated as zero pass edge outline (ZPEO), (b) after the first pass together with ZPEO, (c) after the second pass together with ZPEO, (d) after the third pass together with ZPEO, and (e) after the fourth pass together with ZPEO

Further SEM images presented in Figure 5-6 b and Figure 5-6c viewed from the rake face (pink arrow), show that there was no significant loss on cutting edge.

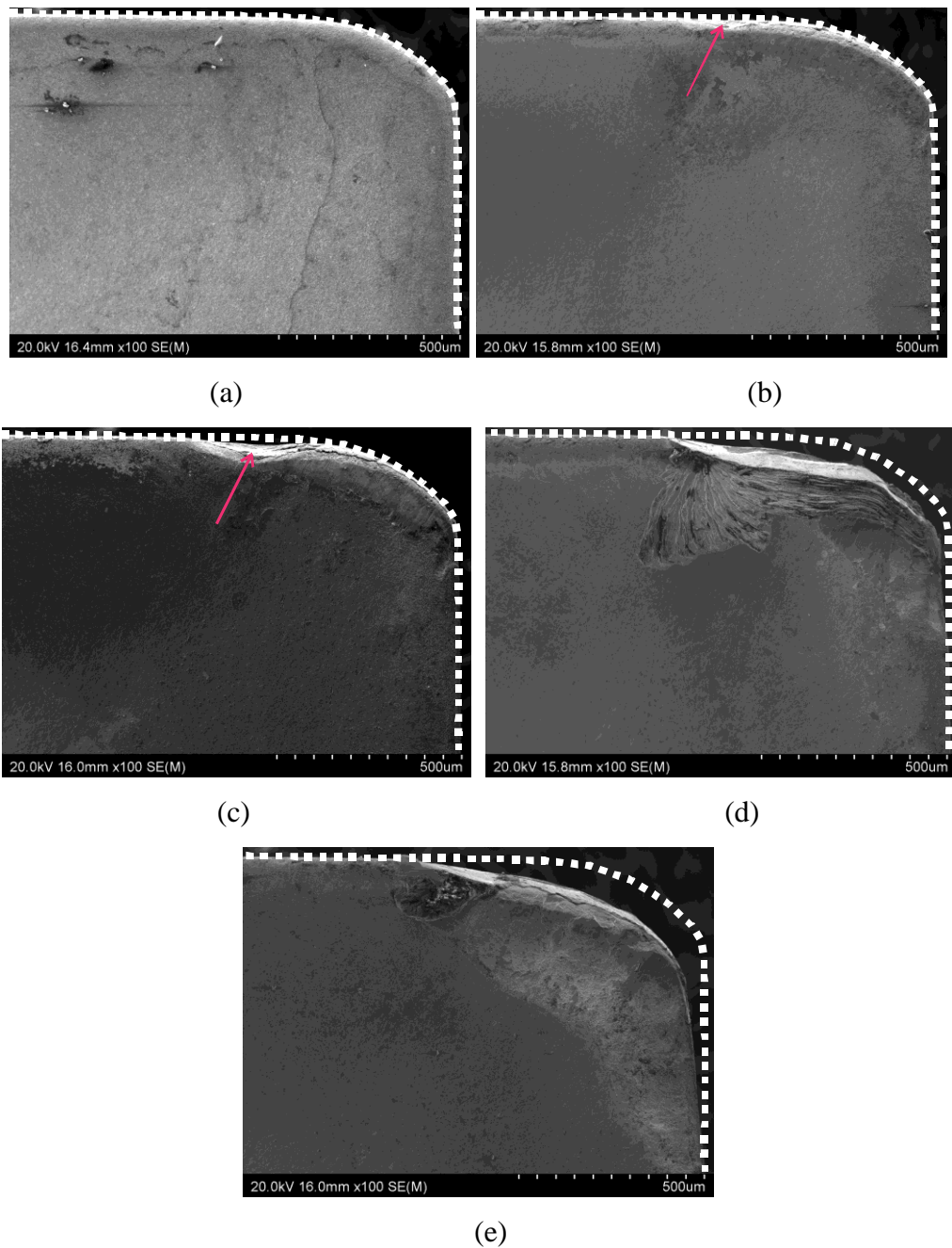


Figure 5-7 SEM images Tool TC13-2 of rake face before and after various milling passes of a hardened workpiece: (a) before milling with edge outlined, designated as zero pass edge outline (ZPEO), (b) after the first pass together with ZPEO, (c) after the second pass together with ZPEO, (d) after the third pass together with ZPEO, and (e) after the fourth pass together with ZPEO

After the second pass local chipping and wear was more apparent as VB_{max} measured about ~ 0.14 - 0.19 mm for these two passes. A large amount of tool material loss occurring on the cutting edge was identified in the third pass as shown in Figure 5-5d, including the huge formation of BUL at the corner region. In reference to Figure 5-5e, the tool severely deteriorated after the fourth pass, where large fracturing occurred on the cutting edge extending far from the edge. This huge fractured area has contributed to elevated tool blunting, whereby the tool only rubs or pushes the workpiece surface instead of milling. Thus, it is observed that the process of tool failure of TC13-2 is consistent with the tool deterioration process described in Chapter 3 and Chapter 4.

Under wet (coolant) cutting conditions, four passes were conducted for both TC14-1 and TC14-2 (Figure 5-1b). For TC14-1 wear progression is low in the first two passes with VB_{max} measured to be ~ 0.11 mm, followed by a rapid increase in VB_{max} in the third pass with VB_{max} reaching ~ 0.3 mm, finally ending its life after the fourth pass with VB_{max} measuring ~ 0.42 mm. It can be seen from Figure 5-7(b-c), that a slow wearing process has taken place in the first and second passes of the cutting tool alike TC13-2. After the third pass, the tool deteriorated severely resulting from chipping and fracturing locally along the cutting edge, with fracture extending ~ 0.3 mm beyond the cutting edge area as displayed in Figure 5-7d. In the final pass seen in Figure 5-7e, large fracturing and heavy chipping dominated altering the tool geometry dramatically with $VB_{max} \sim 0.42$ mm. Figure 5-8e indicates the change in tool geometry, concluding cutting edge blunting and loss of cutting function.

A duplicate number of passes (four passes) was conducted in tooling condition TC14-2 also in wet (coolant) milling as shown in Figure 5-1b. A slow wear rate was observed after the first, second and third pass corresponding to a VB_{max} of 0.1, 0.11 and 0.22 respectively. Significant changes in VB_{max} to a value of ~ 1.25 mm was evident following the fourth pass, implying severe tool deterioration of the cutting tool insert.

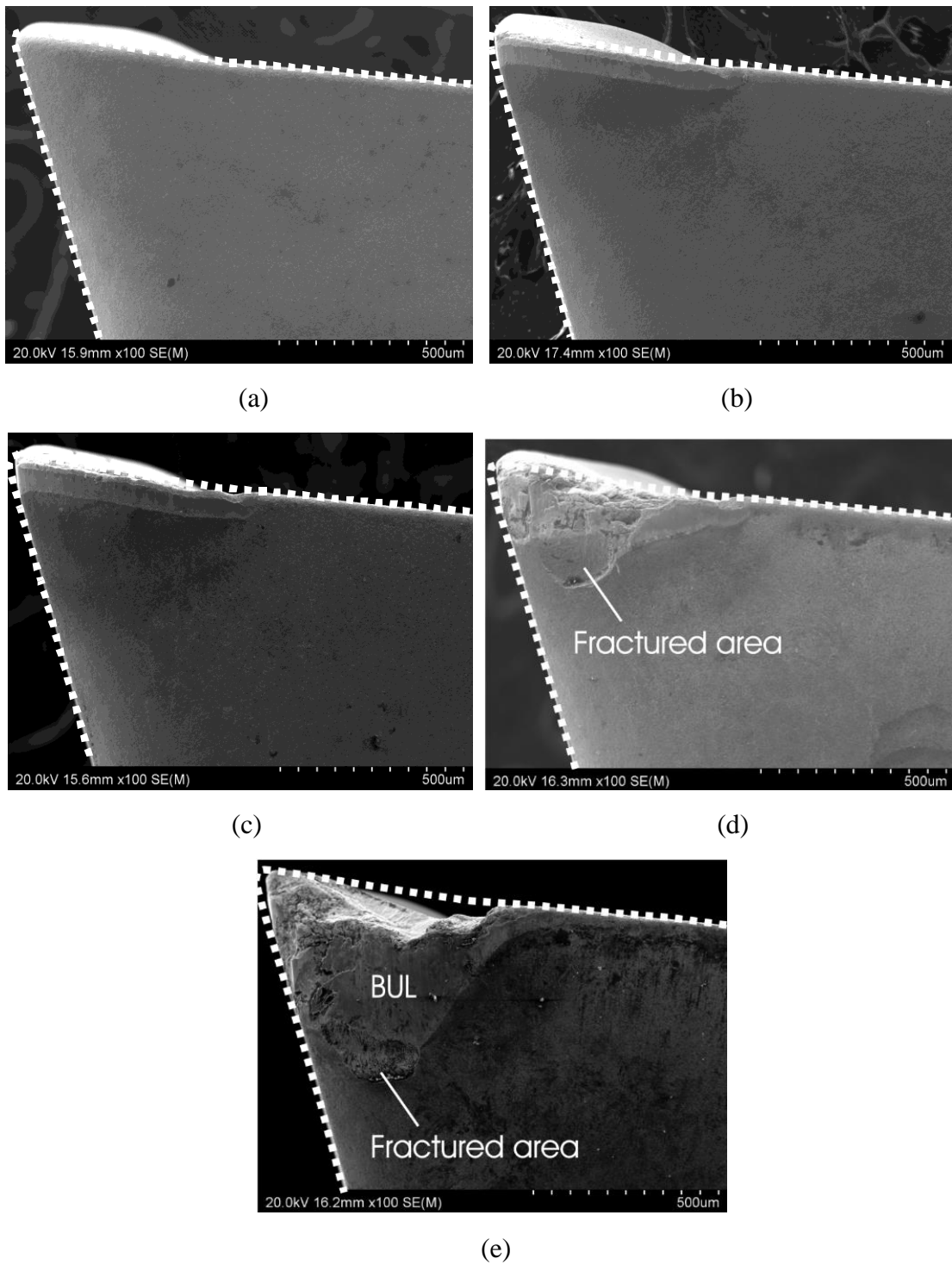


Figure 5-8 SEM images Tool TC14-1 side flank face before and after various milling passes of a hardened workpiece: (a) before milling with edge outlined, designated as zero pass edge outline (ZPEO), (b) after the first pass together with ZPEO, (c) after the second pass together with ZPEO, (d) after the third pass together with ZPEO, and (e) after the fourth pass together with ZPEO

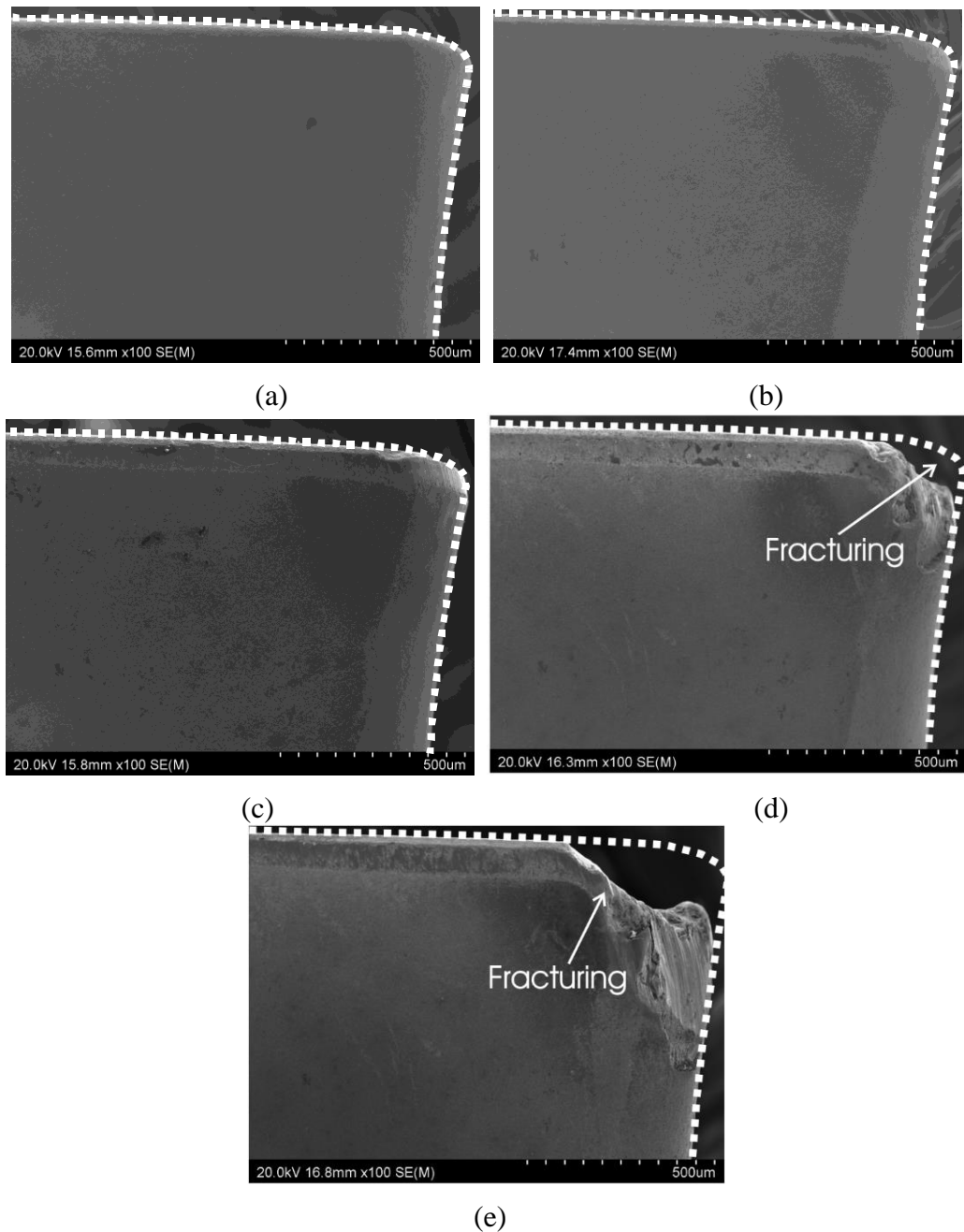


Figure 5-9 SEM images Tool TC14-1 bottom flank face before and after various milling passes of a hardened workpiece: (a) before milling with edge outlined, designated as zero pass edge outline (ZPEO), (b) after the first pass together with ZPEO, (c) after the second pass together with ZPEO, (d) after the third pass together with ZPEO, and (e) after the fourth pass together with ZPEO

For this TC14-2 experiment, observing the side flank face shown in Figure 5-9 (b-c), the cutting tool insert profile has little variation after the first and second pass suggesting a gradual wear process. Only BUL behind the cutting edge area is visible from these images. On the third pass, heavy edge chipping dominated but the tool blunting was not severe. A crack was to initiate in the cutting edge in location A in Figure 5-9d. Greater detail of the

crack is presented in Figure 5-10(a-b), formed by intergranular fracture between WC grains where the phenomenon has been described in Chapter 3 (section 3.6).

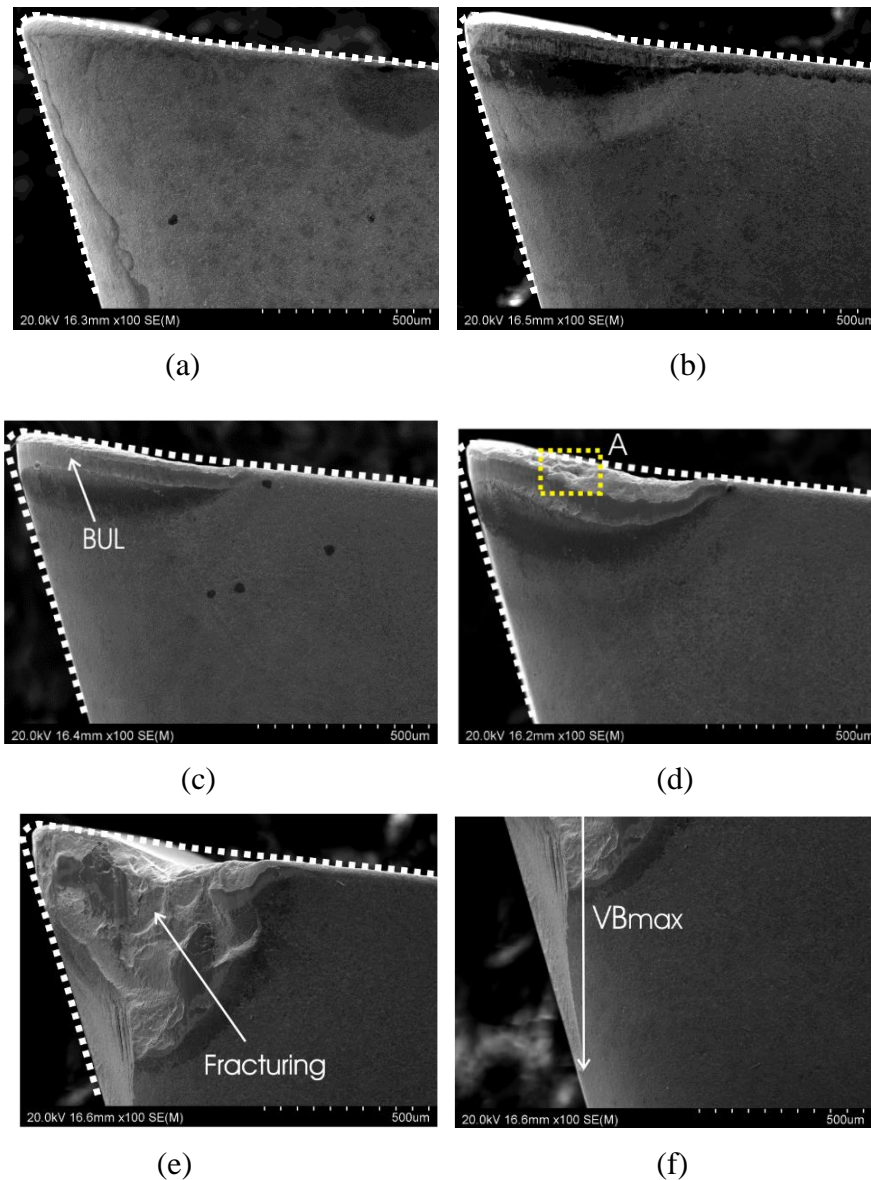


Figure 5-10 SEM images Tool TC14-2 side flank face before and after various milling passes of a hardened workpiece: (a) before milling with edge outlined, designated as zero pass edge outline (ZPEO), (b) after the first pass together with ZPEO, (c) after the second pass together with ZPEO, (d) after the third pass together with ZPEO, and (e) after the fourth pass together with ZPEO

Since cracking and fracturing initiated during the third pass, the rate of crack/fracture propagation was accelerated after the fourth pass culminating in a large fracture shown in Figure 5-9e. The bond between WC grains and Co-binder of the cutting tool insert weakened in the third pass and fractured with ease in the fourth pass especially when subjected to high

cutting forces. Long fracturing along the flank face, visible in Figure 5-9f produced a high VB_{max} of ~ 1.25 mm. SEM images of rake face for TC14-2 are presented in Figure 5-11. From this view no tool material loss is visible after the first two milling passes, suggesting minimal cutting tool edge deterioration as already explained. Nevertheless, after the third pass, the tool geometry changed and cracks were observed in Figure 5-10d at location point B corresponding to location point A in the side flank view.

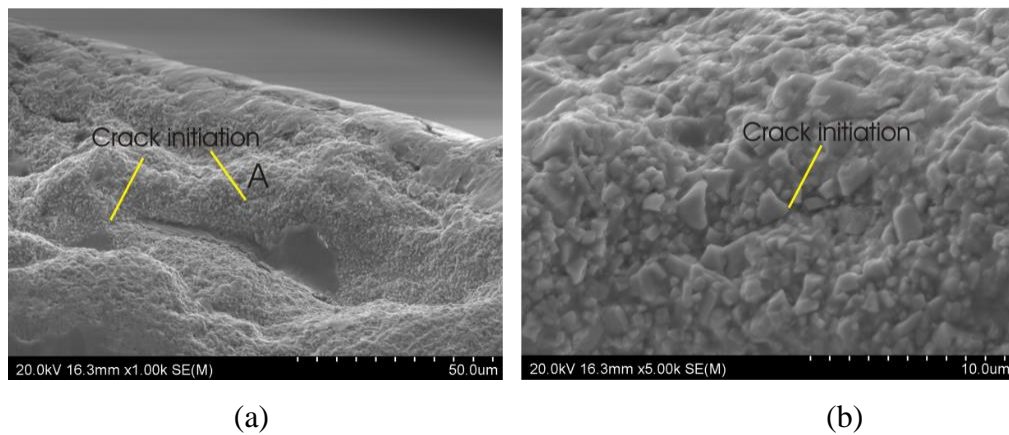


Figure 5-11 SEM images of tool TC14-2 in milling a hardened workpiece: (a) higher magnification image in location of Figure 5-9d at location A, showing crack initiation at side flank face view, and (b) higher magnification of 5000X magnification at side flank face

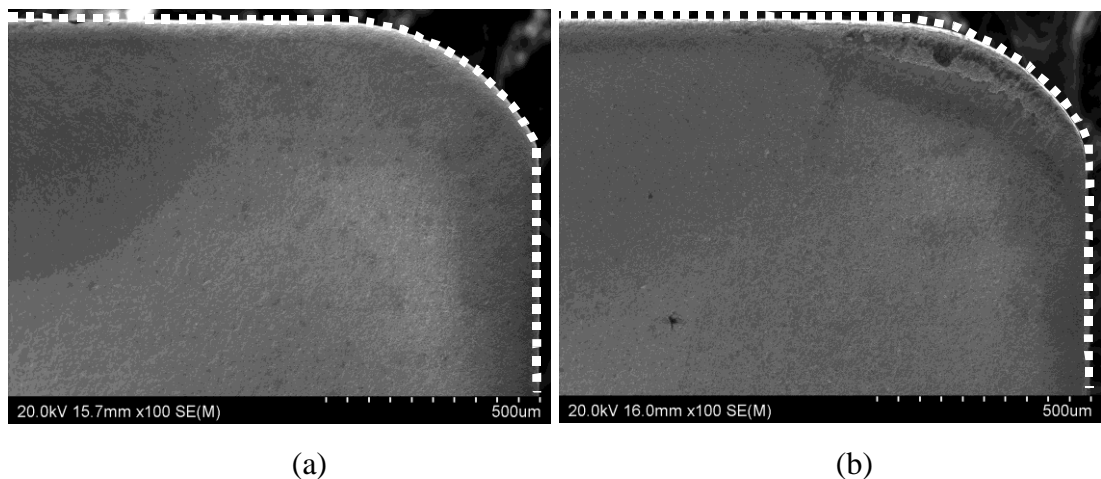
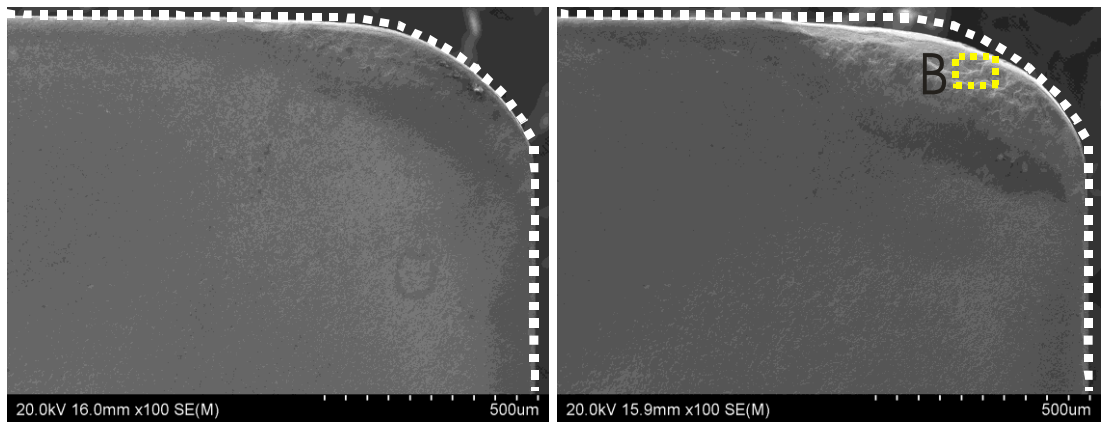
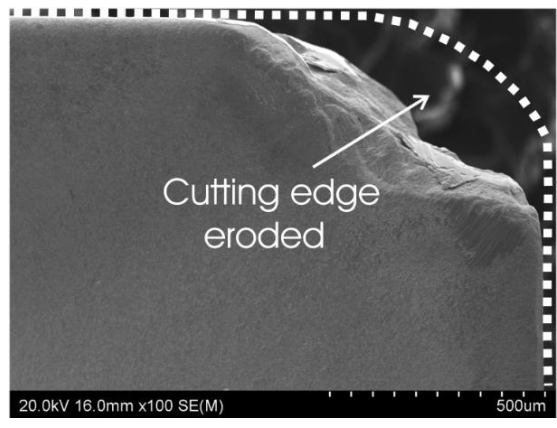


Figure 5-12 SEM images Tool TC14-2 rake face before and after various milling passes of a hardened workpiece: (a) before milling with edge outlined, designated as zero pass edge outline (ZPEO), (b) after the first pass together with ZPEO, (c) after the second pass together with ZPEO, (d) after the third pass together with ZPEO, and (e) after the fourth pass together with ZPEO



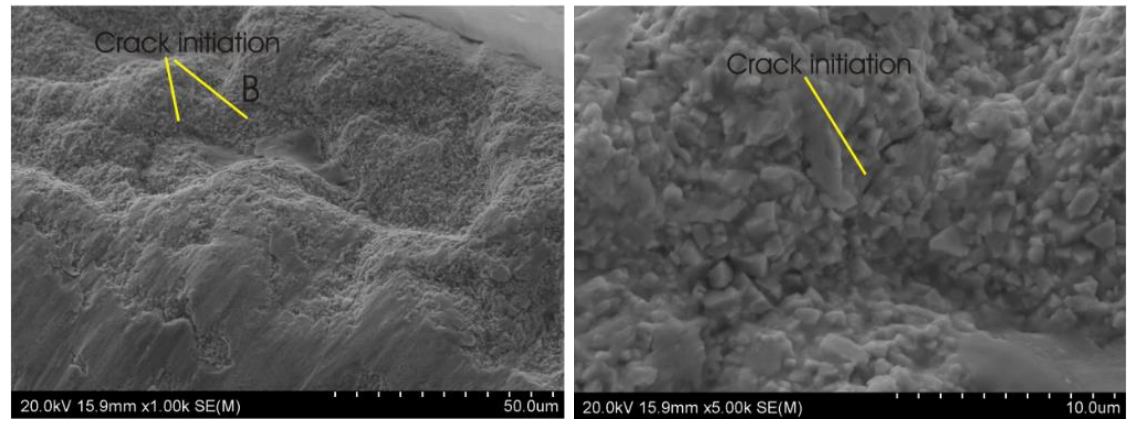
(c)

(d)



(e)

Figure 5-13 Continue



(a)

(b)

Figure 5-14 SEM images of tool TC14-2 in milling a hardened workpiece: (a) higher magnification image in location of Figure 5-11d at location point B, showing crack initiation at rake face view, and (b) higher magnification of 5000X magnification at the rake face

Cracking and fracturing are more apparent in Figure 5-12 (a-b). As shown in Figure 5-11e, a large amount of tool material fractured off at the cutting corner as clearly viewed on the

rake face. At this condition, the cutting tool has been severely deteriorated and was blunt. Overall VB_{max} increases with the number of milling passes irrespective of workpiece metallurgical state. The VB_{max} for the cutting tool was ~ 0.1 mm, indicating gradual wear rate after the first pass. On average, both the hardened and annealed workpieces allowed for four passes (N_{pass}) before the end of tool life. Additionally, the tool life performance of carbide tools on annealed and hardened workpieces under wet (coolant) cutting conditions were similar in which the tool life ended after the fourth pass. Despite of this, the rate of tool deterioration was not as high when machining 718Plus Ni-based superalloy in the hardened state as expected. Thus, in general the cutting tool performance was not significantly affected by the hardened state because there is negligible change in the tool deterioration trend. Additionally, the mode of tool deterioration from the beginning of the milling pass to the severest tool deterioration condition during milling of the hardened workpiece is identical to the annealed workpiece.

5.2 Trend of Cutting Force Increase Verse Milling Pass

Following on the previous section on the progression of cutting edge deterioration as milling pass increases, this section presents cutting forces in response to the tool deterioration. Figure 5-13 shows the cutting force values for the first (a) and fourth (b) pass of milling of coolant condition (TC14-1), one condition is selected, which is representative. By comparing these two passes, the change in cutting force from tool deterioration could be established.

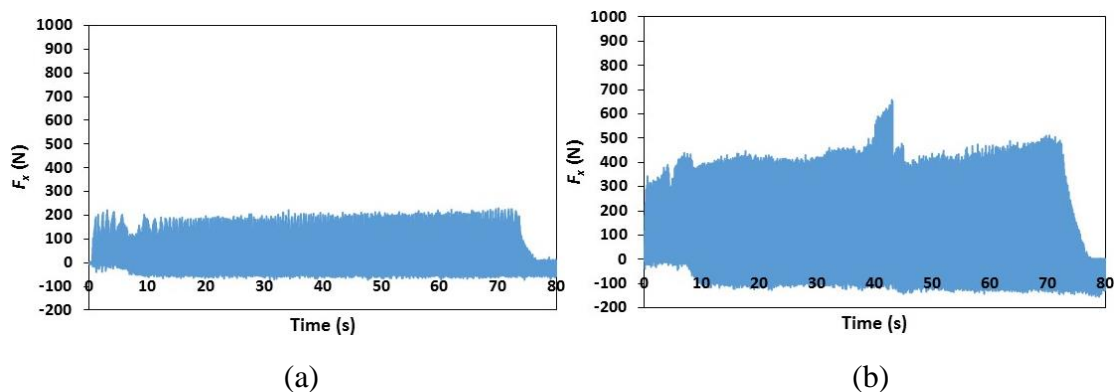


Figure 5-15 The whole F_x , F_y , F_z and F curves (recorded data) of a hardened workpiece (a) the first milling pass and (b) the fourth milling pass. Tooling condition: uncoated and coolant (TC14-1)

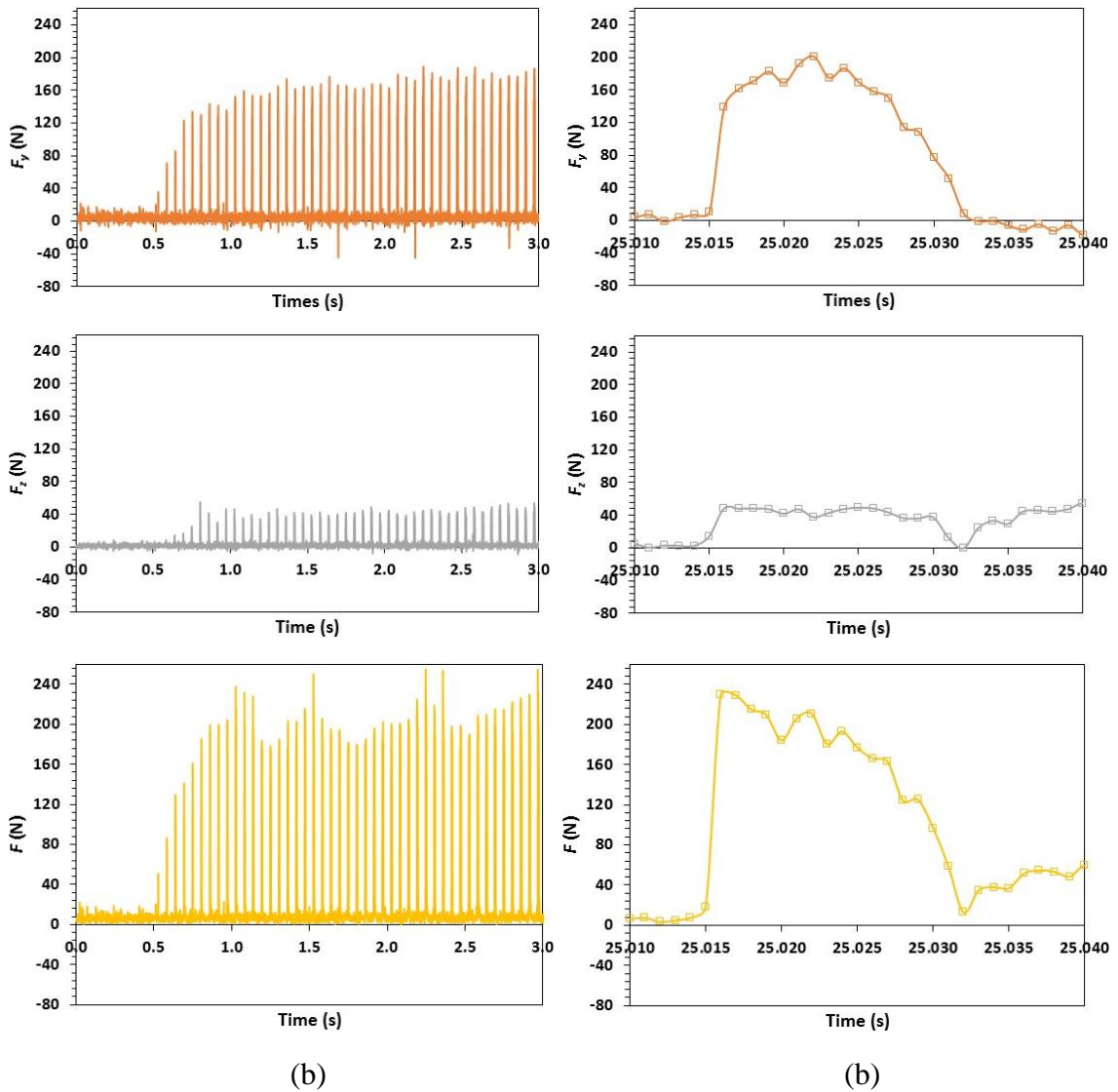


Figure 5-18 Continued

It can be observed in Figure 5-13, that the cutting force values from the first to fourth pass (final) increased from ~ 200 to >800 N. This range matched the trend in increasing cutting force when milling the workpiece in its annealed state as shown and explained in Chapter 4 (section 4.1). The variation and asymmetrical (up and down) in force values were also noticed in the final pass (Figure 5-13b) when the tool has been deteriorated significantly. During the first milling cycle shown in Figure 5-14, F_x and F_y reached a low maximum value of ~ 40 N with no F_z force recorded. From these initial cutting force values, it was not apparent that machining 718Plus Ni-based superalloy in its hardened state would significantly affect cutting force. The range in F_x and F_y cutting forces (both ~ 50 N) were smaller than that of the annealed workpiece and no F_z force was apparent. The cutting force (F), reached a peak of 240 N before gradually decreasing to zero within 0.018s (~ 25.033 s -

25.015 s), comparable to the cutting force (F) when machining the annealed workpiece as shown in Chapter 4 (Figure 4-3).

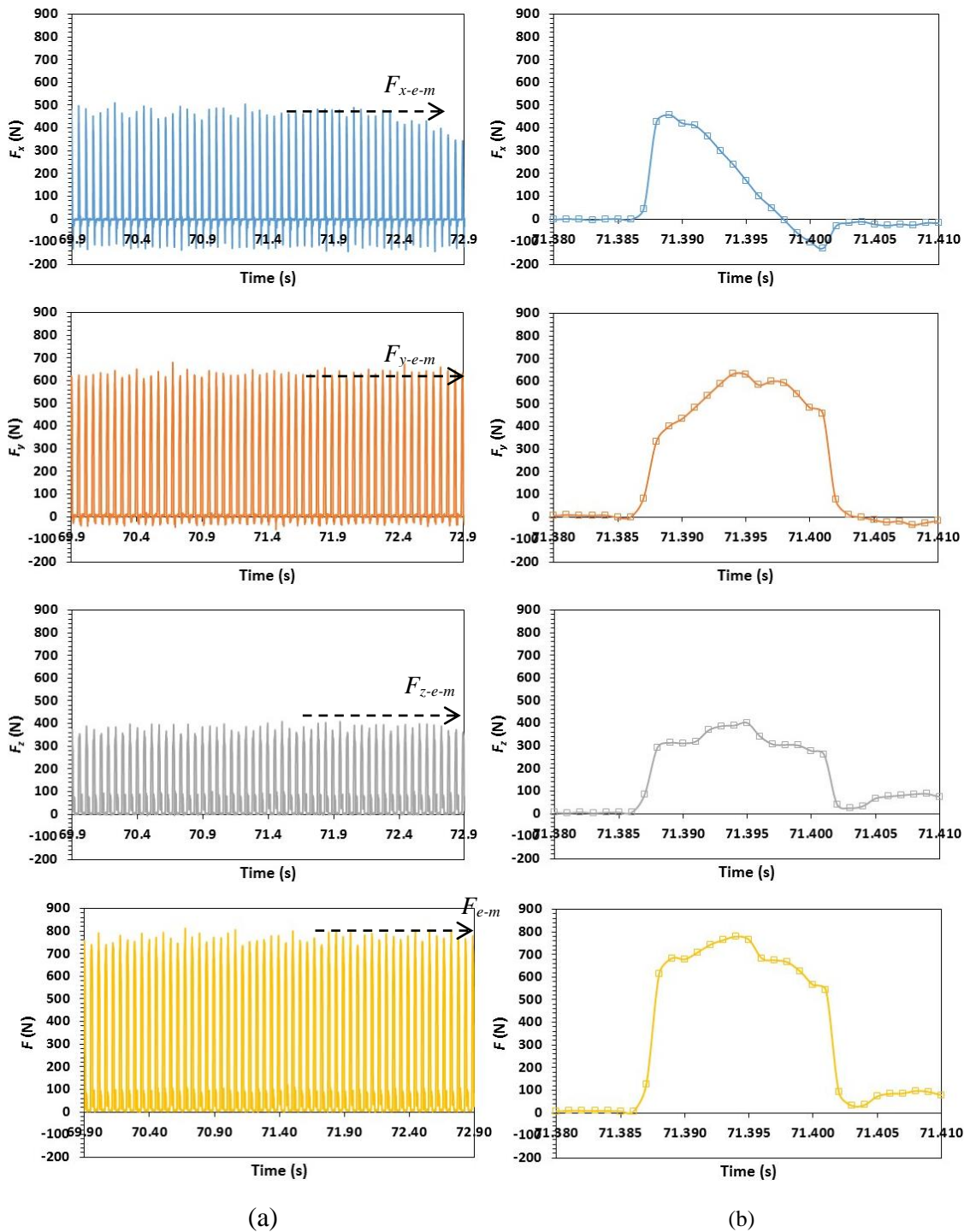


Figure 5-19 F_x , F_y , F_z and F data/curves of the first pass during (a) a 3-s period just before the insert reached the end of the workpiece and (b) a half cycle time within a period. Tooling condition: uncoated and coolant (TC14-1)

The periodicity was still observed in F_x with identical features to tool condition with uncoated tool and coolant (TC7-2) of annealed workpiece. As apparent in Figure 5-15b, the maximum force values towards the end of the pass (F_{x-e-m} , F_{y-e-m} , F_{z-e-m} and F_{e-m}) started to decrease between 73 - 74 s with maximum F of ~ 800 N. Hence, based on cutting force data presented a significant change in cutting force was unseen despite a significant increase in workpiece strength.

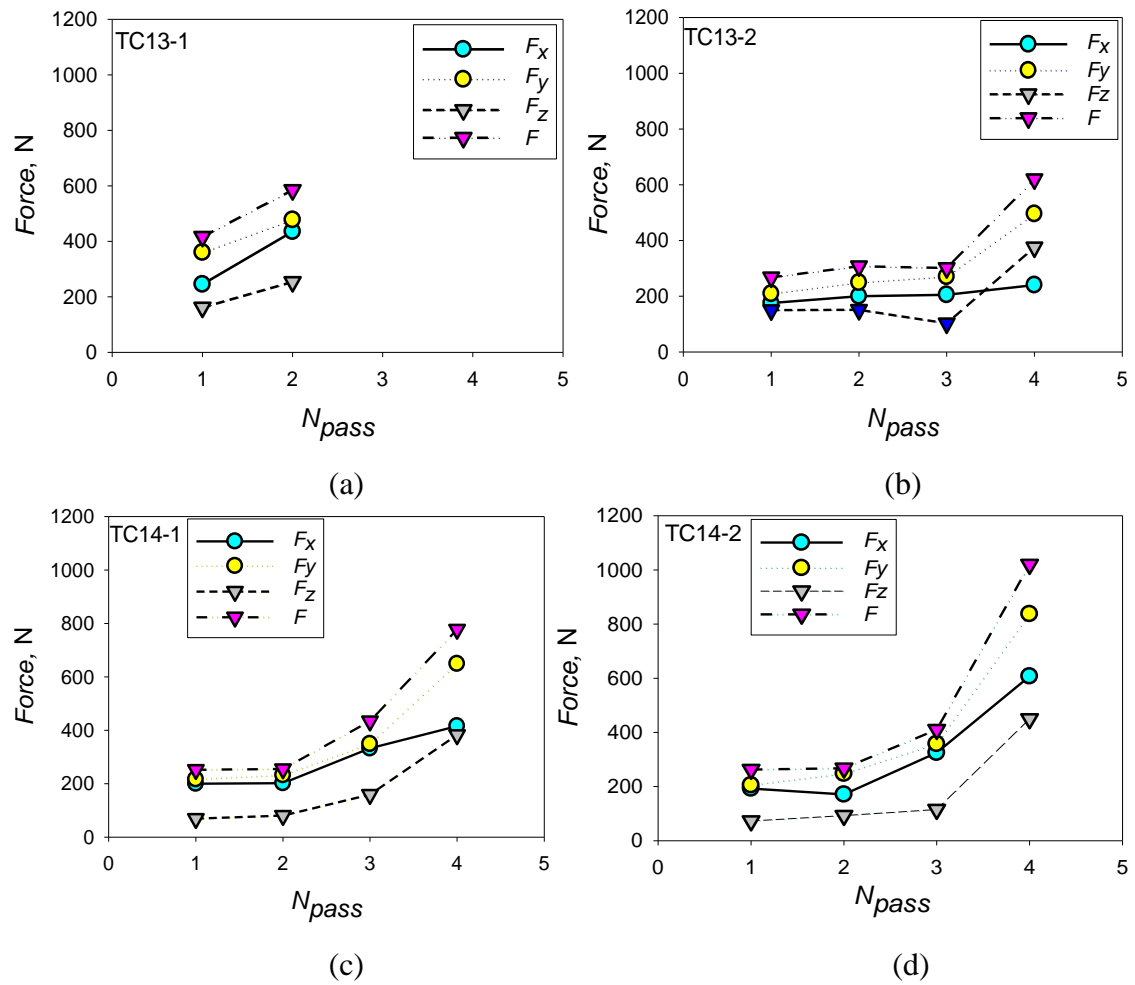


Figure 5-20 Average maximum force values F_{x-e-m} , F_{y-e-m} , F_{z-e-m} and F_{e-m} versus the number of passes four two cooling conditions, (a) TC13-1, (b) TC13-2, (c) TC14-1 and (d) TC14-2

Values of F_{x-e-m} , F_{y-e-m} , F_{z-e-m} and F_{e-m} are plotted against N_{pass} in Figure 5-16. The average F_{e-m} for all first passes was 299.6 N with a standard deviation of 67.7 N across all four data experiments. In particular for TC13-1, F_{e-m} measured an elevated 416.5 N after the first pass. Resulting from this high initial force at the first pass, F_{e-m} easily raised to ~ 585 N after the second pass and the milling experiment was subsequently terminated. As established in the previous chapter, a milling pass is stopped when cutting force (F) reaches ~ 550 N and TC13-

1 reached this criterion after the second pass even though VB_{max} measured ~ 0.22 mm. For all other TC conditions, the value of F_{e-m} was low after the second pass with range ΔF_{e-m} of 3 to 40 N. Meanwhile for tool condition TC13-2, a gradual increase in F was observed from the first to the second pass as shown in Figure 5-16b with VB_{max} measured about ~ 0.14 - 0.19 mm for these two passes. This could be explained by referring to SEM images viewed from side flank face in Figure 5-5 (b-c) and rake face in Figure 5-6 (b-c). Based on the images there was no significant loss after the first and the second passes. In Figure 5-6c, it can be seen that, the cutting edge was still sharp with no major chipping as TC13-1 in Figure 5-3c. Thus, the processes of tool deterioration in TC13-1 and TC13-2 are not consistent though they have similar milling condition. Similar phenomena occurred in milling annealed workpiece material in Chapter 4 (section 4-3) for TC6-1 and TC6-2 in Figure 4-8b. As stated in Chapter 4 (section 4.4), this “randomness” may be the results of the inconsistency of quality and properties of tool insert (WC-Co), which cannot be predicted.

In the third pass, the ΔF_{e-m} moderately increased from 0 to 180 N, followed by a large increase in F_{e-m} for all TC experiments in the fourth pass especially for TC14-2, as shown in Figure 5-16d. The ΔF_{e-m} range was between 319-610 N where the highest F_{e-m} for TC14-2 was ~ 1020 N. Based on the data presented in the graphs above, coolants do not have an effect in reducing the cutting force, same as for the experiments using annealed workpiece as discussed in Chapter 4. By comparing the general trend of cutting force data between hardened (Figure 5-16) and annealed experiments (Figure 4-7), both conditions observe similar features between the first to third pass. A gradual increase in F_{e-m} of ~ 266 - 299 N is noted for the first milling pass of all samples except for TC13-1 which exceeded cutting force criterion. Then, the F_{e-m} moderately increased with the $F_{e-m} < 450$ N at the third pass at all TC. Finally, F_{e-m} further increased in the final pass (fourth and fifth pass) between 450N and 2600N.

The correlation between F_{e-m} and VB_{max} is presented in Figure 5-17 where the high and low dF/VB_{max} curves from Figure 4-11 are given too, showing wide data spread identical with the trend in the series of annealed workpiece experiments. Extrapolating $VB_{max} \sim 0.1$ mm which occurred after the first pass yields the lowest F_{e-m} value (~ 240 N). It is also noted that F_{e-m} increases with increasing VB_{max} , however this correlation is weak. Thus, it can be concluded that the behaviour of tool deterioration of hardened workpiece is similar as annealed workpiece except for TC13-1.

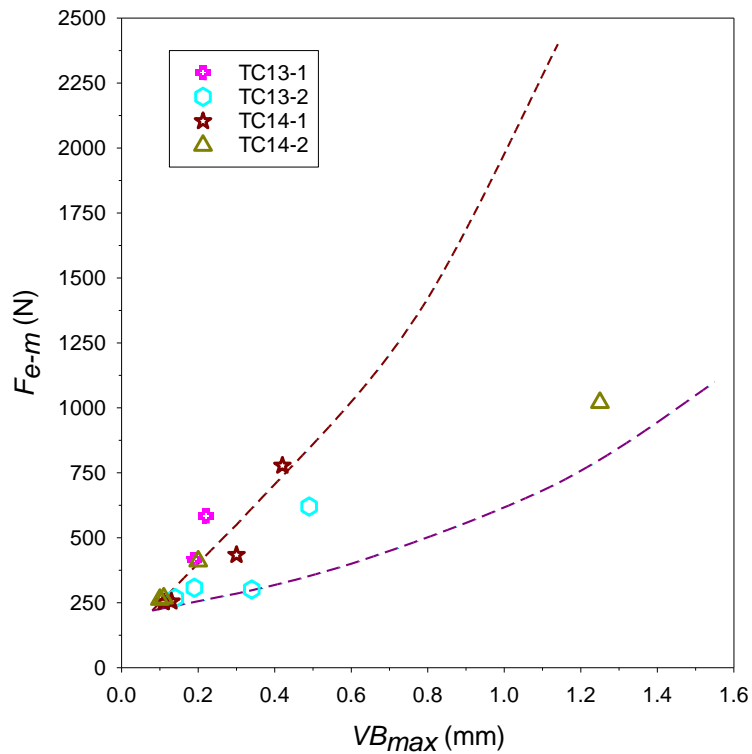


Figure 5-21 F_{e-m} values as a function of VB_{max}

5.3 Cutting Edge Condition Affecting Deformation Zone

Following what has been discussed earlier in Chapter 4 (section 4.5), examination of the workpiece deformation zone using dry milling condition was conducted in order to examine the influence of increase in workpiece hardness. Hardness distribution maps for the hardened workpiece experiments are presented in Figure 5-18. The depth of cut as observed in Figure 5-18 is ~ 0.5 mm, which is the set value of the milling experiment. The map on the left of Figure 5-18 is for first pass using a new tool and map on the right is for the tool that has been deteriorated after the fourth passes. It is clear that the shape of the milled surface observed in the cross section on the right image (Figure 5-18b) has shown severe cutting edge loss. The highest hardness band of ~ 500 - 525 HV obtained in zone 1 of the milled surface as shown in Figure 5-18a. The hardness (band) of the unaffected workpiece material is 400 - 425 HV. Furthermore, the depth of milling affected zone (MAZ) in zone 1 ranged from ~ 0.22 mm along the workpiece surface to ~ 0.36 mm in the bottom section of the zone, similar to the milled surface of annealed workpiece as shown in Figure 4-16. In zone 2, the hardness is near uniform horizontally, from 475 - 500 HV near to milled surface to 400 - 425 HV ~ 0.2 mm below. The rapid hardness transition from zone 1 to zone 2 is identical to the annealed workpiece milled with a new cutting tool (Figure 4-16), discussed previously in Chapter 4 (section 4.5).

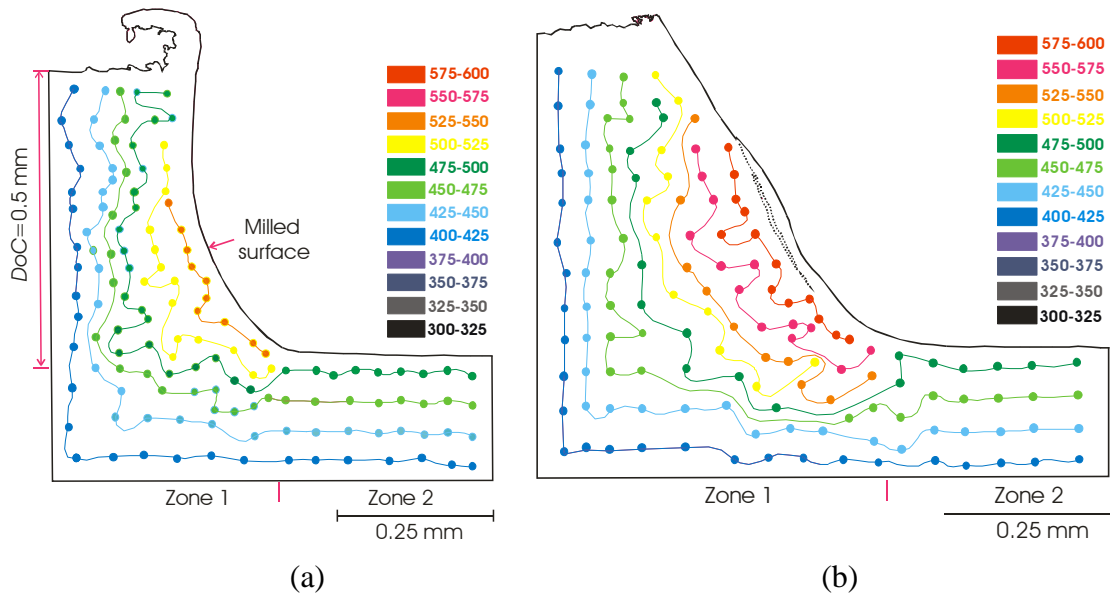


Figure 5-22 Micro hardness map on the cross section machined surface; (a) a new tool insert after the first pass (left image) and a deteriorated tool insert after the fourth milling pass (right image). Tool condition: uncoated tool and dry (TC15)

Furthermore, for the sample of deteriorated tool as shown in Figure 5-18b, the highest band reached 575-600 HV. The deformed zone has widened from slightly over 0.2 mm in the workpiece surface to ~ 0.5 mm to in the bottom zone 1. This suggests that the blunted tool cutting edge has forged/sheared a larger region. This is consistent with the significant cutting edge eroded and material loss shown in Figure 5-19a and Figure 5-19b and the following high increase in cutting force (F) value ~ 700 N after the fourth pass presented in Figure 5-20b.

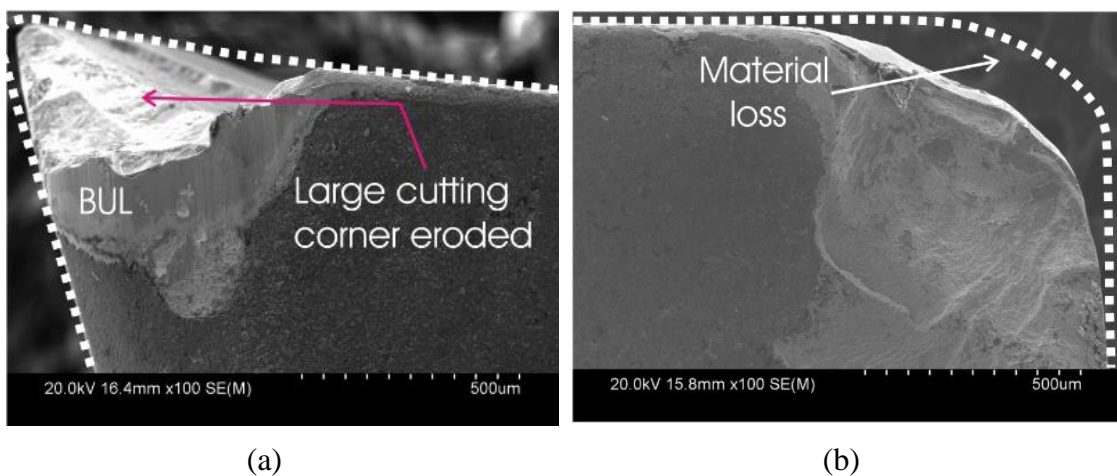


Figure 5-23 SEM images rake face of a deteriorated tool after the fourth pass of milling hardened workpiece in dry condition (TC15)

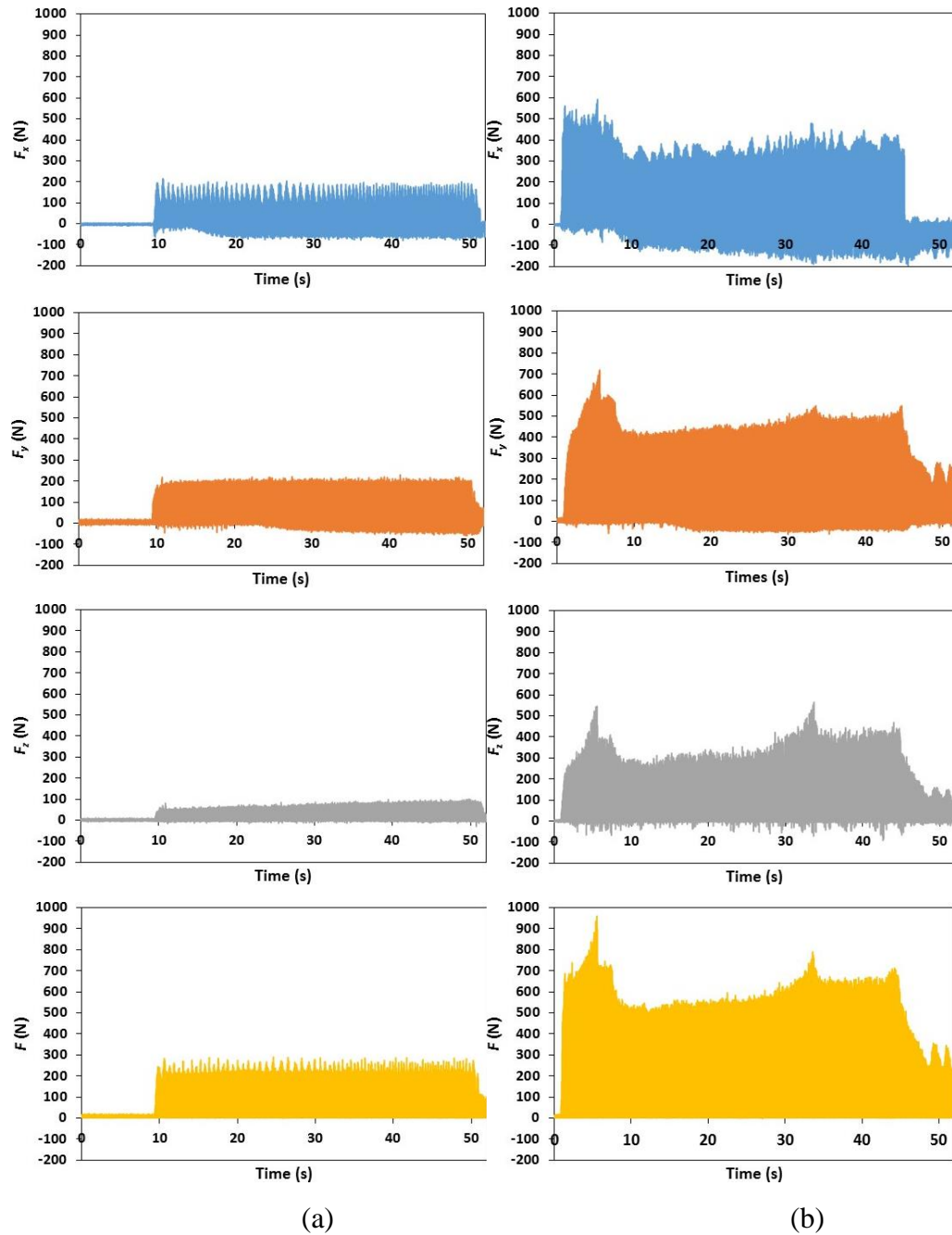


Figure 5-24 F curves (recorded data) of tool insert (a) a new tool after the first pass (b) a deteriorated tool after the fourth pass of milling hardened workpiece in dry condition (TC15)

5.4 Summary Plots on The Effect of Heat Treatment State

To more clearly examine how increasing strength of workpiece affects tool deterioration and cutting force, comparable data are plotted in Figure 5-21a and Figure 5-21b for VB_{max} and F_{e-m} , respectively, versus N_{pass} . Experiment TC13-1 is an exception that cutting edge and corner eroded early in the first and second pass. As has been explained, the result of this exception cannot be provided, as the consistence of cutting tool quality is not known. Other

data in Figure 5-21 have suggested that increasing strength of the workpiece has not a clear effect on tool life and cutting force. The increases in both VB_{max} and F_{e-m} from the first pass to the second are generally small and the increases from the second to third are generally clear. Beyond the third pass, the amounts of increases in VB_{max} and F_{e-m} are not in a predictable manner. These features have also been well observed and explained in Chapter 4 for experiments using annealed workpiece and now apply to experiments using hardened workpiece. A summary $F_{e-m} - VB_{max}$ plot, based on using an uncoated tool, combining both data from using annealed workpiece and hardened workpiece is given in Figure 5-22. This plot again shows the poor $F_{e-m} - VB_{max}$ relationship.

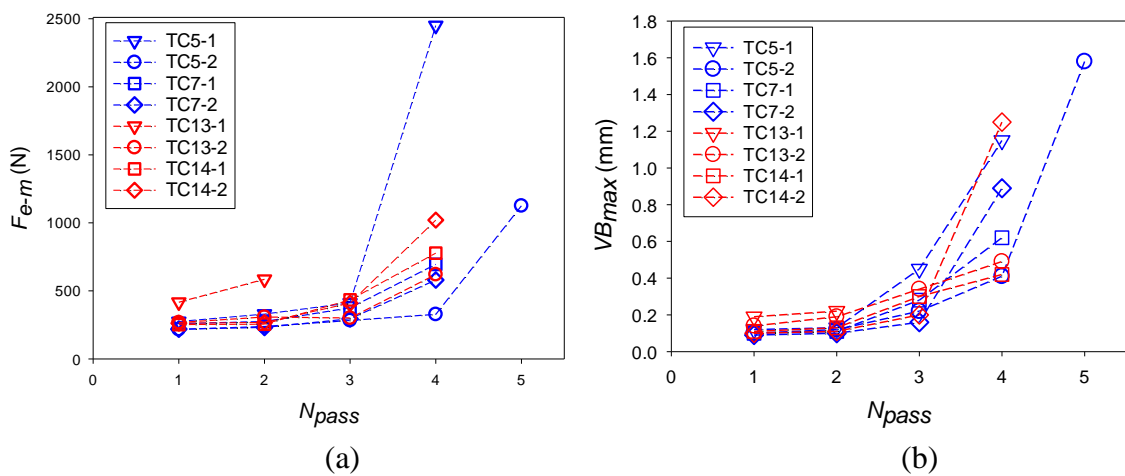


Figure 5-25 (a) Cutting force (F_{e-m}) and (b) flank wear (VB_{max}) values plotted against the number of passes (N_{pass}) for milling experiments conducted using annealed workpiece (TC5 and TC7) and hardened workpiece (TC13 and TC14)

The lack of clear difference in cutting force may explain the lack of difference in tool deterioration and life. However, this lack of difference in cutting force may be difficult to explain. Note, as has already been shown and explained in Figure 4-16, the size of deformation zones appears to be similar for both workpieces. This suggests a similar amount of deformation, although a more detailed analysis has not been conducted to reveal more details of deformation. However, as indicative in these deformation zone plots, hardness values are significantly higher for the hardened workpiece. The flow stress values for the hardened workpiece should then be higher. A high flow stress should mean a higher cutting force for a similar amount of deformation. A logical explanation may

then be the similar flow stresses during milling using either annealed or hardened workpiece.

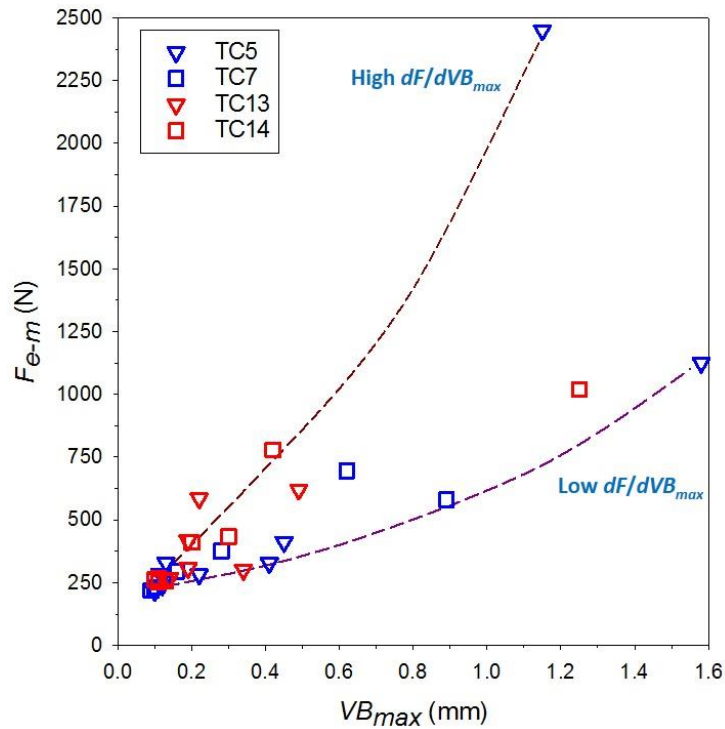


Figure 5-26 F_{e-m} values plotted as a function of VB_{max} for experiments using both annealed and hardened workpieces

This may mean that the temperatures of the deformation zone, either using annealed or hardened workpiece, will increase due to both friction and deformation to high temperatures and hardening mechanisms will stop operational at these high temperatures. Thus, similar cutting forces result. The hardening mechanisms will then reverse upon cooling to room temperature. The complexity of this softening and hardening mechanism is however not further studied in this present thesis.

5.5 Overall Plots of Flank Wear and Cutting Force

For an overview on how varying the milling conditions affects tool deterioration and cutting force, a summary on the results of the milling under various tool conditions are plotted in Figure 5-23 and Figure 5-24 for F_{e-m} and VB_{max} , respectively, versus N_{pass} . In order to construct these plots, an average value of two data points was taken from the same milling condition. For example; in F_{e-m} versus N_{pass} plot as shown Figure 5-23a, TC11 represents the average of TC11-1 and TC11-2 at the defined N_{pass} . An exception to the rule is defined in specific cases when there is an additional comparable pass at a

certain condition e.g. TC11-2 (four passes). For this condition, the prior pass and additional pass are averaged to represent as a non integer N_{pass} e.g 3.5. In the case of TC11, three data points were averaged, the two points corresponding to the third pass for conditions TC11-1 and TC11-2 and the four pass for condition TC11-2. This culminated in a data point at 3.5 passes seen in Fig. 5-23a. The trends of increasing F_{e-m} and VB_{max} as N_{pass} increases both vary significantly. The reasons for this have been explained in Chapter 3-5 of this thesis.

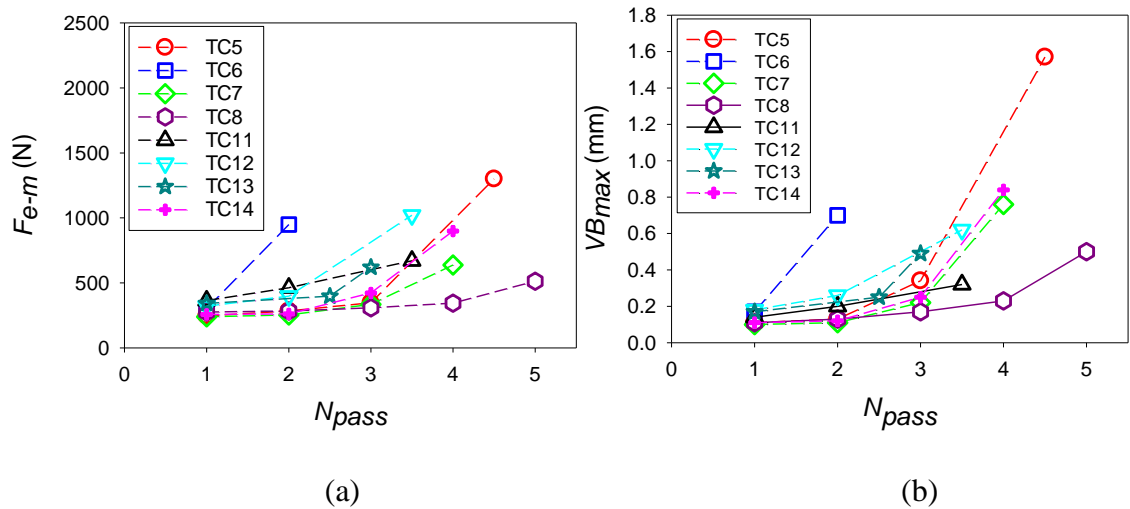


Figure 5-27 (a) Cutting force (F_{e-m}) and (b) flank wear (VB_{max}) values plotted against the number of passes (N_{pass}) for various tool conditions using annealed and heat treatment workpieces

Chapter 6: Conclusion

The main conclusions of this thesis can be summarised as below:

1. The short life of WC–Co tool inserts during the milling of 718Plus Ni alloy is the result of a tool deterioration process dominated by fracturing. After milling starts, chipping as a form of fracture soon follows in the cutting edge region and at the same time cracking/fracturing can extend a longer distance in the subsurface region along the flank face. The forms of these fracture processes directly relate to the forces acting on the cutting region. The process commences by crack initiation in the binder between WC grains and propagates between the grains. The major contribution of this fracture mode is the deformation to fracture of Co binder material. As tool fracturing and thus blunting proceeds, the tool loses its function of cutting the workpiece. Instead, rubbing/forging between the workpiece and the tool dominates. Views from the bottom flank face and rake face in a consistent manner, in addition to viewing the major flank face not only allow the fracturing progression to be revealed but also allow for a correct estimation of tool material loss. Although tool life is short, there is a stage of incubation when cracks initiate in or near the cutting edge on the side of rake face before severe fracturing and thus accelerating tool blunting.
2. Modes of insert deterioration relate to cutting force (F) differently. The trend of increasing flank wear (VB_{max}) as the number of milling passes (N_{pass}) increases broadly agrees with the trend of increasing F as N_{pass} increases. However, the present experimental data have suggested that F correlate poorly with VB_{max} because $\Delta F/\Delta VB_{max}$ can vary considerably. This is the result that, in a specific milling experiment, a deterioration mode may be more dominant than the other as the insert deteriorates. The mode of severe chipping and breakage confined to the cutting edge thus causing severe blunting of the edge corresponds to relatively high $\Delta F/\Delta VB_{max}$. This is suggested to be the result of edge blunting having a major effect on causing the effective rake angle to decrease due to the small feed rate values normally used in milling Ni-based alloys, thus a major effect of increasing F . The mode of fracturing a thin layer extending to outside the cutting edge along the flank face increases the VB_{max} value but the extra VB_{max} does not contribute to the cutting edge contact width and thus no extra F is required. This results in low $\Delta F/\Delta VB_{max}$.

3. Qualitatively, coating of the tool by TiAlN has little effect in preventing the tool deterioration process. This is because the coating in the cutting edge region breaks off under the milling conditions, soon after milling starts. It has also been found that the use of coating has not an influence of cutting force. This finding is consistent with the observation of coating breaking off from the cutting edge, thus losing the effect of lessening friction between the cutting tool and chip (from workpiece).
4. The use of coolant has not been found to affect tool deterioration/life and cutting force. This relates to the deformation zone during milling. It has been determined that the size of deformation zone, which is small, during dry milling is largely the same as one during wet (using coolant) milling. Thus, cutting force required for the similar amount of deformation is largely the same for the two different milling conditions. This lack of the effect from coolant is suggested to be the result of lack of cooling effect on the small deformation zone in workpiece adjacent to the rotating tool at a high speed.
5. As expected, an increase in feed rate from 0.05 mm/min to 0.1 mm/min has reduced the tool life further and higher cutting force. It has been found that, using the higher feed rate, the mode of deterioration has become more edge chipping/fracturing dominant. It has also been found that, due to the dominance of the deterioration mode, F correlates well with VB_{max} . Being the mode of edge chipping/fracturing dominant, a high $\Delta F/\Delta VB_{max}$ trend follows
6. It has been observed that rate of tool deterioration on hardened workpiece was comparable to the annealed workpiece. The modes and progression of deterioration of tools using hardened workpiece were determined to be comparable to those when annealed workpiece was used. Furthermore, the trends of increase in cutting force as milling pass increases have been observed to be similar for both workpiece material conditions. It has been determined that the workpiece at hardened state has not affected the deformation area significantly, although increase in hardness in a similar amount in the severe deformed region has been found for both cases. It is suggested that temperature increases in the narrow deformation zone to be similar for both workpiece conditions and at high temperatures hardening mechanisms do not operate, and thus cutting force values do not differ significantly.

References

- [1] V. P. Astakhov, *Machinability of Advanced Materials*, First Edit. ISTE Ltd and John Wiley & Sons, Inc, 2014.
- [2] S. Pervaiz, A. Rashid, I. Deiab, and M. Nicolescu, "Influence of Tool Materials on Machinability of Titanium- and Nickel-Based Alloys: A Review," *Mater. Manuf. Process.*, vol. 29, no. 3, pp. 219–252, 2014.
- [3] Y. S. Liao, H. M. Lin, and J. H. Wang, "Behaviors of end milling Inconel 718 superalloy by cemented carbide tools," *J. Mater. Process. Technol.*, vol. 201, no. 1–3, pp. 460–465, 2008.
- [4] X. Q. Chen and H. Z. Li, "Development of a tool wear observer model for online tool condition monitoring and control in machining nickel-based alloys," *Int. J. Adv. Manuf. Technol.*, vol. 45, no. 7–8, pp. 786–800, 2009.
- [5] K. Kadirgama, K. A. Abou-El-Hossein, M. M. Noor, K. V. Sharma, and B. Mohammad, "Tool life and wear mechanism when machining Hastelloy C-22HS," *Wear*, vol. 270, no. 3–4, pp. 258–268, 2011.
- [6] A. Devillez, G. Le Coz, S. Dominiak, and D. Dudzinski, "Dry machining of Inconel 718, workpiece surface integrity," *J. Mater. Process. Technol.*, vol. 211, no. 10, pp. 1590–1598, 2011.
- [7] S. Olovsjö and L. Nyborg, "Influence of microstructure on wear behaviour of uncoated WC tools in turning of Alloy 718 and Waspaloy," *Wear*, vol. 282–283, pp. 12–21, 2012.
- [8] S. Zhang, J. F. Li, and Y. W. Wang, "Tool life and cutting forces in end milling Inconel 718 under dry and minimum quantity cooling lubrication cutting conditions," *J. Clean. Prod.*, vol. 32, pp. 81–87, 2012.
- [9] irfan Ucin, K. Aslantas, and F. Bedir, "An experimental investigation of the effect of coating material on tool wear in micro milling of Inconel 718 super alloy," *Wear*, vol. 300, no. 1–2, pp. 8–19, 2013.
- [10] M. Imran, P. T. Mativenga, A. Gholinia, and P. J. Withers, "Comparison of tool wear mechanisms and surface integrity for dry and wet micro-drilling of nickel-base superalloys," *Int. J. Mach. Tools Manuf.*, vol. 76, pp. 49–60, 2014.
- [11] M. S. Kasim, C. H. Che Haron, J. A. Ghani, M. A. Sulaiman, and M. Z. A. Yazid,

- “Wear mechanism and notch wear location prediction model in ball nose end milling of Inconel 718,” *Wear*, vol. 302, no. 1–2, pp. 1171–1179, 2013.
- [12] D. Zhu, X. Zhang, and H. Ding, “Tool wear characteristics in machining of nickel-based superalloys,” *Int. J. Mach. Tools Manuf.*, vol. 64, pp. 60–77, 2013.
- [13] S. Chinchankar and S. K. Choudhury, “Machining of hardened steel - Experimental investigations, performance modeling and cooling techniques: A review,” *Int. J. Mach. Tools Manuf.*, vol. 89, pp. 95–109, 2015.
- [14] L. N. L. De Lacalle, A. Lamikiz, J. F. De Larrinoa, and I. Azkona, “Advanced Cutting Tools.”, *Machining of Hard Materials*, Springer-Verlag, London, 2011, pp.33-86.
- [15] ISO 8688-2, International Organisation for Standardization, Geneva, 1989.
- [16] H. G. Prengel, W. R. Pfouts, and A. T. Santhanam, “State of the art in hard coatings for carbide cutting tools,” *Surf. Coatings Technol.*, vol. 102, no. 3, pp. 183–190, 1998.
- [17] A. Jawaid, S. Koxsal, and S. Sharif, “Cutting performance and wear characteristics of PVD coated and uncoated carbide tools in face milling Inconel 718 aerospace alloy,” *J. Mater. Process. Technol.*, vol. 116, no. 1, pp. 2–9, 2001.
- [18] M. Kuttolamadom, “Prediction of the Wear & Evolution of Cutting Tools in a Carbide / Ti-6Al-4V Machining Tribosystem by Volumetric Tool Wear Characterization & Modeling,” p. 258, 2012.
- [19] M.-D. Jimenez, A.-E. Bermudez, “Friction and wear,” in *Industrial Lubrication and Tribology*, vol. 36, no. 5, J. P. Davim, Ed. Woodhead Publishing Limited, 1984, pp. 168–169.
- [20] M. C. Shaw, *Second Edition*, Second. Oxford series on Advanced manufacturing, , pp. 170, 2005.
- [21] J. a. Charles, *Selection and Use of Engineering Materials*, Third. Butterworth Heinemann, 1997.
- [22] H. Z. Li, H. Zeng, and X. Q. Chen, “An experimental study of tool wear and cutting force variation in the end milling of Inconel 718 with coated carbide inserts,” *J. Mater. Process. Technol.*, vol. 180, no. 1–3, pp. 296–304, 2006.
- [23] W. Akhtar, J. Sun, P. Sun, W. Chen, and Z. Saleem, “Tool wear mechanisms in

- the machining of Nickel based super-alloys: A review,” *Front. Mech. Eng.*, vol. 9, no. 2, pp. 106–119, 2014.
- [24] E. O. Ezugwu, Z. M. Wang, and A. R. Machado, “The machinability of nickel-based alloys: a review,” *J. Mater. Process. Technol.*, vol. 86, no. 1, pp. 1–16, 1999.
- [25] E. O. Ezugwu, J. Bonney, and Y. Yamane, “An overview of the machinability of aeroengine alloys,” *J. Mater. Process. Technol.*, vol. 134, no. 2, pp. 233–253, 2003.
- [26] Y. Huang and S. Y. Liang, “Modeling of CBN Tool Flank Wear Progression in Finish Hard Turning,” *J. Manuf. Sci. Eng.*, vol. 126, no. 1, p. 98, 2004.
- [27] A. Shokrani, V. Dhokia, S. T. Newman, and R. Imani-Asrai, “An initial study of the effect of using liquid nitrogen coolant on the surface roughness of inconel 718 nickel-based alloy in CNC milling,” *Procedia CIRP*, vol. 3, no. 1, pp. 121–125, 2012.
- [28] D. Dudzinski, A. Devillez, A. Moufki, D. Larrouquère, V. Zerrouki, and J. Vigneau, “A review of developments towards dry and high speed machining of Inconel 718 alloy,” *Int. J. Mach. Tools Manuf.*, vol. 44, no. 4, pp. 439–456, 2004.
- [29] T. Obikawa, Y. Kamata, Y. Asano, K. Nakayama, and A. W. Otieno, “Micro-liter lubrication machining of Inconel 718,” *Int. J. Mach. Tools Manuf.*, vol. 48, no. 15, pp. 1605–1612, 2008.
- [30] Y. Kamata and T. Obikawa, “High speed MQL finish-turning of Inconel 718 with different coated tools,” *J. Mater. Process. Technol.*, vol. 192–193, pp. 281–286, 2007.
- [31] F. Pusavec, H. Hamdi, J. Kopac, and I. S. Jawahir, “Surface integrity in cryogenic machining of nickel based alloy—Inconel 718,” *J. Mater. Process. Technol.*, vol. 211, no. 4, pp. 773–783, 2011.
- [32] D. Fernández, V. García Navas, A. Sandá, and I. Bengoetxea, “Comparison of machining inconel 718 with conventional and sustainable coolant,” *MM Sci. J.*, no. December 2014, pp. 506–510, 2014.
- [33] A. Aramcharoen and S. K. Chuan, “An experimental investigation on cryogenic milling of inconel 718 and its sustainability assessment,” *Procedia CIRP*, vol. 14, pp. 529–534, 2014.
- [34] Y. Kaynak, H. E. Karaca, R. D. Noebe, and I. S. Jawahir, “Tool-wear analysis in

cryogenic machining of NiTi shape memory alloys: A comparison of tool-wear performance with dry and MQL machining,” *Wear*, vol. 306, no. 1–2, pp. 51–63, 2013.

- [35] J. A. Ghani, I. A. Choudhury, and H. H. Masjuki, “Wear mechanism of TiN coated carbide and uncoated cermets tools at high cutting speed applications,” *J. Mater. Process. Technol.*, vol. 153–154, no. 1–3, pp. 1067–1073, 2004.
- [36] A. Sharman, R. C. Dewes, and D. K. Aspinwall, “Tool life when high speed ball nose end milling Inconel 718™,” *J. Mater. Process. Technol.*, vol. 118, no. 1–3, pp. 29–35, Dec. 2001.
- [37] H. G. Prengel, P. C. Jindal, K. H. Wendt, A. T. Santhanam, P. L. Hegde, and R. M. Penich, “A new class of high performance PVD coatings for carbide cutting tools,” *Surf. Coatings Technol.*, vol. 139, no. 1, pp. 25–34, 2001.
- [38] L. Li, N. He, M. Wang, and Z. G. Wang, “High speed cutting of Inconel 718 with coated carbide and ceramic inserts,” *J. Mater. Process. Technol.*, vol. 129, no. 1–3, pp. 127–130, 2002.
- [39] C. Ducros, V. Benevent, and F. Sanchette, “Deposition, characterization and machining performance of multilayer PVD coatings on cemented carbide cutting tools,” *Surf. Coatings Technol.*, vol. 163–164, pp. 681–688, 2003.
- [40] M. Sortino, S. Belfio, G. Totis, E. Kuljanic, and G. Fadelli, “Innovative tool coatings for increasing tool life in milling Nickel-coated Nickel-Silver alloy,” *Energy Procedia*, vol. 100, no. C, pp. 946–952, 2015.
- [41] X. Kong, L. Yang, H. Zhang, K. Zhou, and Y. Wang, “Cutting performance and coated tool wear mechanisms in laser-assisted milling K24 nickel-based superalloy,” *Int. J. Adv. Manuf. Technol.*, vol. 77, no. 9–12, pp. 2151–2163, 2015.
- [42] B. Kaya, C. Oysu, and H. M. Ertunc, “Force-torque based on-line tool wear estimation system for CNC milling of Inconel 718 using neural networks,” *Adv. Eng. Softw.*, vol. 42, no. 3, pp. 76–84, 2011.
- [43] M. Nouri, B. K. Fussell, B. L. Ziniti, and E. Linder, “Real-time tool wear monitoring in milling using a cutting condition independent method,” *Int. J. Mach. Tools Manuf.*, vol. 89, pp. 1–13, 2015.
- [44] S. Chinchankar and S. K. Choudhury, “Cutting force modeling considering tool wear effect during turning of hardened AISI 4340 alloy steel using multi-layer

- TiCN/Al₂O₃/TiN-coated carbide tools,” *Int. J. Adv. Manuf. Technol.*, vol. 83, no. 9–12, pp. 1749–1762, 2016.
- [45] C. H. Lauro, L. C. Brandão, D. Baldo, R. A. Reis, and J. P. Davim, “Monitoring and processing signal applied in machining processes - A review,” *Meas. J. Int. Meas. Confed.*, vol. 58, pp. 73–86, 2014.
- [46] L. Whitmore *et al.*, “The microstructure of heat-treated nickel-based superalloy 718Plus,” *Mater. Sci. Eng. A*, vol. 610, pp. 39–45, 2014.
- [47] T. D. Sheet, “ATI 718Plus ® Alloy 1,” vol. 1, pp. 1–5, Allegheny Technologies Incorporated, 2013.
- [48] V. P. Astakhov, “The assessment of cutting tool wear,” *Int. J. Mach. Tools Manuf.*, vol. 44, no. 6, pp. 637–647, 2004.
- [49] M. Kuttolamadom, P. Mehta, L. Mears, and T. Kurfess, “Correlation of the Volumetric Tool Wear Rate of Carbide Milling Inserts With the Material Removal Rate of Ti–6Al–4V,” *J. Manuf. Sci. Eng.*, vol. 137, no. 2, p. 21021, 2015.
- [50] M. A. Kuttolamadom and M. L. Mears, “Msec2011-50278 on the Volumetric Assessment of Tool Wear in Machining,” pp. 1–10, 2011.
- [51] Chetan, B. C. Behera, S. Ghosh, and P. V. Rao, “Wear behavior of PVD TiN coated carbide inserts during machining of Nimonic 90 and Ti6Al4V superalloys under dry and MQL conditions,” *Ceram. Int.*, vol. 42, no. 13, pp. 14873–14885, 2016.
- [52] N. H. Razak, Z. W. Chen, and T. Pasang, “Modes of tool deterioration during milling of 718Plus superalloy using cemented tungsten carbide tools,” *Wear*, vol. 316, pp. 92–100, 2014.
- [53] A. Introduction, M. F. Ashby, and D. R. H. Jones, *Engineering Materials 2*. 1986.
- [54] T. Kitagawa, A. Kubo, and K. Maekawa, “Temperature and wear of cutting tools in high-speed machining of Inconel 718 and Ti–6Al–6V–2Sn,” *Wear*, vol. 202, no. 2, pp. 142–148, 1997.
- [55] L. Zhang, X. Qu, X. He, D. Rafi-Ud, M. Qin, and H. Zhu, “Hot deformation behavior of Co-base ODS alloys,” *J. Alloys Compd.*, vol. 512, no. 1, pp. 39–46, 2012.
- [56] R &D ISCAR Ltd., “of ISCAR Grades Substrate - IC 28 Grade - IC 928 Typical Layers,” *Gen. Inf. ISCAR Grades*, p. 9970165, 2013.

- [57] X. Ren and Z. Liu, "Influence of cutting parameters on work hardening behavior of surface layer during turning superalloy Inconel 718," *Int. J. Adv. Manuf. Technol.*, pp. 2319–2327, 2016.